NUREG/CR-0797
PNL-2975
R-3

1 -

Post-Irradiation Data Analysis for NRC/PNL Halden Assembly IFA-431

C. Nealley
D. D. Lanning
M. E. Cunningham
C. R. Hann

October 1979

Prepared for
the U.S. Nuclear Regulatory Commission

Pacific Northwest Laboratory
Operated for the U.S. Department of Energy
by Battelle Memorial Institute

Battelle

PNL-2975

PACIFIC NORTHWEST LABORATORY
operated by
BATTELLE
for the
UNITED STATES DEPARTMENT OF ENERGY
Under Contract EY-76-C-06-1830

Printed in the United States of America
Available from
National Technical Information Service
United States Department of Commerce
5285 Port Royal Road
Springfield, Virginia 22151

Price: Printed Copy $____*; Microfiche $3.00

*Pages	NTIS Selling Price
001-025	$4.00
026-050	$4.50
051-075	$5.25
076-100	$6.00
101-125	$6.50
126-150	$7.25
151-175	$8.00
176-200	$9.00
201-225	$9.25
226-250	$9.50
251-275	$10.75
276-300	$11.00

NUREG/CR-0797
PNL-2975

POST-IRRADIATION DATA ANALYSIS FOR NRC/PNL HALDEN ASSEMBLY IFA-431

C. Nealley
D. D. Lanning
M. E. Cunningham
C. R. Hann

October 1979

Prepared for
the U.S. Nuclear Regulatory Commission
under a Related Services Agreement
with the U.S. Department of Energy
Contract EY-76-C-D6-1820
Fin. No. B-2043

Pacific Northwest Laboratory
Richland, Washington 99352

DOE Richland, WA

ABSTRACT

This report presents results of the post irradiation examination performed on IFA-431, which was a 6-rod test fuel assembly irradiated in Halden Reactor, Norway, under sponsorship of the Nuclear Regulatory Commission. The irradiation conditions included: peak powers of 33 kW/m; coolant pressure and temperature of 3.3 MPa and 240°C, respectively; and peak burnup of 4300 MWd/-MTM. IFA-431 included instrumented rods of basic boiling water reactor design, with variations in fill gas composition, gap size, and UO_2 fuel type. The irradiation was designed to measure the effect of these variations upon fuel rod thermal and mechanical performance.

The post irradiation examination assessed the permanent changes to the rods, including induced radioactivity, cladding deformation, fission gas release, and fuel densification. The induced gamma ray activity confirmed previous estimates of power distribution in the test rods. No significant cladding deformation was observed. Fission gas release was negligible (0.25% cumulative release). Densification of an unstable fuel type was confirmed at ~4% (from 92% to 96% of theoretical density). However, this densification did not result in increased fuel temperatures. It is concluded that under the conditions of the IFA-431 test, thermal effects of densification up to 4% are offset by fuel relocation.

SUMMARY

Nuclear fuel test assembly IFA-431 was designed by Pacific Northwest Laboratory to determine the uncertainties in fuel rod thermal stored energy calculations. This assembly was also designed to allow cross correlation of the results among other tests and commercial fuel assemblies. After irradiation to 4300 MWd/MTM in the Halden Boiling Water Reactor (HBWR), nondestructive examination consisting of visual examination, gamma scanning, profilometry, length measurements and gap measurement was performed at Kjeller Hot Cell. Rod 6 of assembly IFA-431 was destructively examined at Harwell. This examination consisted of fill gas and internal volume determinations, burnup analysis, bulk UO_2 density measurement, metallographic examination, and burnup and UO_2 density measurements across the pellet. Rods 1 thru 5 are scheduled for re-irradiation in the Power Burst Facility (Idaho Falls, Idaho).

The results of these examinations and an analysis of the results are presented in this report. From the analysis, it was concluded that 92% TD unstable fuel does densify, but that fuel relocation may override the fuel shrinkage to reduce rod temperature.

ACKNOWLEDGEMENTS

The authors wish to thank the Fuel Behavior Research Branch, Office of Reactor Safety Research, Nuclear Regulatory Commission, for their continued support and encouragement of the experimental program. We also recognize the contributions that personnel in several European laboratories made to the effort to obtain the data reported here. J. A. Christensen, NRC representative at Halden, and the Halden staff coordinated the final assembly design and irradiation. Nondestructive precharacterization and post irradiation measurements were carried out by the staff at Kjeller Hot Lab. John Williams and David Clough of Harwell were in charge of the destructive examination performed at that laboratory.

CONTENTS

FIGURES

TABLES

1.0 INTRODUCTION

Several unresolved questions pertaining to fuel rod thermal performance were causing delays in nuclear power plant licensing at the time the IFA-431 test was designed. These included the initial stored energy in rods prior to postulated loss-of-coolant accidents (LOCA's); the thermal effects of densification; and the extent of pellet-cladding interaction as a function of power and burnup. Many of the uncertainties in these phenomena were attributed to the lack of well-characterized data for fuel irradiated throughout the normal operating power range of commercial nuclear power plants.

This lack of well-characterized data resulted in inadequate computer-coded mathematical models that were developed to simulate fuel rod behavior over a wide range of postulated conditions. All of these factors have contributed substantially to the stored energy uncertainty. Specifically, the effects of fuel densification and fission gas on the fuel-cladding gap conductance were difficult to quantify, primarily because the applicable data were extremely sparse.

To focus on these uncertainties, Pacific Northwest Laboratory (PNL), under contract to the U.S. Nuclear Regulatory Commission (NRC) designed two instrumented Halden Boiling Water Reactor (HBWR) fuel assemblies. Experiments using these assemblies have provided well-characterized data under conditions that realistically simulate light water reactor conditions. This data will be used to verify NRC fuel codes, as well as provide bench mark data for commercial fuel licensing codes.

These two assemblies were designated IFA-431 and IFA-432, and were irradiated in HBWR. Assembly IFA-431 had a design power of 328 W/cm (10 kW/ft) and reached its goal burnup of 4300 MWd/MTM in February 1976. The second assembly, IFA-432, has a design power of 492 W/cm (15 kW/ft) and is expected to reach its goal burnup of 30,000 MWd/MTM in mid-1980.

The post irradiation examination (PIE) of assembly IFA-431 has been completed. Nondestructive PIE work was performed at Kjeller Hot Cell in Norway. This examination included visual inspection, gamma scanning, profilometry,

length measurements and inferred gap measurement. Harwell performed the destructive PIE work on rod 6 of IFA-431. Included in this examination was fill gas and internal volume measurement, burnup analysis, bulk UO_2 density measurements, metallographic and scanning electron microscope (SEM) examination, UO_2 density measurement across the fuel pellet and burnup profile measurement across the fuel pellet. Fuel rods 1 thru 5 are scheduled for re-irradiation in the Power Burst Facility, Idaho. This report includes general information on the post irradation examination of IFA-431 and the important results. Detailed metallographic and SEM results will be reported later.

2.0 CONCLUSIONS

The significant conclusions reached as a result of the post irradiation examination (PIE) of assembly IFA-431 are:

1. The fuel in rod 6 (initially 92% TD) definitely densified about 4%. This was concluded from bulk density measurements on the irradiated fuel, as well as from apparent fuel stack length and pellet diameter decreases.

2. In spite of the fuel densification in rod 6, the temperatures in that rod over the ∿4,300 MWd/MTM IFA-431 irradiation remained nearly identical to those of rod 1, which did not experience densification. It is presumed that the effects of fuel relocation overrode any effective gap widening due to densification.

3. The flux depression and local power estimates used for these test rods are well verified by the detailed PIE gamma scan and burnup analysis.

4. Incidental pellet cladding mechanical interaction (PCMI) was indicated by the cladding elongation detectors on all rods throughout the irradiation. However, only rod 3 (50 μm initial diametral gap) showed permanent cladding ridging. Therefore, PCMI and permanent cladding strain are definitely not synonymous.

5. The fission gas release for rod 6 was very low (0.25%) over the 4,300 MWd/MTM irradiation.

3.0 TEST DESCRIPTION

The following section describes the overall test parameters.

3.1 ASSEMBLY DESCRIPTION

Assembly IFA-431 was designed in July 1974 to test the effects of gap size, fill gas composition and fuel densification on fuel temperatures. The design parameters for this assembly are shown in Table 3.1, while the rationale for selecting these parameters is presented in the precharacterization report for IFA-431.[1]

TABLE 3.1. Design Parameters and Instrumentation for IFA-431 Peak Power 328 W/cm (10 kW/ft)

Rod No.	Pellet Diameter mm	Pellet Diameter in.	Cold Diametral Gap[a] mm	Cold Diametral Gap[a] in.	Fill Gas	Fuel Density % TD	Fuel Type[b]	Burnup MWd/MTM	Instrumentation: Temperature Upper	Temperature Lower	Pressure	Cladding Length
1	10.681	0.4205	0.229	0.009	He	95	Stable	4,000	TC[c]	TC	PT[d]	ES[e]
2	10.528	0.4145	0.381	0.015	He	95	Stable	4,000	TC	TC	--	ES
3	10.858	0.4275	0.051	0.002	He	95	Stable	4,000	TC	TC	--	ES
4	10.681	0.4205	0.229	0.009	Xe	95	Stable	4,000	TC	TC	--	ES
5	10.681	0.4205	0.229	0.009	He	92	Stable	4,000	TC	TC	PT	ES
6	10.681	0.4205	0.229	0.009	He	92	Unstable	4,000	TC	TC	PT	ES

(a) Cladding for all rods has an OD of 12.789 mm (0.5035 in.) and an ID of 10.909 mm (0.4295 in.). Diametral gap is cladding ID minus pellet diameter.
(b) With respect to in-reactor densification.
(c) TC = Thermocouple
(d) PT = Pressure Transducer
(e) ES = Elongation Sensor

This test allows cross correlation of available data. In addition to the rod-to-rod comparisons, top-to-bottom comparisons can be made in each rod and separate effects as a function of burnup and power can be evaluated. The design also facilitates comparison of this test with other test programs and commercial operation. Table 3.2 shows the cross correlation that is possible.

TABLE 3.2. Cross-Correlation Matrix

Rod Number	Gap Size	Fuel Relocation	Fuel Eccentricity	Fuel Stability	Gas Composition	Fuel Density	Rod Power	Rod Pressure	Dynamic Temperature
1 (9-He-95-s)[a]	X	X			X	X		X	X
2 (15-He-95-s)	X	X							X
3 (9-He-95-s)	X	X					X		X
4 (9-Xe-95-s)		X	X		X				X
5 (9-He-92-s)		X		X		X		X	X
6 (9-He-92-u)		X		X				X	X

(a) Example 1 (9-He-95-s): 1 identifies the rod, 9 is the nominal dimetral gap in mils, He is the fill gas, 95 is the fuel percent theoretical density, and s indicates stable fuel (u designates unstable fuel).

The fuel rods designed for use in IFA-431 had a BWR-6 pellet geometry. Each of these rods nominally contained 45 fuel pellets, 1.27 cm (0.5 in.) in length, for an active cold fuel length of 57.15 cm (22.5 in.). All the pellets were fabricated from 10 wt% U-235 enriched UO_2 powder by compacting and sintering. These pellets were made with flat ends. Dysprosium oxide pellets were located at both ends of the fuel column to prevent flux peaking. A helical plenum spring maintained a compact fuel column within the seamless, annealed Zircaloy-2 cladding. Supplied in accordance with ASTM B353-71, this cladding had an inside diameter of 1.0909 cm (0.4295 in.) and a wall thickness of 0.094 cm (0.037 in.).

Three types of fuel pellets were selected for the test, the reference fuel type was 95% theoretical density (TD) stable fuel to assure a densification-resistant fuel and to provide a density typical of current fuel designs. And, since new designs being considered for commercial reactor fuels will use stable, low density fuel, the other two types were fuel of 92% TD with stable or unstable structures.

Initial cold diametral fuel-cladding gap sizes of 0.0051, 0.0229 and 0.0381 cm (0.002, 0.009, and 0.015 in.) were selected for IFA-431. The rod with a 0.0229 cm gap was selected as the test standard. The rod with a gap size of 0.0381 cm provided an upper limit for the postulated effects of densification, while the small-gap rod (0.0051 cm) produced fuel-cladding contact at power, thus producing high gap conductance.

Five of the six rods in IFA-431 were backfilled with helium at atmospheric pressure. Due to the fission gas release, these rods experienced gas thermal conductivity degradation during irradiation. The sixth was backfilled with xenon at atmospheric pressure to eliminate the variables of changing gas composition and gas thermal conductivity, and to study the thermal effects of simulated fission gas.

Each of the six rods in assembly IFA-431 was designed to test specific parameters. A summary of these parameters follows:

Rod 1: Standard Fuel Rod - Rod 1 was selected as the standard rod for this test. This rod was fabricated with a 95% TD stable fuel, a 0.0229 cm initial diameter gap and helium fill gas.

Rod 2: Instantaneous Fuel Densification - The major calculated impact of fuel densification is the assumption that fuel undergoes instantaneous isotropic shrinking directly proportional to the difference between the fabricated and terminal densities. To simulate this condition, rod 2 was designed with a 0.0381 cm diametral gap. Other parameters for this rod were 95% TD stable fuel and helium fill gas.

Rod 3: Internal Reference - Rod 3 was designed as an independent check of rod powers. It also provided an upper bound for gap conductance and was used to simulate high burnup rods where the initial gap was closed by fuel relocation mechanisms. This rod contained 95% TD stable fuel, had a diametral gap of 0.0051 cm and was backfilled with helium. The small gap closed at power, thus producing high gap conductances, minimizing the temperature drop across the fuel-cladding interface, and providing a good check of the effective in-reactor thermal conductivity of the fuel.

Rod 4: Effects of Xenon Fill Gas - Experimental irradiations[2] have indicated that the apparent gap conductance in rods filled with either xenon or xenon-krypton is better than the values calculated by accepted analytical codes. To aid in understanding the reported anomalous thermal behavior of xenon-filled rods, rod 4 was designed with 95% TD stable fuel, a 0.0229-cm diametral gap, and 100% xenon fill gas.

Rod 5: Verification of Fuel Densification Stability - The new commercial reactor fuel designs that were being considered at the time IFA-431 was designed were to use low-density, stable fuel. Thus, rod 5 was designed to verify the recent fuel fabrication technology with regards to the effects of fuel structures on irradiation temperature. Rod 5 contained 92% TD stable fuel and had an initial gap of 0.0229 cm.

Rod 6: Densification Kinetics - Rod 6 contained 92% TD unstable fuel, had a 0.0229 cm diametral gap and was backfilled with helium. Earlier studies[3] conducted by the Pacific Northwest Laboratory have indicated that fuel with a similar structure underwent significant densification during irradiation and resintering. Data from rod 6 will be used to verify NRC densification models[4] and to provide a check of applicant-supplied models.

The following instrumentation was used to acquire experimental operating data for IFA-431:

- Fuel centerline thermocouples - The thermocouples had grounded junctions with 0.1575 cm (0.062 in.) outer diameter W/22%Rh sheaths and W5%Re/W26%Re seven-stranded thermocouple wires. The insulators were beryllium oxide.
- Pressure transducers - Measurement of the internal gas pressure of the fuel rods was performed by the pressure transducers, which were mounted on top of the rods. These instruments were thin platinum membrane barriers that separated the fuel rod gases from an external helium source with controlled pressure. The pressure balance across the membrane was indicated by an electric contact that rested against the membrane.
- Elongation detectors - The elongation detectors were linear variable differential transformer (LVDT) types. The LVDT is an electric mechanical transducer that produces an electrical output proportional to the displacement of a separate movable core. At Halden, the fuel rods are fixed at the top end and are allowed to elongate in a downward direction. Therefore, these instruments were positioned below the lower end of the fuel rods with the spring-loaded LVDT core in contact with the end of each fuel rod. Axial elongation of the fuel rods caused the core to move, which produced a change in the ouput voltage of the transducer.

- Self-powered neutron detectors (SPND) - The IFA-431 assembly was equipped with seven self-powered beta current neutron detectors. One of these detectors used cobalt as the absorber material, while the remaining six used vanadium. The vanadium detectors were used to determine assembly power during steady-state operation. For transient experiments, the assembly power was determined by the cobalt detector.

- Data Acquisition - The outputs from the in-reactor instruments (except the pressure transducers) were connected to a process computer which scanned and logged all the signals at 15 minute intervals. This recorded data was stored on discs for 24 hours, and then transferred to magnetic tape for permanent storage.

  The pressure transducer measurements were taken manually on a demand basis.

Figure 3.1 shows the location of the assembly instrumentation relative to the core and the normal neutron flux profile. A schematic arrangement of the

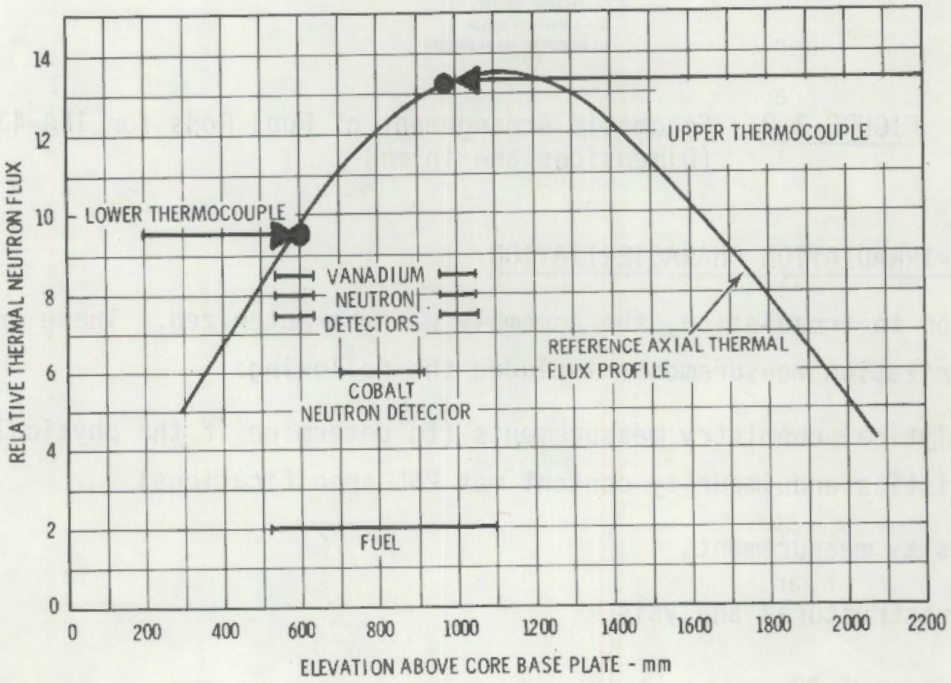

FIGURE 3.1. Arrangement of Temperature Sensors, Neutron Detectors, and Fuel Relative to Reference Axial Thermal Flux Profile, IFA-431 (Dimensions are in mm)

fuel rods and attached instrumentation is presented in Figure 3.2. Figure 3.3 is a schematic of assembly IFA-431.

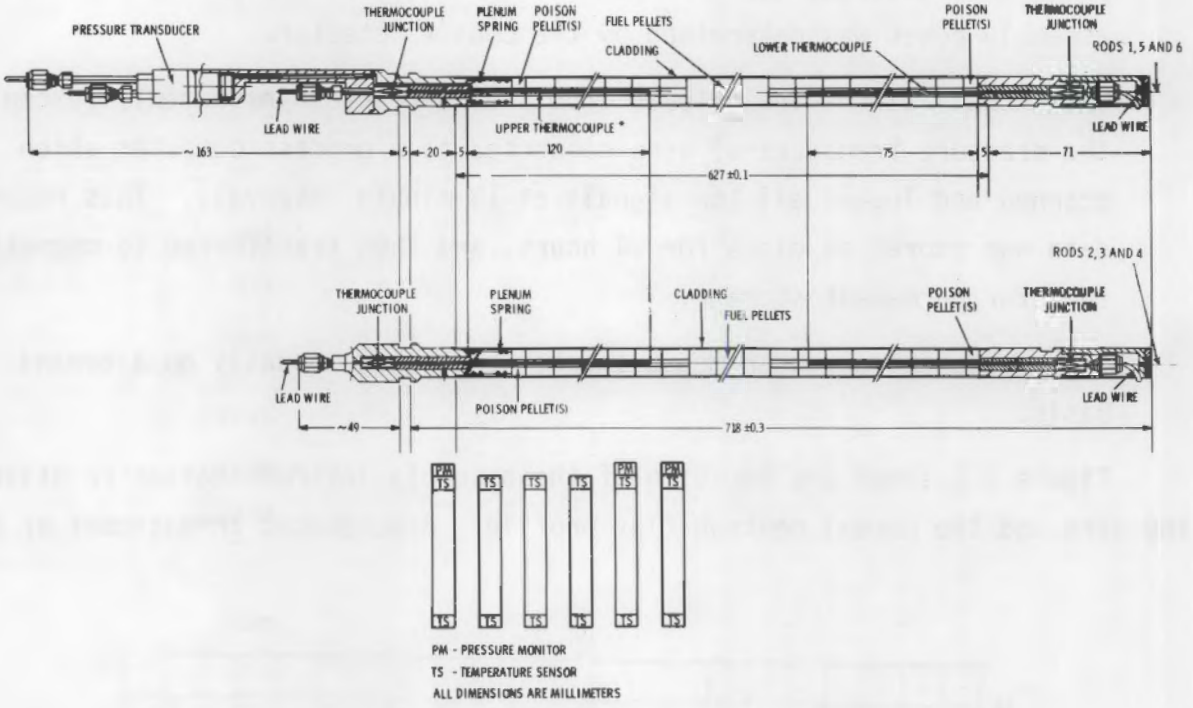

FIGURE 3.2. Schematic Arrangement of Fuel Rods for IFA-431 (Dimensions are in mm)

3.2 PRE-IRRADIATION CHARACTERIZATION

Prior to irradiation, the assembly was characterized. These pre-characterization measurements included the following:

- analytical chemistry measurements (to determine if the physical characteristics and impurity content met PNL specifications)
- density measurements
- microstructural analysis

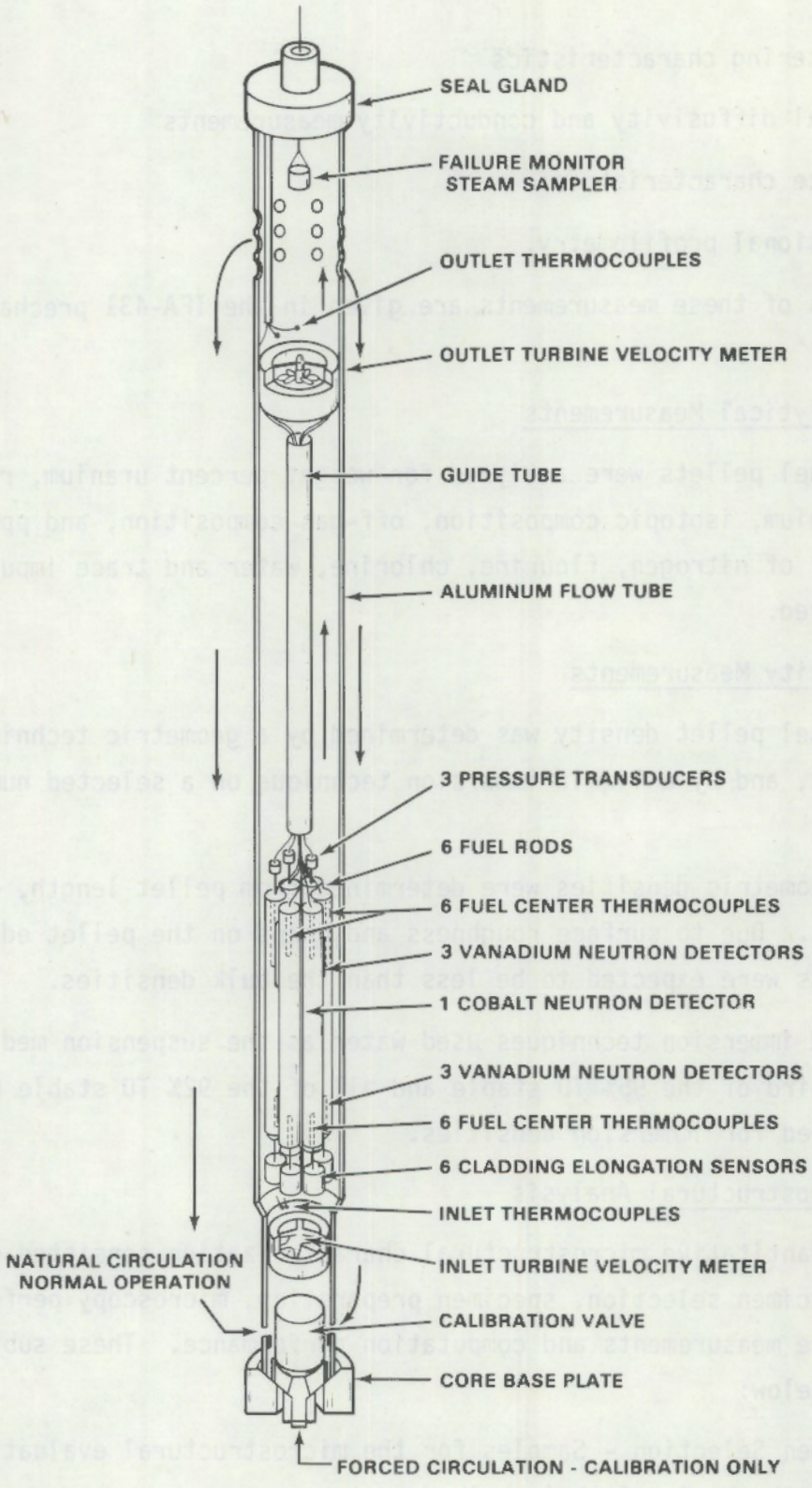

FIGURE 3.3. Schematic of Instrumented Fuel Assembly IFA-431

- resintering characteristics
- thermal diffusivity and conductivity measurements
- surface characteristics
- dimensional profilometry.

The results of these measurements are given in the IFA-431 precharacterization report.[1]

3.2.1 Analytical Measurements

The fuel pellets were analyzed for weight percent uranium, ratio of oxygen to uranium, isotopic composition, off-gas composition, and ppm of carbon. The amounts of nitrogen, flourine, chlorine, water and trace impurities were also measured.

3.2.2 Density Measurements

The fuel pellet density was determined by a geometric technique on all the pellets, and by a liquid immersion technique on a selected number of pellets.

a. The geometric densities were determined from pellet length, diameter and weight. Due to surface roughness and chips on the pellet edges, the results were expected to be less than the bulk densities.

b. Liquid immersion techniques used water as the suspension medium. About one-third of the 95% TD stable and all of the 92% TD stable pellets were measured for immersion densities.

3.2.3 Microstructural Analysis

The quantitative microstructural characterization consisted of five subtasks: specimen selection, specimen preparation, microscopy performance, quantitative measurements and computation performance. These subtasks are explained below:

Specimen Selection - Samples for the microstructural evaluation were selected on the basis of their bulk density.

Specimen Preparation - Grain size and pore distributions were evaluated on polished pellet cross section surfaces. The samples were prepared by polishing in a series of steps, ultimately utilizing a Lyntron vibratory polisher with 0.3 μm AlO_2 polishing agent in a 2% chromic acid bath.

Microscopy Performance - Both light and electron microscopy were required to cover the entire range of pores present in the fuel. A Zeiss "Ultraphot" light microscope was used to prepare micrographs at 9X, 31X, and 125X to 1000X magnification. Observation and measurement of the small pores required a higher magnification (up to 15000X), and this was achieved with a JSM-U3 scanning electron microscope.

Quantitative Measurements - The measuring and counting of the pores was a critical step in the process that required high accuracy with reasonable speed. A Quantimet 720 (a commercial quantitative image analyzer) was used to analyze the prepared micrograph prints. The standards used were reference micrographs measured independently with a Zeiss particle size analyzer.

Computation Performance - Mathematical and statistical methods were developed for converting two-dimensional pore data into three-dimensional data. These methods were incorporated into a computer code called LINEST II. The printout from this code includes tabulation of input pore count and measurement data; data summation for each magnification; tabulation of calculated relationships between pore size, density and volume; a summary of calculated and interpolated values for selected pore sizes or volume fractions; and a graphic display of represented data histograms. Pellet grain sizes were evaluated using the linear intercept method on peripheral, midradius and centerline position micrographs.

3.2.4 Resintering Characteristics

Resintering tests were conducted under five test conditions at 1600°C (2912°F) and 1700°C (3092°F). A test involving sintering at 1700°C for 24 hours was selected as a standard test because it was in compliance with the proposed NRC guidelines for predicting maximum irradiation density changes based on resintering test results. The 1600°C-for-24-hour condition was selected as a less severe test. A test pellet that was resintered at 1700°C

for 24 hours was heated for an additional hour to determine if the 1700°C-for-24-hour test resulted in a stable pellet. Resintering tests were run at 1700°C for 7.8 hours to see if Marlowe's equivalency model was correct. Finally, a 4-hour test at 1700°C was chosen to more fully characterize the densification kinetics at 1700°C.

3.2.5 Thermal Diffusivity and Conductivity Measurements

The purpose of these measurements was to determine the thermal diffusivity and conductivity of the three fuel types and to evaluate the effect of heat treatment on the diffusivity and conductivity. Thermal diffusivity of the fuel types was determined using a laser-pulse technique from 100°C (212°F) to 1600°C (2912°F). The thermal conductivity was calculated from the measured thermal diffusivity, the measured density and the known heat capacity.

3.2.6 Surface Characteristics

The surface roughness and roundness measurements were made on three fuel pellets and on six samples of cladding. These measurements, taken both axially and circumferentially, were made on the cylindrical surface of the pellets and the inside surface of the cladding.

3.2.7 Dimensional Profilometry

After Halden assembled IFA-431, the fuel rods were dimensionally characterized at the Kjeller Hot Laboratory. Measurements were taken of the length, diameter and profile.

3.3 PRETEST PREDICTIONS

Pretest predictions for IFA-431 were made with GAPCON-THERMAL-2[5] and FRAP-S[6] codes. The major difference in the input to these codes was the lack in FRAP-S of a xenon fill gas option and a fuel densification model. These predictions are shown in Figures 3.4 to 3.9.

A schematic view of the planned HBWR core loading as of November 1975 is shown in Figure 3.10. IFA-431 was irradiated in channel 6-14, as shown. The assembly was charged into the bottom half of the core.

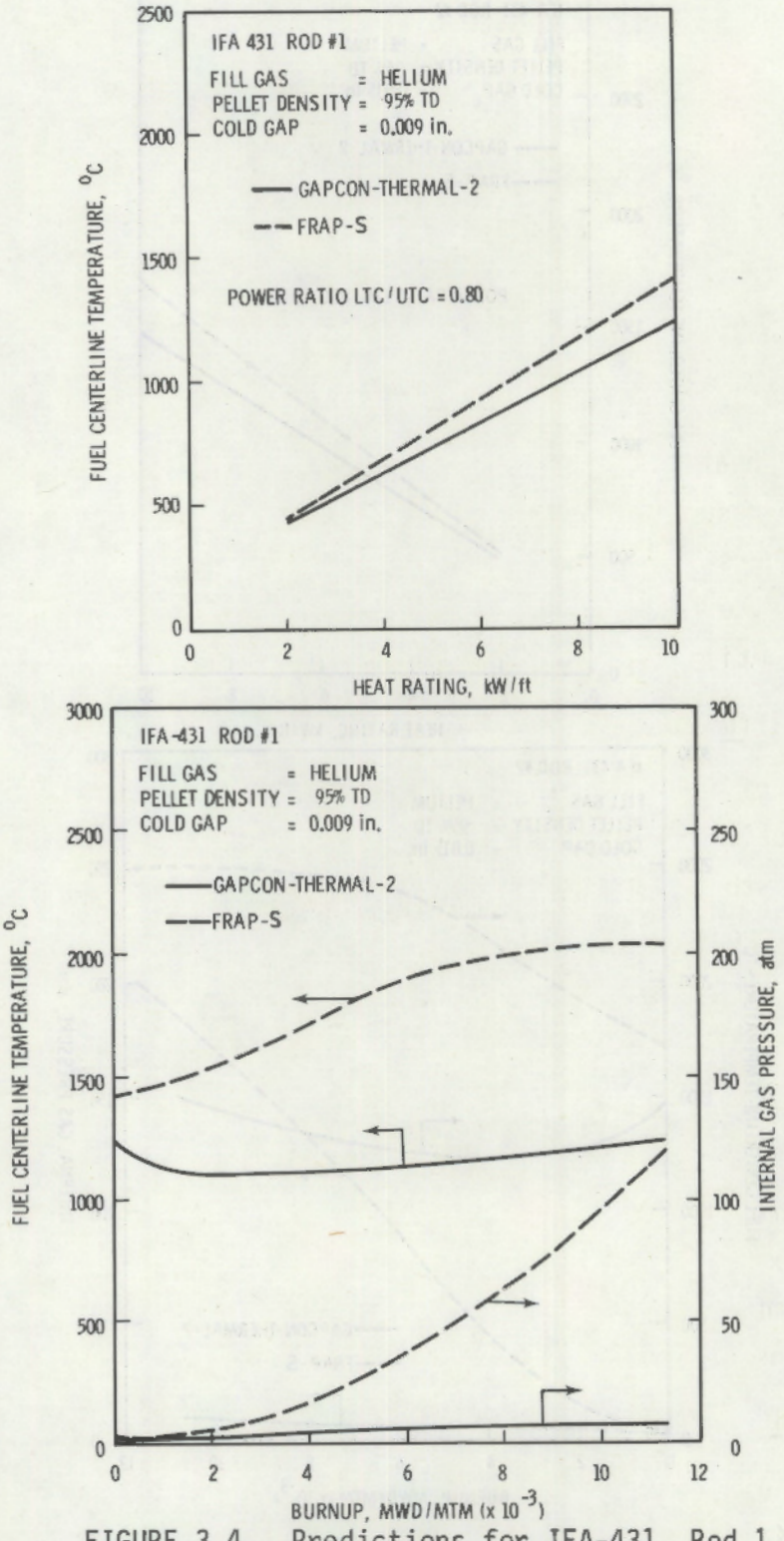

FIGURE 3.4. Predictions for IFA-431, Rod 1 (100% He, 95% TD-S UO_2, 0.022⁹ cm cold gap)

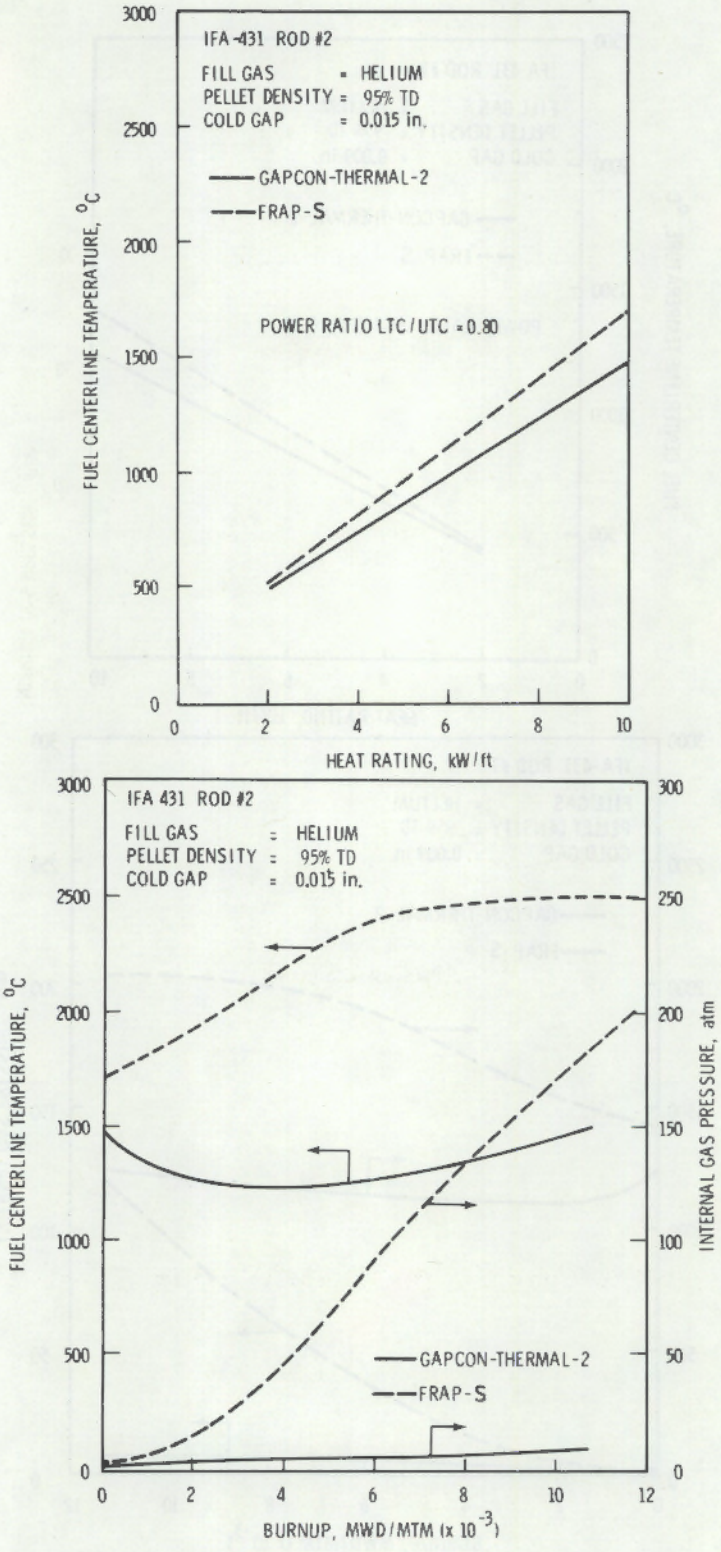

FIGURE 3.5. Predictions for IFA-431, Rod 2 (100% He, 95% TD-S UO_2, 0.0381 cm cold gap)

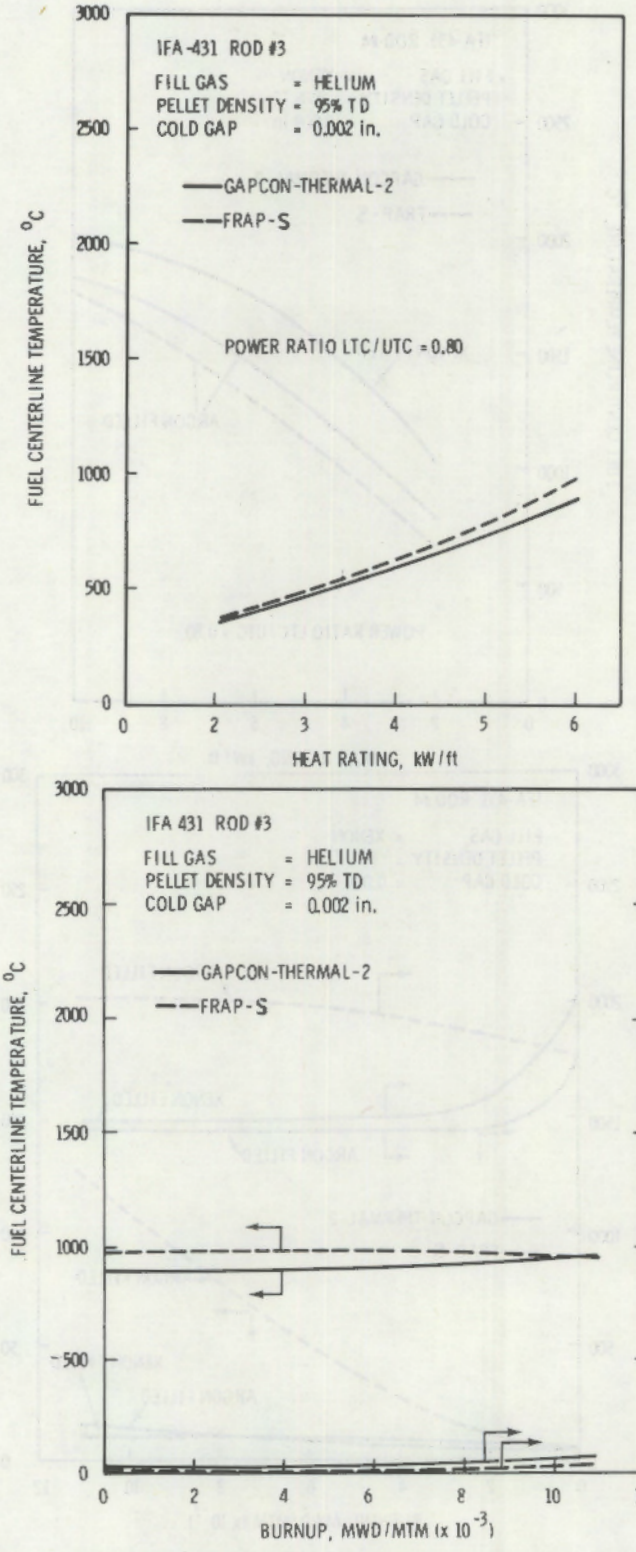

FIGURE 3.6. Predictions for IFA-431, Rod 3 (100% He, 95% TD-S UO_2, 0.0051 cm cold gap)

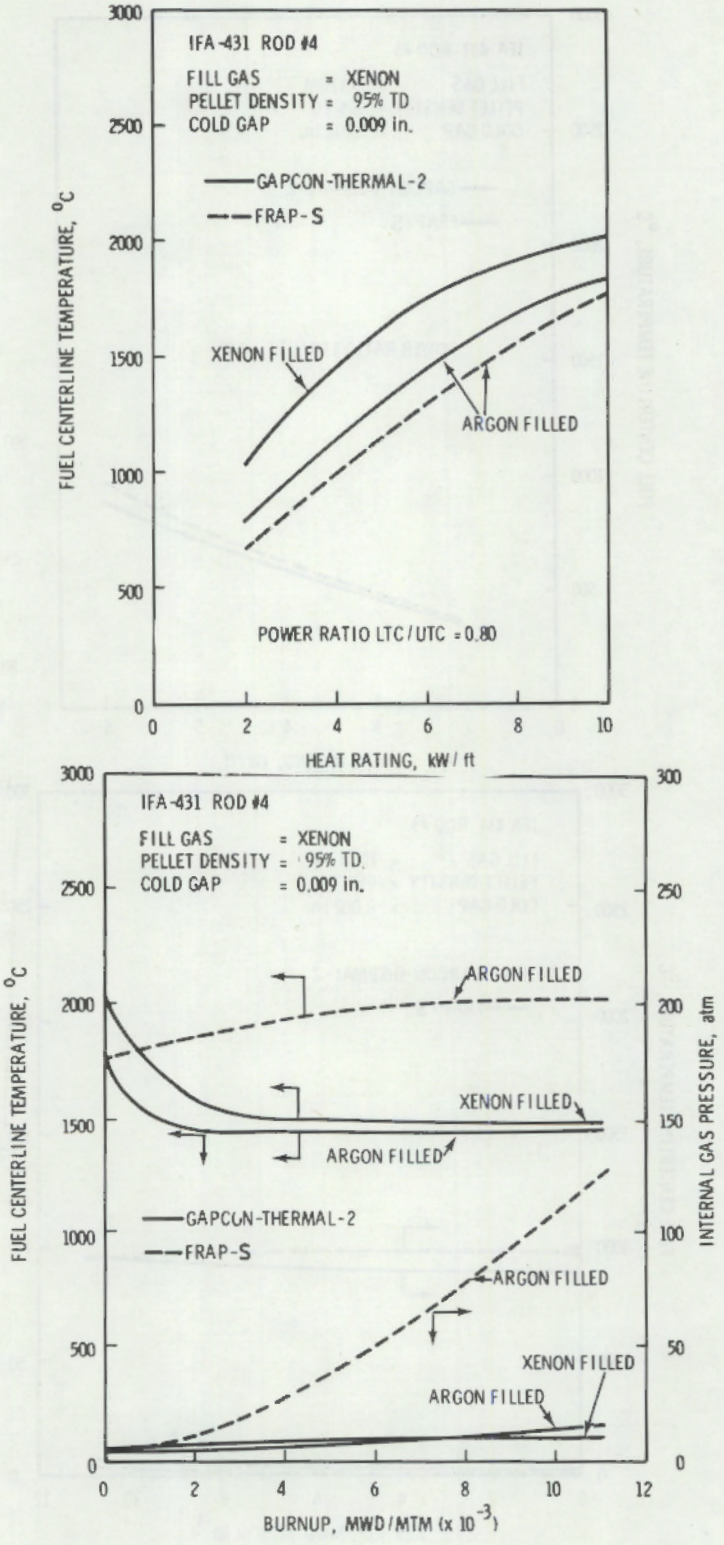

FIGURE 3.7. Predictions for IFA-431, Rod 4 (100% Xe, 95% TD-S UO_2, 0.0229 cm cold gap)

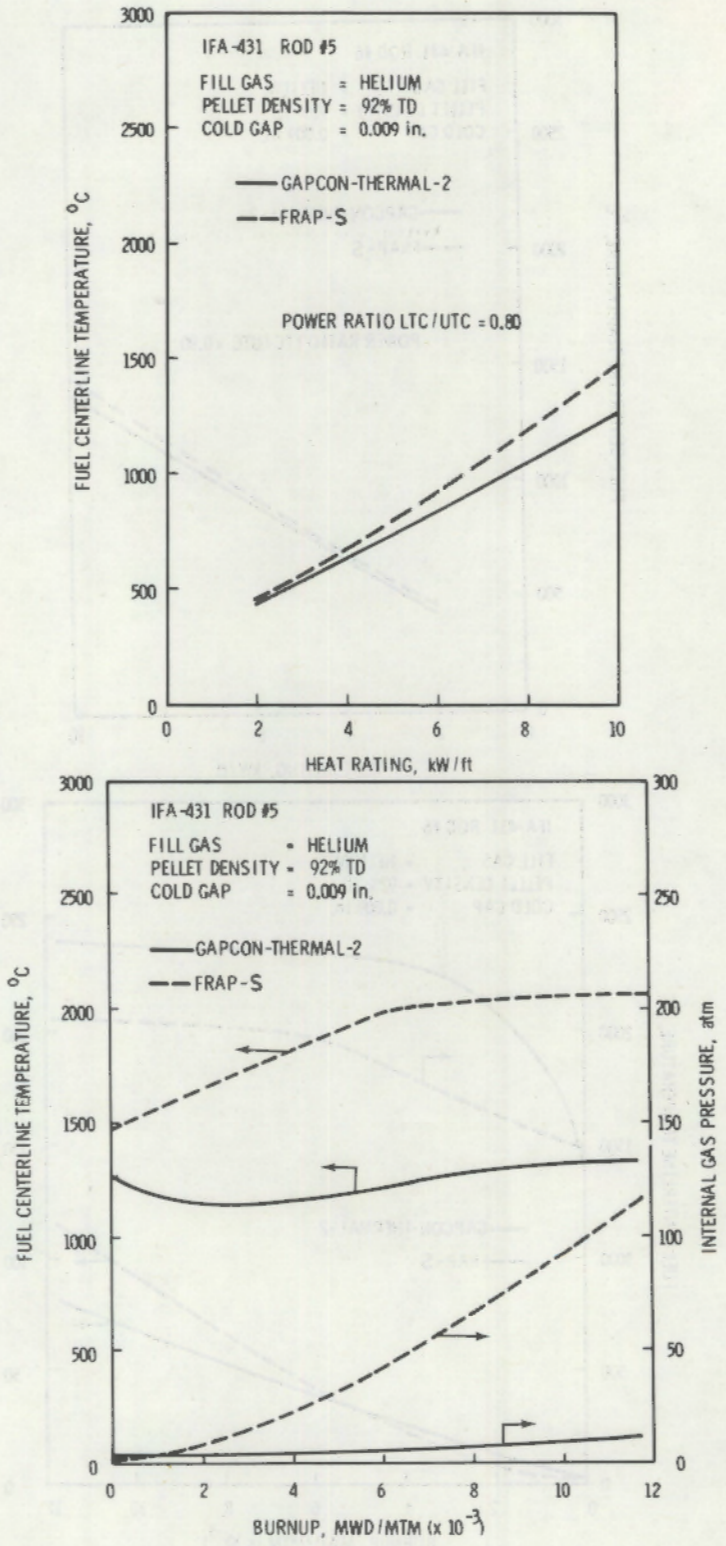

FIGURE 3.8. Predictions for IFA-431, Rod 5 (100% He, 92% TD-S UO_2, 0.0229 cm cold gap)

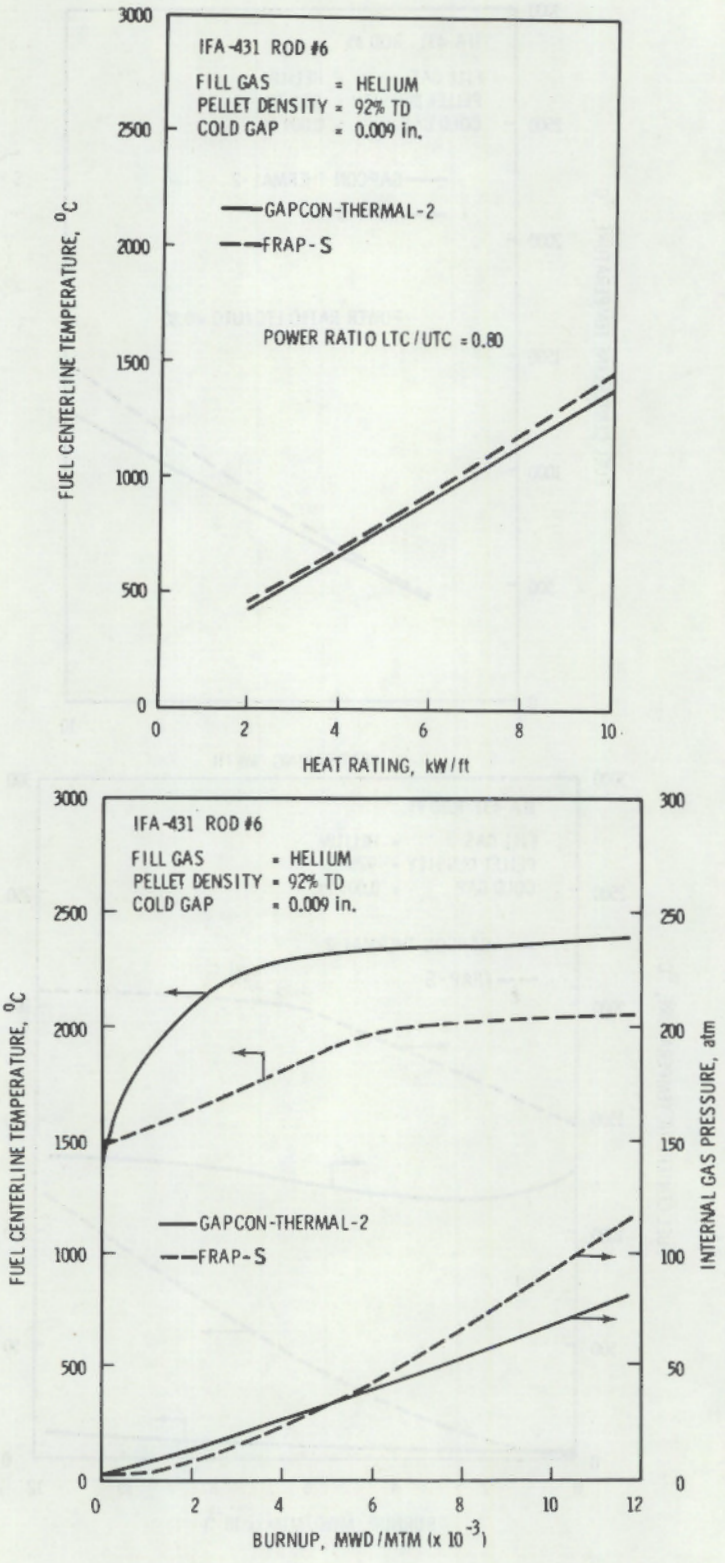

FIGURE 3.9. Predictions for IFA-431, Rod 6 (100% He, 92% TD-U UO_2, 0.0229 cm cold gap)

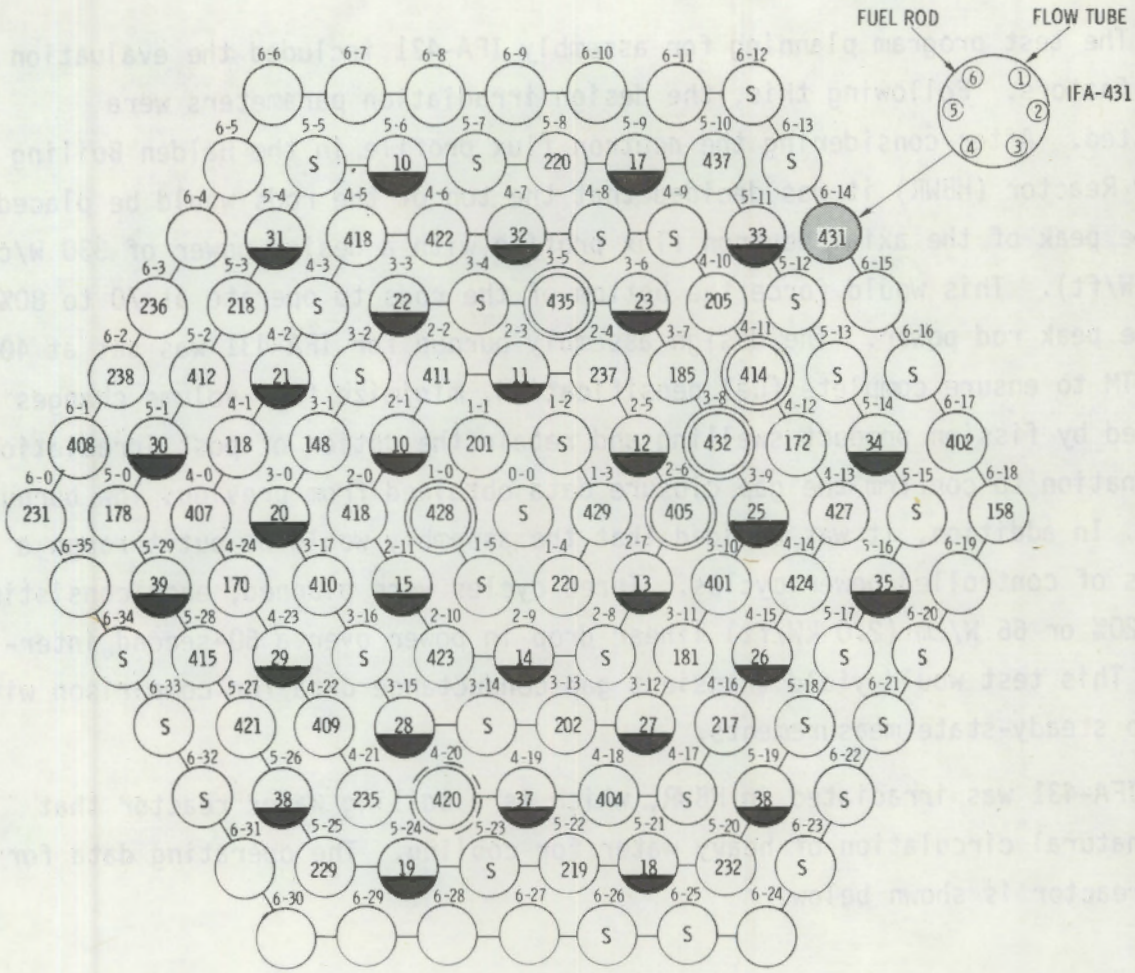

FIGURE 3.10. IFA-431 Arrangement in the HBWR Core

3.4 IRRADIATION HISTORY

The test program planning for assembly IFA-431 included the evaluation of many factors. Following this, the design irradiation parameters were selected. After considering the neutron flux profile in the Halden Boiling Water Reactor (HBWR) it was decided that the top of the rods would be placed at the peak of the axial neutron flux profile with a design power of 330 W/cm (10 kW/ft). This would force the bottom of the rods to operate at 70 to 80% of the peak rod power. The design assembly burnup for IFA-431 was set at 4000 MWd/MTM to ensure complete fuel densification, minimize fuel volume changes induced by fission product swelling and retain the option of post irradiation examination to confirm the gap closure data obtained from previous low burnup rods. In addition, it was decided that the assembly would be put through a series of controlled power cycles. Three cycles were planned, each consisting of a 20% or 66 W/cm (2.0 kW/ft) linear drop in power over a 60-second interval. This test would yield transient gap conductance data for comparison with pseudo steady-state measurements.

IFA-431 was irradiated in HBWR, which is a boiling water reactor that uses natural circulation of heavy water for cooling. The operating data for this reactor is shown below.

Power Level	12 MW
Reactor Pressure	3.4 MPa (500 psi)
Heavy Water Saturation Temperature	240°C (464°F)
Plenum Inlet Temperature	237°C (459°F)
Thermal Flux	$\sim 3 \times 10^{13}$ n/cm^2-sec
Fast Flux (>1 MeV)	$\sim 5 \times 10^{11}$ n/cm^2-sec
Average Fuel Power Density	14.8 W/g

The irradiation of assembly IFA-431 lasted from June 1975 to February 1976 and a burnup of 4300 MWd/MTM was achieved. There were no indications of fuel failure or other unusual occurrences during this period. Actual power and

fuel temperature histories are shown in Appendix A and Appendix B, respectively. The data for these plots was obtained by the Halden IBM/1800 on-line computer data acquisition system. Data densities (versus time) in these plots vary from 15 minutes to 12 hours, depending on whether the reactor was experiencing transient (startup, power cycling, etc.) or steady-state conditions.

4.0 NONDESTRUCTIVE MEASUREMENTS

IFA-431 was discharged to the Halden fuel pool for cooling following irradiation. After 123 days, the assembly was transported to the Kjeller Hot Lab where it was disassembled and underwent nondestructive examination that included visual examination, gamma scanning, dimensional profilometry and gap measurements.

4.1 TEST BUNDLE DISASSEMBLY

Part of the shroud tube was removed while the assembly was at Halden, and the instrument cables were isolated by sealing the ends in a cup with two component resin. When the assembly arrived at Kjeller, the shroud tube was completely removed, then the upper and lower parts of the assembly were removed, and finally the rods were removed from the bundle.[7]

To remove the rods, the bundle was suspended in two rope loops from the power manipulator and the cell crane. A clip holding each rod in the upper grid plate was removed first. Then the two thermocouple cables were cut and the fuel rod was drawn out of the bundle from the bottom. Immediately after removal of the fuel rod, the ends of the thermocouples were sealed separately by putting them into prepared perspex cups with Hysol two-component resin. These thermocouple wires were coiled to facilitate handling and shipping. Finally the rods were placed in a corrugated tray and photographed.

4.2 VISUAL EXAMINATION

For the detailed visual inspection, each rod was placed on a movable table for inspection under the fixed through-wall periscope. The surface of each rod was systematically scanned at four different angular orientations. The 0^{o} orientation was obtained by placing an axial groove that had been engraved into the upper end cap out towards the objective lens of the periscope. The 90^{o} orientation was obtained by rotating the rod clockwise through 90^{o} (when looking at the top end).

Visual inspection of all six IFA-431 rods revealed no cracks, blisters or corroded welds. No regular pattern of circumferential discolorations, indicating pellet-to-pellet interfaces, was seen. However, two small crud particles were observed at the 90^{o} orientation on rod 1, 415 mm above the lower weld. On rod 2 at the 110^{o} orientation there was an axial scratch running the whole length of the fuel rod. From the dull appearance of this scratch, it was concluded that it occurred before irradiation. There was a slight outward bulge of the cladding on rod 3 just below the sealing weld of the upper end cap. There were also two discolorations at 540 mm at the 90^{o} orientation on rod 3. Besides these minor irregularities, no indications of irradiation damage were found during visual inspection.

4.3 GAMMA SCANNING

All six IFA-431 fuel rods were gamma scanned, using a germanium/lithium detector. The first step in the gamma scanning process was to determine the fission product that produced the greatest activity. To accomplish this, the gamma spectrum for rod 1 was recorded at the lower end of the fuel stack (for results, see Figure C-1 in Appendix C). This was performed with a Kevex Model 5000A, 1024 channel analyzer. Because of the assembly's short irradiation and the long cooling time, the Zr 95/Nb 95 dominated with an effective half life of 65 days. Thus, two energy windows for the gamma scanning were chosen: channel A with 584 to 775 keV (gross gamma scan) and channel B with 752 to 777 keV (double peak of Zr 95/Nb 95). This was accomplished by adjusting the lower and upper discrimination levels of the two independent, single-channel pulse height analyzers.

The gamma scan of the fuel rods was performed with the fuel rods resting on a horizontal support that was moved with a stepping motor. Each fuel rod had a scribe mark indicating the edge of the rod that faced the outer edge of the assembly. During gamma scan, this scribe mark was turned toward the collimator, which eliminated differences from transverse activity gradients (flux depression in the bundle) and from self-shielding by the fuel. Scanning was

begun 50 mm below the lower end of the bottom enriched pellet at a speed of 0.5 mm/sec.

The pulses in the two energy channels were counted by two 4-decade scalers. For every 0.1 mm of axial movement, the number of pulses accumulated and the exact axial positions were recorded on magnetic tape. Off-line processing was done by a computer; the tables and curves of the results are shown in Appendix C. Two curves were plotted for each fuel rod: one for channel A (gross gamma) and one for channel B (Zr 95/Nb 95). However, the low count rate for channel B resulted in a rather large statistical error that is shown on these curves. The plots also show a smooth curve that was determined by a least-squares fit method. In addition, two different values for average count rate, one including the end pellets and one excluding the end pellets, are shown on each plot.

The curves show an activity distribution that reflects normal power distribution for the HBWR core height. No pellet-to-pellet interface effects were seen since the pellets were not dished. However, rod 4 showed some pellet separation near the upper and lower end.[8] End peaking, which occurs near the ends of the enriched stack was slight due to the presence of the poisoned end pellets. Table 4.1 shows condensed results of the gamma scan.

TABLE 4.1. Condensed Results from Gamma Scanning for IFA-431

Measured Results	Energy Channel	Pin Number 1	3	3	4	5	6
Stack Length (incl. end pellets, mm)	A	600.6	594.0	601.8	593.4	597.9	596.1
	B	600.0	594.3	600.9	594.9	597.3	596.4
Stack Length (excl. end pellets, mm)	A	575.7	576.0	582.6	570.0	580.2	570.6
	B	575.1	575.7	582.9	568.8	579.9	570.6
Axial Form Factor (AFF 2 - mean-to-average ratio)	A	1.10	1.10	1.11	1.09	1.10	1.10
	B	1.04	1.04	1.04	1.05	1.04	1.05
Average Count Rate (MEAN 2)	A	6302	6487	6675	6379	6272	6120
	B	1224	1234	1236	1226	1225	1211
Radial Form Factor (rod-to-average ratio)	A	0.989	1.018	1.047	1.001	0.984	0.961
	B	0.999	1.007	1.008	1.000	0.998	0.988

The stack length values, which were determined by the computer program searching for the end discontinuities in the data curve, are not very accurate. Therefore, a better method for determining this stack length was developed. This method involved the single-step movement of the fuel rod, and the observation of the count rate changes near the ends of the enriched stack. Readings from the scaler displayed the axial position of the rod (in units of 0.01 mm). By repeated upward and downward stepping, the enriched stack position, and thus the stack length, was determined to an accuracy of 0.3 mm. The results of this analysis are shown in Table 4.2.

TABLE 4.2. Stack Length Change Determined from Gamma Scanning

Rod No.	Stack Length, mm Initial	Final	Change mm[a]	Percent[b]
1	574.4	573.8	-0.6	-0.10
2	574.6	574.7	+0.1	+0.02
3	580.6	581.8	+1.2	+0.21
4	566.1	568.2	+2.1	+0.37
5	579.1	578.9	-0.2	-0.03
6	575.9	569.4	-6.5	-1.13

(a) The length change was calculated by subtracting the initial length from the final length.
(b) The percentage of length change was calculated by dividing the length change by the initial length and multiplying by 100.

4.4 PROFILOMETRY

Profilometry was performed on a vertical bench with two measurements taken 90^{o} apart on each fuel rod. The rods were inserted in the bench with the bottom end down and the engraved fuel rod number towards the transducer that gave the profile signal. This 0^{o} orientation is not the same as the orientation used in the visual examination or gamma scanning, but it is the same as was used during pre-irradiation profilometry. The 90^{o} orientation was obtained by looking down from the top end and rotating the rod clockwise.

The profile measuring device consisted of two knife edges formed by 2-mm diameter polished sapphire rods. These knives were mounted on slides and drawn into contact with the fuel rod surface by two springs. One slide was fixed to the core while a linear variable displacement transducer (LVDT) was connected to the other slide. This measured the distance between the two slides and, thus, the fuel rod diameter. A second LVDT measured the position of the right hand slide relative to the bench, and this produced the profile signal.

The movement of the transducer along the length of the rod was accomplished by a stepping motor with a step of 0.01 mm. Values for the axial position diameter signal and the profile signal were recorded digitally on magnetic tape every 10th step (0.1 mm). This profile data was processed off line by a CDC-Cyber computer and the results are shown in Appendix D.

4.5 LENGTH MEASUREMENT

Length measurements were performed while the fuel rods were on the profilometry bench by using the V-grooves that had been machined into both end caps. The exact location of these grooves was determined by manually stepping the bench and monitoring a profile digital voltmeter for a minimum reading. Thus, the rod length was determined to an accuracy of $\pm$ 0.01 mm. Two measurements each were taken at the 0^{o} and 90^{o} orientation.

The length measurements were corrected for the slightly higher cladding temperature that occurs as a result of residual gamma heating of the fuel rod. In addition, the length measurements made at 0^{o} and 90^{o} were averaged. The results obtained after these corrections are shown in Table 4.3.

4.6 GAP MEASUREMENT

Figure 4.1 is a schematic diagram of the Kjeller equipment for residual gap measurement. A 15-mm long rectangular lever applies a line force over its length along two opposite edges of the fuel rod, which rests on a flat support. The force necessary to reshape the rod as an oval is generated by a pneumatic cylinder acting on the end of the lever, and the force is measured by a transducer incorporated in the lever. Displacement of the clad surface

TABLE 4.3. Corrected and Reduced Length Measurement

Rod No.	V-Groove Distance, mm Initial	Final	Elongation mm	Percent(a)
1	645.68	645.92	0.24	0.04
2	645.36	645.53	0.17	0.03
3	645.58	645.83	0.25	0.04
4	645.48	645.87	0.39	0.06
5	645.62	645.80	0.18	0.03
6	645.60	645.76	0.16	0.02

(a) The percentage of elongation was calculated by dividing the elongation by the initial distance and multiplying by 100.

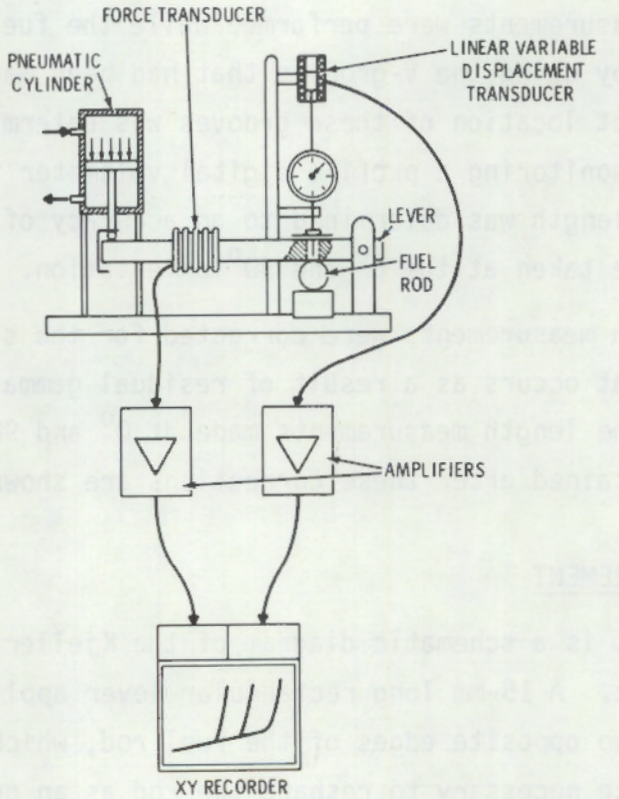

FIGURE 4.1. Schematic Diagram of Gap Measurement Equipment

is measured by a linear variable displacement transducer, which touches the fuel rod through a hole in the lever. A dial gauge provides a small contact force and the capability of calibrating the displacement signal. The signals from the two transducers are fed to the measuring bridges/amplifiers and from there to an XY recorder.

Initial experiments were performed on an open tube section, approximately 150 mm long, into which steel mandrels of different diameters were inserted. A typical XY-plot obtained with the Kjeller equipment is shown in Figure 4.2. The straight part of the curve corresponds to the elastic behavior of the empty tube. Interaction with the mandrel starts where the curve begins to deviate from a straight line. The curves are evaluated by projecting the "zero force point" and the "interaction force point" down onto the abscissa and directly reading the gap in microns. There was very good agreement between the gap values found in this way and the predicted gap values.

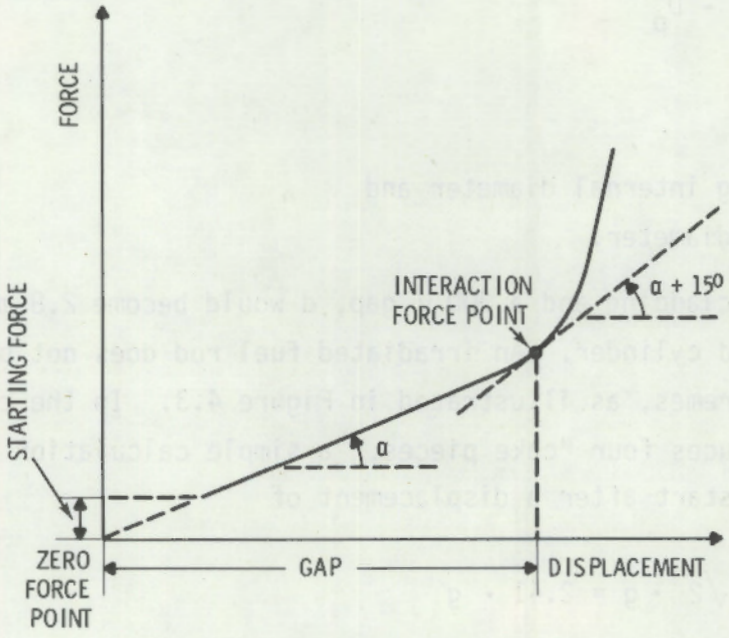

FIGURE 4.2. Evaluation of Force-Displacement Curves for Gap Measurement

An irradiated fuel rod containing cracked fuel pellets will behave differently than a tube with a solid cylinder inside. Depending on the crack pattern, the fuel will more easily follow the oval shape of the cladding than would the solid cylinder. The solid cylinder represents one extreme; the other extreme is represented by powder that is allowed to flow both transversely and longitudinally. This would not produce any interaction with the cladding at all, at least not as long as there is some open volume available. A more "realistic extreme" would be a powder with its longitudinal movement inhibited. In this case, interaction will occur as soon as the inner cross-sectional area of the tube has been reduced by pressure to the size of the cross-sectional area of the fuel. Assuming that the cladding retains an elliptical shape (true for small deformations) the displacement for interaction can be calculated to be

$$d = \sqrt{D_c^2 - D_p^2}$$

where

D_c = cladding internal diameter and

D_p = pellet diameter.

For a 12.9 mm ID cladding and a 300 μ gap, d would become 2.8 mm compared to 0.3 mm for a solid cylinder. An irradiated fuel rod does not behave like either of the extremes, as illustrated in Figure 4.3. In the case of a crack pattern that produces four "cake pieces," a simple calculation shows that interaction will start after a displacement of

$$d = g + \sqrt{2} \cdot g = 2.41 \cdot g$$

Calculations can be performed for a larger number of "cake pieces", however, they get more complicated as the number of pieces increases.

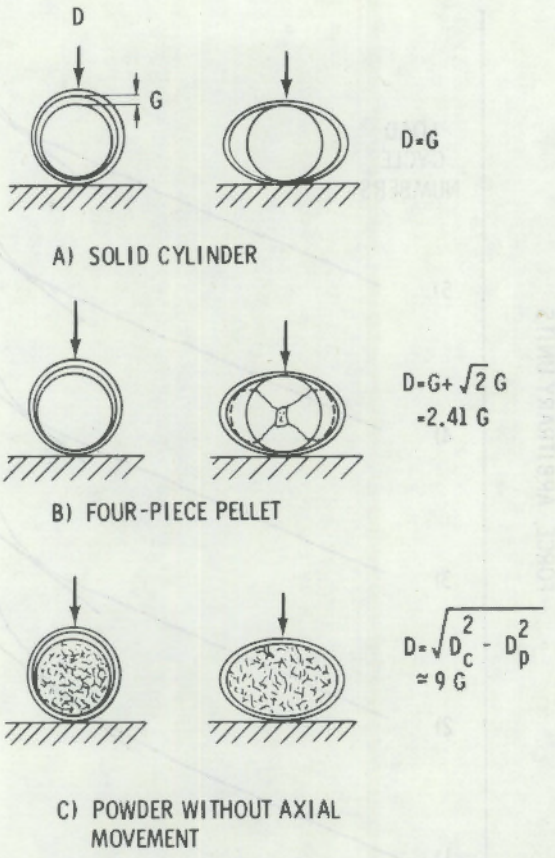

FIGURE 4.3. Radial Relocation of Fuel in Compression Test

The interaction curve of an irradiated fuel rod is shown in Figure 4.4 where five successive experiments, all performed at the same rod location (rod 5 at the 370 mm axial position) are reproduced (with some zero displacement in the force direction, in order to separate the curves). The first compression (curve 1) produced a rather rounded XY plot, with no clear transition point from empty-tube to filled-tube behavior. All the other curves are nearly identical. These curves also have a marked straight portion and an easy-to-determine transition point. The rounded shape of the first compression curve is believed to be caused by the crushing and/or displacement of very fine particles located in the gaps and cracks, and the unlocking of slip systems. Once this "conditioning" is accomplished, the rod behaves in a completely reversible, elastic way in the later tests.

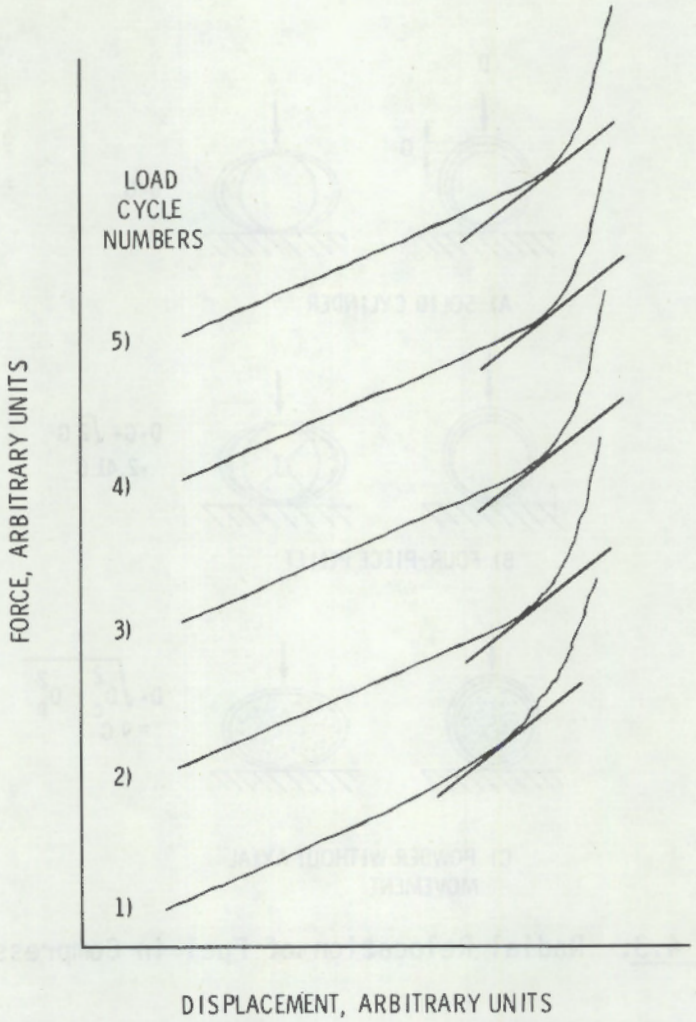

FIGUR E 4.4. Typical Force - Displacement Curves for Irradiated Fuel Rods

Gap measurements were performed on all six rods at eight different axial positions: 75, 112, 170, 270, 370, 470, 534 and 570 mm. These values correspond to the distance from a position on the lower end plug, 27 mm below the V-groove. This was chosen as zero because the gamma scans and profilometry started there. The positions at 112 mm and 534 mm coincide with the tips of the lower and upper thermocouples, respectively. The compressions were repeated five times at each location and the results are given in Table 4.4. The results are also plotted in Figure 4.5, which includes a schematic fuel rod drawing and the superimposed power profile from gamma scanning.

TABLE 4.4. Results of Gap Measurement (in Microns)

Axial Position, mm	Pin Number 1	2	3	4	5	6
75	195	347	-	72	202	288
112 (TC)	178	260	-	140	226	292
170	201	283	-	146	259	271
270	181	286	15	102	192	298
370	164	264	20	94	199	269
470	160	268	22	110	248	291
534 (TC)	195	309	24	109	247	277
570	198	309	31	108	230	284

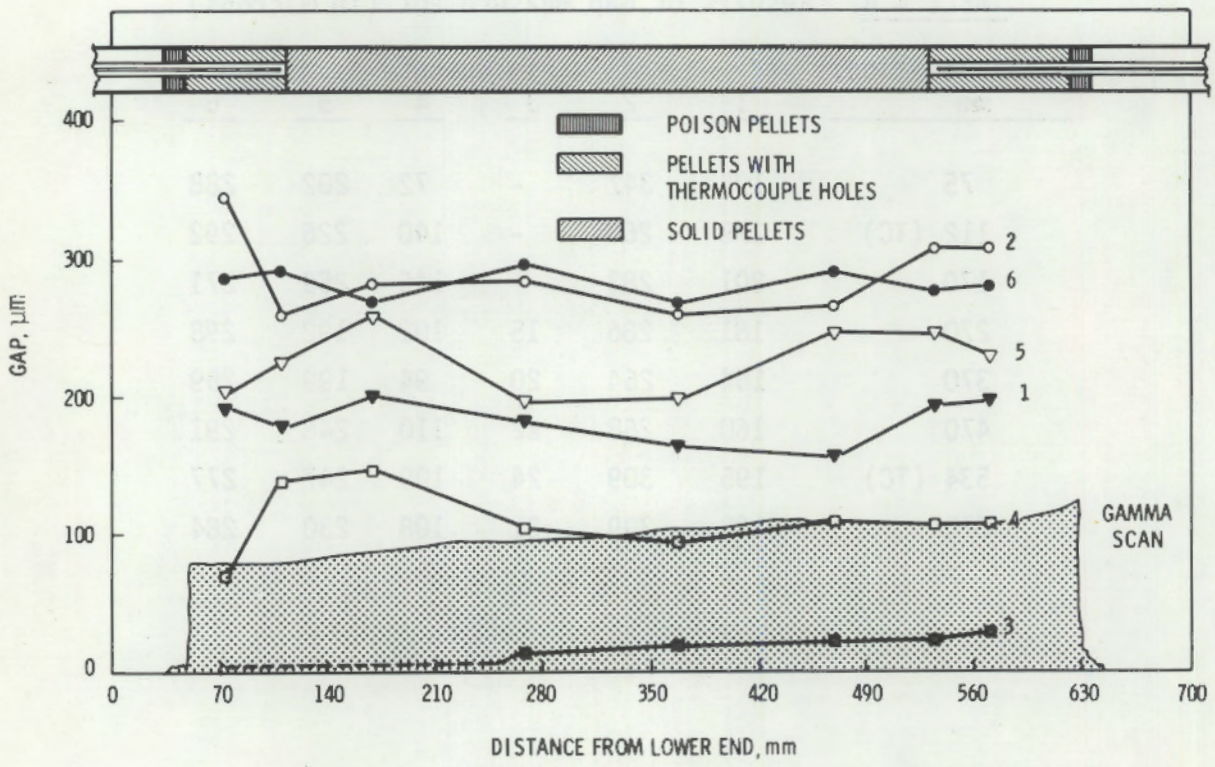

FIGURE 4.5. Gap Measurement Results for IFA-431

4.7 HARWELL GAMMA SCANNING FOR ROD 6

At this point, rod 6 was sent to Harwell for destructive examination. Before the destruction examination, Harwell gamma scanned the rod. For gamma scanning, the equipment consisted of a stepping motor-driven table, a shielded assembly with a collimator system, and a gamma ray detecting and analyzing system. The collimator used a germanium/lithium diode detector for gamma activity.

For rod 6, a large collimator (1.143 mm x 12.7 mm in size) was used for gamma scanning because of the low burnup and the long cooling period. The gamma activity, which resulted in the energy peaks, was due to Cs 137 and Zr 95/Nb 95, and is shown on page C-15.

The lengths of the fuel pellet stack and the overall stack, including top and bottom spacer pellets, were measured from the gamma scan. The results of these measurements are shown in Table 4.5. There was good agreement between the values obtained by the different gamma activities. In addition, the results are good when compared with the length measurements made in a similar way at Kjeller (Table 4.1).

TABLE 4.5. Fuel Stack Length Measurements from the Gamma Scans at Harwell

Isotope	Measured Lengths	Measurement Length in mm 1st Scan	2nd Scan	Mean
Cs 137	Total stack length (fuel + spacer pellets)	597.4	596.0	596.7
Cs 137	Fuel stack length	570.4	570.1	570.25
Zr 95/Nb 95	Total stack length (fuel + spacer pellets)	596.3	595.5	595.9
Zr 95/Nb 95	Fuel stack length	570.3	570.1	570.2

5.0 DESTRUCTIVE EXAMINATION

After nondestructive examination of the IFA-431 fuel rods, rod 6 was sent to Harwell where destructive examination began in 1977. The following is a summary of the examinations performed:

1. To find the fission gas release, the volume of gas in the fuel rod was measured and its composition was determined. The internal volume of the pin was measured to determine the amount of fuel densification that had occurred, and to calculate the gas pressure in the pin.
2. The rod was cut to provide samples for the other examinations.
3. The burnup of a section of UO_2 pellet from near the peak burnup position was determined. This, together with the gamma scan, was used to assess the burnup along the rod.
4. The bulk density of UO_2 pieces from two pellets close to the two metallographic solid pellet samples was measured to determine the amount of fuel densification.
5. Four sections of fuel rod were examined metallographically:
   a. One section was taken from the hot junction region of each of the thermocouples to determine the structure of the UO_2 in the region of the thermocouple.
   b. A solid section was taken from both high and low burnup regions in order to examine the fuel cross-section structure and pellet/ cladding geometry. After detailed optical microscopy, the finer pores of these two samples were examined with the scanning electron microscope (SEM).

   The metallographic analysis was extensive and provided a large number of photomicrographs for the quantitative assessment of pore structure. The same areas of the specimens that were examined with the optical microscope were also examined with the SEM.
6. Radial density variation across the two solid UO_2 pellet metallographic samples was determined in order to assess the densification as a function of radial position and fuel temperature.

5.1 FILL GAS AND INTERNAL VOLUME DETERMINATIONS

The equipment used to determine the fill gas and internal volume consisted of a puncturing head connected to the gas collecting and measuring equipment by stainless steel flexible vacuum pipe. The fuel rod was seated to the puncturing head through pressure on an "O" ring seal. The puncturing head was fitted with a 0 to 50 psi pressure transducer and a tungsten carbide-tipped tool. The gas measuring part of the system used a mercury booster (diffusion) pump and an automatic toepler pump to move the gas to a storage bulb where a transducer measured gas pressure.

The fuel rod was seated to the puncturing head and the complete system was evacuated and checked for leaks. After the dead volume of the equipment was determined, the fuel rod was punctured and the pressure in the puncturing head was measured. The released gas was pumped into a storage bulb and the pressure of the gas measured. Sample bottles of fuel rod gas were filled, sealed and sent for mass spectrometric analysis.

The internal volume of the rod was measured by filling the fuel rod and puncturing head with helium at atmospheric pressure and measuring the volume of the gas. The fuel rod internal volume was the difference between the measured volume and the dead volume. This process was completed five times, and the mean measured volume was 7.58 ml. The NTP ($0^{o}C$, 760 mm Hg) volume of gas recovered was 3.33 ml. Mass spectrometric analysis results are presented in Table 5.1, while Table 5.2 shows the isotopic composition of the fission gas.

TABLE 5.1. Results of Mass Spectrometric Analysis of 3 Samples of Gas from Rod 6 (given in volume percent)

Gas	Sample 1	Sample 2	Sample 3
Helium	85.2	84.3	83.7
Nitrogen/Carbon Monoxide[a]	9.48	10.0	10.3
Oxygen	0.08	0.57	0.69
Argon	0.57	0.56	0.57
Carbon Dioxide	<0.014	<0.024	0.13
Krypton	0.73	0.71	0.71
Xenon	3.91	3.80	3.87

(a) Nitrogen or carbon monoxide was not part of the fill gas in this rod, and could have come from the binder used in fuel fabrication.

TABLE 5.2. Isotopic Composition of Fission Gases in Three Gas Samples from Rod 6

Isotope	Composition in Volume Percent Sample 1	Sample 2	Sample 3
Kr 86	50.54	50.67	51.64
Kr 85	6.49	6.40	6.26
Kr 84	27.76	27.73	26.45
Kr 83	15.22	15.21	15.65
Xe 136	35.50	35.54	35.27
Xe 134	29.12	29.15	29.32
Xe 132	23.74	23.70	23.70
Xe 131	11.65	11.61	11.71

The value of the fission gas production rate was 0.249 cc of fission gas per gram of UO_2 per 1% burnup (neglecting Xe 135 Xe 137 neutron capture reactions at high fluxes). Thus, the volume of fission gas produced in the rod for a mean burnup of 0.49% was calculated as 62.9 ml at NTP. This yields a release of stable fission gasses of 0.25%.

5.2 FUEL ROD CUTTING

Before cutting fuel samples, the 0^{o} orientation from the top of the fuel rod was scribed down the entire fuel rod length. The cutting positions were determined from the gamma scan trace, and transverse cuts were made.

Cutting of the samples was difficult. First, a cut was made through the plenum at the top of the fuel rod. Epoxy resin was used to seal the end of the fuel rod. The next cut was made through the fuel just below the upper thermocouple hot junction (pellet 9 region). At this point, a cut was made below pellet 10. However, the UO_2 began falling out of the rod during the cutting process. Since burnup and bulk density samples must be resin free, resin impregnation could not be done to hold pellet 10 together, and therefore, a new cut was made. By carefully cutting in the region of pellets 11 and 12, samples from pellet 12 were obtained for burnup analysis and samples from pellets 11 and 12 were obtained for bulk density measurement. Care was

also taken to prepare pellet 14 for radial gamma scanning. In spite of this, some pieces of UO_2 fell out of the fuel cladding. A spare section from the region of pellets 14 and 15 was therefore substituted.

A summary of the samples taken from fuel rod 6 is given in Table 5.3.

TABLE 5.3. List of Samples Cut from Rod 6

Pellet No.	Use	Metallographic Mount Identity
8-9	Top thermocouple hot junction-for metallographic examination	ACF
11-12	Bulk density	
12	Bulk burnup	
13	Metallographic examination	ACI
14	Study of burnup profile	ACE
14-15	Spare sample - but actually used for burnup profile because large piece of UO_2 was missing from ACE; pellet 14	ACJ
15	Spare sample	
37	Spare sample	
38	Spare sample	
39	Metallographic examination	ACH
40	Bulk burnup	
42	Bottom thermocouple hot junction for metallographic examination	ACD

5.3 BURNUP ANALYSIS

Part of pellet 12 was analyzed chemically for burnup, using the procedures outlined by Fudge and Foster.[9] Isotopic compositions of uranium, plutonium and neodymium were determined as well as the Pu:U and Nd 148:U weight ratios. The results are shown in Table 5.4 with an accuracy of ± one standard deviation. These results are reported as the percentage ratio of total number of atoms fissioned to the initial total number of uranium atoms.

TABLE 5.4. Results of Bulk Burnup Analysis from a Section of Pellet 12 from Rod 6[a]

Isotopic Composition	Presence of Isotope, %
U 234	0.05 ± 0.01
U 235[b]	9.62 ± 0.03
U 236	0.21 ± 0.01
U 238	90.11 ± 0.01
Pu 238	0.02 ± 0.01
Pu 239	0.02 ± 0.01
Pu 240	96.92 ± 0.07
Pu 241	0.16 ± 0.01
Pu 242	0.01 ± 0.01
Nd 142	0.05 ± 0.01
Nd 143	29.71 ± 0.08
Nd 144	24.19 ± 0.05
Nd 145	19.46 ± 0.05
Nd 146	14.95 ± 0.03
Nd 148[c]	8.37 ± 0.02
Nd 150	3.27 ± 0.01
Pu/U ratio by weight	0.000591 ± 0.000006
Nd 148/U ratio by weight	0.0000574 ± 0.0000006
Atom percent burnup by Nd 148	0.55 ± 0.01[d]

(a) The errors quoted are one-sigma standard deviations.
(b) Initial U 235 content was 10 wt%.
(c) The fission yield value for Nd 148 used in the calculations was 1.68%.
(d) In fissions/U atom. Calculated, thusly:

$$\text{Fissions/U atom}(\%) = 100 \left(\frac{\text{Nd at.}}{\text{U at.}}\right) \div \left(\frac{\text{Nd at.}}{\text{fission}}\right) = \left(\frac{238}{148} \times 5.74 \times 10^{-5} \quad 0.0168\right) \times 100$$

$$= 0.55\%$$

Burnup along the length of the fuel rod was estimated from a Zr 95/Nb 95 gamma scan trace and the bulk burnup of pellet 12. These results are presented in Table 5.5.

TABLE 5.5. Burnup Along Rod 6 Estimated from the Gamma Scan and Bulk Burnup Measurement

Pellet Number	Burnup (atom percent of total fissions to initial total number of uranium atoms)
4	0.56
8	0.55
12	0.55
16	0.54
20	0.52
24	0.52
28	0.50
32	0.47
36	0.46
40	0.41
44	0.39

5.4 BULK UO_2 DENSITY MEASUREMENT

The bulk density of the UO_2 was measured on several pieces of pellets 11 and 12, and on several pieces of pellet 40 that were removed from the zircaloy cladding. Since the UO_2 fuel was badly broken up, a number of the largest samples were used for the density measurements.

The density of each sample was determined by weighing in air and then weighing when submerged in carbon tetrachloride. The carbon tetrachloride density was corrected for temperature. Results of these measurements are presented in Table 5.6.

TABLE 5.6. Bulk Densities of UO_2 Pellet Pieces

Pellet Number	Number of Sample Pieces	Density g/cm^3 (1)	(2)	(3)	(4)	Mean
11-12	1	10.469	10.490	10.473	-	10.477
11-12	1	10.628	10.553	10.562	-	10.581
11-12	4	10.537	10.536	10.644	10.642	10.590
						10.549 (average)
40	6	10.592	10.590	10.589		10.590

5.5 METALLOGRAPHIC EXAMINATION

Four samples from the fuel rod were prepared for metallographic examination. Each of these samples, which had been impregnated with resin during the cutting process to keep the pieces in place, were mounted with the prepared surface being the surface that was toward the top of the fuel rod during irradiation. These sections were ground with 320-grade silicon carbide abrasive papers until a full UO_2 pellet cross section was observed. At this stage the pellets were reimpregnated with resin and the resin was allowed to harden. Then, the samples were ground on 600-grade silicon carbide paper. Following lapping with 14 μm diamond compound, each specimen was polished with 6 μm, 3 μm and then 1 μm diamond powder on rotary machines. Then the samples were attack polished with 2% Cr_2O_3 (by weight) in water with gamma grade alumina polishing agent.

After polishing and cleaning, the samples were photographed at 8x. The microstructure of the samples was examined in a remote optical microscope. Then four diameters were drawn at 45-degree intervals on a photomacrograph of each cross section. Each radius was numbered from one to eight. On each radius, locations were marked near the outer surface and at midradius, and on four of the radii additional locations were marked near the center of the pellet. These were the areas picked for photomicrographs to allow quantitative metallographic analysis.

At each site on each specimen, photomicrographs were taken at 125x and 650x. Overlapping photomicrographs at 50x were also taken to cover the whole area of the two solid pellet samples (pellets 13 and 39). A series of overlapping photomicrographs along one radius of the two thermocouple samples was taken at 63x.

Each sample was then lightly etched with a 10% H_2SO_4 and 90% H_2O_2 mixture diluted with water. The etching time was selected just to delineate the UO_2 grain boundaries and prevent pore enlargement if the sample over-etched. Some of the locations examined before etching were rephotographed at 650x.

The polished and etched surfaces of the two samples without thermocouple holes were examined in a scanning electron microscope (SEM) at magnifications up to 10,000x. On each section, nine of the twenty sites that had been photographed with the optical microscope were examined and photographed at 120x, 600x, 3000x, and two of the twenty sites were examined and photographed at 6000x and 10,000x. This was done to enable comparison of the SEM and the optical micrographs. Four locations at the outer edge, three at midradius, and two at the pellet center were also examined.

This procedure was adopted to obtain photographs for a detailed quantitative assessment of the pore structure as a function of pellet radius (UO_2 temperature) and to show the variation along the length of the fuel rod. Because pore-size measurments were to be made, the magnifications of all the optical micrographs were calibrated by photographing a stage micrometer at each magnification used. Also, each of the magnifications of the scanning electron microscope were calibrated by photographing a standard mesh of known pitch.

A detailed analysis of the metallographic results will be presented in another report. Some micrographs are shown here as representative structures. Figure 5.1 is the total polished cross section of pellet 13, the optical photomicrographs of pellet 13 are presented in Figure 5.2, and Figure 5.3 is the scanning electron micrographs of pellet 13.

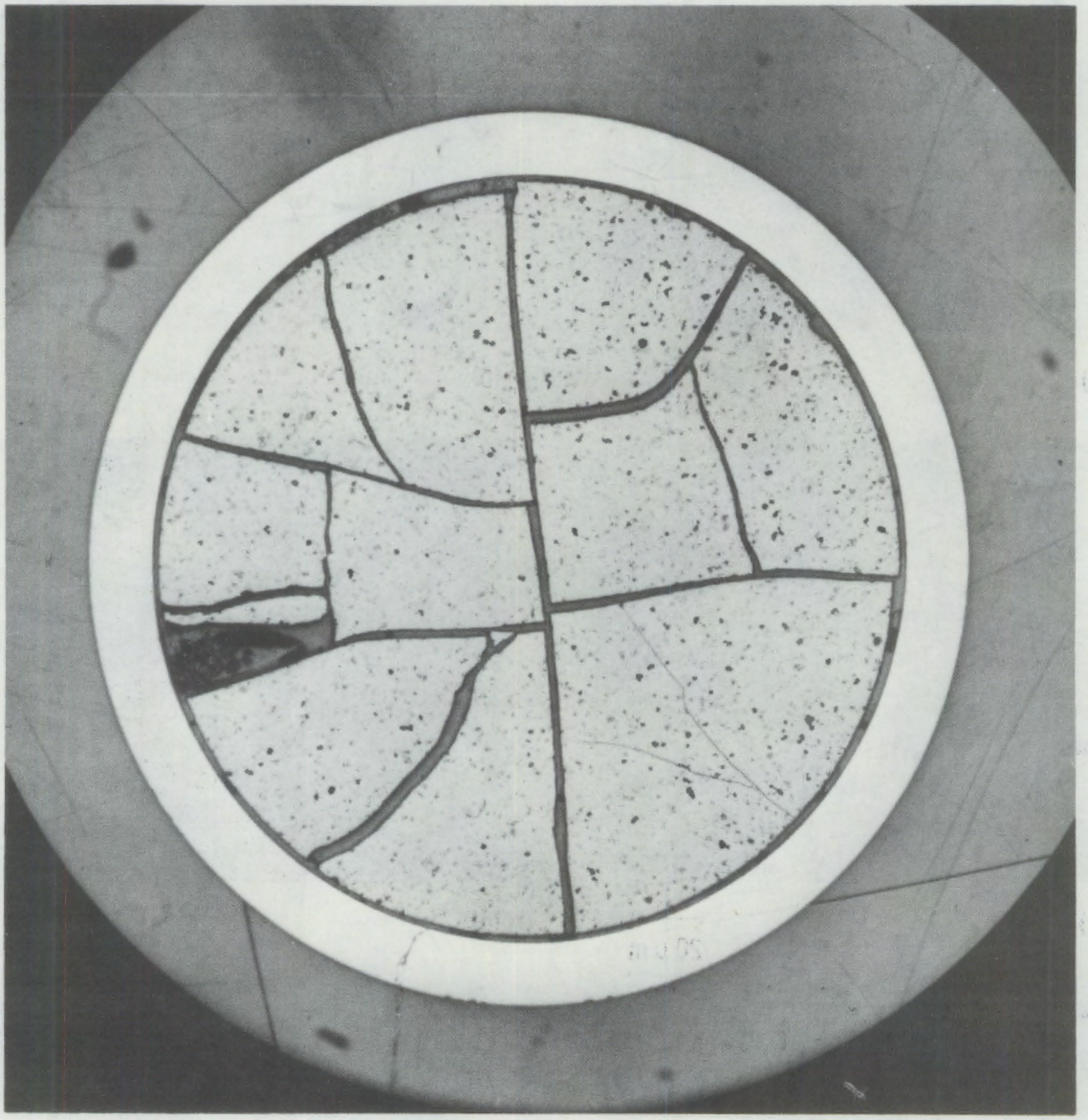

FIGURE 5.1 Polished Cross Section of Pellet 13.

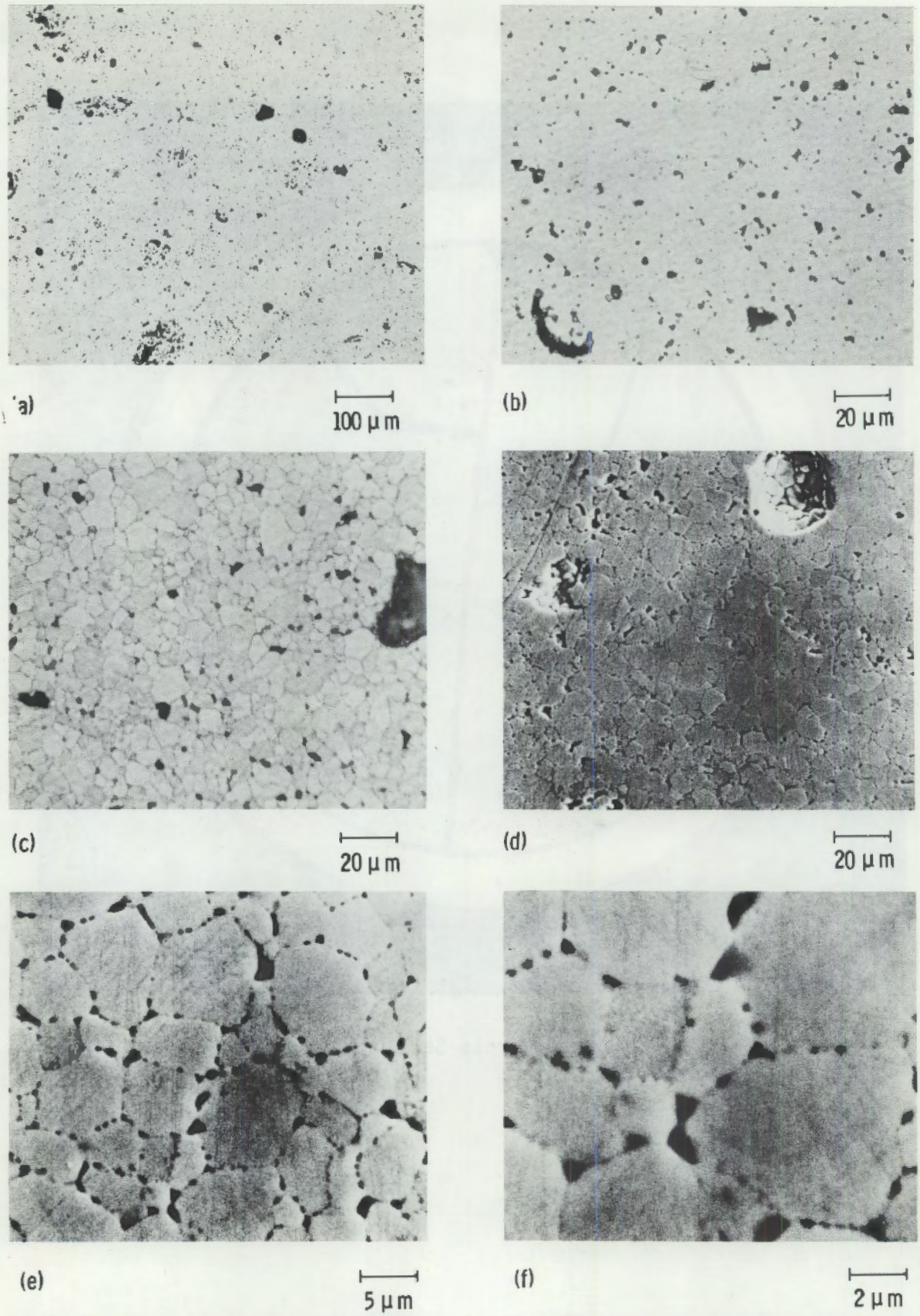

FIGURE 5.2. Optical Photomicrographs of Archive UO_2 Pellet of Type Used in Rod 6: (1) to (5) Unetched, (6) Etched

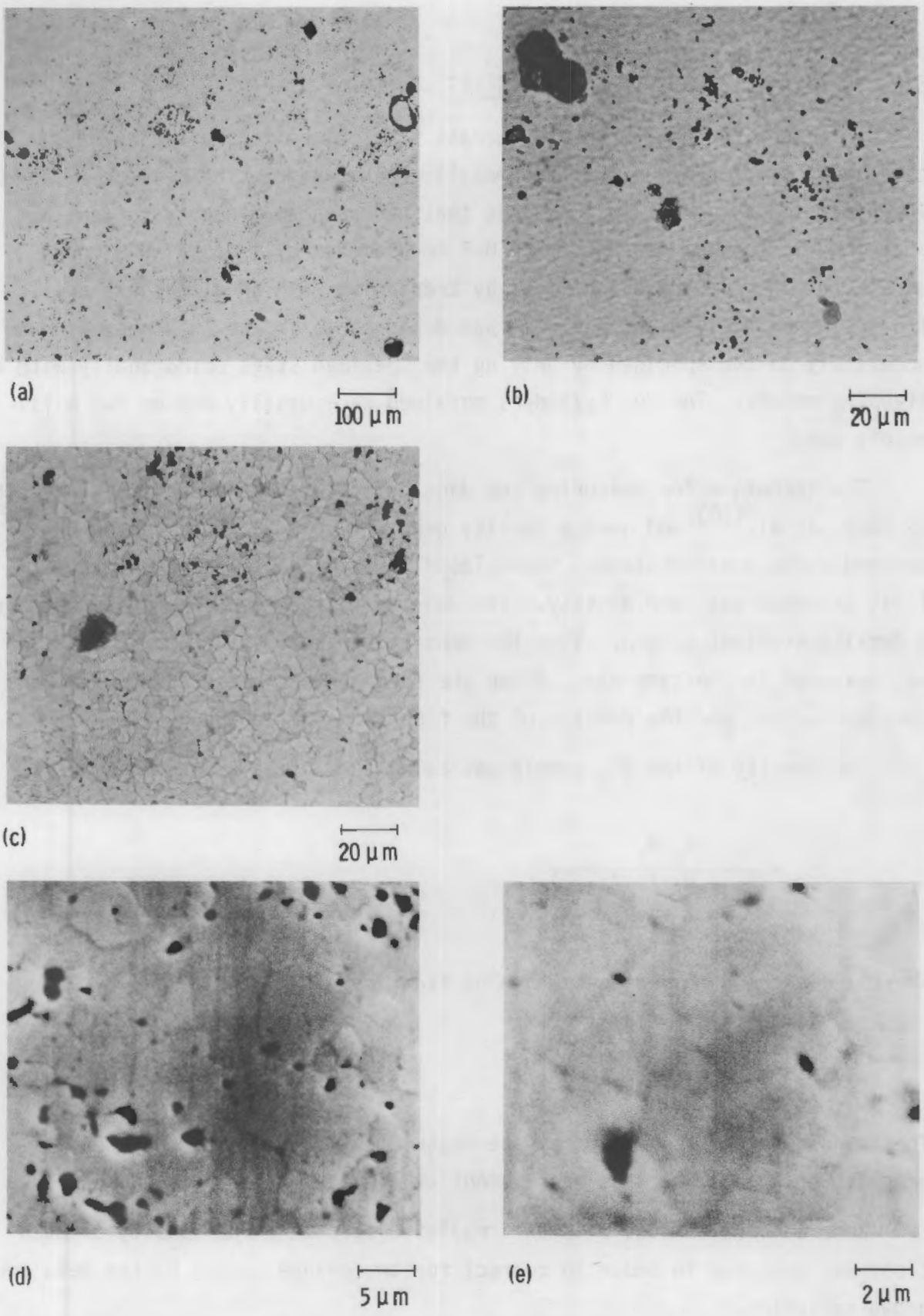

FIGURE 5.3. Scanning Electron Micrographs of Archive UO_2 Pellet of Type Used in Rod 6. Polished Surface Examined After Etching

5.6 UO_2 DENSITY ACROSS THE FUEL PELLET

To determine the UO_2 density across the fuel pellet, a series of small core samples was removed from the metallographic samples of pellets 13 and 39. The core samples were from locations that had been examined by optical and scanning electron microscopy. The 0.5 mm-diameter cylindrical UO_2 cores were obtained from these locations by trepanning with an ultrasonic drill. The equipment used in the hot cell was designed to locate the trepanning drill accurately on the specimen by driving the specimen stage orthogonally with two stepping motors. The UO_2 cylinders obtained were usually one or two millimeters long.

The technique for measuring the density of these cores has been described by Rose, et al.[10] and uses a density gradient column. Each sample was weighed using a microbalance, then placed in a specially designed carrier float of known mass and density. The density of the float was measured using a density gradient column. Then the density of the float plus the specimen was measured in the same way. After the specimen was removed the float and specimen masses and the density of the float were remeasured.

The density of the UO_2 sample was calculated using the formula:

$$\rho_s = \frac{\rho_c M_s}{M_s - M_f (\rho_c/\rho_f - 1)}$$

where ρ_c is the combined specimen plus float density,
ρ_f is the float density,
M_s is the specimen mass, and
M_f is the float mass.

The technique relies on the accurate measurement of density using density gradient columns as well as measurement of the mass of small specimens.

Before and after use with an irradiated specimen, the density of each float was measured in order to correct for any change caused by the beta and gamma radiation.

The results of the UO_2 density measured across the fuel pellet are presented in Table 5.7.

TABLE 5.7. Densities of Small Cores from Pellets 13 and 39 of Rod 6

Pellet Number	Core Identity	Measured Density g/cm^3	Core Location
13	3	10.268(a)	Center - radius 3
13	7	10.906	Midradius - radius 3
13	8	10.917	Midradius - radius 7
13	6	10.128	Outer region - radius 3
13	9	10.118	Outer region - radius 7
39	1	10.238	Center - radius 1
39	9	10.169	Midradius - radius 1
39	10	10.198	Midradius - radius 5
39	8	9.580(b)	Outer region - radius 1
39	7	10.068	Outer region - radius 5

(a) When the density of this specimen was first measured it was very low ($\sim$8 g/cm^3). It was found to have epoxy resin down one side. The value given above was obtained after dissolving away the resin. This value might be in error if all the resin was not removed.
(b) After rechecking.

5.7 BURNUP PROFILE ACROSS FUEL PELLET

A UO_2 pellet from near the peak burnup position (pellet 14) was selected and prepared so that its cross section could be gamma scanned. The pellet was prepared by mounting in the same way as the metallographic samples, the prepared surface being the end of the pellet that had been towards the top of the rod, and by grinding the top surface flat. However, the radial gamma scanning exercise was unsuccessful because of the low gamma activity of the sample in relation to the normal background levels at the detector position. Thus, a series of 0.5-mm diameter cores were then removed from the sample using the trepanning technique described in Section 5.6. The cores were removed across two diameters that were at right angles to one another from near the surface of the pellet, at midradius position and in the center of the

pellet. One of the diameters selected was in line with the orientation mark scribed on the outside of the zircaloy cladding before cutting and in line with the centerline mark on the top fitting of the rod.

The core samples weighed about 4 mg each. This small amount of material limited the amount of chemical analysis and mass spectrometry that could be carried out on each sample. The samples were dissolved to complete solution under reflux in 8M nitric acid containing 0.01M hydrofluoric acid. Although sample 2 was lost at this stage as a result of an accident, it was still possible to measure the isotopic composition of the uranium in a small amount of residual liquid that was recovered.

The remaining samples were analyzed for uranium, plutonium and neodymium concentrations using isotope dilution and surface ionization mass spectrometry. However, the remaining samples were too small to determine the plutonium and neodymium isotopic composition. After dissolution, known amounts of tracer uranium, plutonium and neodymium were added to known amounts of each sample solution. Standard methods of ion exchange chromatography were used to separate these three elements, which were then mounted on filaments for thermal ionization mass spectrometry. From these measurements the isotopic composition of the uranium in each sample was calculated and these are given in Table 5.8.

In addition, the ratio of plutonium to uranium, by weight, and the atom percent burnup from the Nd 148/U ratio were calculated. These results are given in Table 5.9. The results are given in the percentage ratio of total number of atoms fissioned to the initial total number of uranium atoms. The isotopic composition of an archive UO_2 sample is given below.

Isotope	Atom Percent
U 234	0.04 ± 0.01
U 235	10.14 ± 0.05
U 236	0.08 ± 0.02
U 238	89.74 ± 0.02

TABLE 5.8. Uranium Isotopic Composition of Samples Cored from Pellet 14 of IFA-431 Rod 6[a]

Sample No.	Atom Per Cent U 234	U 235	U 236	U 238
2	0.05 ± 0.01	9.67 ± 0.05	0.21 ± 0.02	90.07 ± 0.02
5	0.06 ± 0.01	9.76 ± 0.05	0.20 ± 0.02	89.98 ± 0.02
10	0.06 ± 0.01	9.73 ± 0.05	0.20 ± 0.02	90.01 ± 0.02
11	0.07 ± 0.01	9.66 ± 0.05	0.22 ± 0.02	90.05 ± 0.02
12	0.05 ± 0.01	9.71 ± 0.05	0.21 ± 0.02	90.03 ± 0.02
15	0.05 ± 0.01	9.50 ± 0.05	0.22 ± 0.02	90.23 ± 0.02
17	0.06 ± 0.01	9.74 ± 0.05	0.20 ± 0.02	90.00 ± 0.02
18	0.06 ± 0.01	9.54 ± 0.05	0.24 ± 0.02	90.16 ± 0.02
20	0.05 ± 0.01	9.67 ± 0.05	0.21 ± 0.02	90.07 ± 0.02

(a) The accuracy of the results given in this table is to within ± one standard deviation.

TABLE 5.9. Plutonium/Uranium, Neodymium 148/Uranium Ratios and Calculated Burnup of Samples Cored from Pellet 14 of IFA-431, Rod 6[a]

Core Number	Pu/U Ratio by weight	Nd 148/U Ratio by weight	Atom Per Cent Burnup
2	Sample lost due to accident at dissolution stage		
5	0.000489 ± 0.000008	0.0000479 ± 0.0000009	0.458 ± 0.009
10	0.000485 ± 0.000008	0.0000482 ± 0.0000009	0.461 ± 0.009
11	0.000560 ± 0.000011	0.0000616 ± 0.0000012	0.589 ± 0.012
12	0.000518 ± 0.000010	0.0000532 ± 0.0000010	0.509 ± 0.010
15	0.000686 ± 0.000013	0.0000696 ± 0.0000014	0.666 ± 0.014
17	0.000632 ± 0.000012	0.0000473 ± 0.0000009	0.452 ± 0.009
18	0.000778 ± 0.000015	0.0000700 ± 0.0000014	0.669 ± 0.014
20	0.000528 ± 0.000010	0.0000535 ± 0.0000010	0.512 ± 0.010

(a) The accuracy of the results given in this table is to within ± one standard deviation.

6.0 ANALYSIS OF THE POST IRRADIATION EXAMINATION RESULTS

Analysis of the PIE results for IFA-431 showed that significant findings were obtained in three areas: dimensional changes, gamma scanning and burnup, and densification. The finding in each of these areas will be discussed in this section.

6.1 DIMENSIONAL CHANGES

The three types of dimensional change that were observed in IFA-431 are length, diametral ridging, and gap size.

Length - The fuel length changes, shown in Table 6.1, were obtained by two different methods. In the first method, performed at Kjeller (on all six rods) and at Harwell (on rod number 6), the pellet stack start and end were observed by noting where the gamma activity in the gamma scans took a sudden jump. The fuel lengths for rod 6 obtained at both labs agree fairly well. However, this method was not very exact.

TABLE 6.1. Fuel Rod Length Changes

Fuel Rod Number	Original Stack Length, (mm)	Stack Length[a] gross/Zr 95 + Nb 95 , (mm)	Change in Length (mm)	Stack Length, by Step Method (mm)	Change in Length (mm)
1	574.4	575.7/575.1	+1.3/+0.7	573.8	-0.6
2	574.6	576.0/575.7	+1.4/+1.1	574.7	+0.1
3	580.6	582.6/582.9	+2.0/+2.3	581.8	+1.2
4	566.1	570.0/568.8	+3.9/+2.7	568.2	+2.1
5	579.1	580.2/579.9	+1.1/+0.8	578.9	-0.2
6	575.9	570.6/570.6	-5.3/-5.3	569.4	-6.5

(a) The stack lengths and length changes given here were obtained by gamma scans performed at Kjeller. The gamma scans at Harwell were performed on rod 6 only. Cs 137 was used to measure the gross gamma activity, and Zr 95 to Nb 95 activity was also measured. Stack lengths of 570.25 and 570.2 were obtained with corresponding length changes of -5.65 and -5.7.

In the second method, the exact fuel start and end were determined by using manual, single-step movement of the fuel rod in both directions while observing the gamma activity rate changes.

The fuel rod lengths obtained by these methods are presented in Table 6.1. They indicate a small stack elongation in rods 3 and 4, and a strong (>1%) stack shortening in rod 6. The other changes are too small to be significant. Note that rod 6 is the only rod that contained unstable fuel.

Diametral Ridging - Pre-irradiation diameter curves were fairly smooth with outer diameter variations of less than 10μ along the length of the rods. All values were very near the range of 12.780 mm to 12.782 mm. Comparing these values to the overall average values shown in the diameter tables of Appendix D shows that only rod 3 had a significant diameter increase on the order of 15μ.

All of the PIE diameter curves (Appendix D) show periodic variations in diameter. However, these variations are not caused by pellet-cladding mechanical interaction (PCMI) or ridging since the wave length of the variations is not the same as the pellet length, which was 13 mm. These diameter variations were caused by the noncontinuous feeding action in the last tube step of the milling process and were also observed prior to irradiation.

Only rod 3 showed some ridging, which was in the 360 mm area. These diameter variations had a correct wave length of 13 mm and a different shape of narrow-pointed maxima instead of rounded ones. The height of the ridging was 12μ.

Gap Size - The gap in the irradiated fuel rods was measured by a squeeze test. Results of this test were presented in Table 4.4, and they are reproduced here as Table 6.2. The gap values of various rods were compared to one another as follows:

1. Rod 6 and rod 5 - The unstable fuel structure resulted in a 70μ larger post irradiation gap than did the stable fuel structure.
2. Rod 1 and rod 5 - There is little difference in the residual gap between high-density and low-density stable fuel.

3. Rod 1 and rod 2 - The large gap rod still has the largest gap after irradiation, although the difference between the two has decreased.

4. Rod 4 and rod 1 - The gap decrease was greater in the xenon-filled rod than in the helium-filled rod. The xenon-filled rod had a higher operating temperature.

The gap values along one rod were compared to one another. The axial gap dependence indicates a large gap decrease near the middle of the rod. Near the lower end, the lower temperature may have caused less relocation. Gap values near the ends of the fuel rod were erratic because of the presence of the hollow pellets.

TABLE 6.2. Result of Gap Measurement (in microns)

Axial Position, mm	Pin Number 1	2	3	4	5	6
75	195	347	-	72	202	288
112 (TC)	178	260	-	140	226	292
170	201	283	-	146	259	271
270	181	286	15	102	192	298
370	164	264	20	94	199	269
470	160	268	22	110	248	291
534 (TC)	195	309	24	109	247	277
570	198	309	31	108	230	284

6.2 ANALYSIS OF GAMMA SCANNING AND BURNUP OETERMINATIONS

The axial gamma scans of the rods, which begin on page C-3, represent the time-averaged axial power profile over the last two months or so of the irradiation. Since the total irradiation time for IFA-431 was only about 7 months, and since the axial neutron flux was undisturbed over most of the assembly life, we can expect the gamma activity axial variation to be close to the neutron flux variation as registered by the assembly's neutron detectors.

Figure 6.1 shows the Kjeller gross gamma scan for rod 1: it includes the counts per second at both the upper and lower neutron detector positions. The ratio of upper to lower counts/sec is approximately 1.38 for all six rods, and this was also found in the gamma scan of rod 6 at Harwell. The ratio of the upper/lower neutron detector readings was in the range of 1.35 to 1.45 throughout the life of the assembly. This ratio is confirmed by the axial gamma scans. In addition, the "normal" axial flux shape assumed by Halden between the upper/lower locations seems to be fairly well confirmed by the gamma scans. This is illustrated in Figure 6.1, where the normal axial flux shape (Figure 3.1) is superimposed on the gross gamma scan for rod 1. The end peaking is slight, but discernible.

The gamma scans also give the ratio of average gamma intensity from each rod to the average of all six rods. This ratio should be indicative (for this short, stable irradiation) of the partition of assembly power among the various rods. That partition is a function of the fuel/unit length variations among the rods plus the radial tilt of the neutron flux. Since the tilt varies from day to day throughout the assembly's life, we have compared the end-of-life calculated relative burnup of the rods to the relative gamma intensity.[(a)] The results are listed in Table 6.3. The agreement is very good. Thus, the gamma scans confirm partition of assembly power among the rods that was made for power and burnup calculations.

(a) The burnup calculation represents a time integration of the tilt factor.

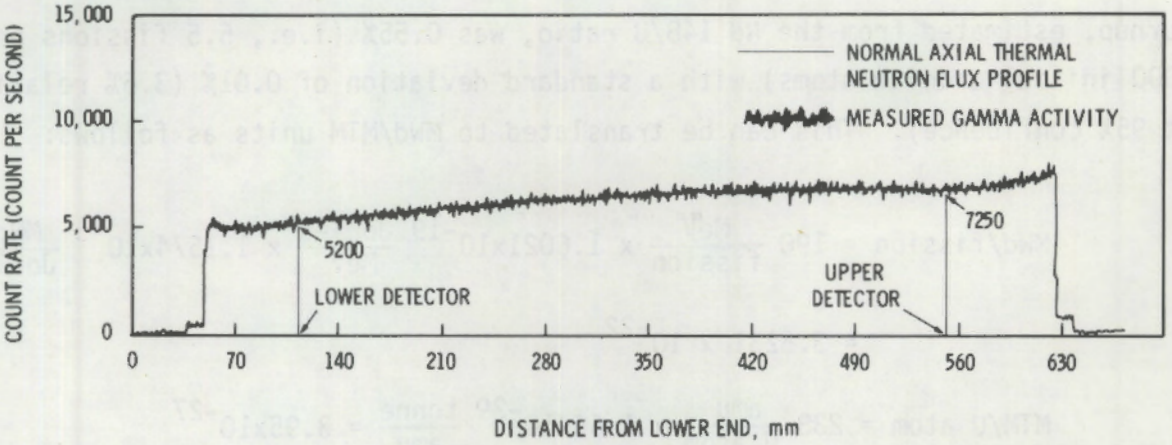

FIGURE 6.1. Element IFA-431, Pin 1, Axial Gamma Scan Channel A

TABLE 6.3. Comparison of Relative Gamma Intensity and Relative Burnup for the IFA-431 Rods

Rod Number	Calculated EOL[a] Burnup (Rod Average), MWd/MTM	Relative Burnup[b]	Relative Gross Gamma Intensity (Rod Average)
1	4315	0.979	0.989
2	4459	1.012	1.018
3	4621	1.048	1.047
4	4478	1.016	1.001
5	4333	0.983	0.984
6	4241	0.962	0.961

(a) Pacific Northwest Laboratory performed these end-of-life calculations.
(b) The ratio of rod average burnup to assembly average burnup.

The absolute connection between calculated and measured burnup can only be made at one point - pellet 12 from the top of the rod. At that point Harwell made a (pellet average) burnup determination. The pellet was dissolved and the isotopic concentrations of the uranium, plutonium and neodynium

isotopes were determined, along with the Pu/U and Nd 148/U weight ratios. The burnup, estimated from the Nd 148/U ratio, was 0.55% (i.e., 5.5 fissions per 1000 initial uranium atoms) with a standard deviation of 0.01% (3.6% relative at 95% confidence). This can be translated to MWd/MTM units as follows:

$$\text{MWd/fission} = 190 \frac{\text{MeV}}{\text{fission}} \times 1.6021\text{x}10^{-19} \frac{\text{Joules}}{\text{MeV}} \times 1.1574\text{x}10^{-5} \frac{\text{MWd}}{\text{Joule}}$$

$$= 3.5231 \times 10^{-22}$$

$$\text{MTM/U atom} = 238 \frac{\text{amu}}{\text{U atom}} \times 1.66\text{x}10^{-29} \frac{\text{tonne}}{\text{amu}} = 3.95\text{x}10^{-27}$$

$$\text{MWd/MTM} = 0.055 \frac{\text{fission}}{\text{U atom}} \times \frac{\text{MWd}}{\text{fission}} \div \frac{\text{MTM}}{\text{U atom}} = 4^{\circ}05.$$

The calculated peak value for rod 6 was 4914 MWd/MTM. The measured/calculated difference is barely significant, given the 3.6% uncertainty in the measured value plus the 5% uncertainty in the calculated value. Thus, the absolute estimation of burnup (and hence rod power) seems well confirmed by the PIE burnup analysis.

A final question in the distribution of power has to do with the volumetric heat generation rate as a function of radial and azimuthal position within the pellet. This may seem to be a fine point, but it considerably affects the interpretation of fuel temperature data with respect to inference of gap conductance,[11] which was one of the original objectives of the test. Failure to account for the "flux depression" in the 10% enriched pellets can lead to a 50°C (90°F) error in the estimated surface temperature at 30.0 kW/m, which amounts to a 15% or more error in typical conductance values. Failure to account for flux tilt across the rod has less effect on the calculated mean surface temperature, but the error is not insignificant. Accordingly, Harwell was requested to attempt the determination of radial and azimuthal burnup variation.

There are at least two ways to determine the radial distribution of burnup: gamma scans across the pellet face, and burnup determination of microcores. The former is much easier and less expensive than the latter, but it requires gamma activity high enough to give good counting statistics with extremely narrow collimation. Unfortunately, rod 6 of IFA-431, with low burnup and a 6 month cooling time prior to arrival at Harwell, just did not have the required gamma activity. Therefore the burnup distribution determination rests on the tedious process of removing ~5-mg. microcores approximately 0.5 mm in diameter. Pellet 14 from the top of the rod was selected for this purpose, and cores were taken from edge, mid-radius and center positions across two diameters, at right angles to one another. One of the diameters was in line with an orientation mark on the outside of the cladding. The locations of these cores are shown in Figure 6.2, which is approximately to scale.

The cores were dissolved and analyzed for isotopic composition of the Pu, Nd and U. In Figure 6.2, b, c, and d show, respectively, the burnup, Pu/U ratio, and U 235 content of the cores. The standard deviation of the burnup results is approximately 0.01 atom %.

There is evidence of a definite flux tilt across the rod as indicated in Figure 6.2. The maximum edge-to-edge difference indicated is in line with the orientation mark and amounts to about 14%. On the other hand, the neutron detectors indicated a maximum flux tilt of 5-10% across the entire assembly for most of the irradiation, which translates to only a one or two percent variation across each rod. The much larger tilt evidenced here is, therefore, an assembly effect rather than a reactor effect. Support for such a possibility lies in some results of flux wire activation in the NORA reactor, Kjeller.[12] A copper wire was threaded laterally through a 6-rod assembly (directly through two fuel rods) and the assembly was irradiated in a flat reactor flux at low power. Figure 6.3 shows the results, which conclusively indicate a flux tilt of about 15% across the rods, with the higher flux at the outside of the rods. From the IFA-431 assembly data package, we found that the orientation mark of all rods faced outward and was in line with the assembly center. Referring again to Figure 6.2b, we see that the azimuthal burnup distribution determined by Harwell definitely is in agreement with the NORA flux wire data.

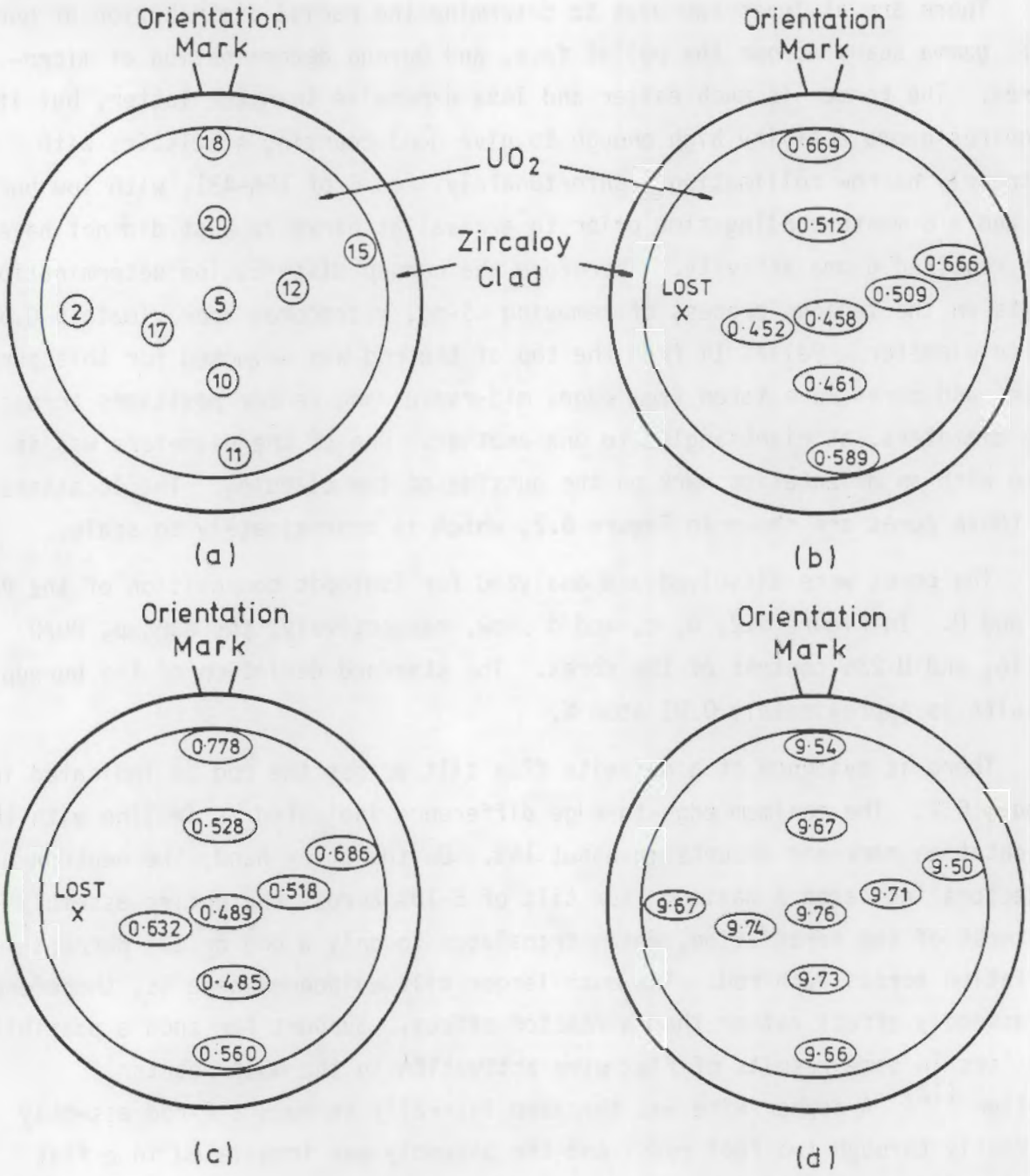

FIGURE 6.2. Schematic Diagram of Pellet 14 from IFA-431, Rod 6 Showing the Locations of the Core Samples Taken for Analysis

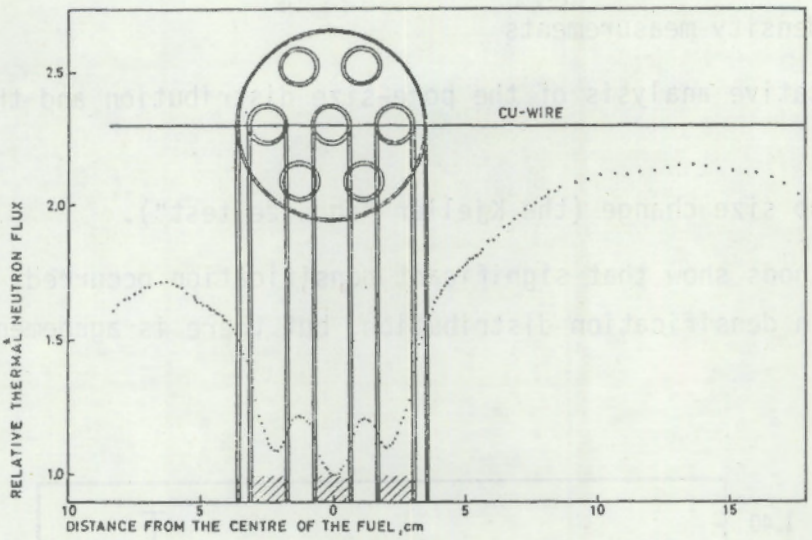

FIGURE 6.3. Relative Flux Variation Through a Fuel Assembly

The radial variation of burnup also agrees with our expectations. In Figure 6.4 we show the calculated fission rate for a 10% enriched solid pellet, as determined from the Battelle-revised THERMOS code[14] normalized to 1.0 at the center. Harwell data points for burnup are superimposed on the calculated curve. The Harwell points were averaged azimuthally and normalized to 1.0 at the rod center. The error bars indicate 95% (2σ) confidence intervals. The agreement is good, and confirms the basic flux depression function used up to this point for interpreting IFA-431 data.

6.3 DETERMINATION OF FUEL DENSIFICATION IN ROD 6

The fuel pellets in rod 6 were deliberately made susceptible to in-reactor densification. This was accomplished by incomplete sintering, as explained earlier. Resintering at 1600°C (2912°F) and 1700°C (3092°F) caused 2-3% increases in the theoretical density. Several techniques and indicators that were used to evaluate the in-reactor densification, include:

- fuel stack shortening (from gamma scan)
- void volume change
- bulk fuel density checks

- microcore density measurements
- SEM quantitative analysis of the pore-size distribution and the overall porosity
- apparent gap size change (the Kjeller "squeeze test").

All of these methods show that significant densification occurred. There are some anomalies in densification distribution, but there is agreement on the overall range.

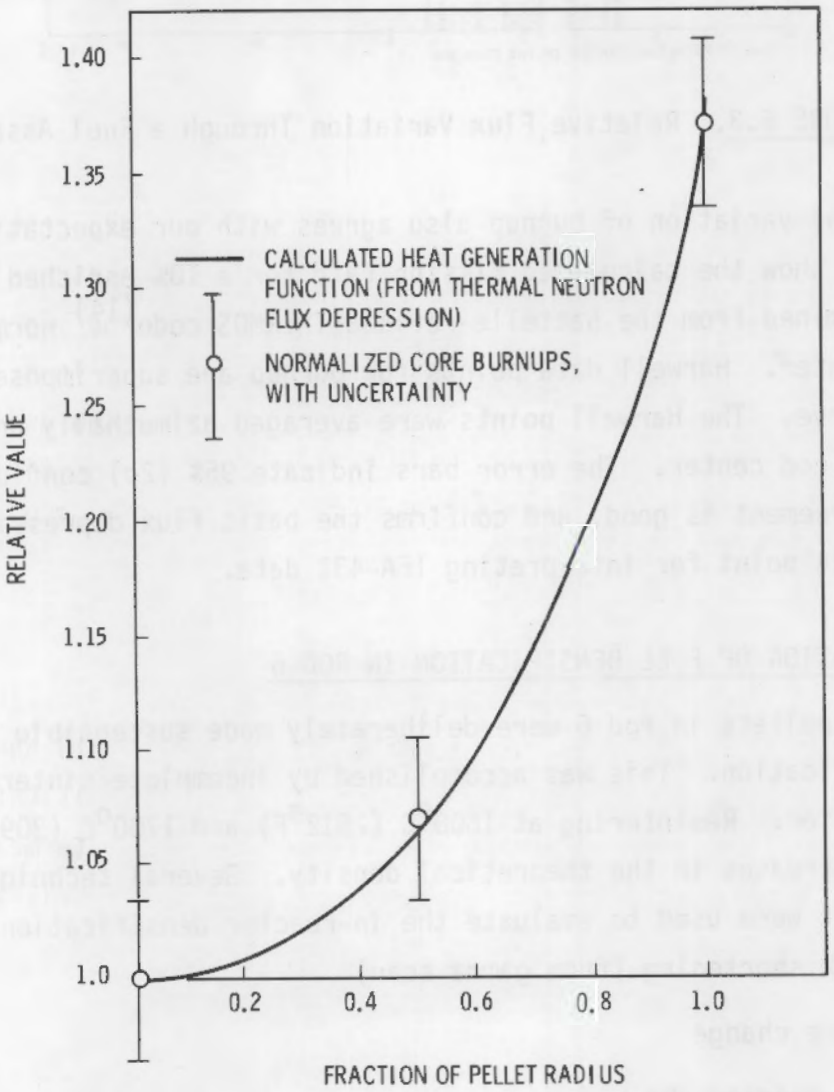

FIGURE 6.4. Measured and Estimated Burnup/Power Profile Across Pellet 14, Rod 6

In summary, significant in-reactor densification was confirmed for rod 6, in the range of 4.0 ± 1.5% TD. In spite of this densification, which probably occurred early in life, the fuel temperatures over the short irradiation (∿4,000 MWd/MTM) of rod 6 remained very close to those of rod 1, which was of identical design and had stable, high-density fuel.

6.3.1 Fuel Stack Shortening

The gamma scan of rod 6 at Kjeller indicated a fuel stack shortening of 6.5 mm, or about 1.1%. If this were due to densification, and if the reduction in radius is also 1%, then the total volume reduction, and hence the densification, would be 3%.

6.3.2 Void Volume Change

The estimated free volume in the pin before irradiation was 4.13 ml. The void volume measured at Harwell during rod puncture was 7.58 ml. Assuming the difference can all be assigned to densification, the computed densification is (7.98 - 4.13)/51.18 = 6.7%. This is rather large, probably as a result of inaccuracies in the initial void volume estimate.

6.3.3 Bulk Fuel Density Measurements

Six pieces from the upper end of the rod (pellets 11-12) and six from the lower end were measured for density by immersion in carbon tetrachloride. Three or four measurements were performed on each piece. The mean of all upper location measurements was 96.2% TD and the mean of the lower position measurements was 96.6% TD. The density difference between the two positions does not appear significant, even though they operated at significantly different temperatures and powers. Assuming an initial density of 91.5% TD, the average densification in the rod appears to be 4.9% TD.

6.3.4 Microcore Density Measurements

An attempt was made to determine the radial distribution of fuel density from the densities of 5 mg microcores extracted from pellets 13 and 39 of rod 6. Cores were taken from center, mid-radius and edge positions along 2 diameters in each pellet. The difficulty of obtaining accurate measurements on such small samples led to anomalous results. The mean for all 10 cores was 93.6 ± 6% TD.

6.3.5 SEM Analysis

Quantitative estimates of the pore size distribution and total porosity have been made at PNL from micrographs of the irradiated rod 6 fuel taken at Harwell. A detailed description of the analysis procedure and the results will be in a future report. Overall densification of the fuel in the range of from 3% to 5% is confirmed by the SEM analysis.

6.3.6 Apparent Change in Gap Size

The difference in apparent end-of-life gap between rod 1 and rod 6 is 100μ. Thus the shrinkage in rod 6 is approximately 1%, and the apparent densification is 3%.

REFERENCES

1. C. R. Hann, et al. 1977. Test Design, Precharacterization, and Fuel Assembly Fabrication for Instrumented Fuel Assemblies IFA-431 and IFA-432. BNWL-1988, Pacific Northwest Laboratory, Richland, WA 99352.

2. I. Cohen, et al. 1960. Measurment of the Thermal Conductivity of Metal-Clad Uranium Oxide During Irradiation, WAPD-228, Pittsburg, PA.

3. P. E. Hart and J. L. Daniel. 1975. "The Role of Microstructure in Thermal and Irradiation-Induced Densification of UO_2 Fuels," presented at the 77th annual Meeting of the American Ceramic Society, Washington, D.C., May 3-8, 1975.

4. R. O. Meyer. 1976. The Analysis of Fuel Densification, NUREG-0085, Nuclear Regulatory Commission, Washington, D.C.

5. C. E. Beyer, C. R. Hann, D. D. Lanning, F. E. Panisko, and L. J. Parchen. 1975. GAPCON-THERMAL-2: A Computer Program for Calculating the Thermal Behavior of an Oxide Fuel Rod, BNWL-1898, Pacific Northwest Laboratory, Richland, WA 99352.

6. J. A. Dearien, G. A. Berna, M. P. Bohn, D. R. Coleman, P. E. MacDonald, J. M. Broughton, "FRAP-S: A Computer Code for the Steady State Analysis of Oxide Fuel Rods," Volume 1 FRAP-S Analytical Models and Input Manual, Report I-309-13.1, Idaho National Engineering Laboratory, Idaho Falls, ID. January 1975.

7. K. D. Olshausen. The Non-Destructive Post Irradiation Examination of Test Fuel Assembly IFA-431, ME-110, Kjeller, Norway.

8. R. E. Williford and C. R. Hann. 1977. Effects of Fill Gas Composition and Pellet Eccentricity, BNWL-2285, Pacific Northwest Laboratory, Richland, WA 99352.

9. E. Foster and A. J. Fudge. 1972. "Post-Irradiation Chemical Analysis," Paper No. 40 at the BNES Conference on Postirradiation Examination Techniques, Reading, England (UK).

10. K. S. B. Rose, I. Williams and G. Potts. 1974. "A Technique for Measuring the Density of Small Fragments of High Density Materials both Before and After Irradiation," Journal of Nuclear Materials 51.

11. C. R. Hann, D. D. Lanning, R. K. Marshall, A. R. Olson and R. E. Williford. 1977. A Method for Determining the Uncertainty of Gap Conductance Deduced from Measured Centerline Temperatures, BNWL-2091, Pacific Northwest Laboratory, Richland, WA 99352.

12. K. Ingebrigtsen and K. Jarhen. 1964. Flux Distributions in the HBWR Second Fuel Charge, HPR-56, Halden Reactor Project, Halden, Norway.

13. C. R. Hann, E. R. Bradley, M. E. Cunningham, D. D. Lanning, R. K. Marshall and R. E. Williford. 1978. Data Report for NRC/PNL Halden Assembly IFA-431. PNL-2494, Pacific Northwest Laboratory, Richland, WA 99352.

14. L. J. Page and D. R. Skeen. 1967. THERMOS/BATTELLE: The Battelle Version of the THERMOS Code, BNWL-516, Pacific Northwest Laboratory, Richland, WA 99352.

APPENDIX A

POWER HISTORIES

POWER HISTORIES

Figures A-1 through A-42 show the power histories of the upper and lower thermocouple locations for all six rods in IFA-431. This data was collected by the Halden IBM/1800 on-line computer data acquisition system while IFA-431 was being irradiated between June 1975 and February 1976. Power is plotted versus time for each month. The rod number for each curve appears in the upper left hand corner of the figure in a position relative to the curve's corresponding position.

The power values were deduced from the vanadium self-powered neutron detector readings after applying many correction factors. These correction factors accounted for local mass distribution, radial flux tilt, axial flux shape, and burnup dependent depletion of U 235. Plutonium buildup, which was negligible, was not considered. In addition, the neutron detector readings during transient periods were not corrected for the response lag of the detector due to incomplete saturation of the vanadium emitter.

Neutron detector six, which monitored the flux near the top of rods 4 and 5, failed early in life. As discussed in the 431 Data Report[13], an equivalent value was calculated by assuming that the upper and lower flux planes defined by the neutron detectors were parallel.

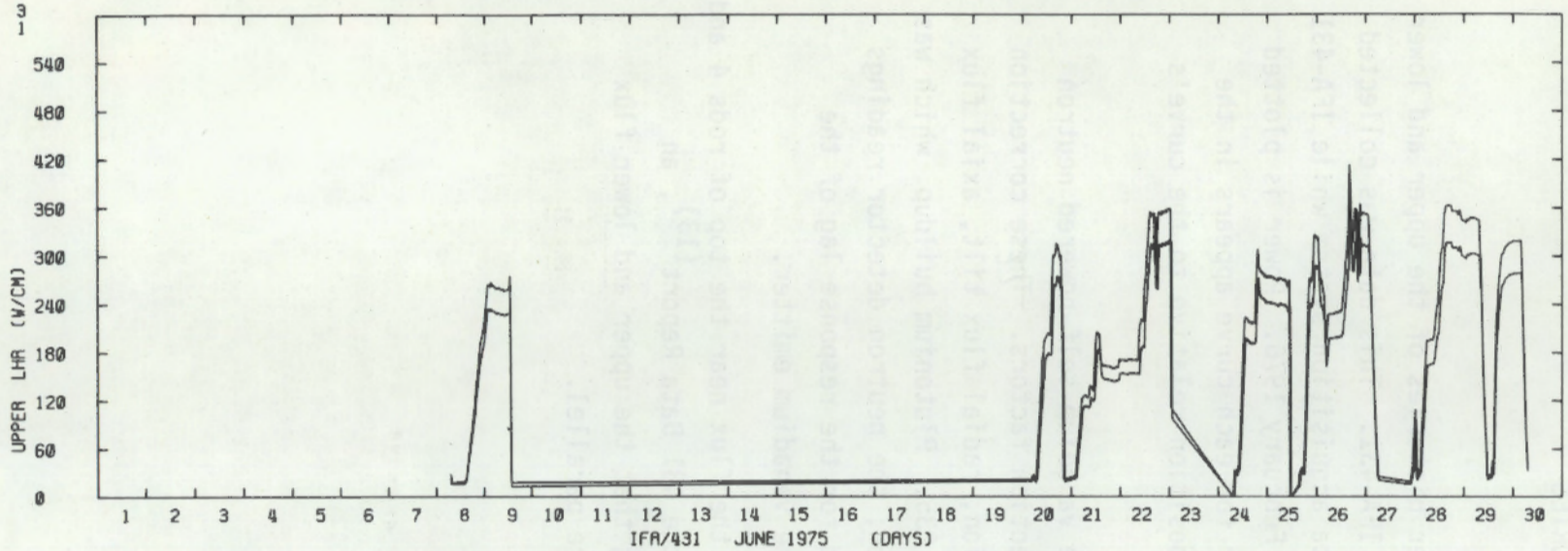

FIGURE A.1. Local Linear Heat Ratings at Upper Thermocouple Locations for Rods 1,3 of IFA 431 - June 1975

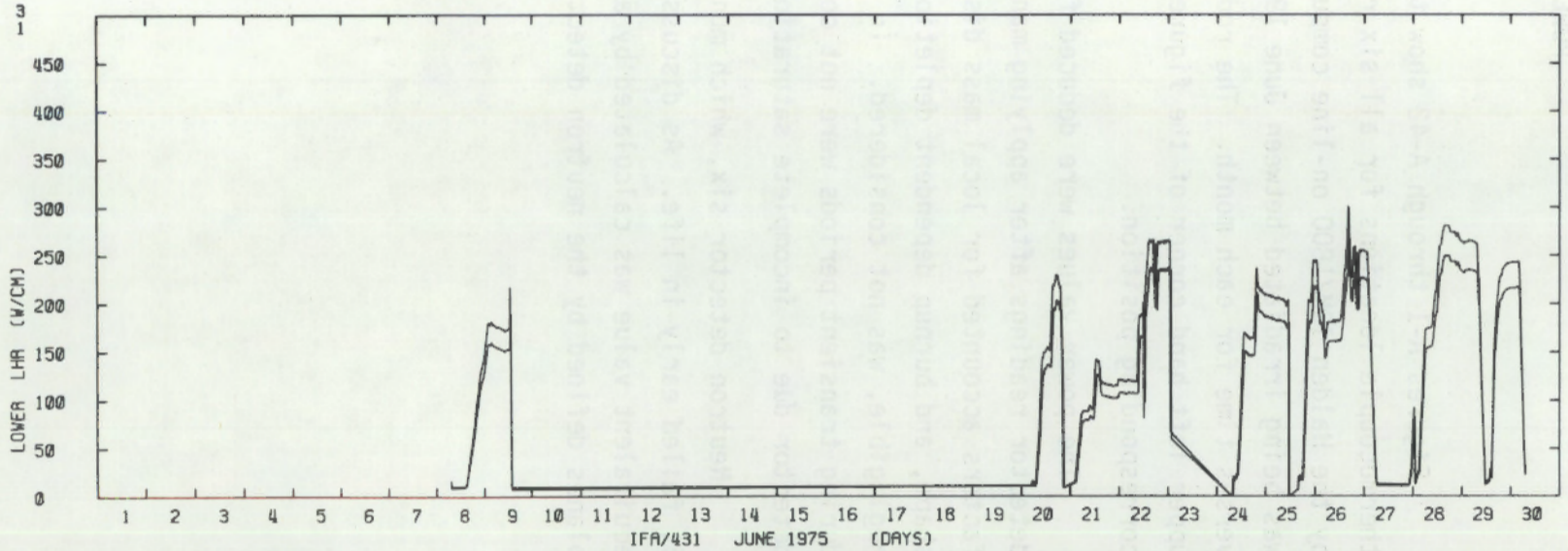

FIGURE A.2. Local Linear Heat Ratings at Lower Thermocouple Locations for Rods 1,3 of IFA 431 - June 1975

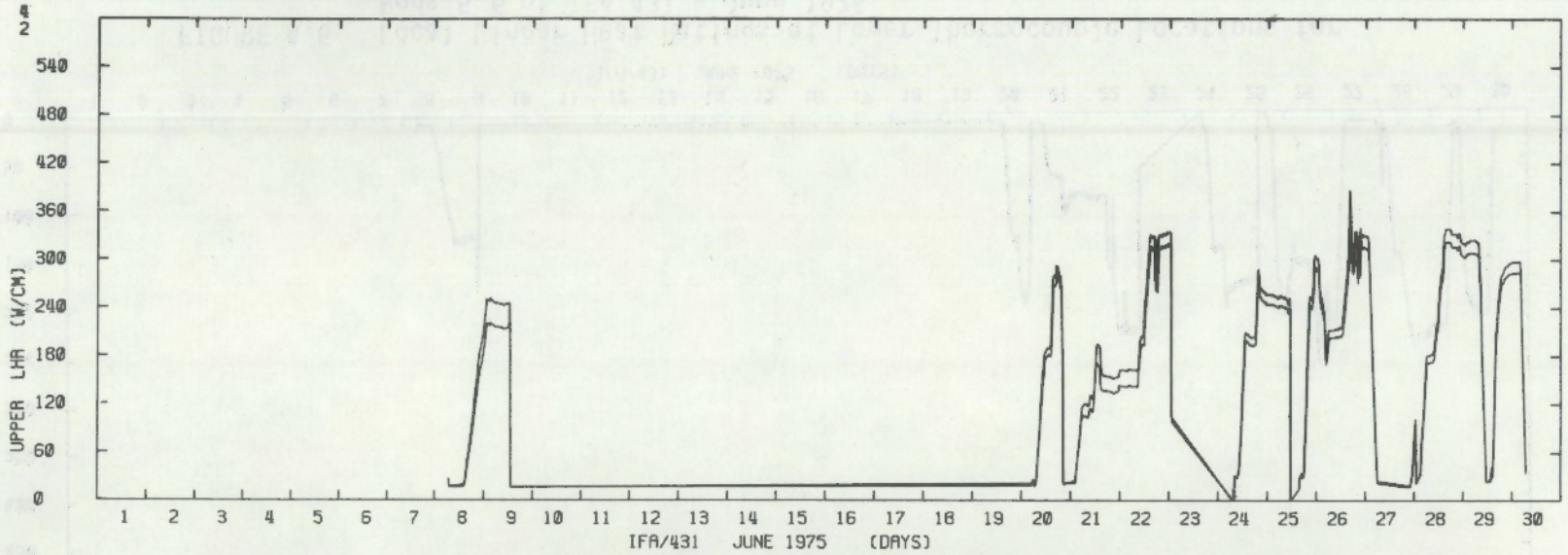

FIGURE A.3. Local Linear Heat Ratings at Upper Thermocouple Locations for Rods 2,4 of IFA 431 - June 1975

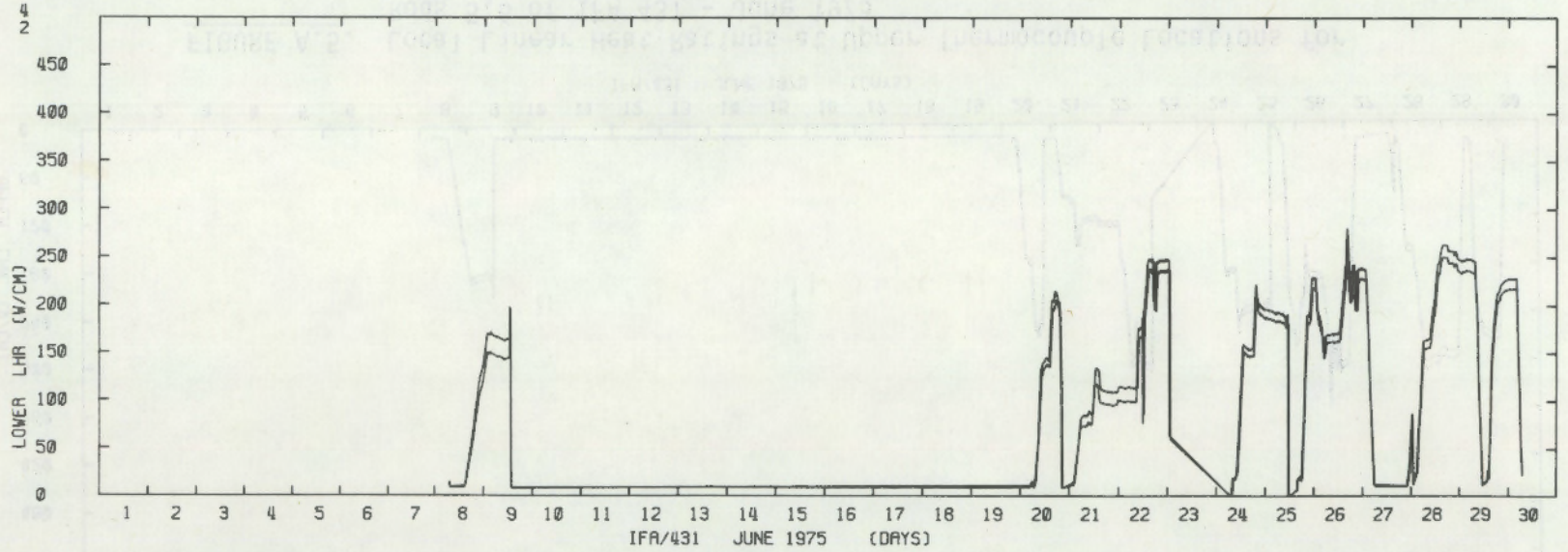

FIGURE A.4. Local Linear Heat Ratings at Lower Thermocouple Locations for Rods 2,4 of IFA 431 - June 1975

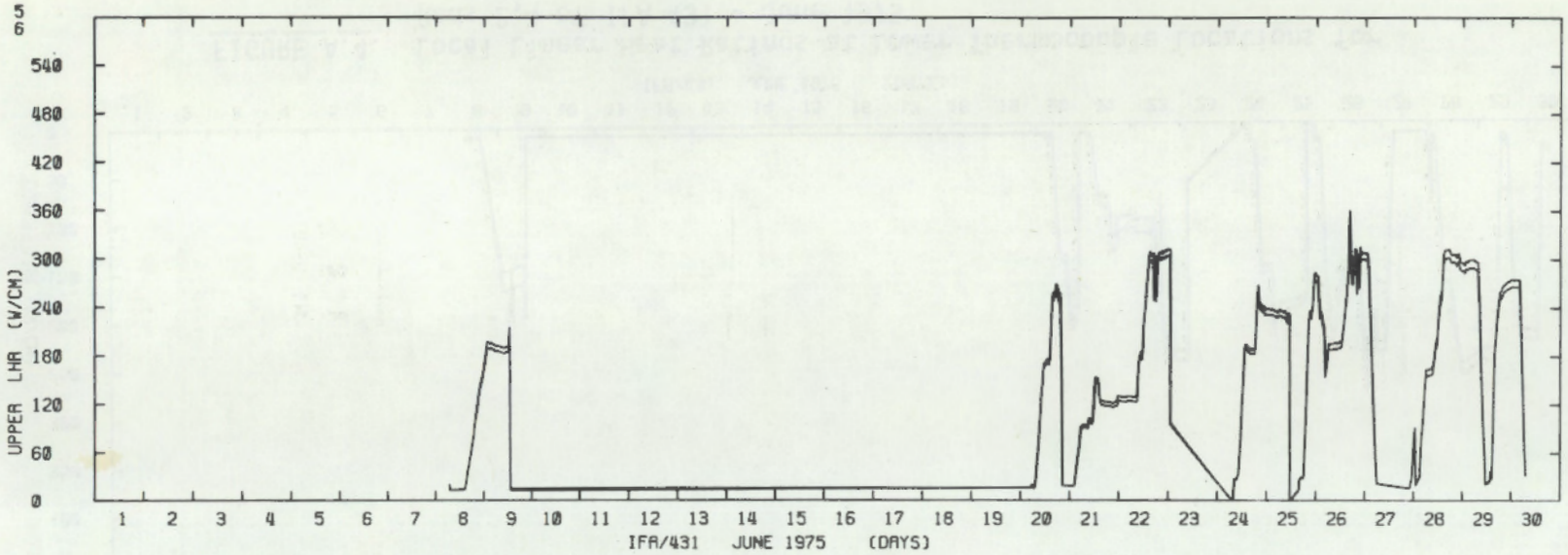

FIGURE A.5. Local Linear Heat Ratings at Upper Thermocouple Locations for Rods 5,6 of IFA 431 - June 1975

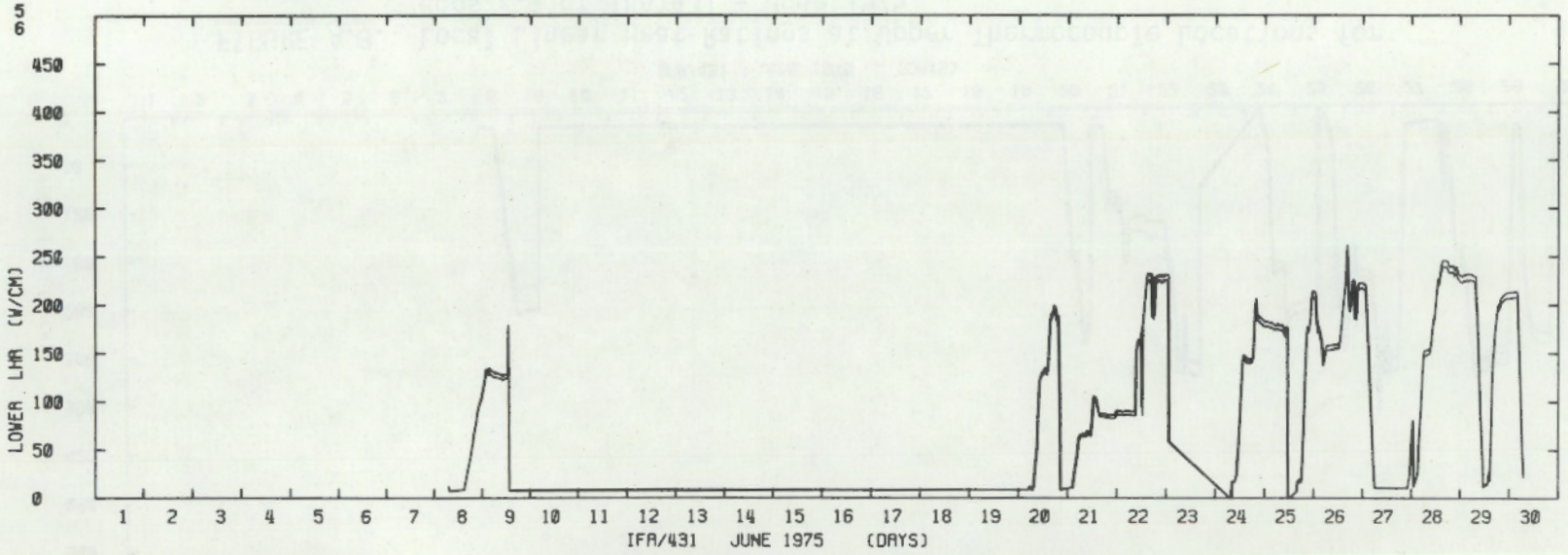

FIGURE A.6. Local Linear Heat Ratings at Lower Thermocouple Locations for Rods 5,6 of IFA 431 - June 1975

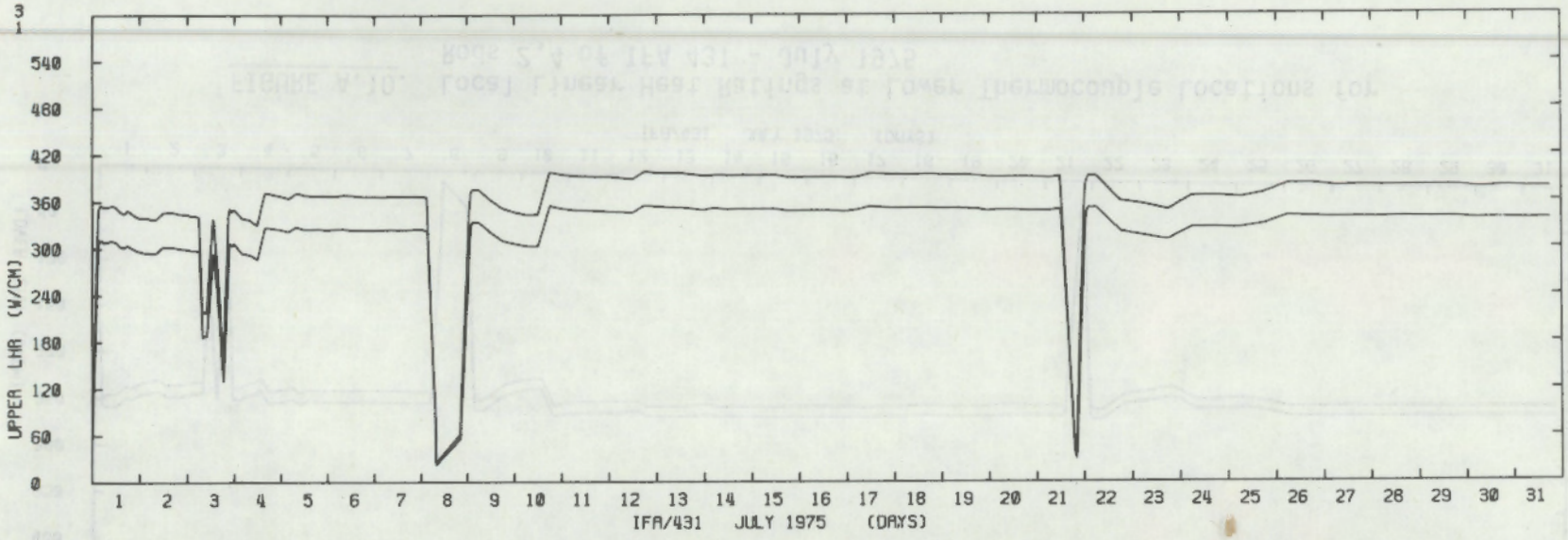

FIGURE A.7. Local Linear Heat Ratings at Upper Thermocouple Locations for Rods 1,3 of IFA 431 - July 1975

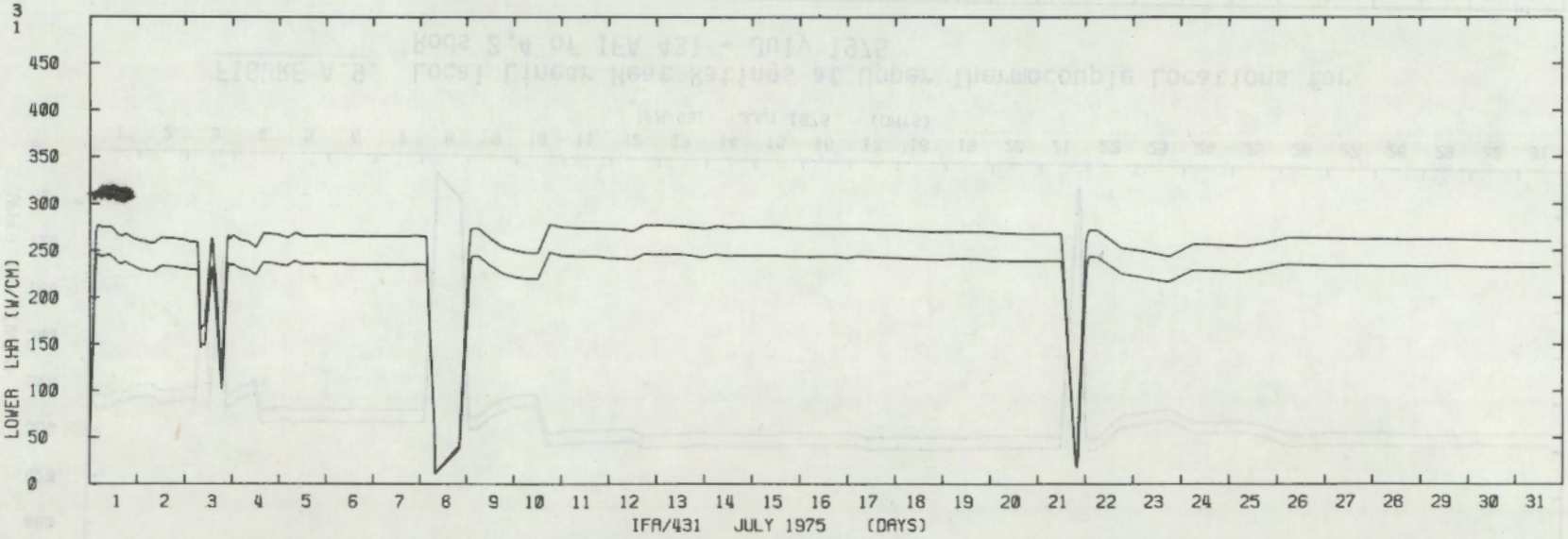

FIGURE A.8. Local Linear Heat Ratings at Lower Thermocouple Locations for Rods 1,3 of IFA 431 - July 1975

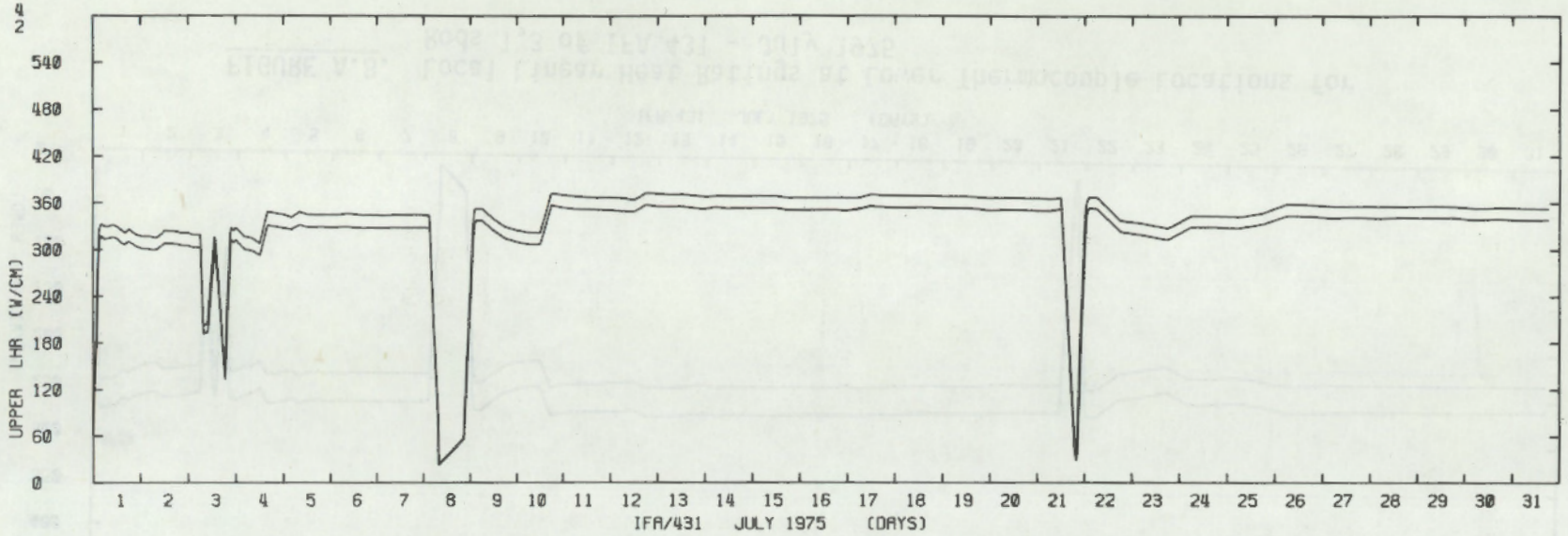

FIGURE A.9. Local Linear Heat Ratings at Upper Thermocouple Locations for Rods 2,4 of IFA 431 - July 1975

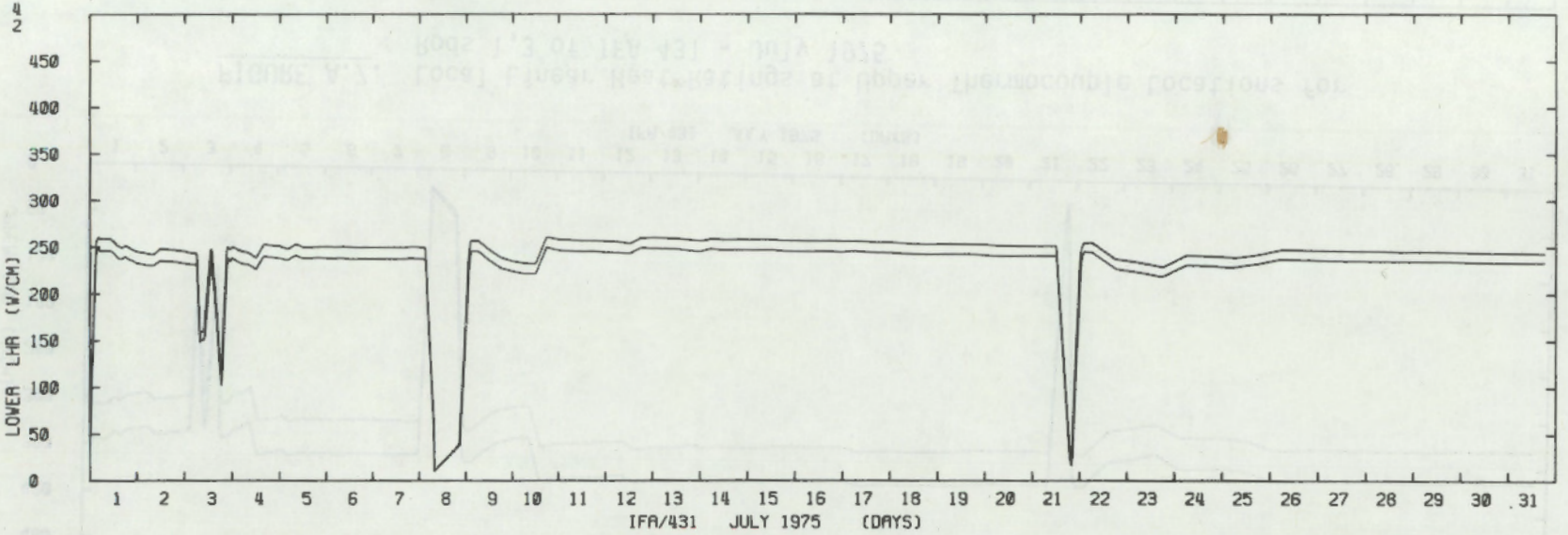

FIGURE A.10. Local Linear Heat Ratings at Lower Thermocouple Locations for Rods 2,4 of IFA 431 - July 1975

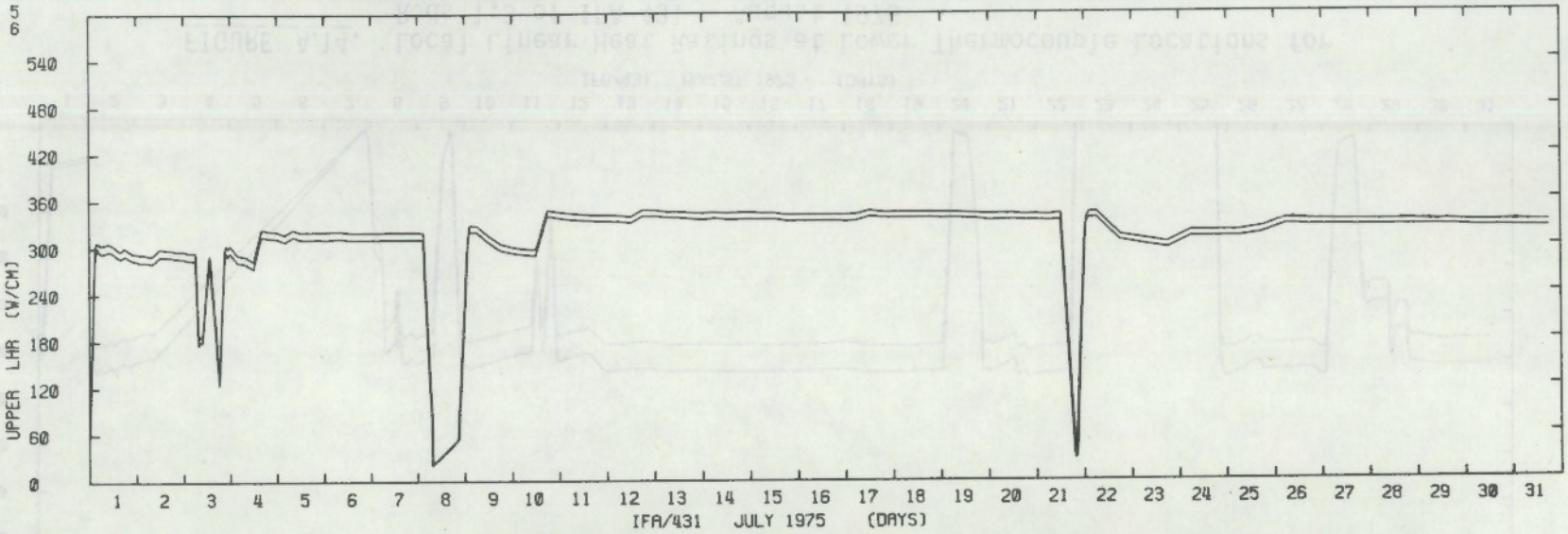

FIGURE A.11. Local Linear Heat Ratings at Upper Thermocouple Locations for Rods 5,6 of IFA 431 - July 1975

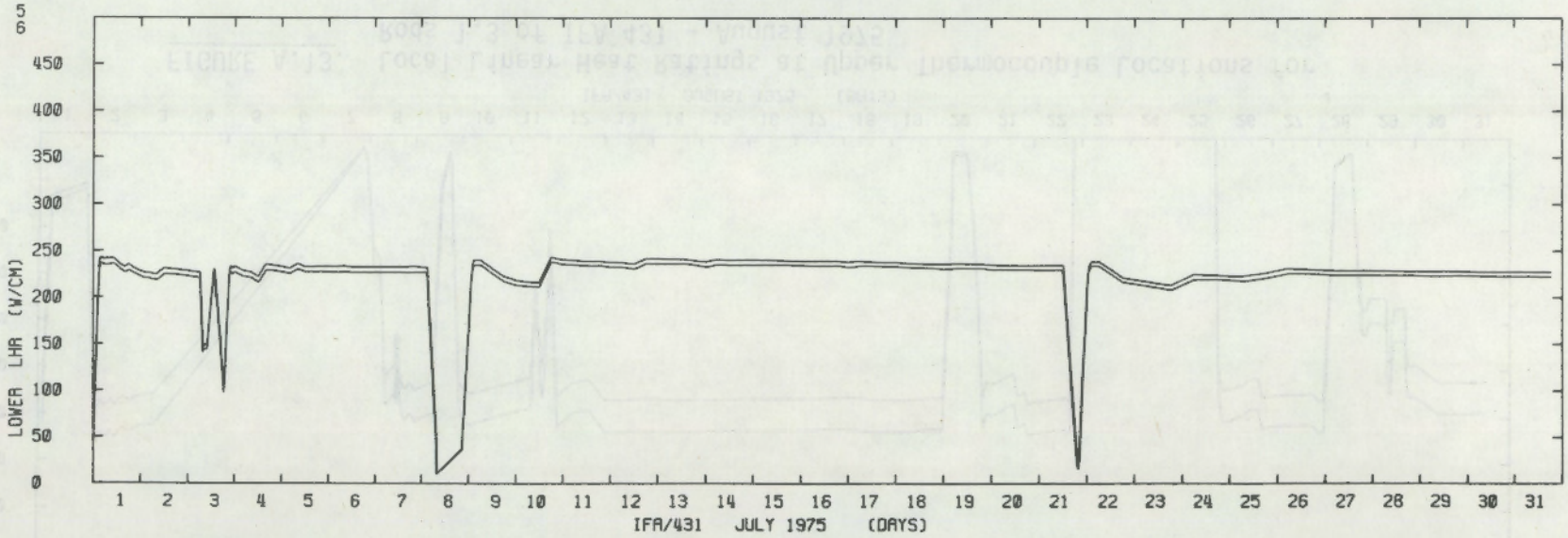

FIGURE A.12. Local Linear Heat Ratings at Lower Thermocouple Locations for Rods 5,6 of IFA 431 - July 1975

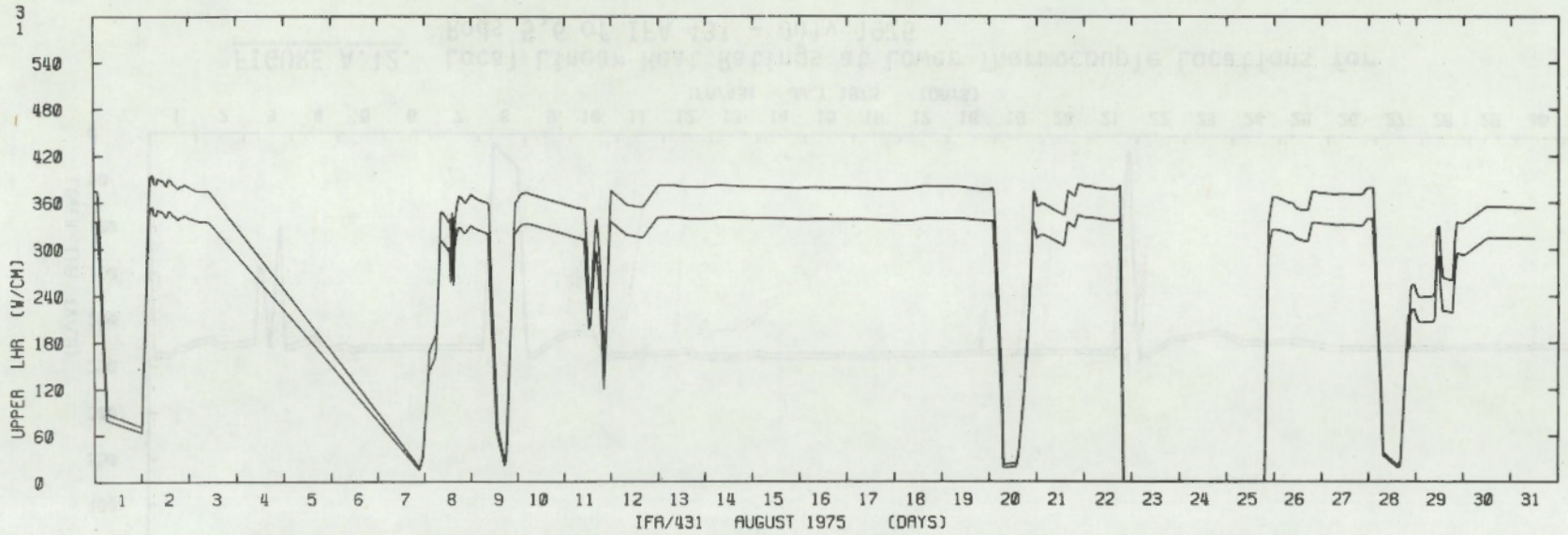

FIGURE A.13. Local Linear Heat Ratings at Upper Thermocouple Locations for Rods 1,3 of IFA 431 - August 1975

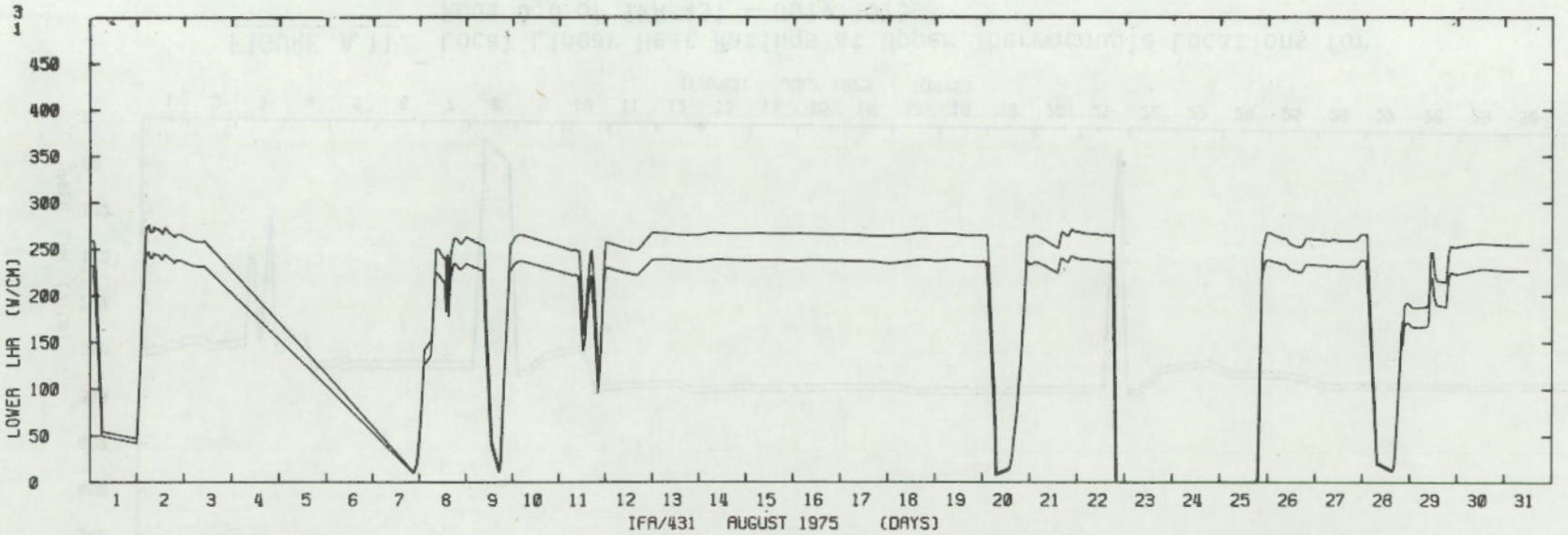

FIGURE A.14. Local Linear Heat Ratings at Lower Thermocouple Locations for Rods 1,3 of IFA 431 - August 1975

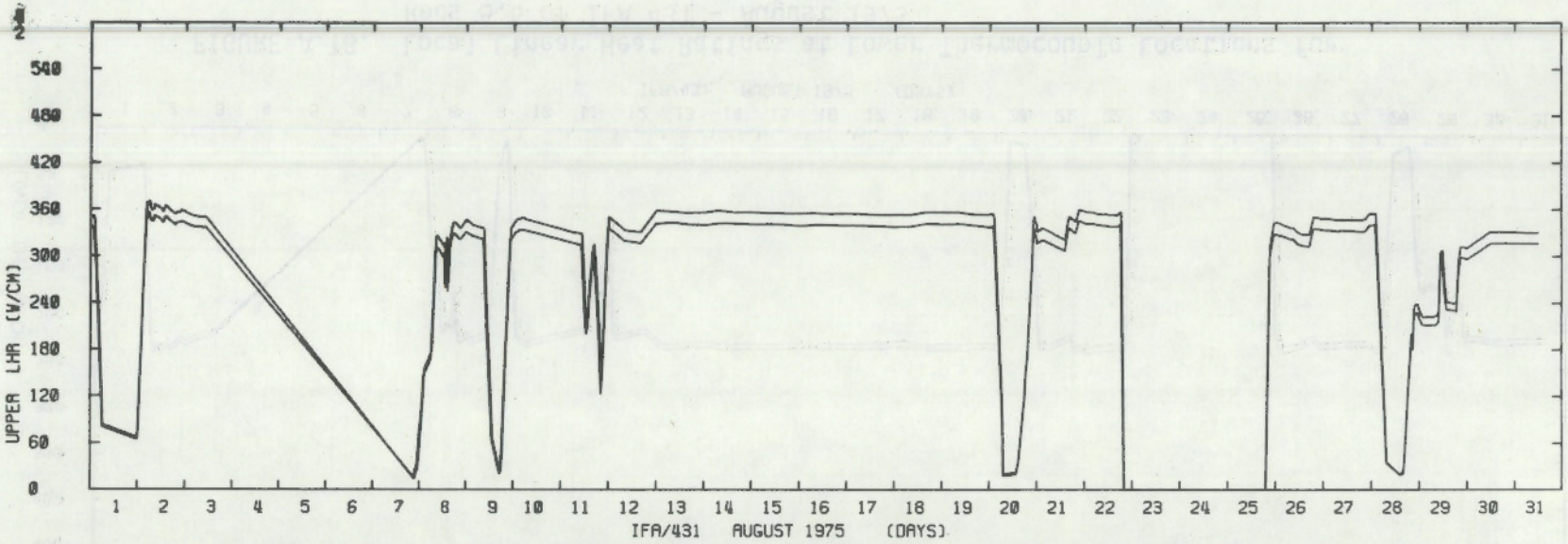

FIGURE A.15. Local Linear Heat Ratings at Upper Thermocouple Locations for Rods 2,4 of IFA 431 - August 1975

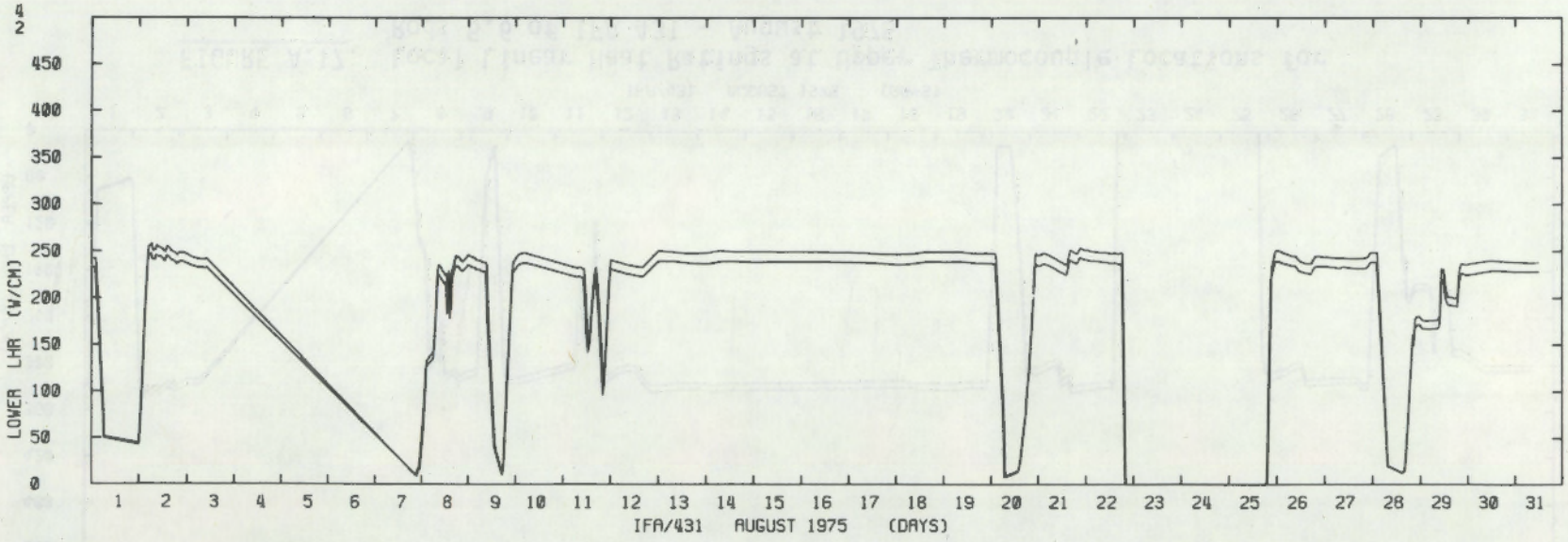

FIGURE A.16. Local Linear Heat Ratings at Lower Thermocouple Locations for Rods 2,4 of IFA 431 - August 1975

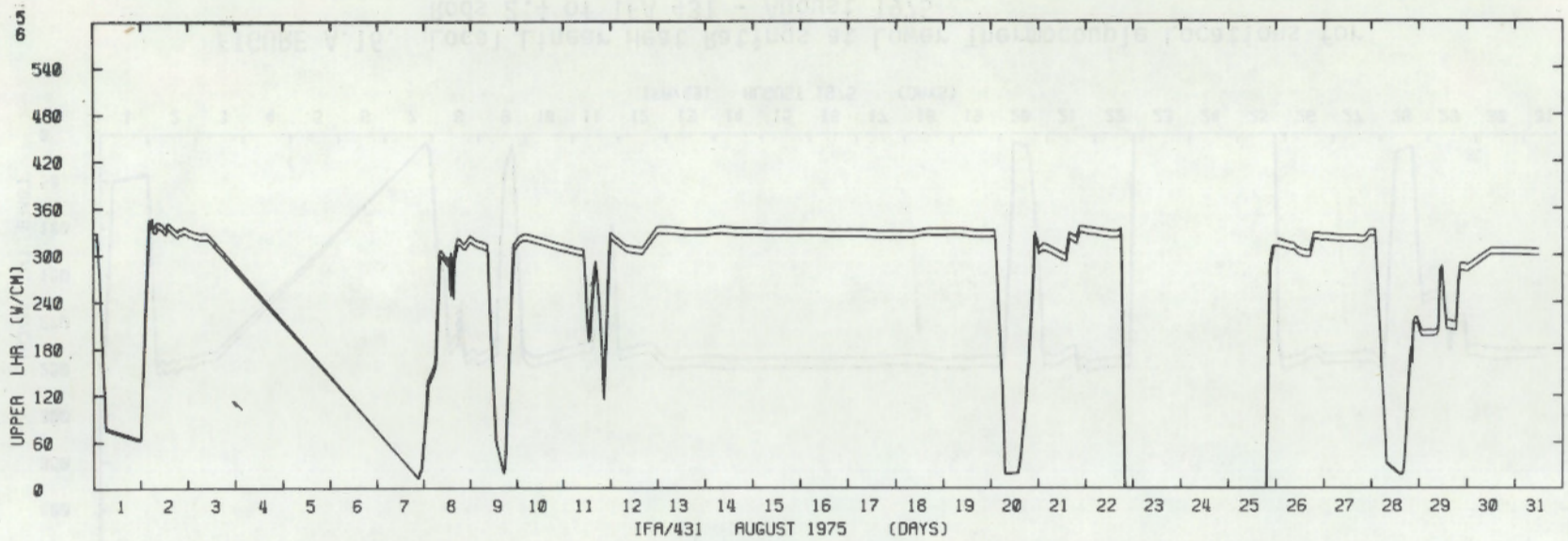

FIGURE A.17. Local Linear Heat Ratings at Upper Thermocouple Locations for Rods 5,6 of IFA 431 - August 1975

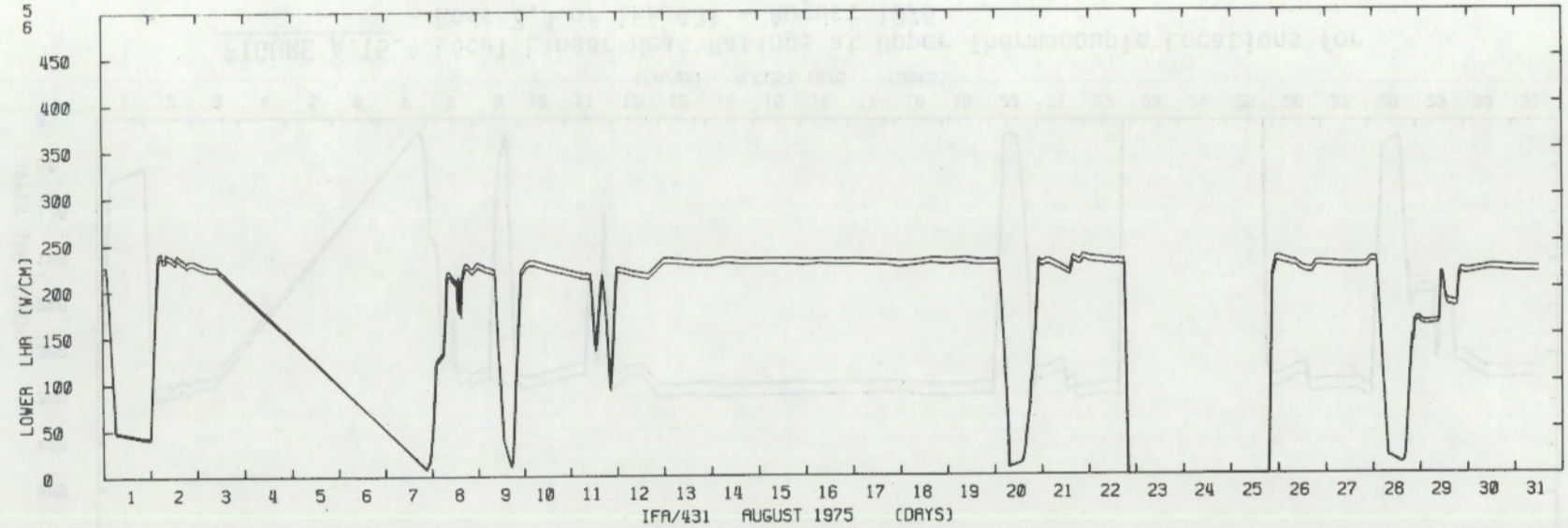

FIGURE A.18. Local Linear Heat Ratings at Lower Thermocouple Locations for Rods 5,6 of IFA 431 - August 1975

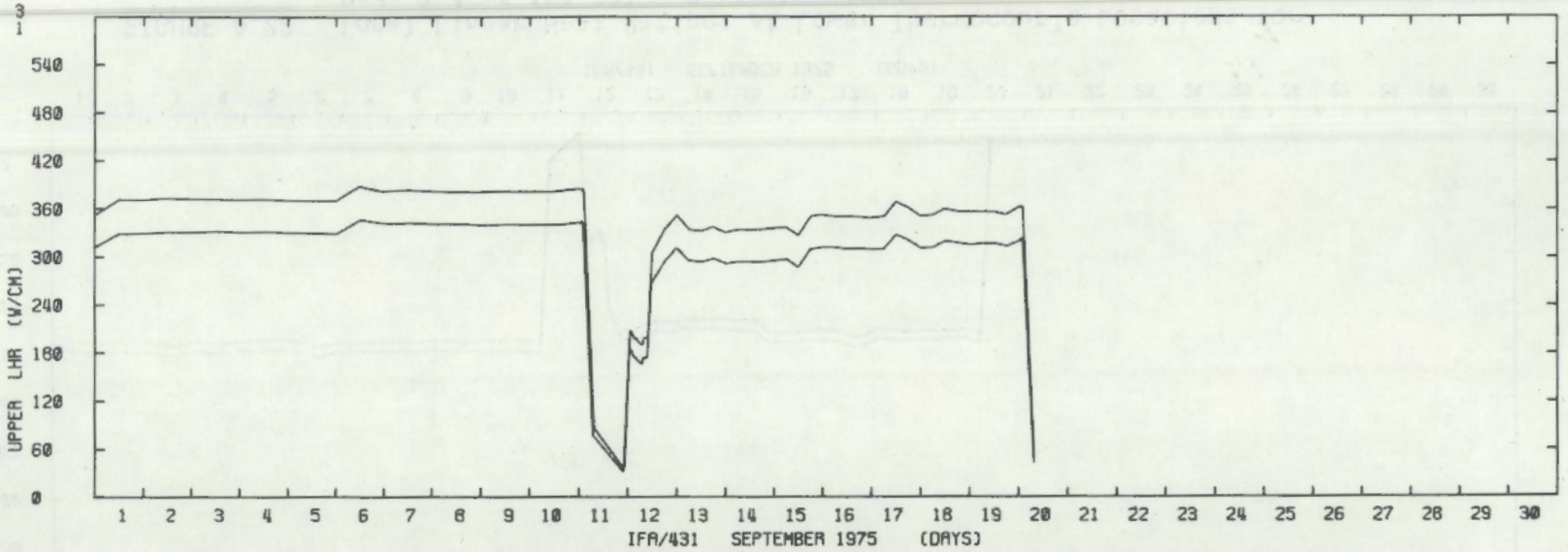

FIGURE A.19. Local Linear Heat Ratings at Upper Thermocouple Locations for Rods 1,3 of IFA 431 - September 1975

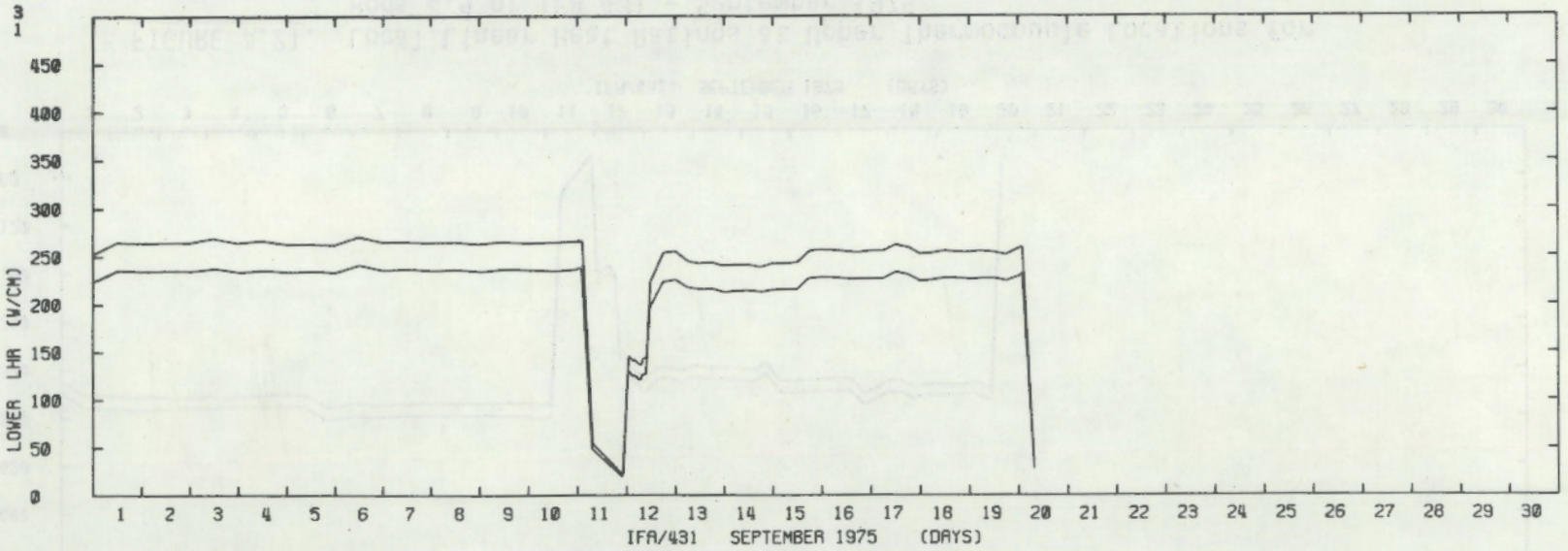

FIGURE A.20. Local Linear Heat Ratings at Lower Thermocouple Locations for Rods 1,3 of IFA 431 - September 1975

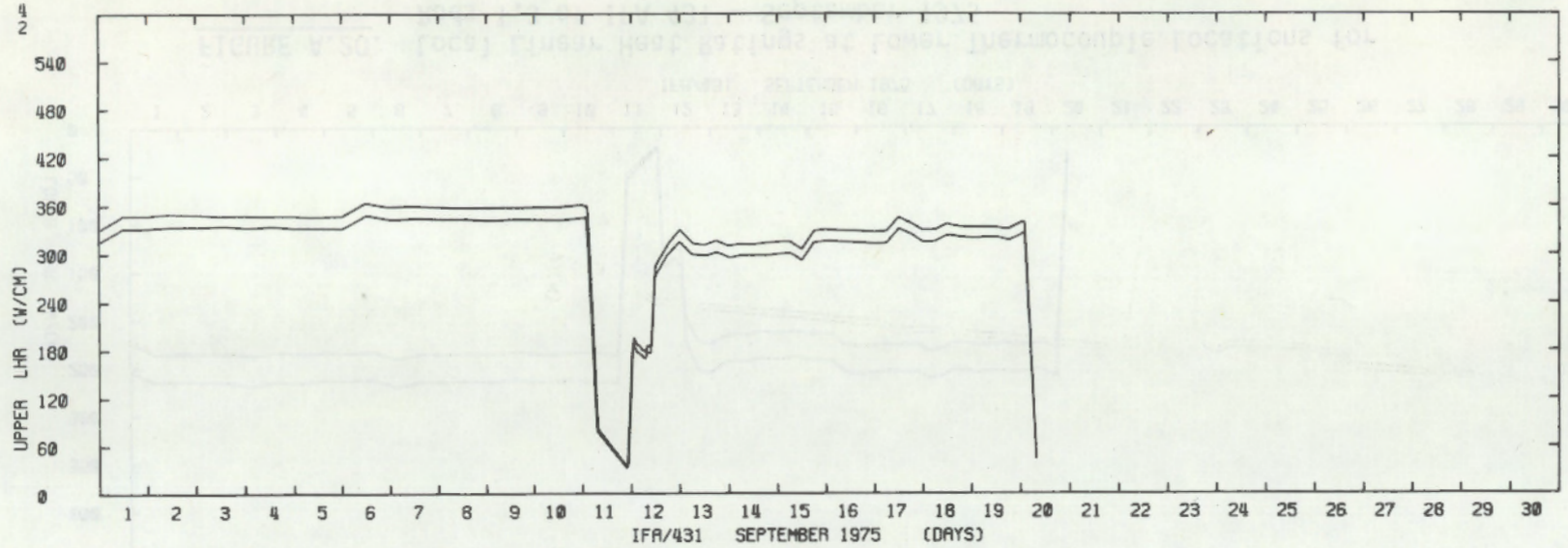

FIGURE A.21. Local Linear Heat Ratings at Upper Thermocouple Locations for Rods 2,4 of IFA 431 - September 1975

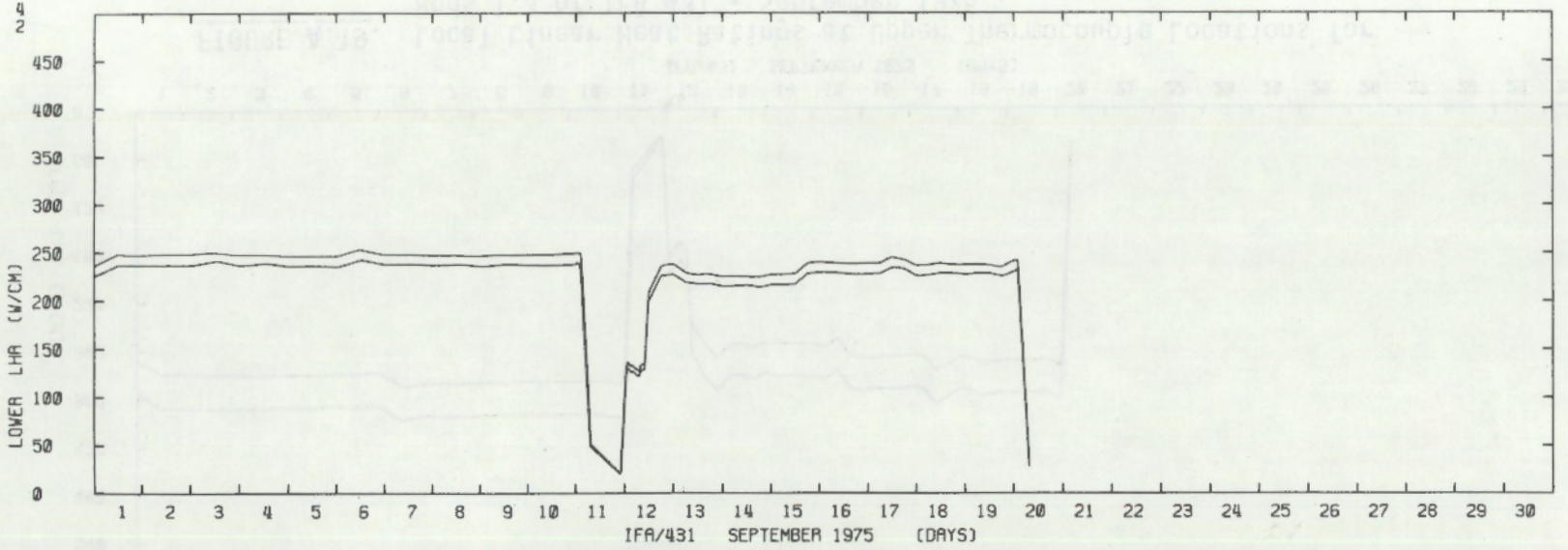

FIGURE A.22. Local Linear Heat Ratings at Lower Thermocouple Locations for Rods 2,4 of IFA 431 - September 1975

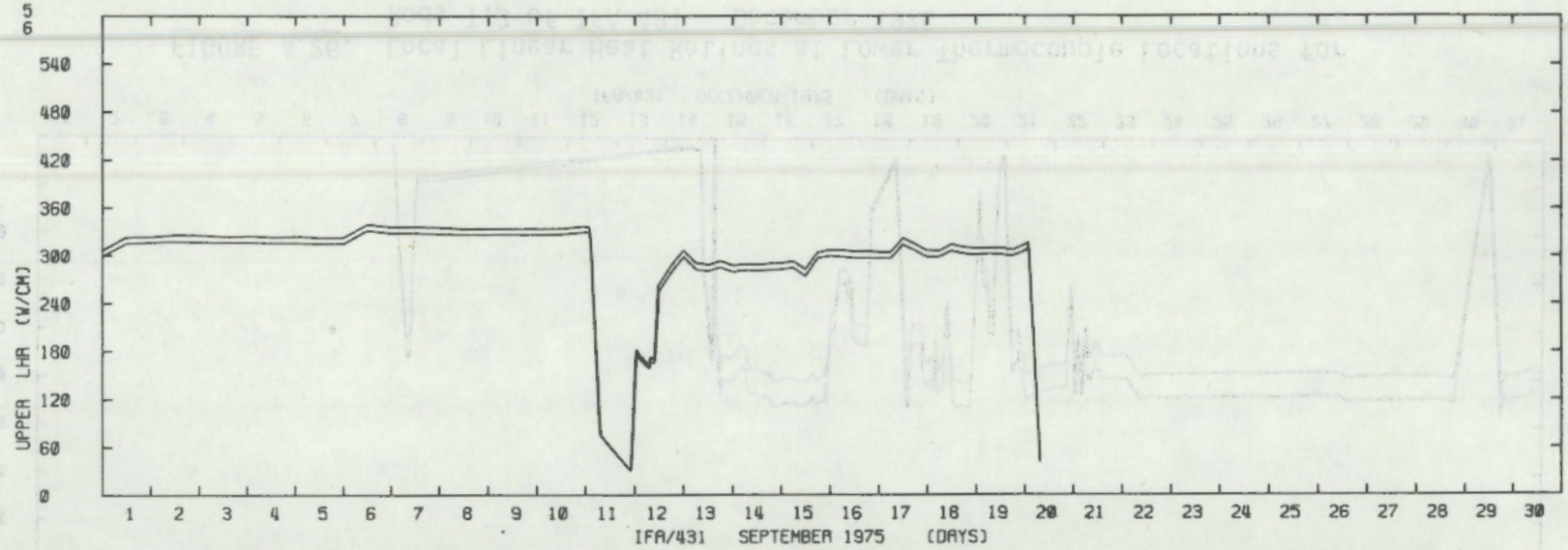

FIGURE A.23. Local Linear Heat Ratings at Upper Thermocouple Locations for Rods 5,6 of IFA 431 - September 1975

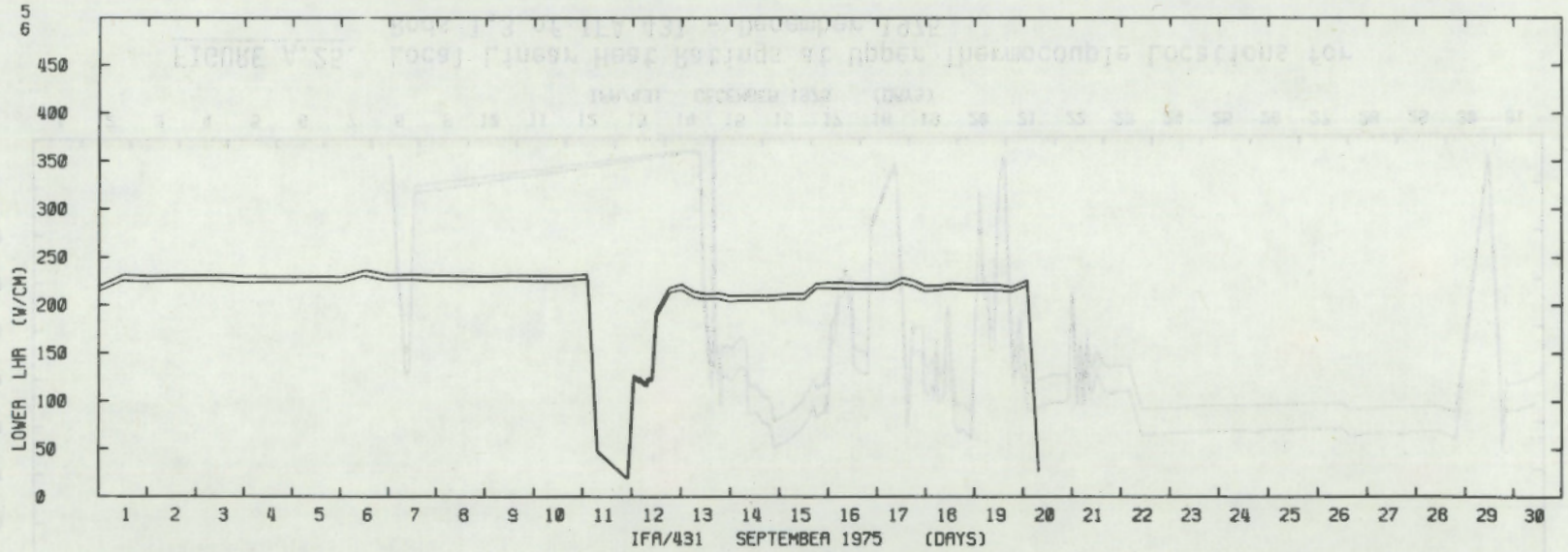

FIGURE A.24. Local Linear Heat Ratings at Lower Thermocouple Locations for Rods 5,6 of IFA 431 - September 1975

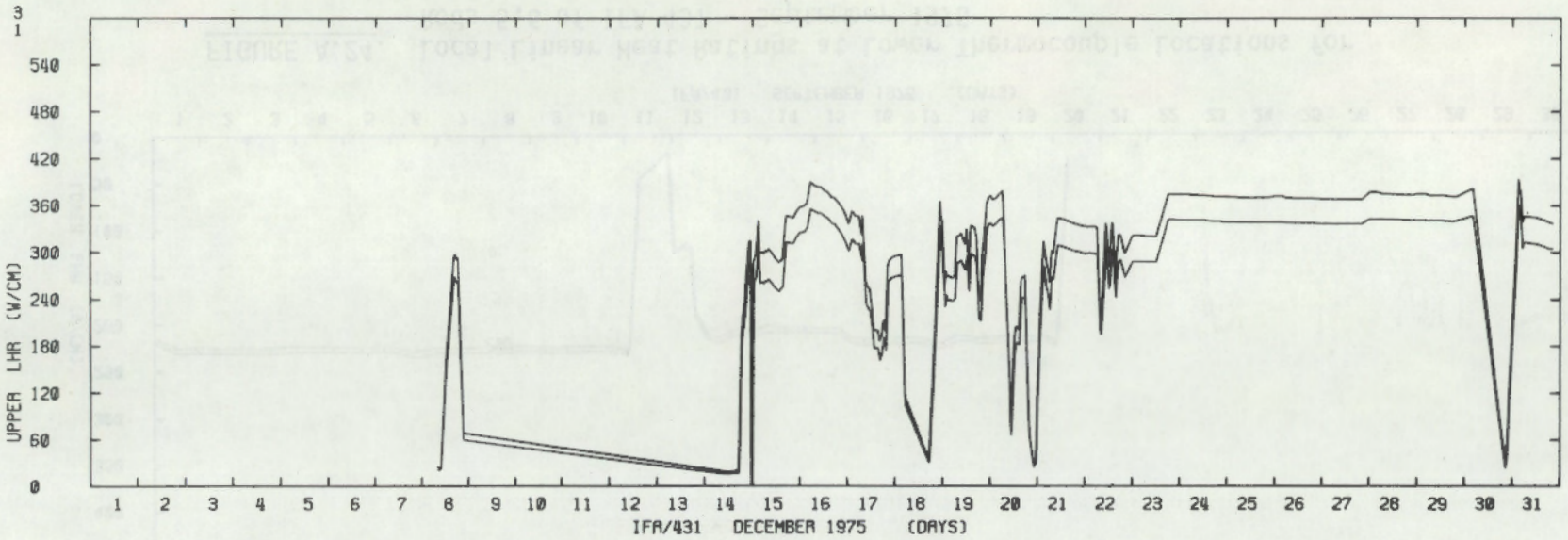

FIGURE A.25. Local Linear Heat Ratings at Upper Thermocouple Locations for Rods 1,3 of IFA 431 - December 1975

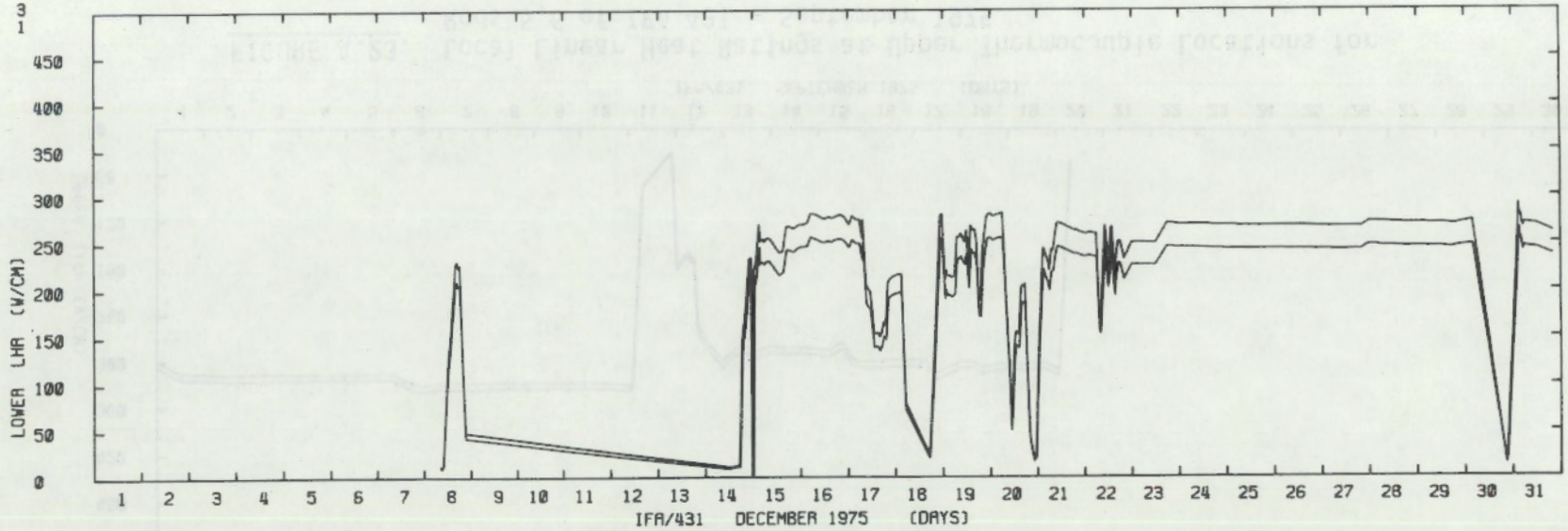

FIGURE A.26. Local Linear Heat Ratings at Lower Thermocouple Locations for Rods 1,3 of IFA 431 - December 1975

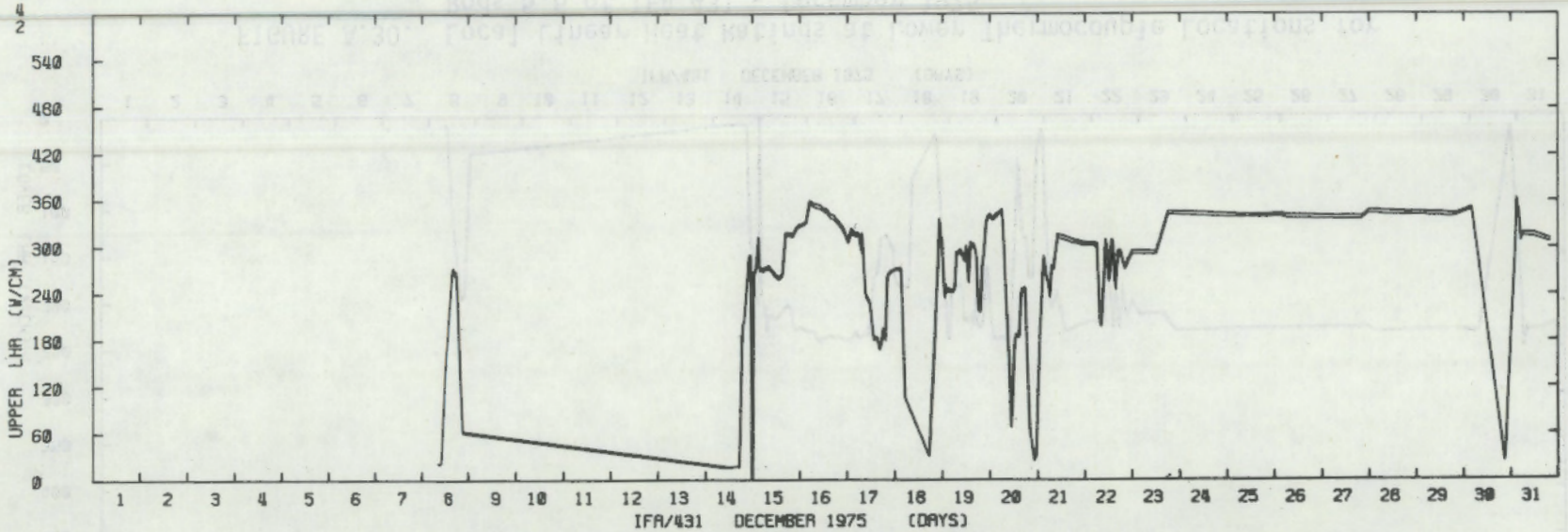

FIGURE A.27. Local Linear Heat Ratings at Upper Thermocouple Locations for Rods 2,4 of IFA 431 - December 1975

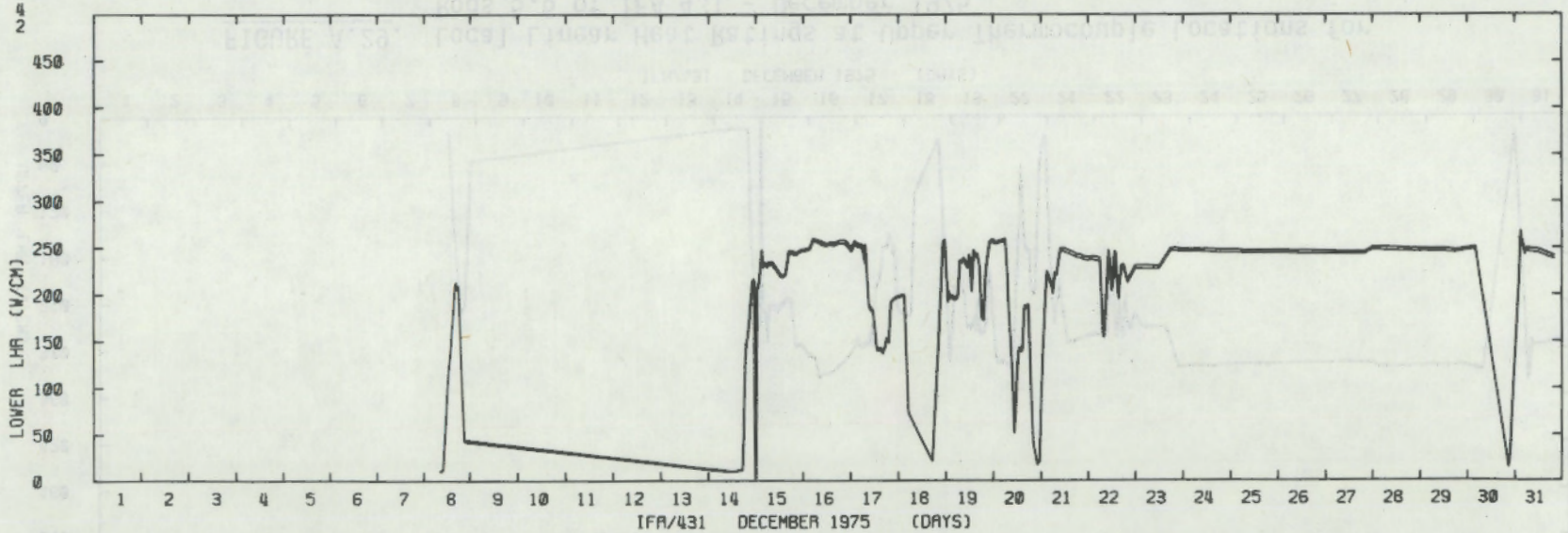

FIGURE A.28. Local Linear Heat Ratings at Lower Thermocouple Locations for Rods 2,4 of IFA 431 - December 1975

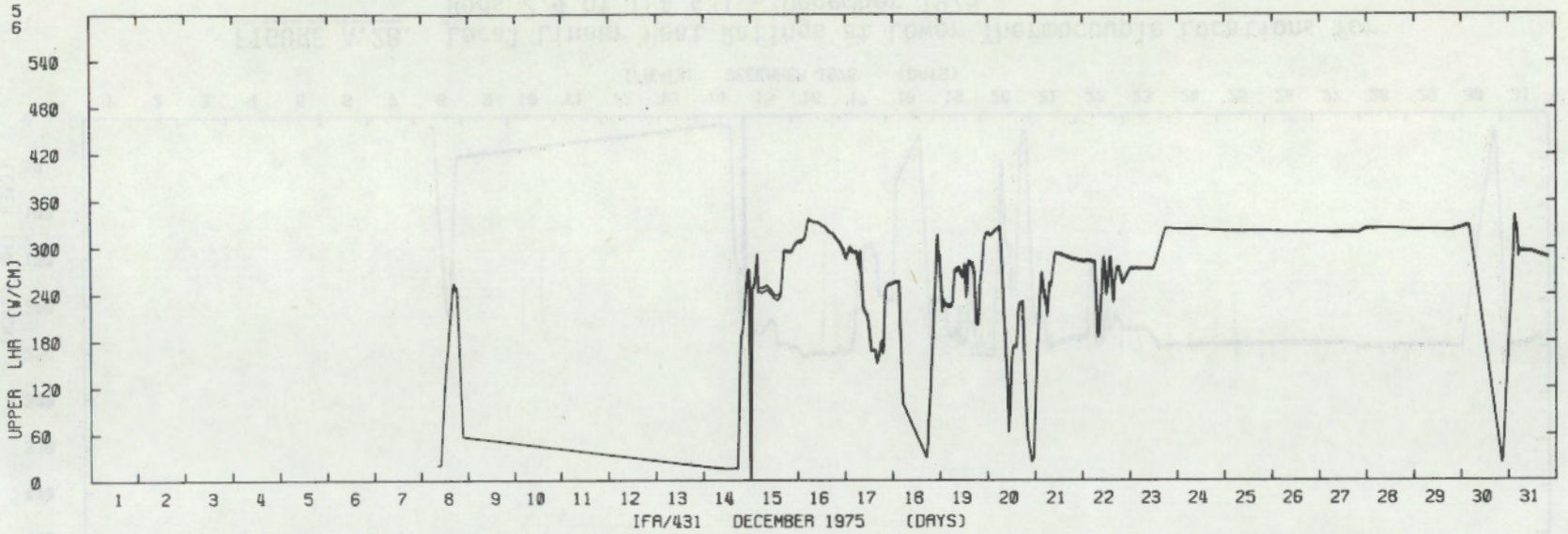

FIGURE A.29. Local Linear Heat Ratings at Upper Thermocouple Locations for Rods 5,6 of IFA 431 - December 1975

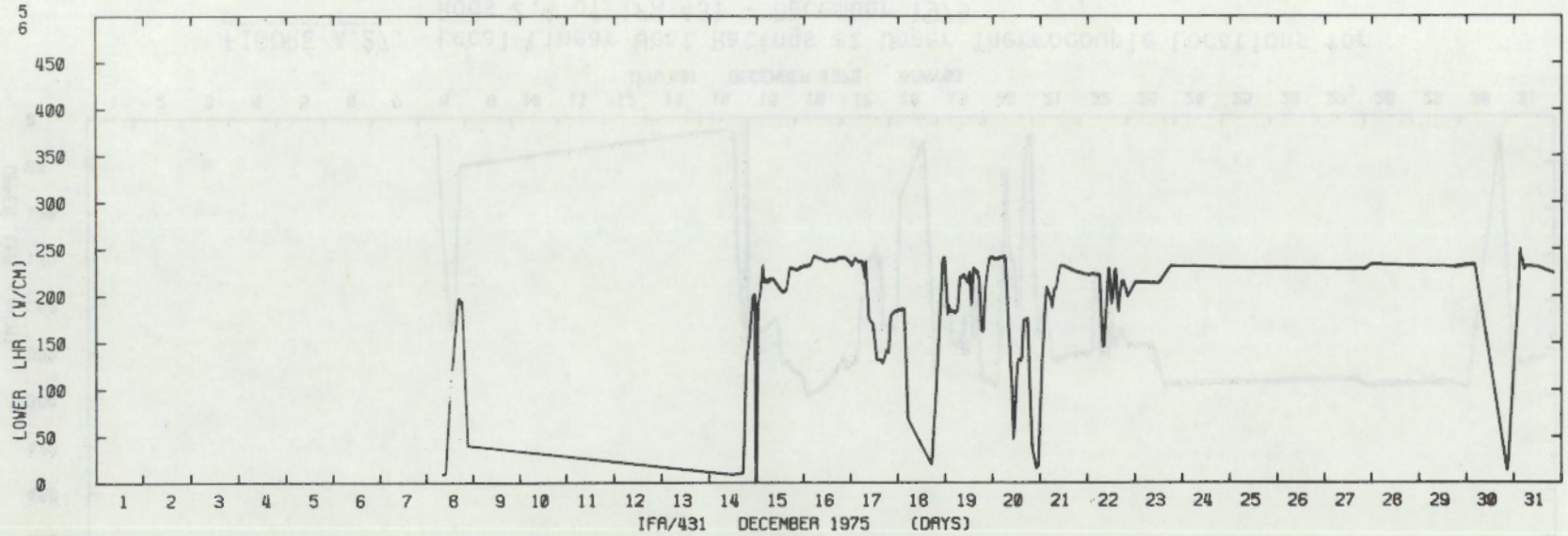

FIGURE A.30. Local Linear Heat Ratings at Lower Thermocouple Locations for Rods 5,6 of IFA 431 - December 1975

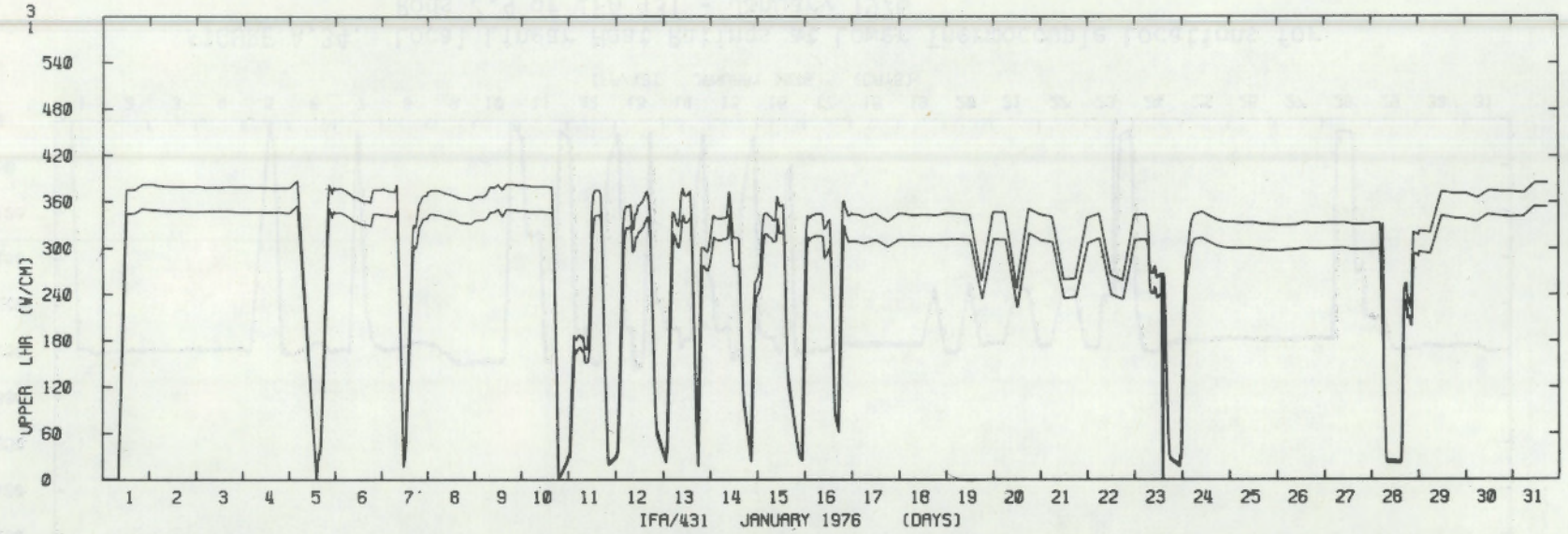

FIGURE A.31. Local Linear Heat Ratings at Upper Thermocouple Locations for Rods 1,3 of IFA 431 - January 1976

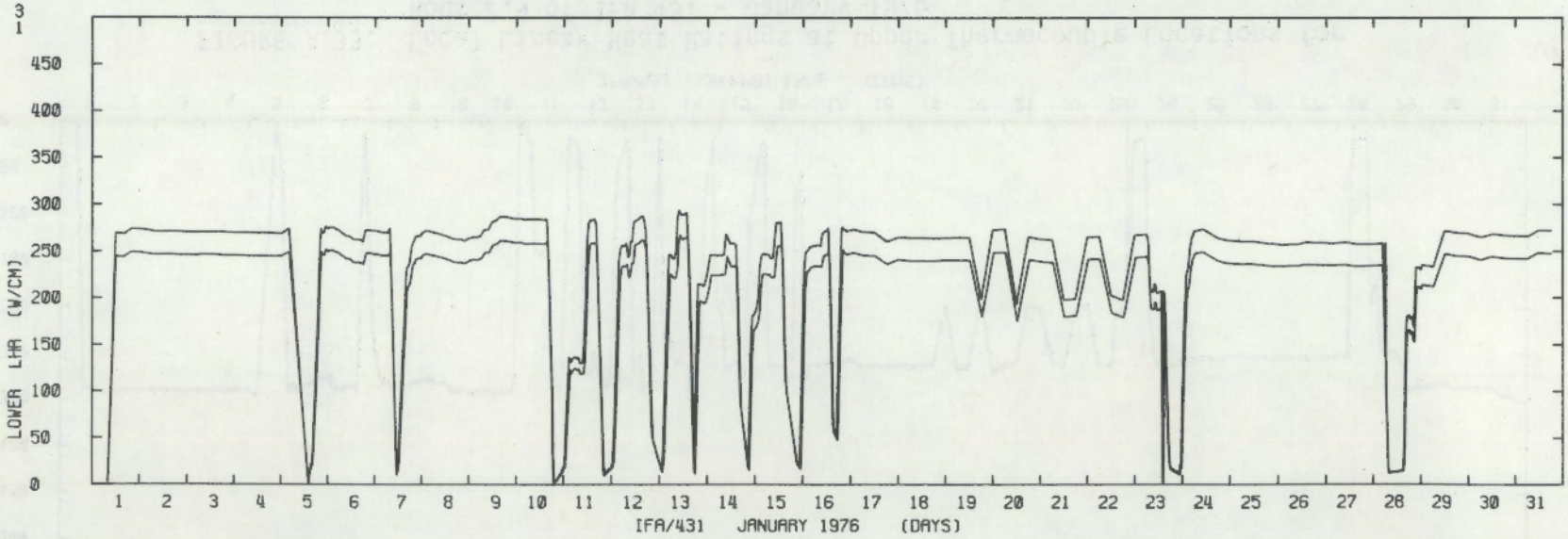

FIGURE A.32. Local Linear Heat Ratings at Lower Thermocouple Locations for Rods 1,3 of IFA 431 - January 1976

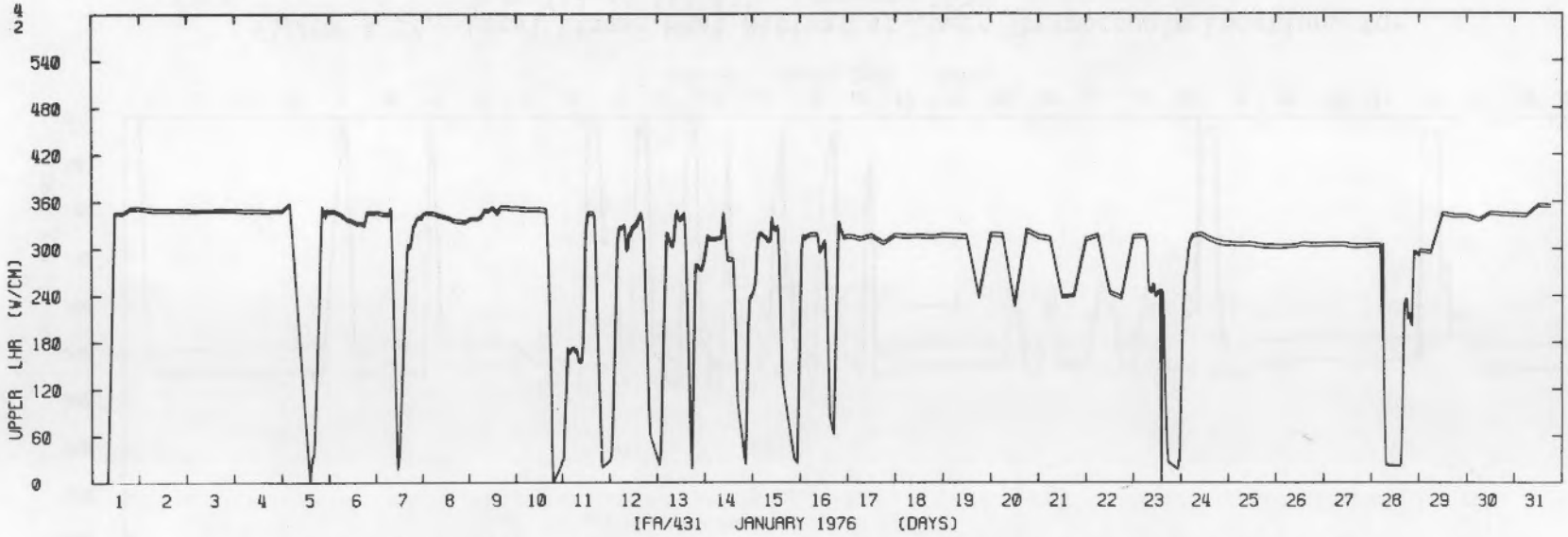

FIGURE A.33. Local Linear Heat Ratings at Upper Thermocouple Locations for Rods 2,4 of IFA 431 - January 1976

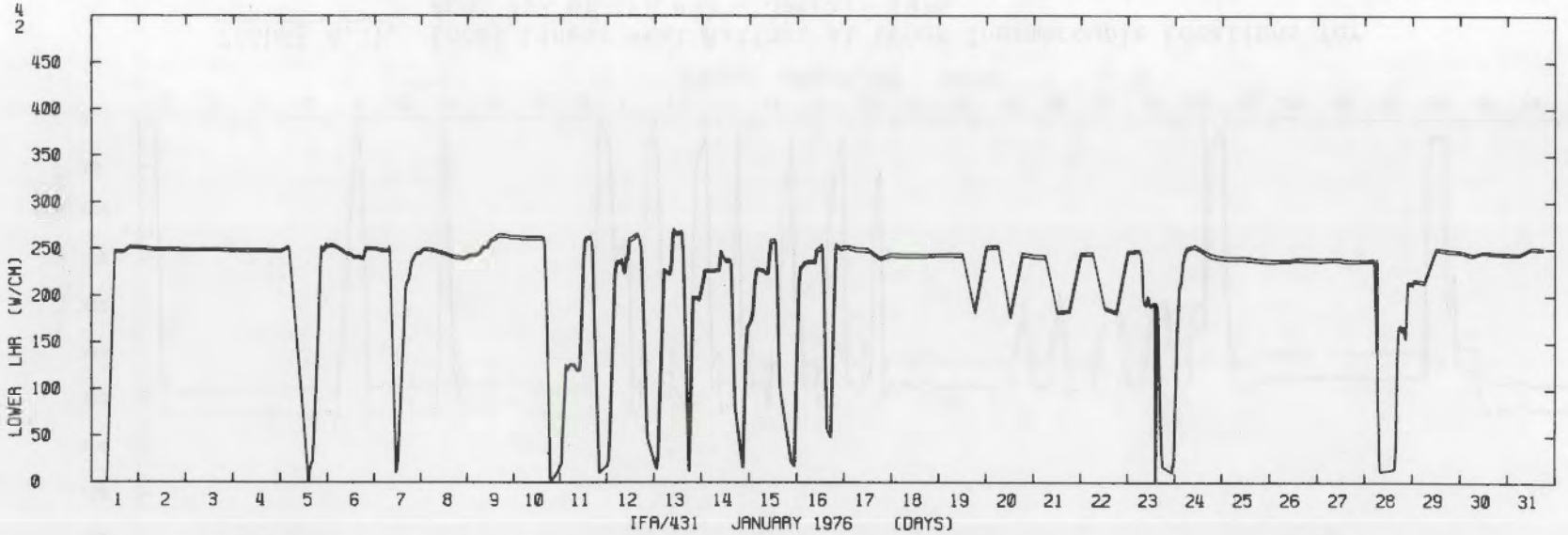

FIGURE A.34. Local Linear Heat Ratings at Lower Thermocouple Locations for Rods 2,4 of IFA 431 - January 1976

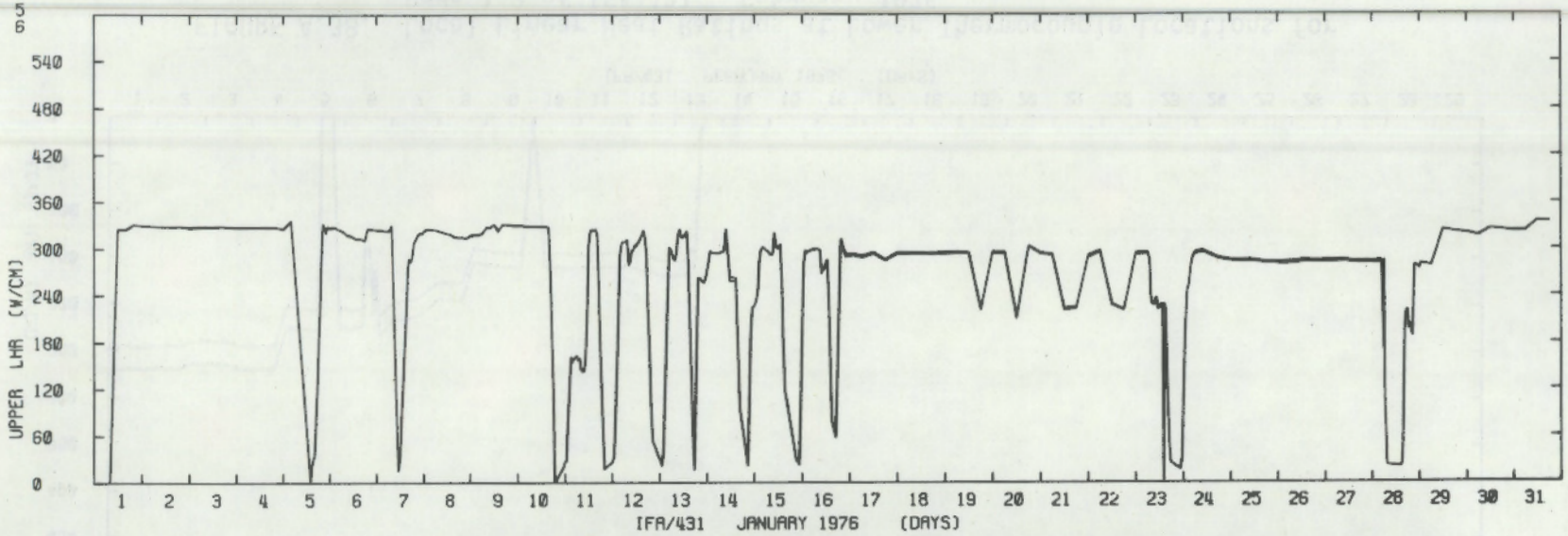

FIGURE A.35. Local Linear Heat Ratings at Upper Thermocouple Locations for Rods 5,6 of IFA 431 - January 1976

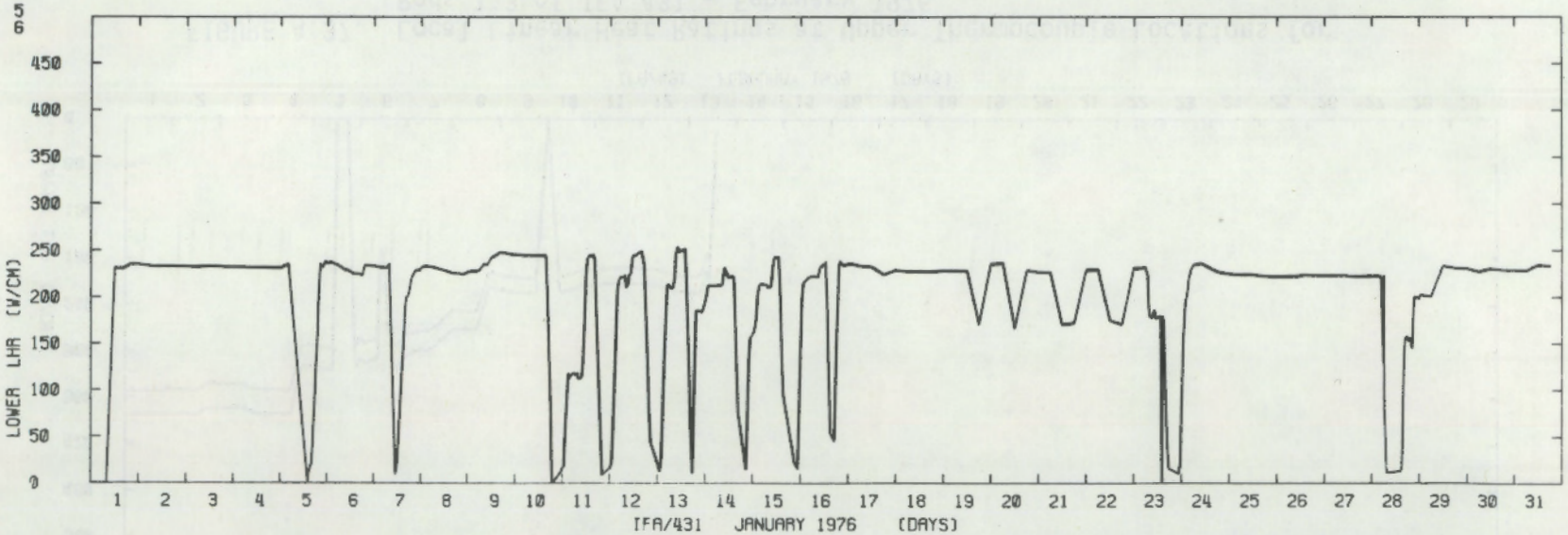

FIGURE A.36. Local Linear Heat Ratings at Lower Thermocouple Locations for Rods 5,6 of IFA 431 - January 1976

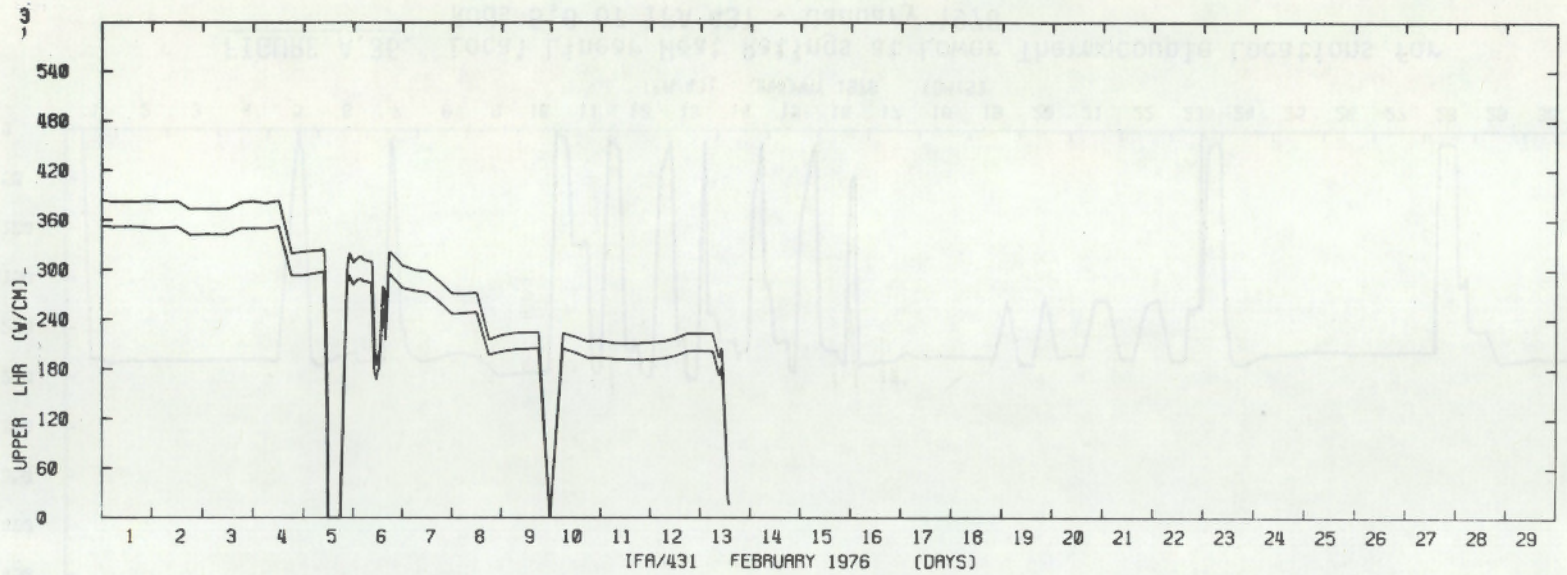

FIGURE A.37. Local Linear Heat Ratings at Upper Thermocouple Locations for Rods 1,3 of IFA 431 - February 1976

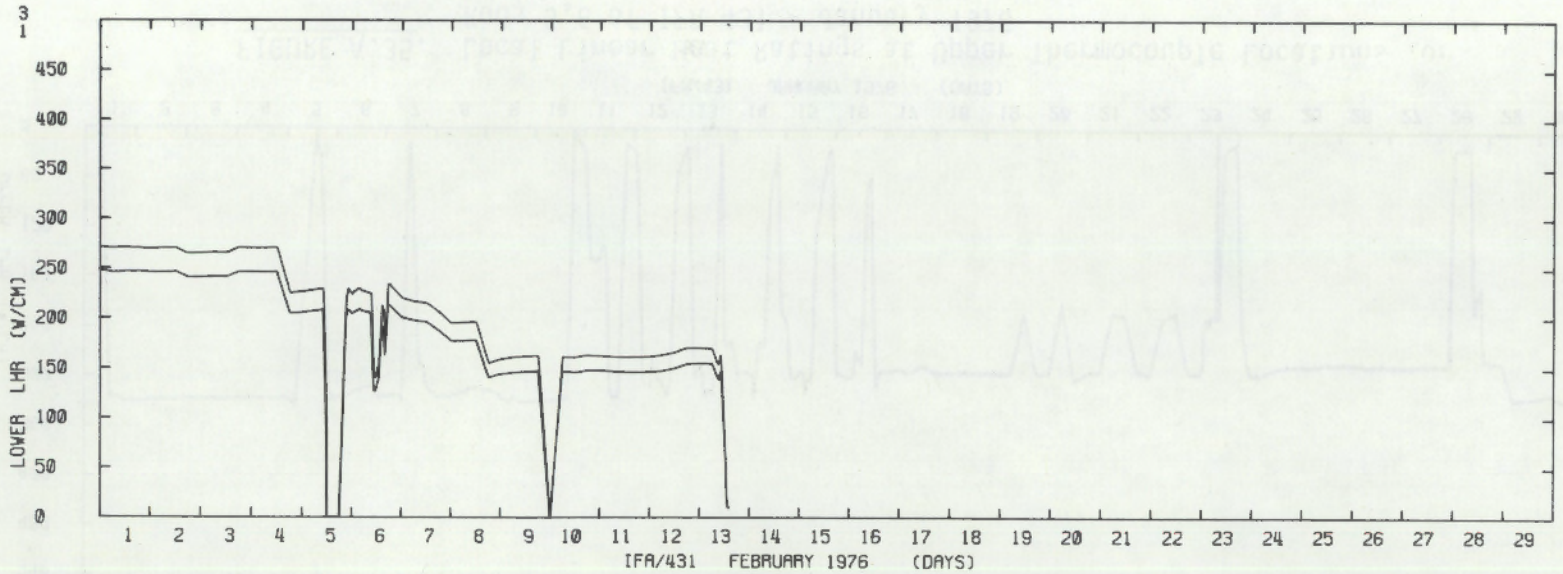

FIGURE A.38. Local Linear Heat Ratings at Lower Thermocouple Locations for Rods 1,3 of IFA 431 - February 1976

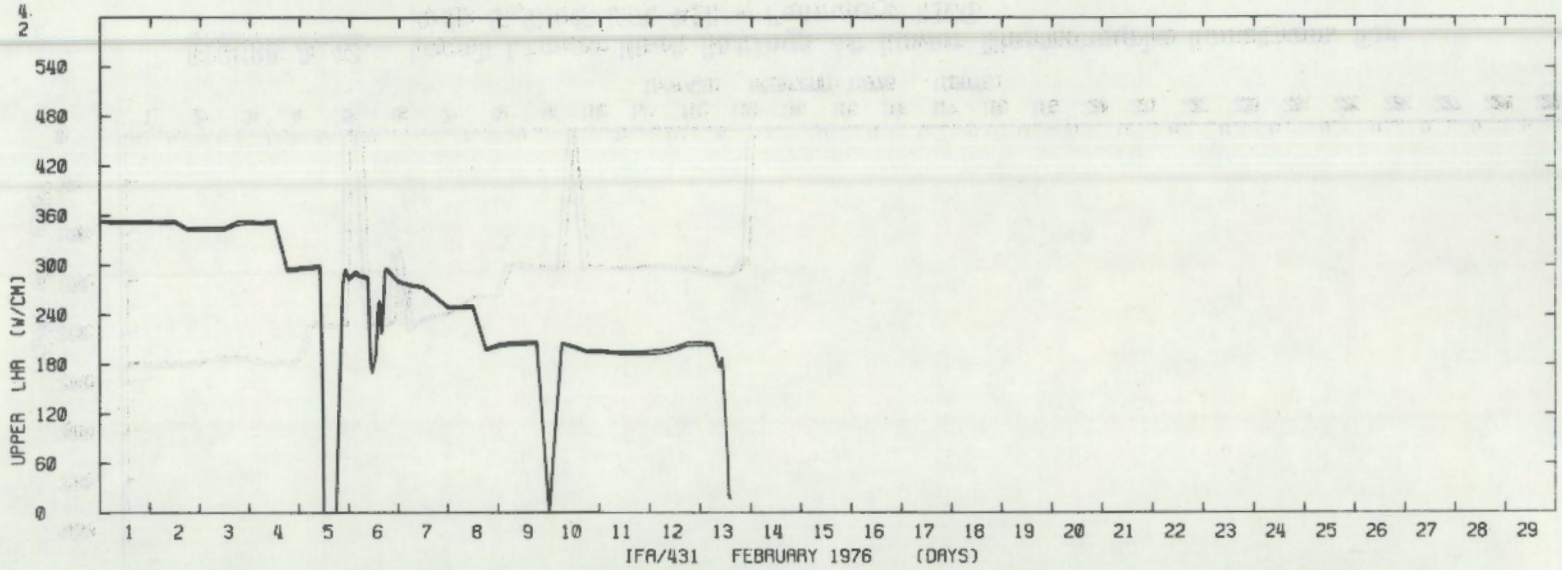

FIGURE A.39. Local Linear Heat Ratings at Upper Thermocouple Locations for Rods 2,4 of IFA 431 - February 1976

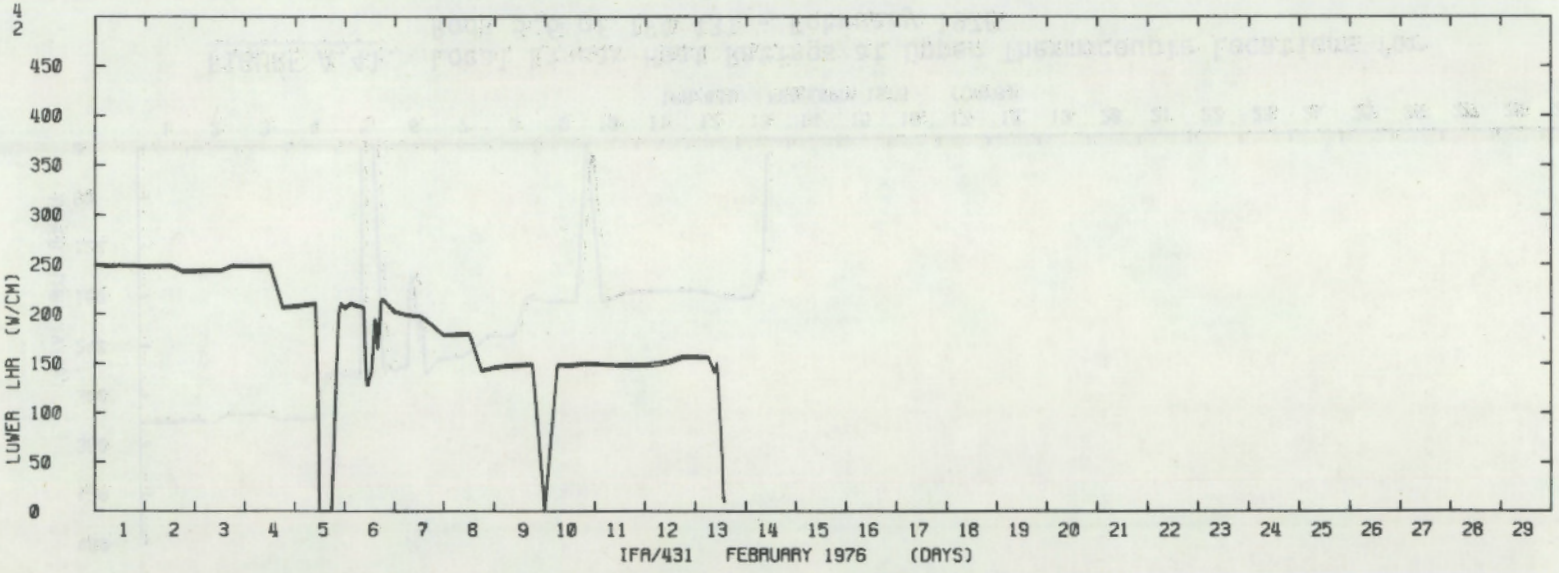

FIGURE A.40. Local Linear Heat Ratings at Lower Thermocouple Locations for Rods 2,4 of IFA 431 - February 1976

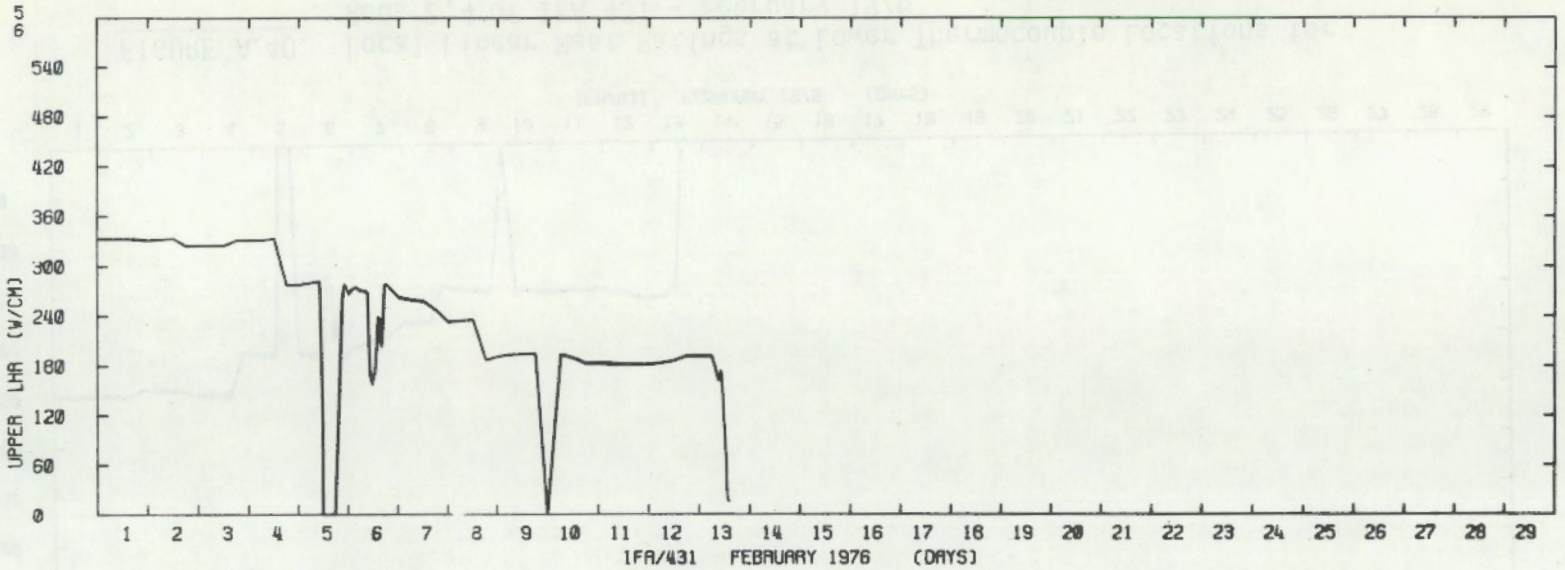

FIGURE A.41. Local Linear Heat Ratings at Upper Thermocouple Locations for Rods 5,6 of IFA 431 - February 1976

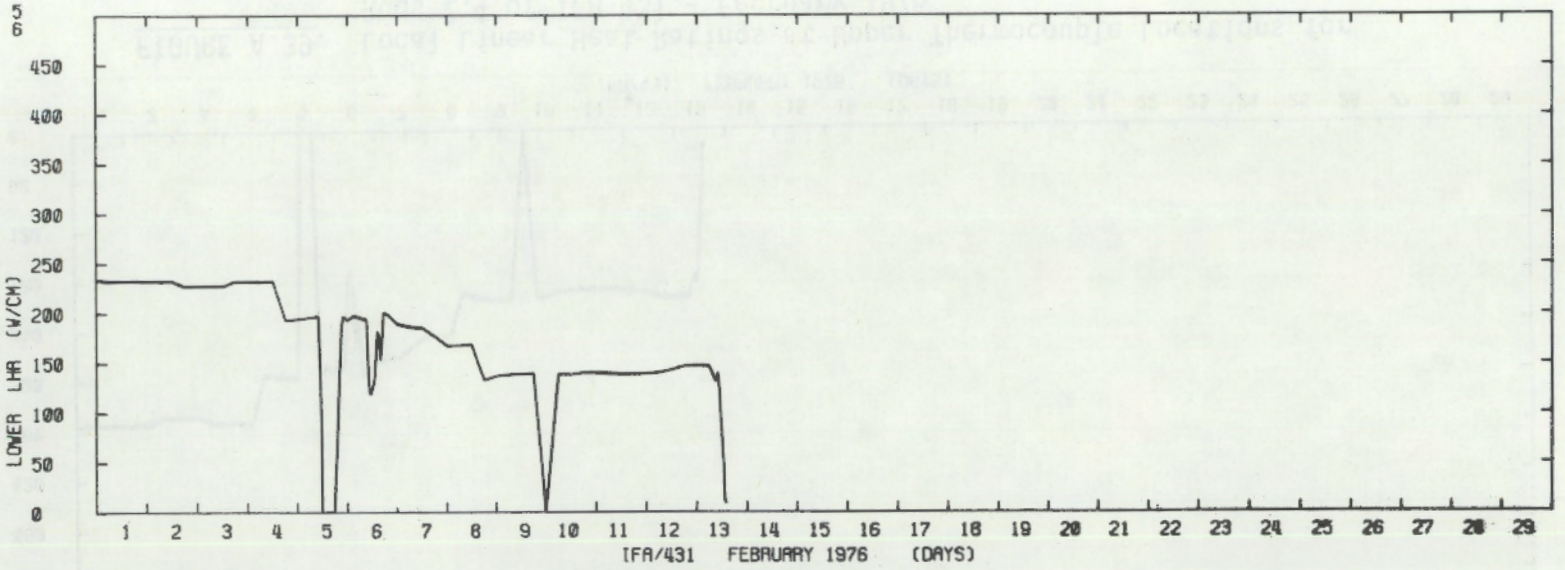

FIGURE A.42. Local Linear Heat Ratings at Lower Thermocouple Locations for Rods 5,6 of IFA 431 - February 1976

APPENDIX B

FUEL TEMPERATURE HISTORIES

FUEL TEMPERATURE HISTORIES

The fuel centerline temperature for the upper and lower themocouple locations was plotted versus time by months. These plots are included as Figures B-1 through B-42. This data was collected (on the Halden IBM/1800 on-line computer data acquisition system) from all six IFA-431 rods using W 5% Re/W 26% Re sheathed, grounded thermocouples. As in Appendix A, the rod number is in the upper left hand corner of each figure. The relative position of the rod number on each figure corresponds to the relative position of the curve.

Note that there are some anomalies between the upper and lower thermocouples in the same rod. This suggests that the fuel at one end of the rod may be relatively decoupled from the fuel at the other end.

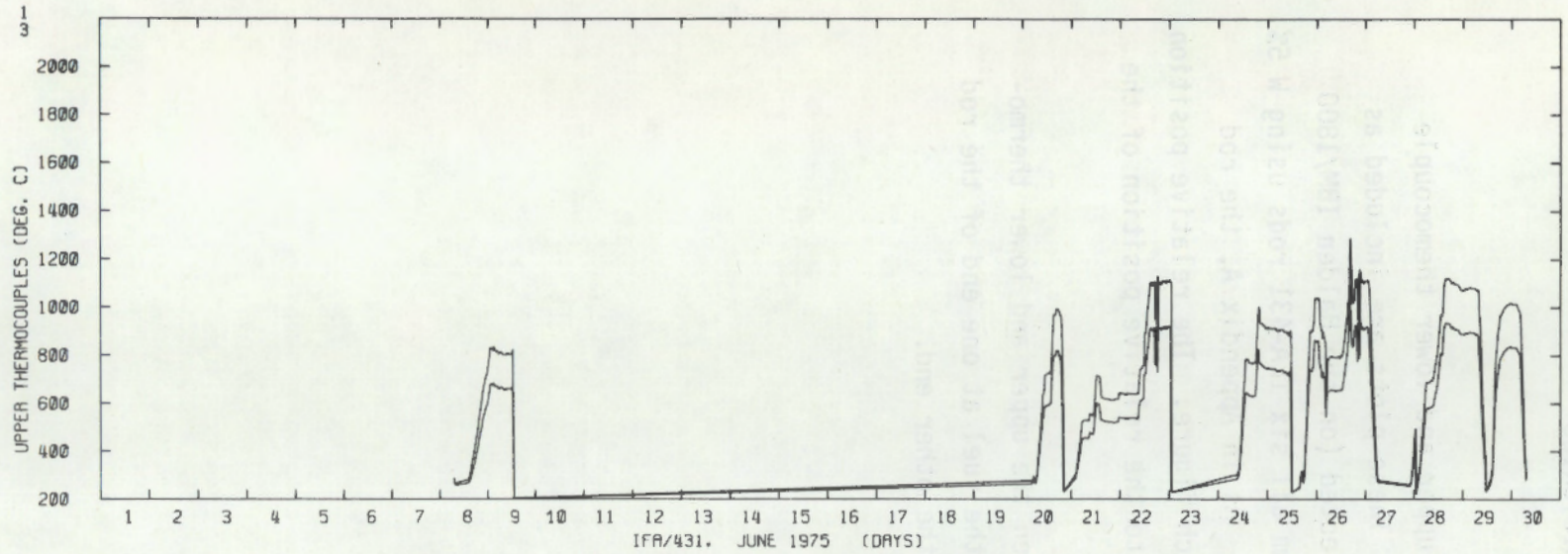

FIGURE B.1. Upper Thermocouple Readings for Rods 1,3 of IFA 431 - June 1975

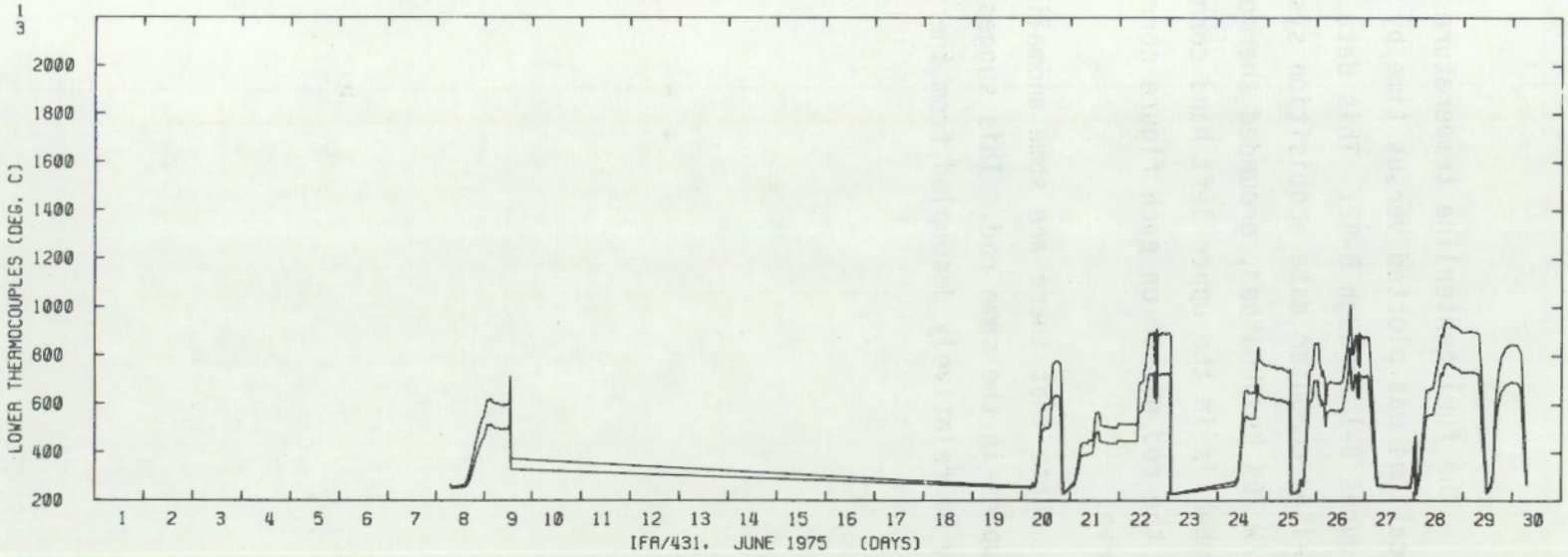

FIGURE B.2. Lower Thermocouple Readings for Rods 1,3 of IFA 431 - June 1975

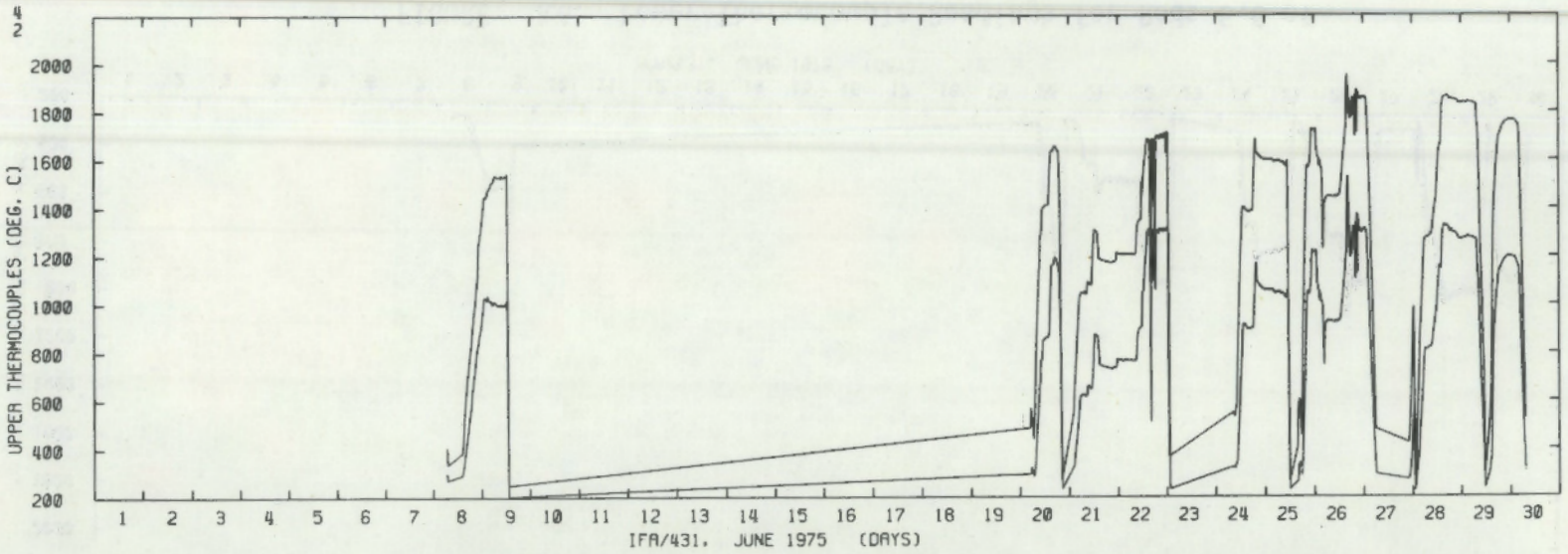

FIGURE B.3. Upper Thermocouple Readings for Rods 2,4 of IFA 431 - June 1975

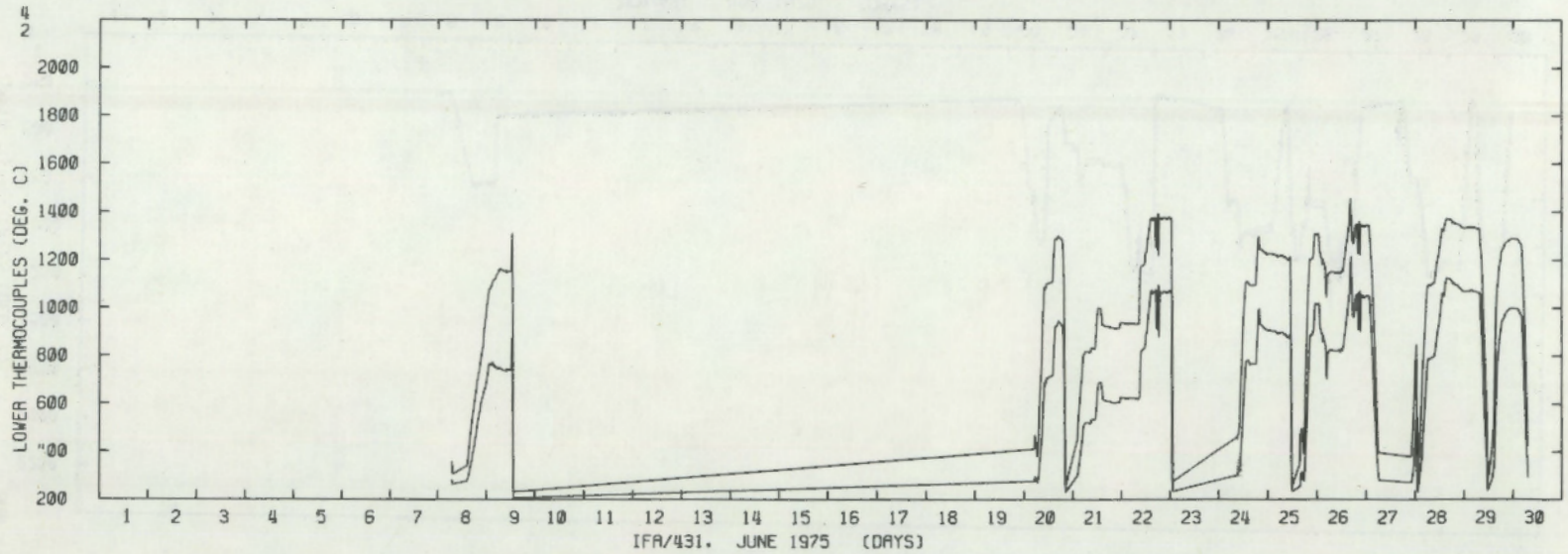

FIGURE B.4. Lower Thermocouple Readings for Rods 2,4 of IFA 431 - June 1975

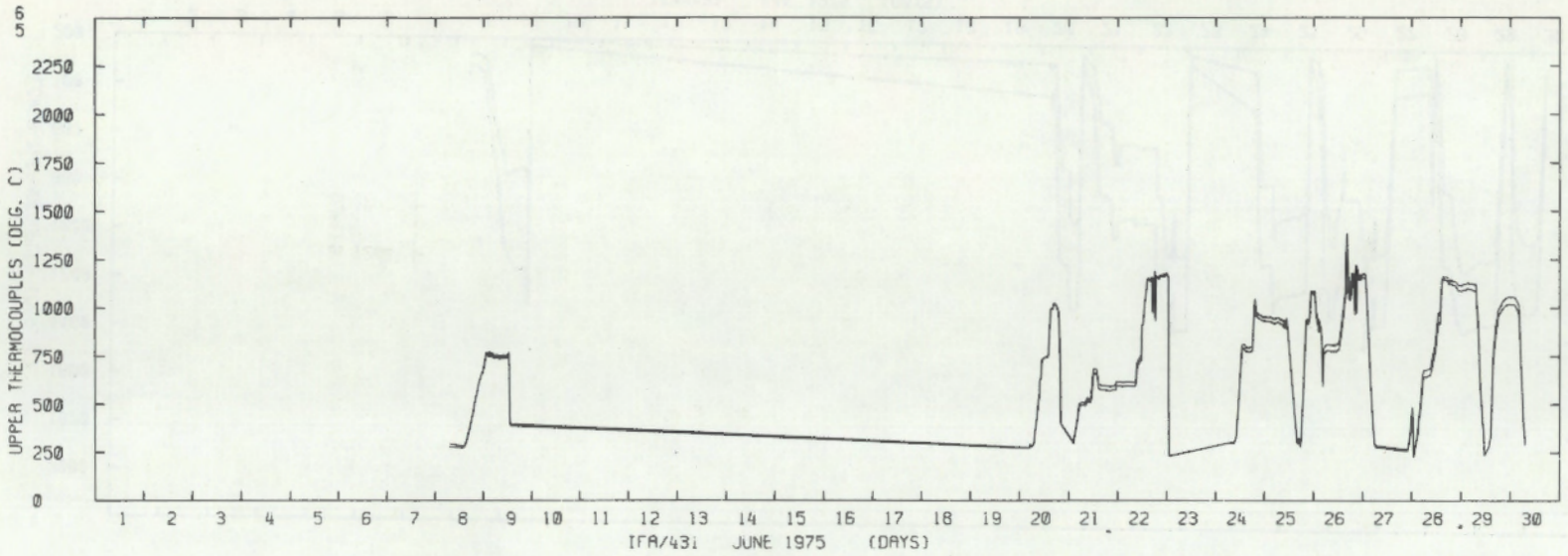

FIGURE B.5. Upper Thermocouple Readings for Rods 5,6 of IFA 431 - June 1975

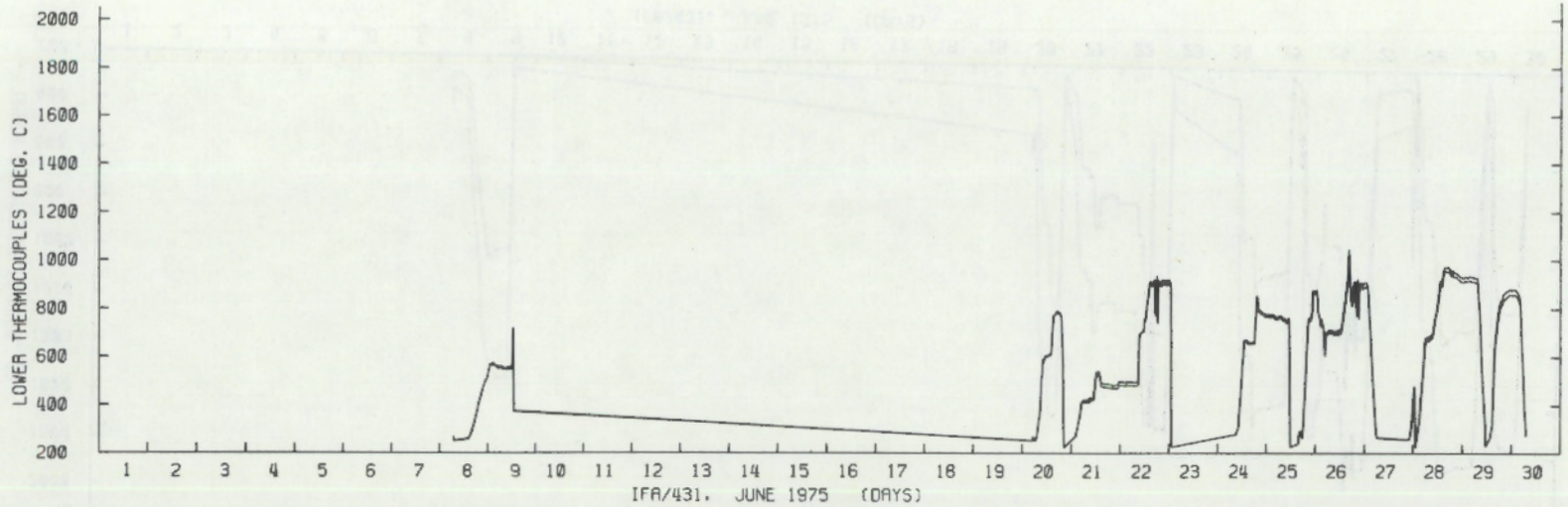

FIGURE B.6. Lower Thermocouple Readings for Rods 5,6 of IFA 431 - June 1975

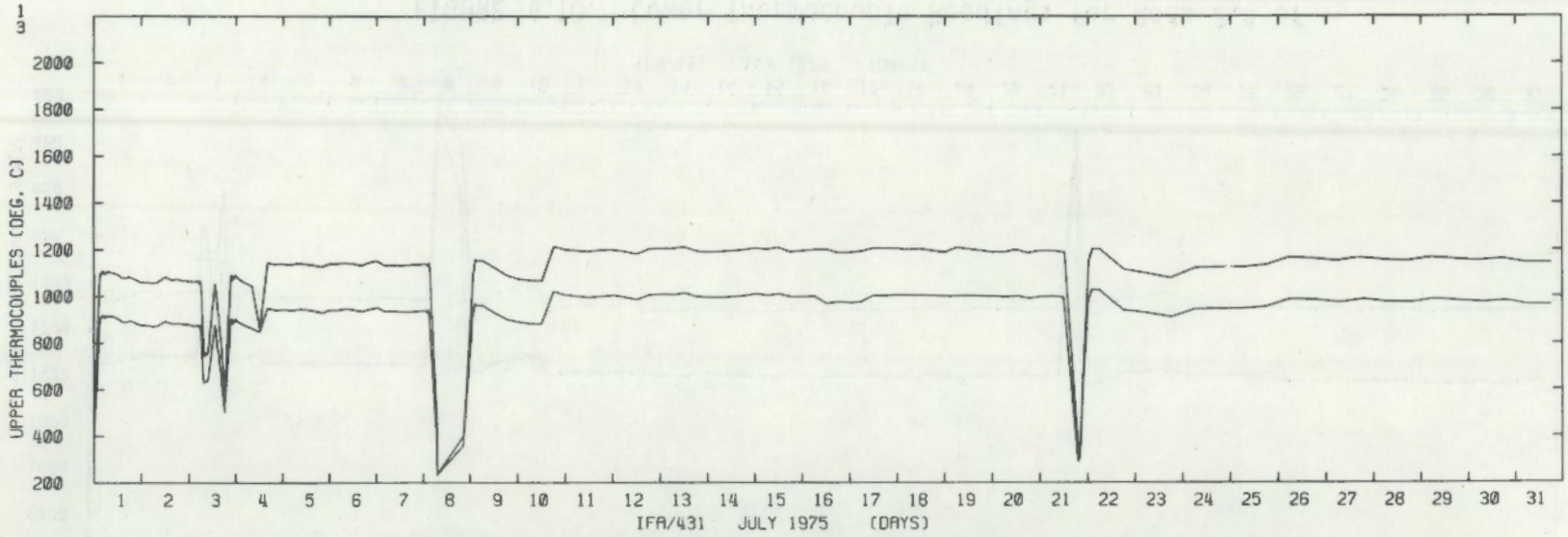

FIGURE B.7. Upper Thermocouple Readings for Rods 1,3 of IFA 431 - July 1975

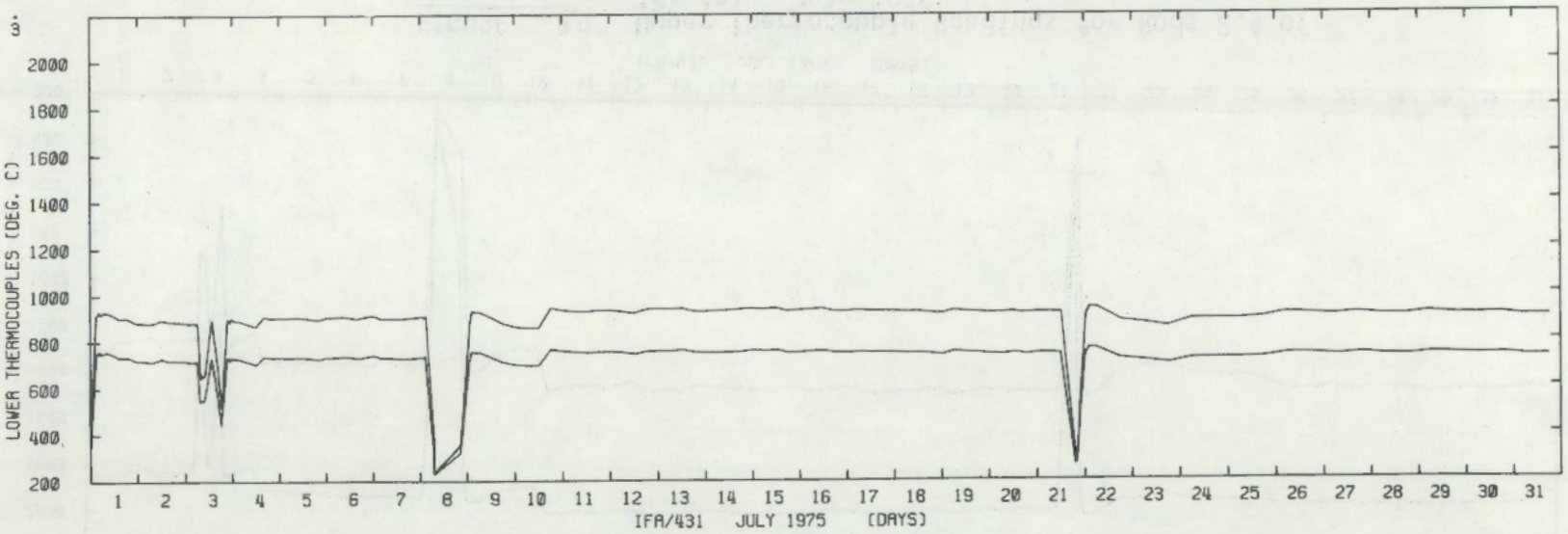

FIGURE B.8. Lower Thermocouple Readings for Rods 1,3 of IFA 431 - July 1975

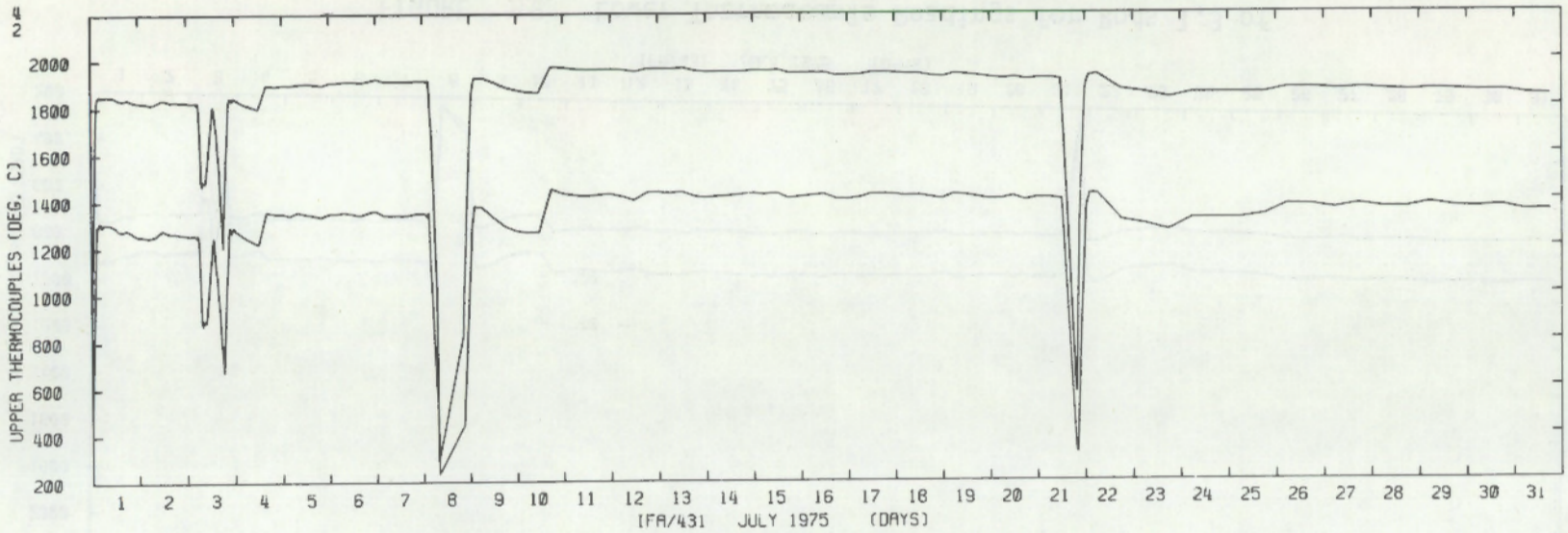

FIGURE B.9. Upper Thermocouple Readings for Rods 2,4 of IFA 431 - July 1975

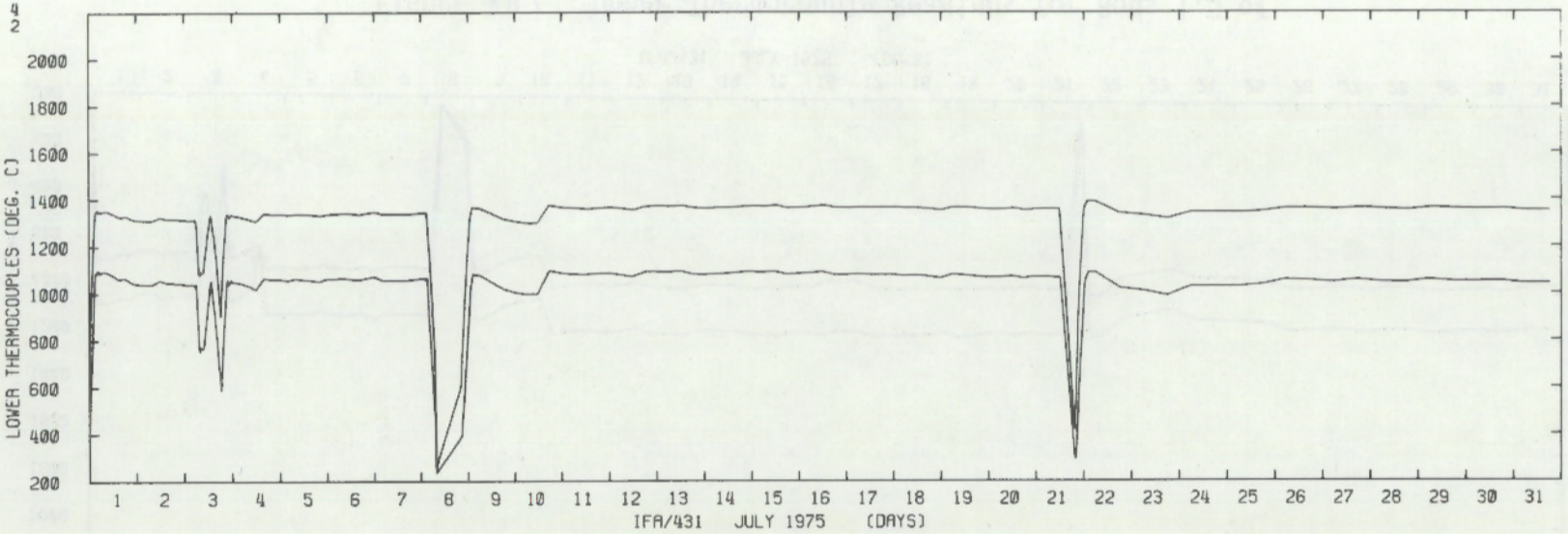

FIGURE B.10. Lower Thermocouple Readings for Rods 2,4 of IFA 431 - July 1975

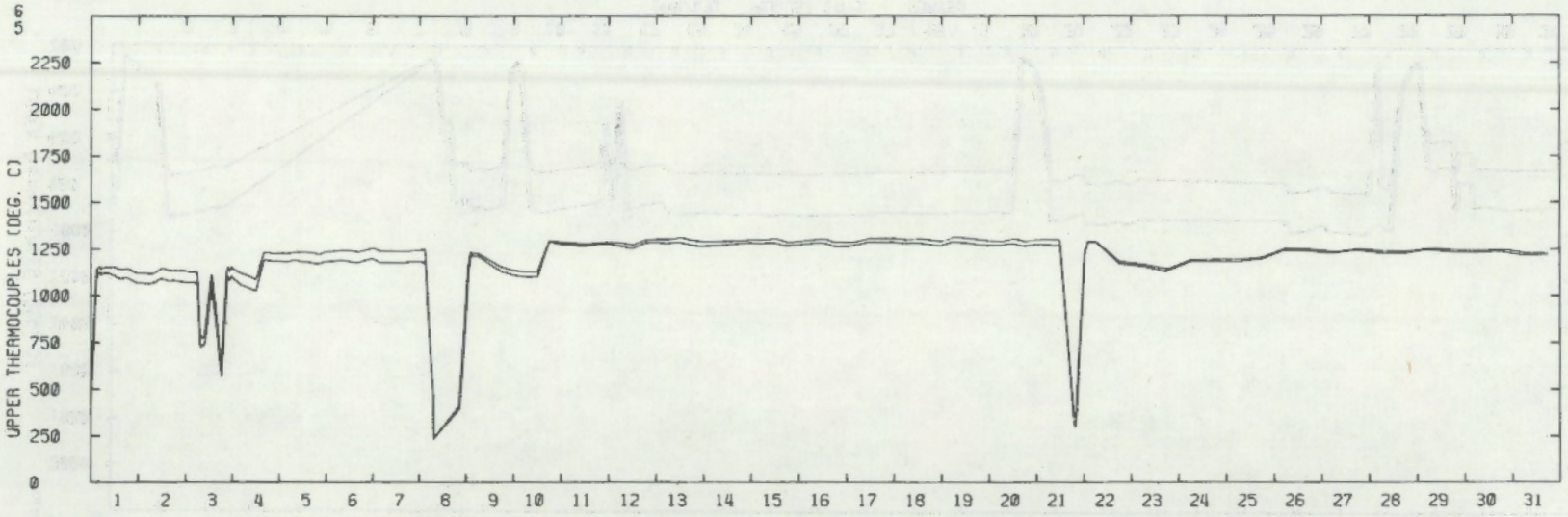

FIGURE B.11. Upper Thermocouple Readings for Rods 5,6 of IFA 431 - July 1975

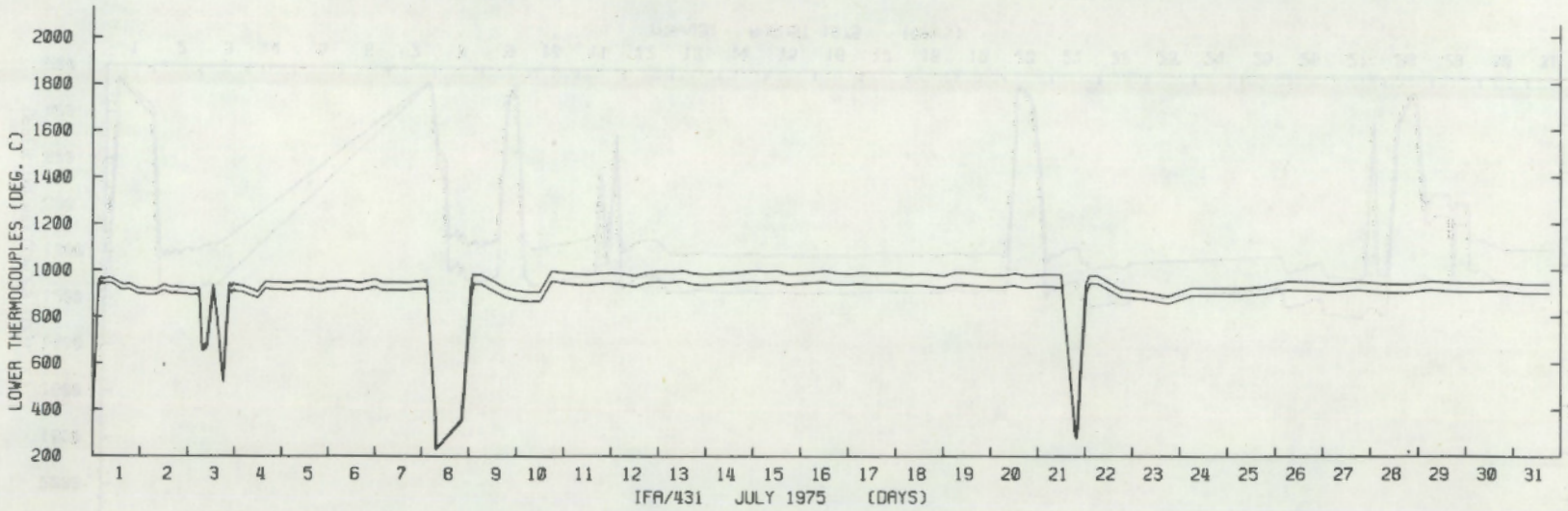

FIGURE B.12. Lower Thermocouple Readings for Rods 5,6 of IFA 431 - July 1975

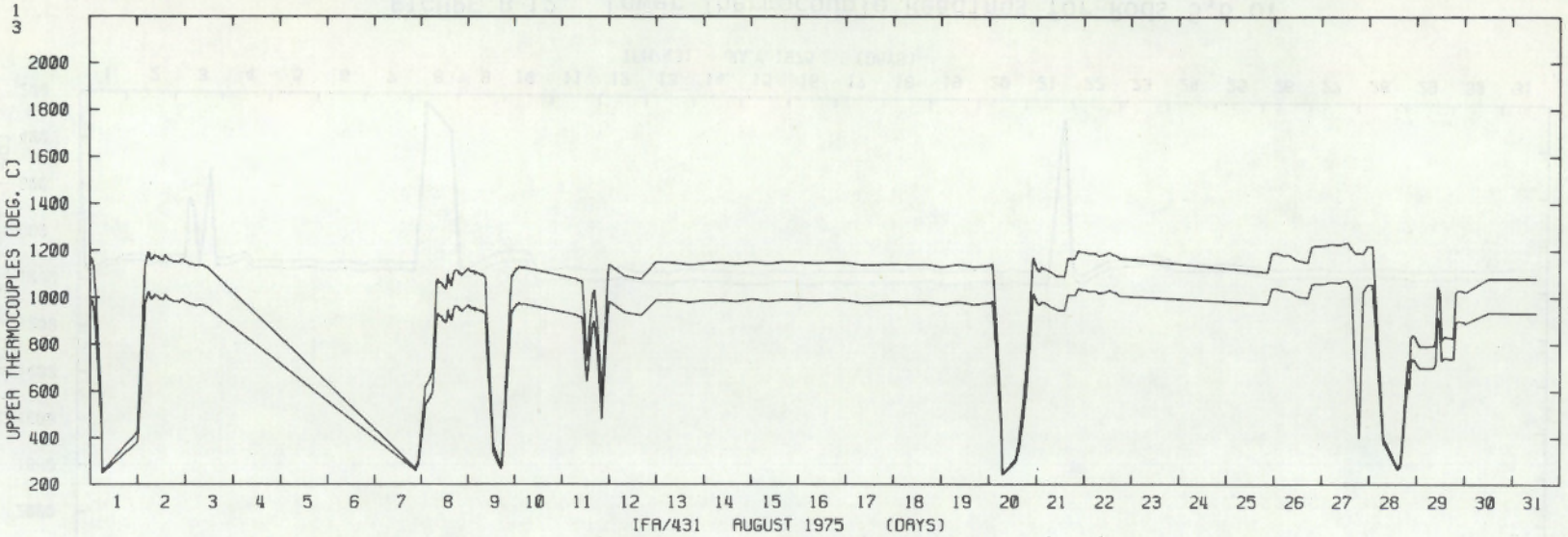

FIGURE B.13. Upper Thermocouple Readings for Rods 1,3 of IFA 431 - August 1975

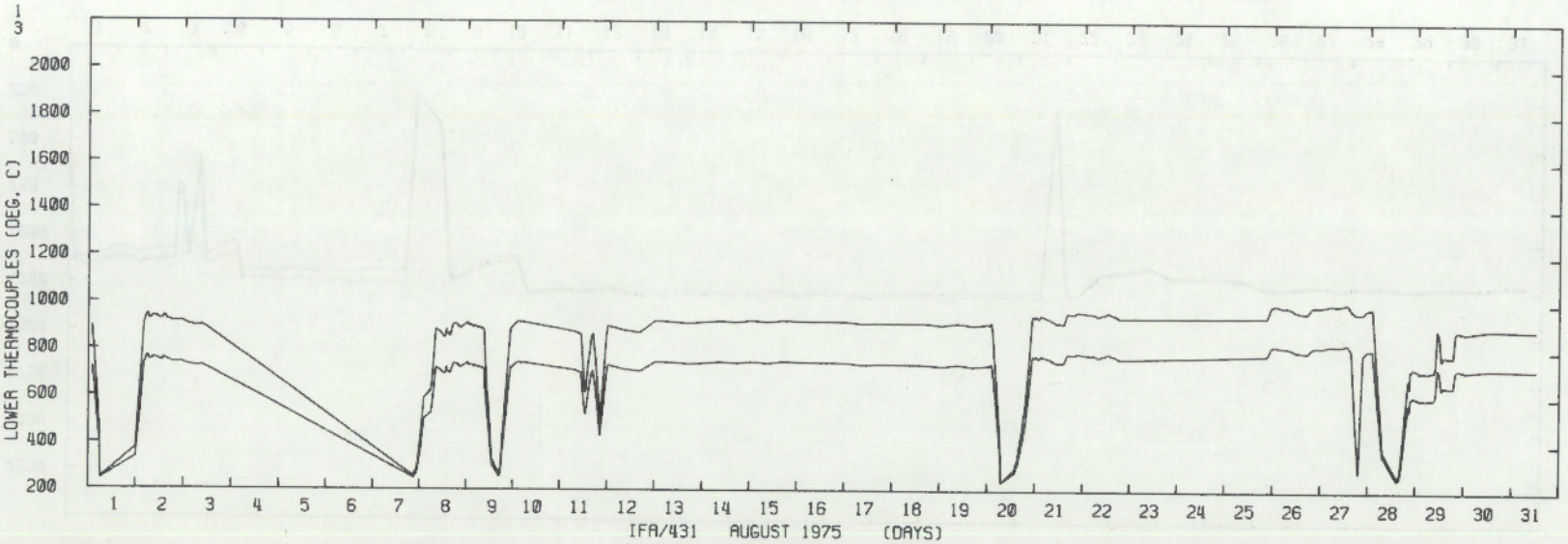

FIGURE B.14. Lower Thermocouple Readings for Rods 1,3 of IFA 431 - August 1975

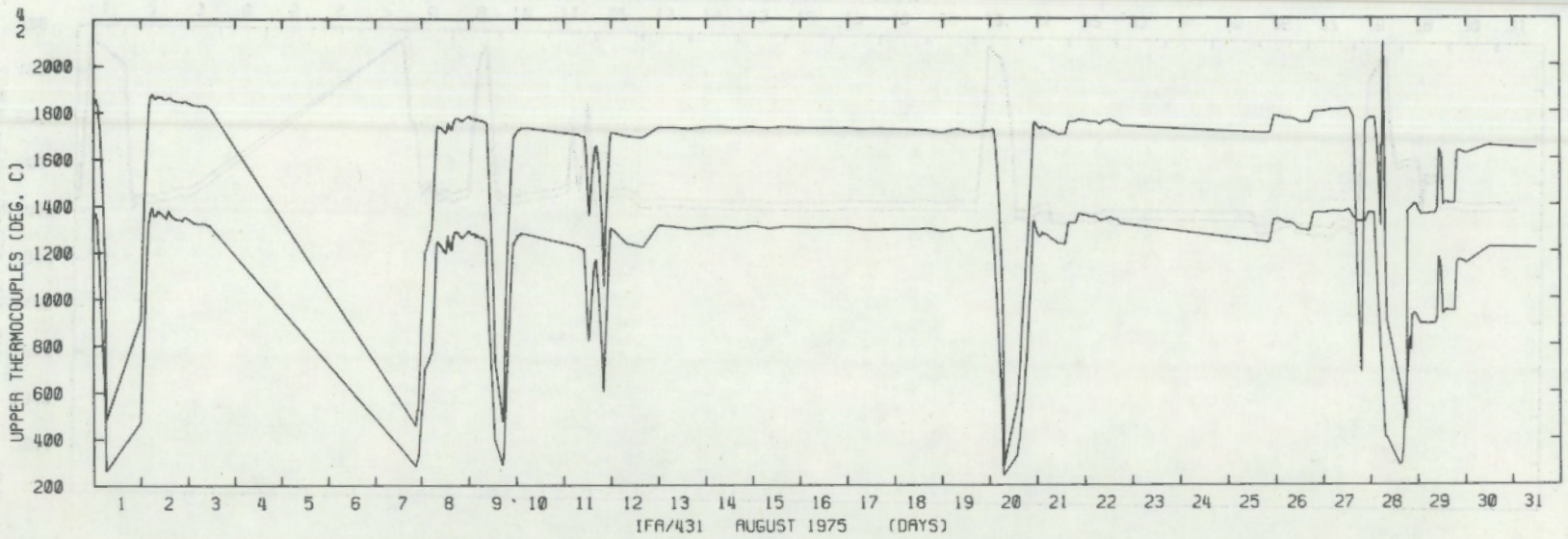

FIGURE B.15. Upper Thermocouple Readings for Rods 2,4 of IFA 431 - August 1975

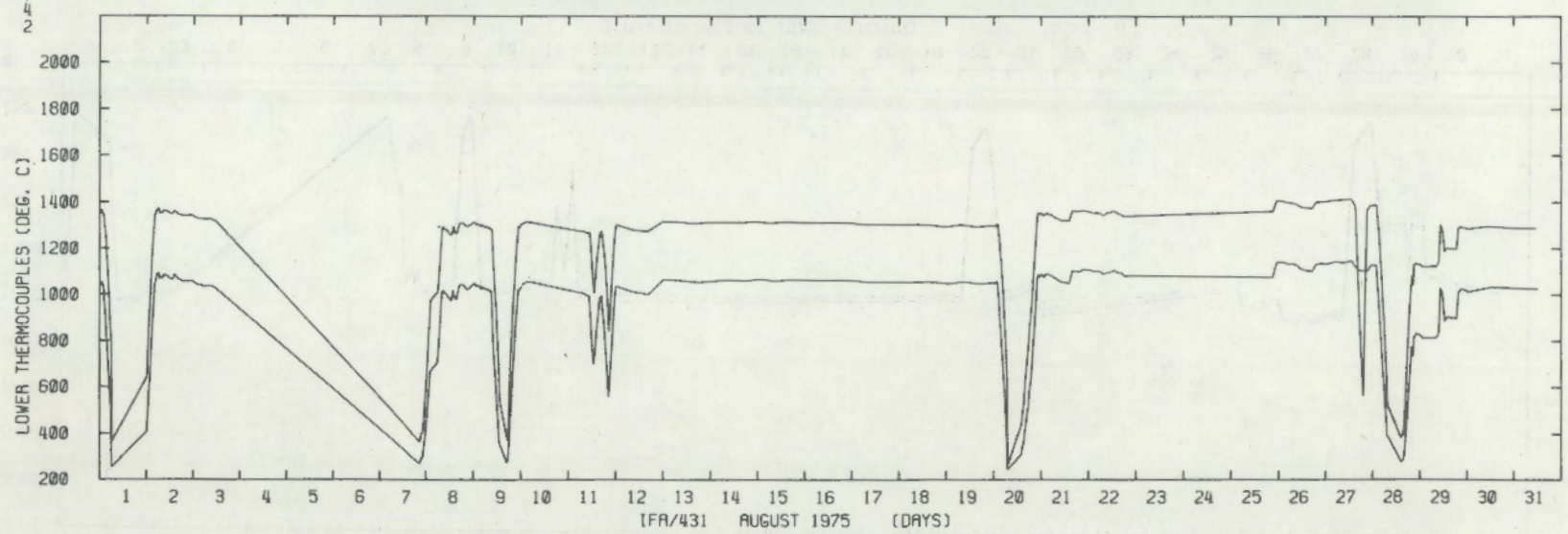

FIGURE B.16. Lower Thermocouple Readings for Rods 2,4 of IFA 431 - August 1975

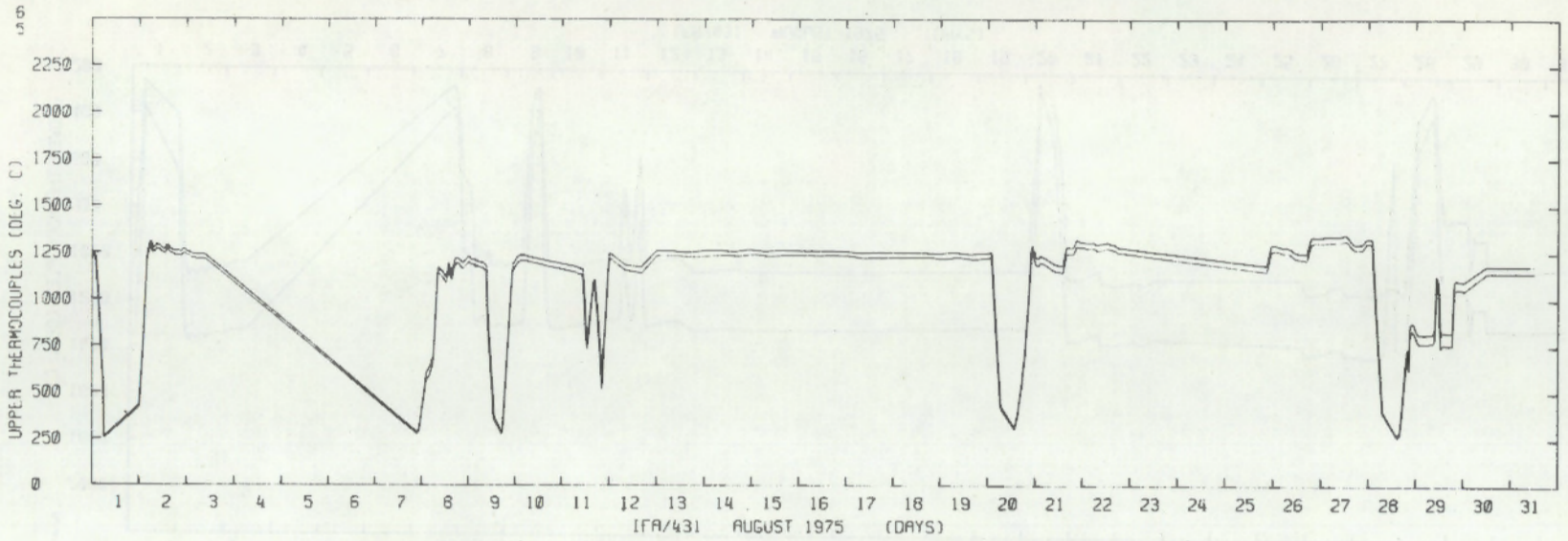

FIGURE B.17. Upper Thermocouple Readings for Rods 5,6 of IFA 431 - August 1975

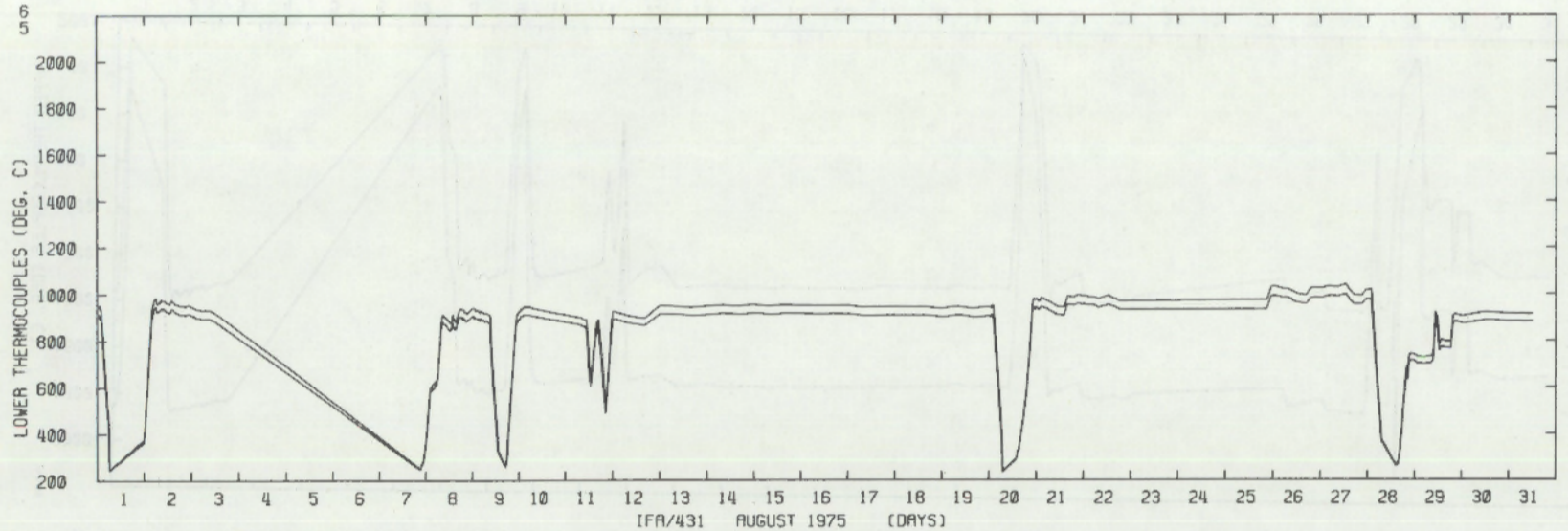

FIGURE B.18. Lower Thermocouple Readings for Rods 5,6 of IFA 431 - August 1975

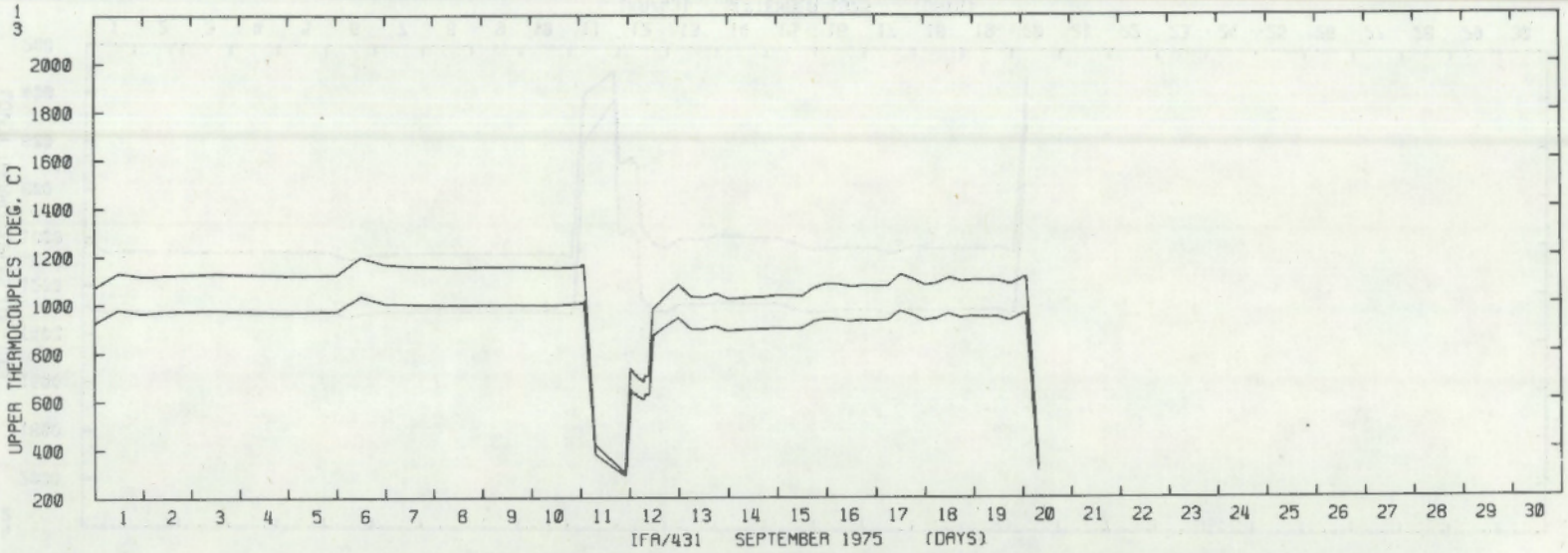

FIGURE B.19. Upper Thermocouple Readings for Rods 1,3 of IFA 431 - September 1975

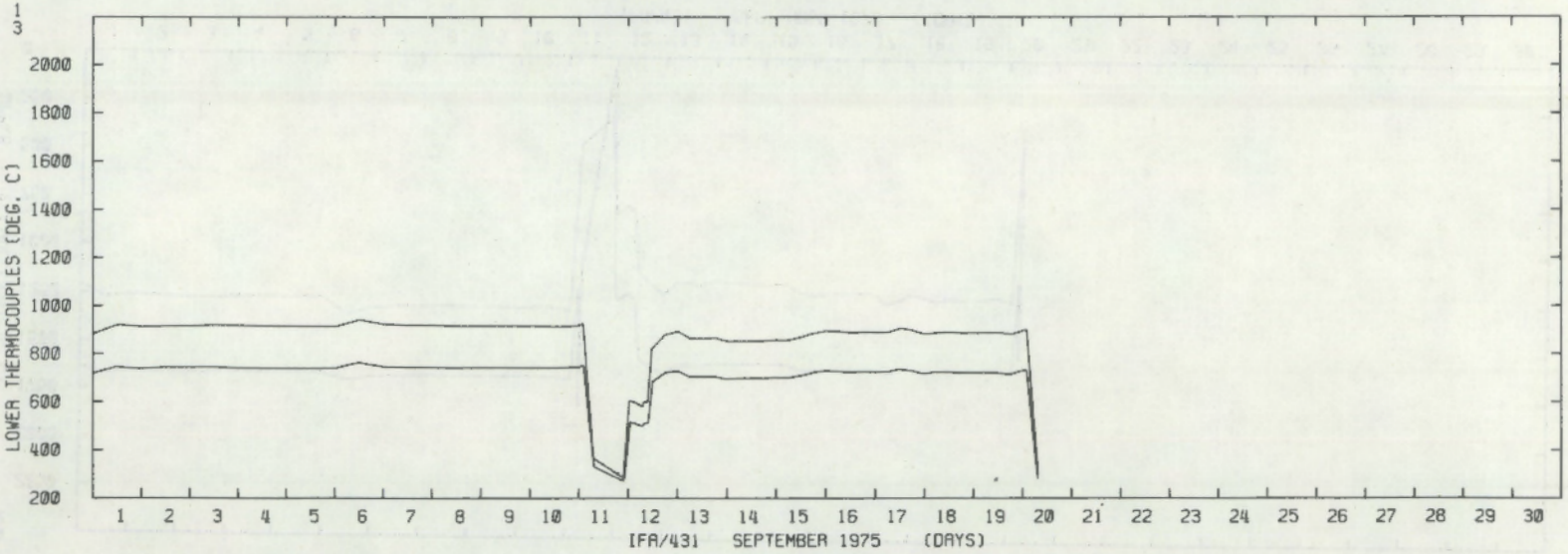

FIGURE B.20. Lower Thermocouple Readings for Rods 1,3 of IFA 431 - September 1975

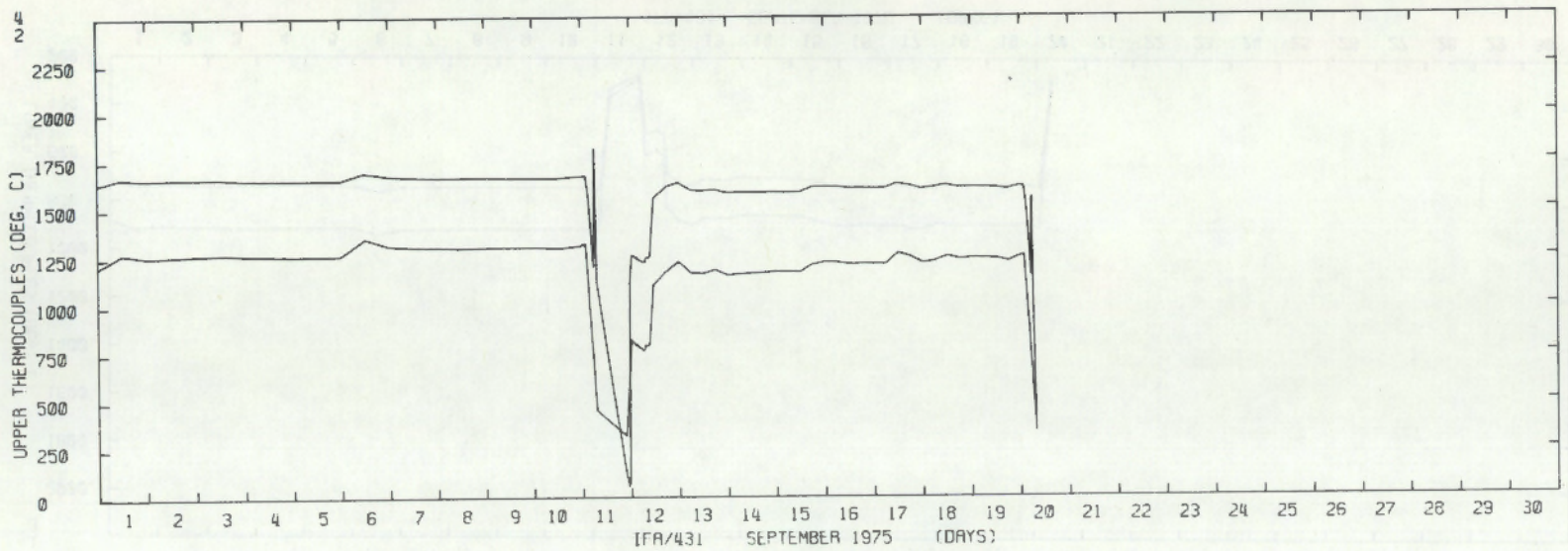

FIGURE B.21. Upper Thermocouple Readings for Rods 2,4 of IFA 431 - September 1975

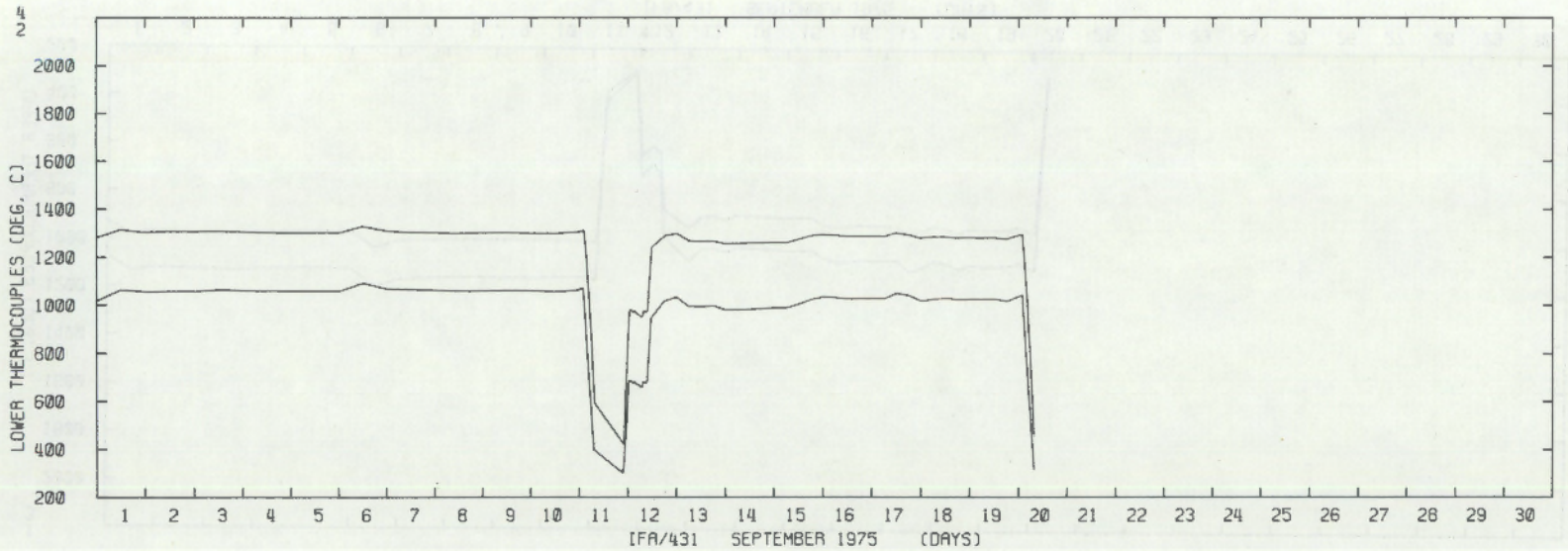

FIGURE B.22. Lower Thermocouple Readings for Rods 2,4 of IFA 431 - September 1975

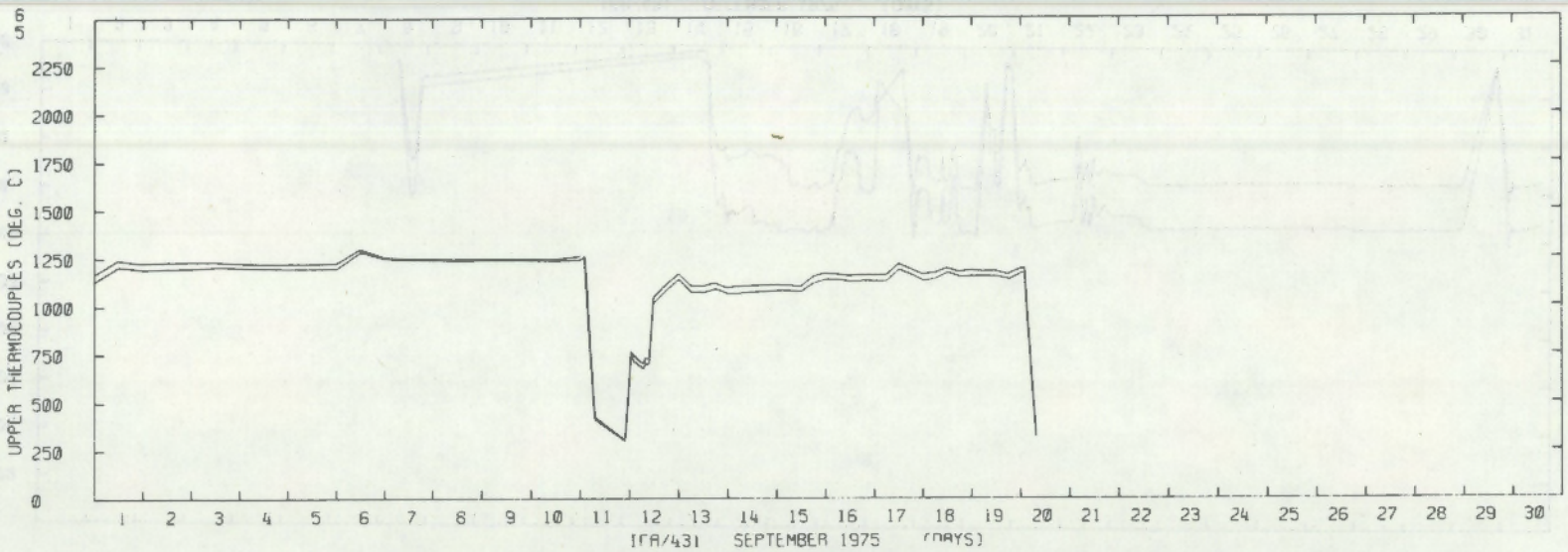

FIGURE B.23. Upper Thermocouple Readings for Rods 5,6 of IFA 431 - September 1975

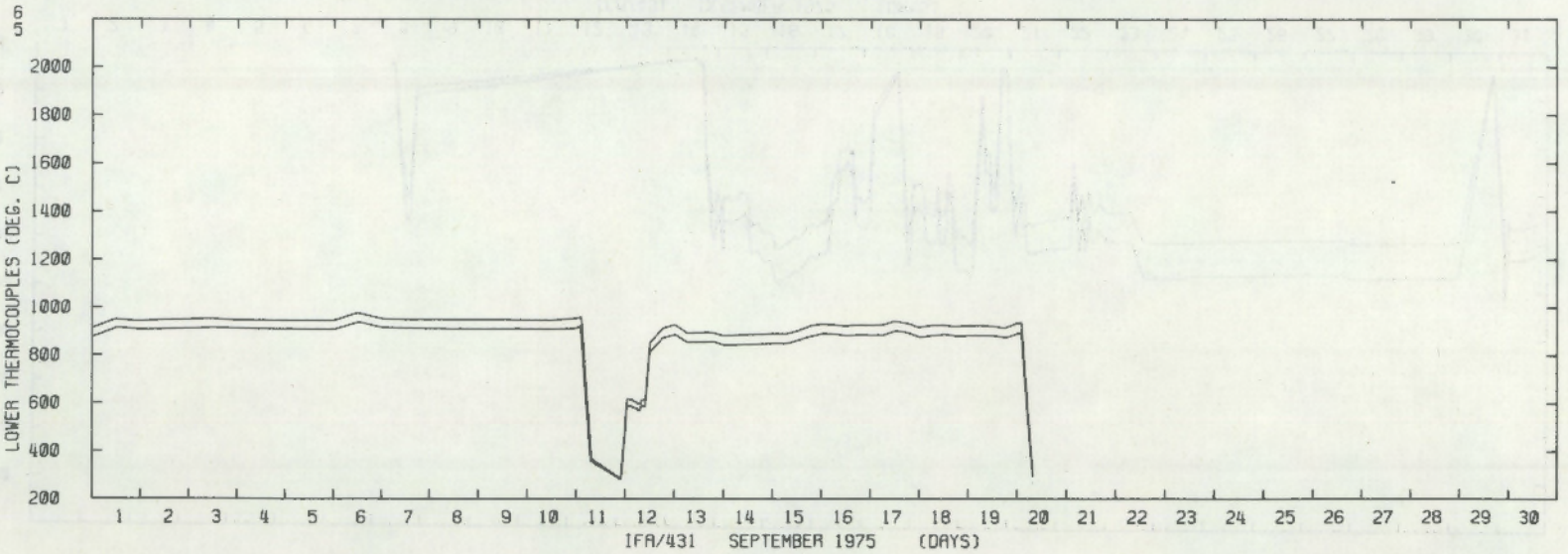

FIGURE B.24 Lower Thermocouple Readings for Rods 5,6 of IFA 431 - September 1975

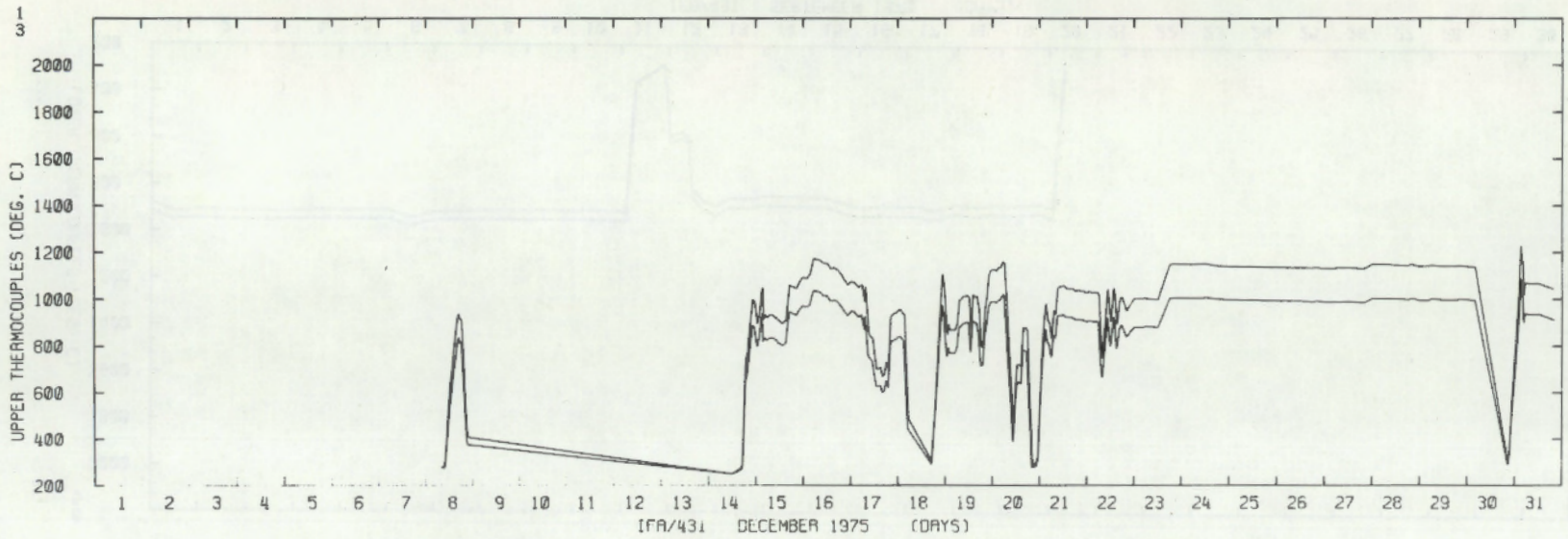

FIGURE B.25. Upper Thermocouple Readings for Rods 1,3 of IFA 431 - December 1975

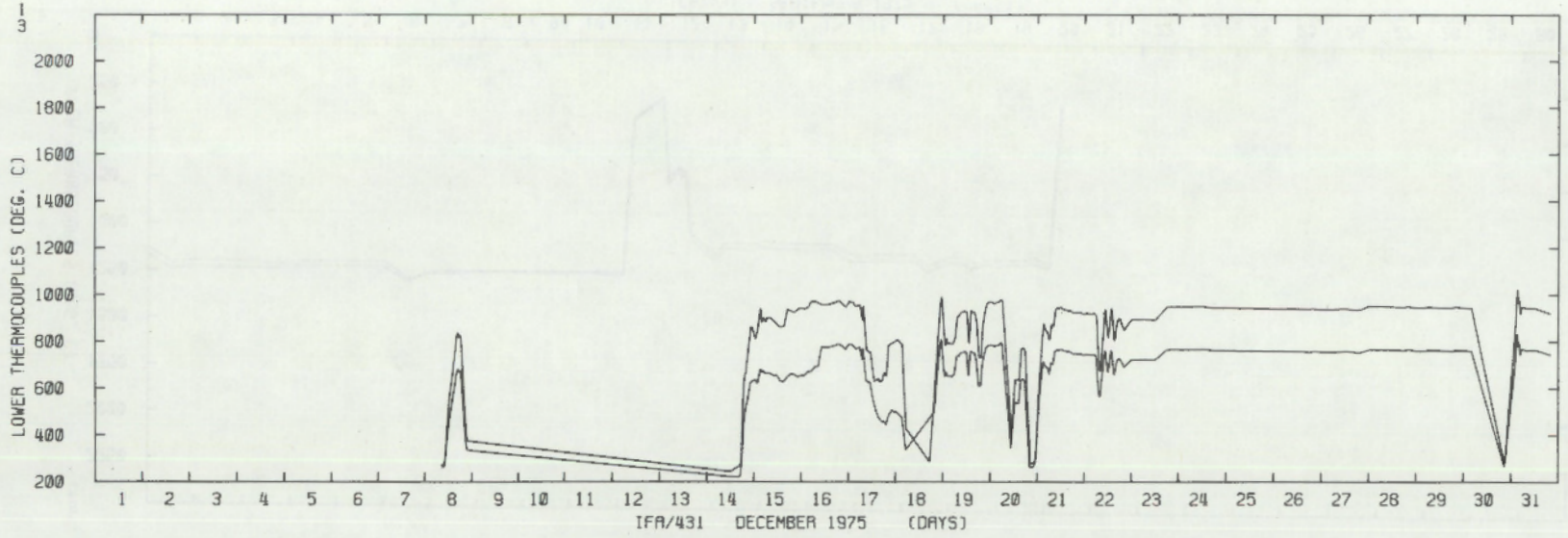

FIGURE B.26. Lower Thermocouple Readings for Rods 1,3 of IFA 431 - December 1975

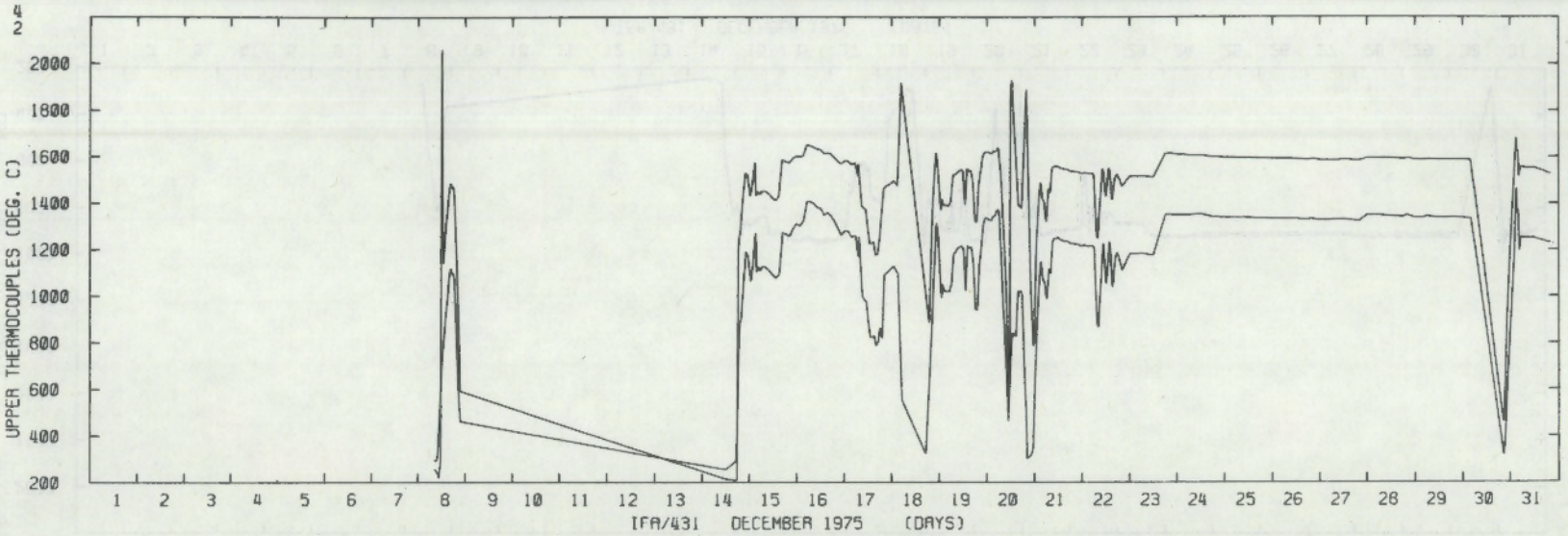

FIGURE B.27. Upper Thermocouple Readings for Rods 2,4 of IFA 431 - December 1975

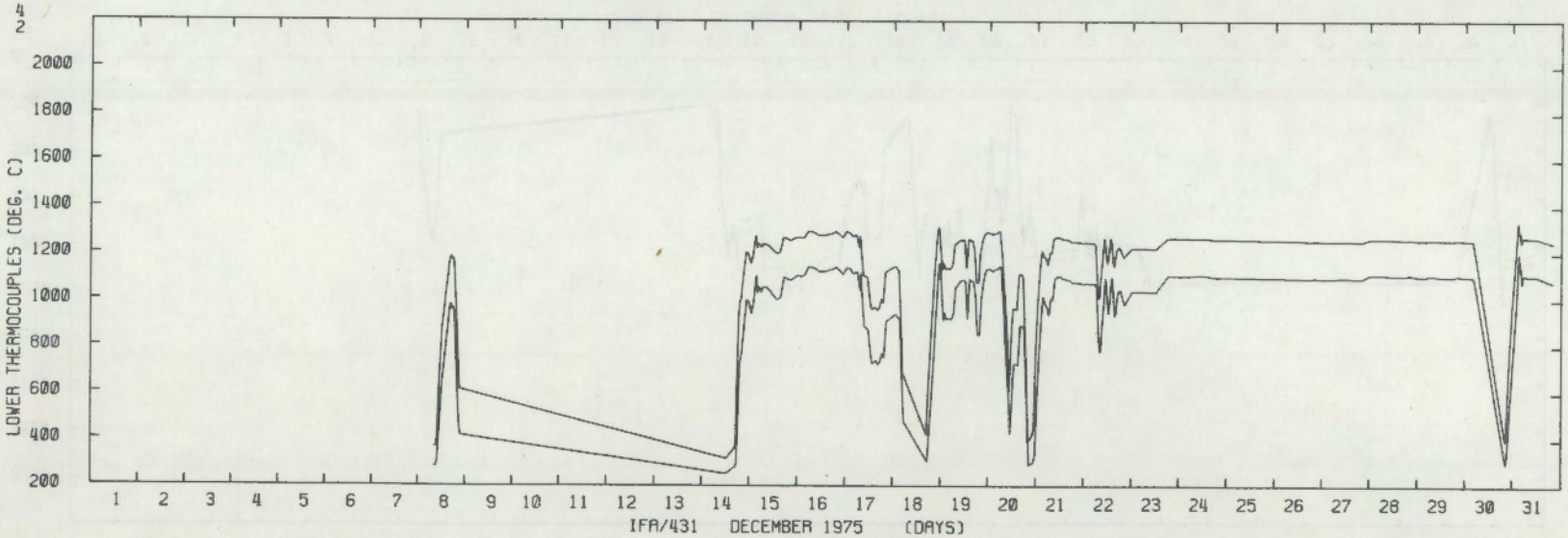

FIGURE B.28. Lower Thermocouple Readings for Rods 2,4 of IFA 431 - December 1975

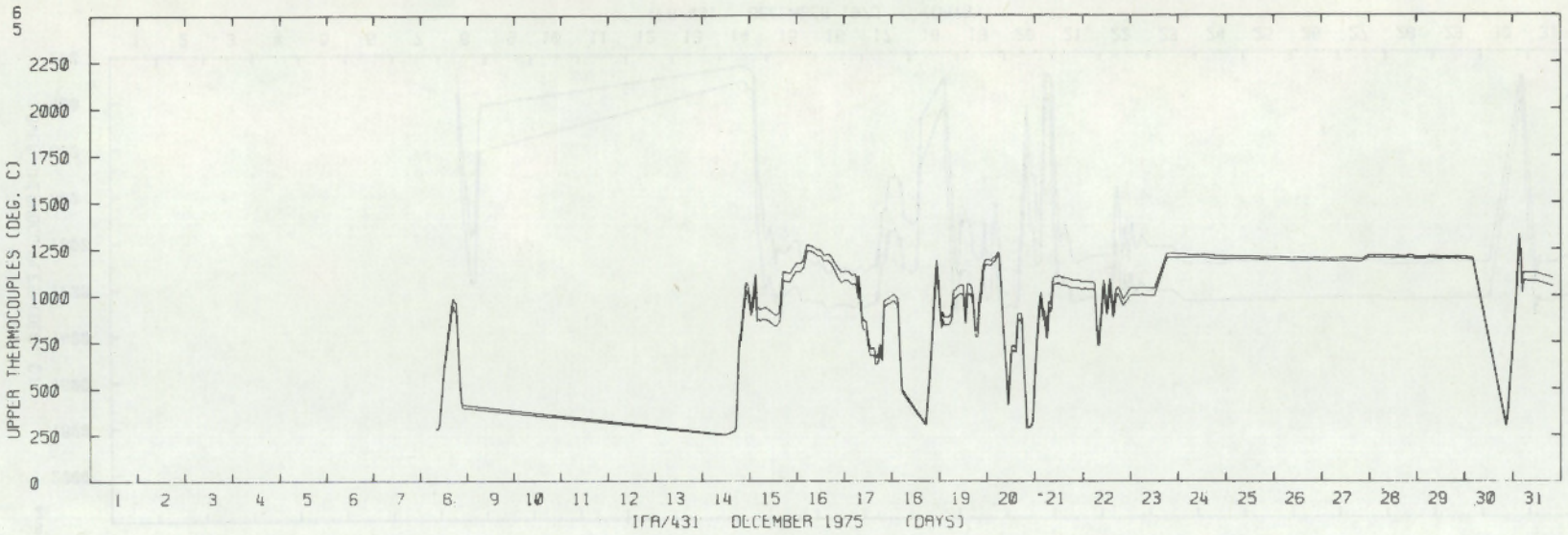

FIGURE B.29. Upper Thermocpuple Readings for Rods 5,6 of IFA 431 - December 1975

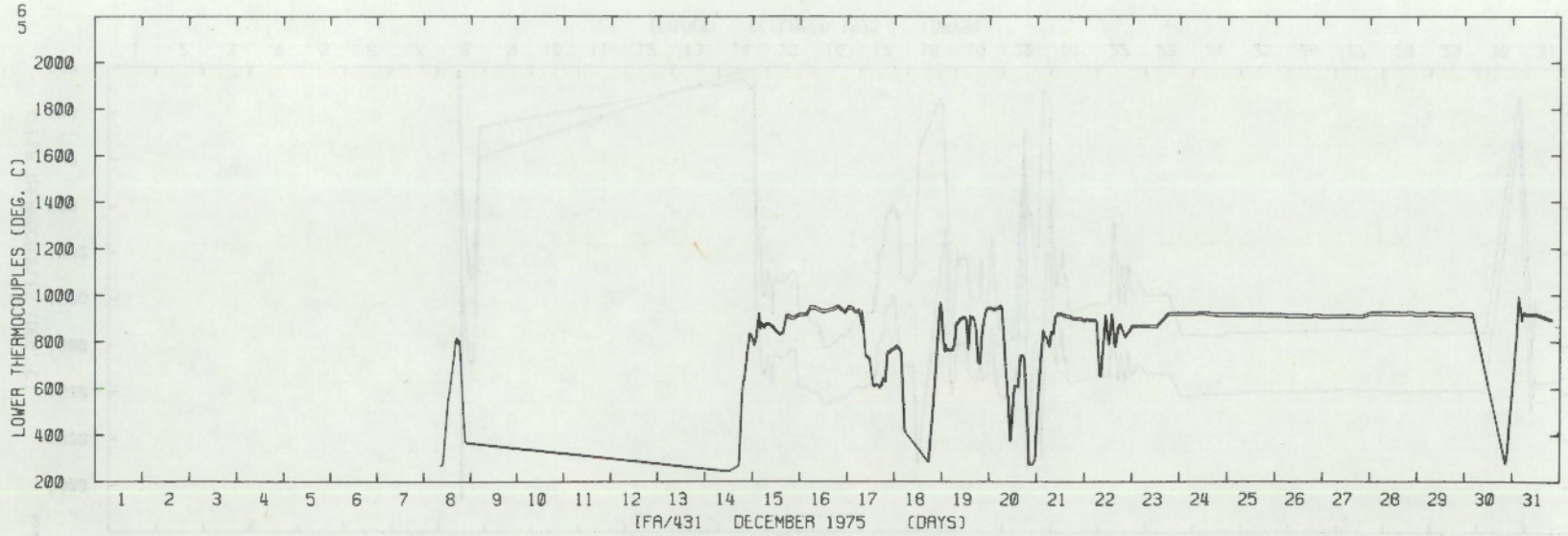

FIGURE B.30. Lower Thermocouple Readings for Rods 5,6 of IFA 431 - December 1975

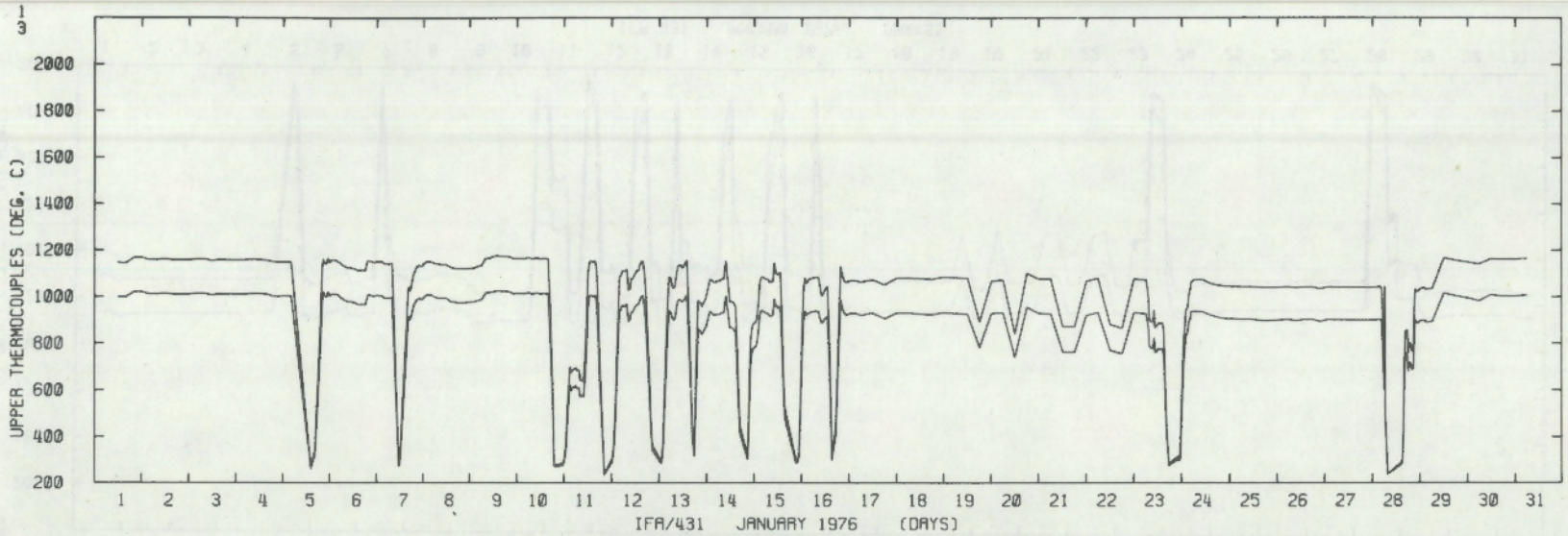

FIGURE B.31. Upper Thermocouple Readings for Rods 1,3 of IFA 431 - January 1976

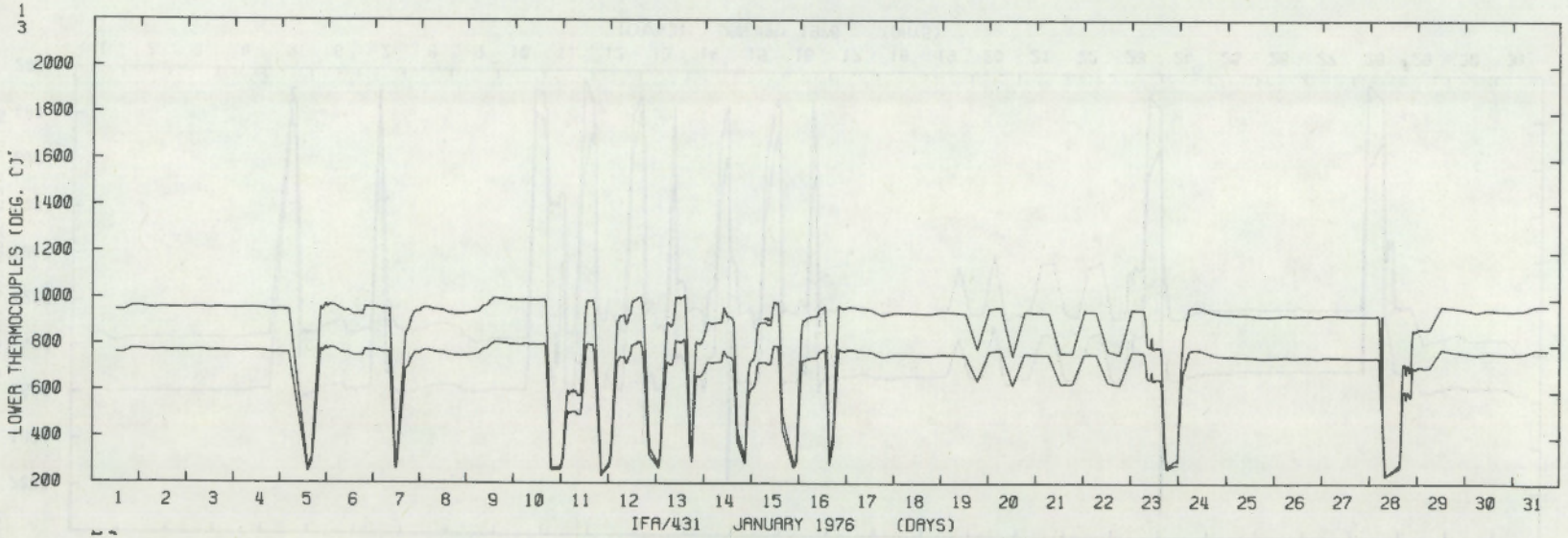

FIGURE B.32. Lower Thermocouple Readings for Rods 1,3 of IFA 431 - January 1976

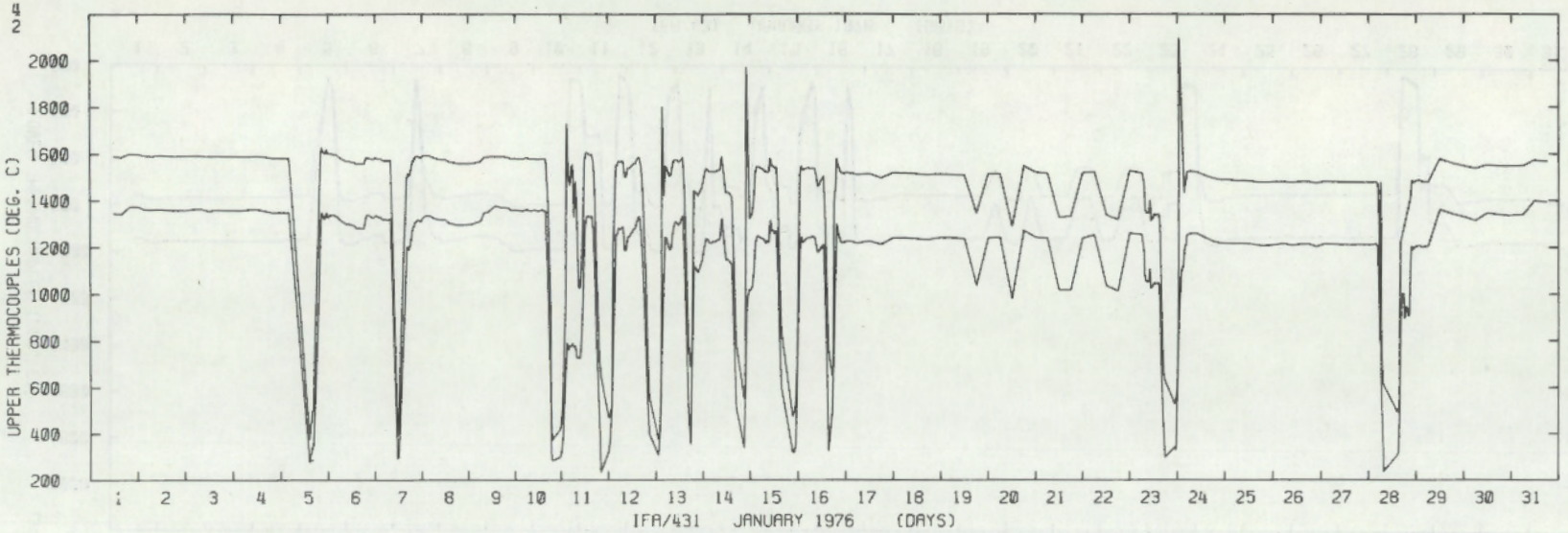

FIGURE B.33. Upper Thermocouple Readings for Rods 2,4 of IFA 431 - January 1976

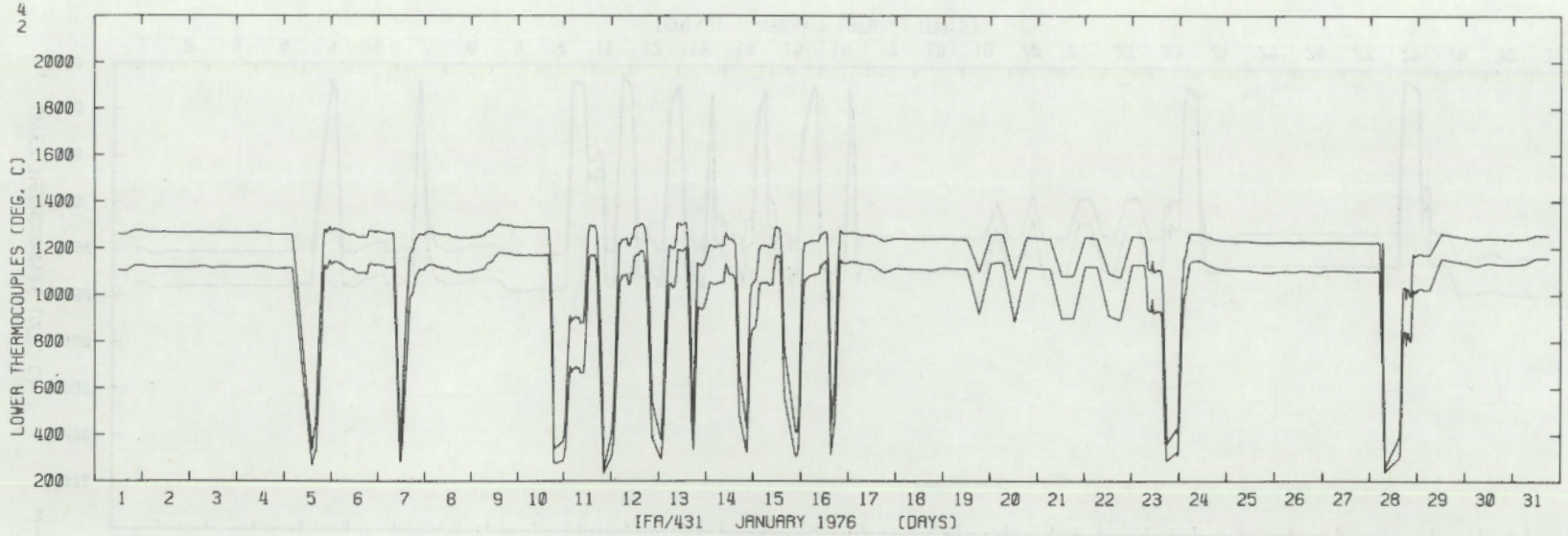

FIGURE B.34. Lower Thermocouple Readings for Rods 2,4 of IFA 431 - January 1976

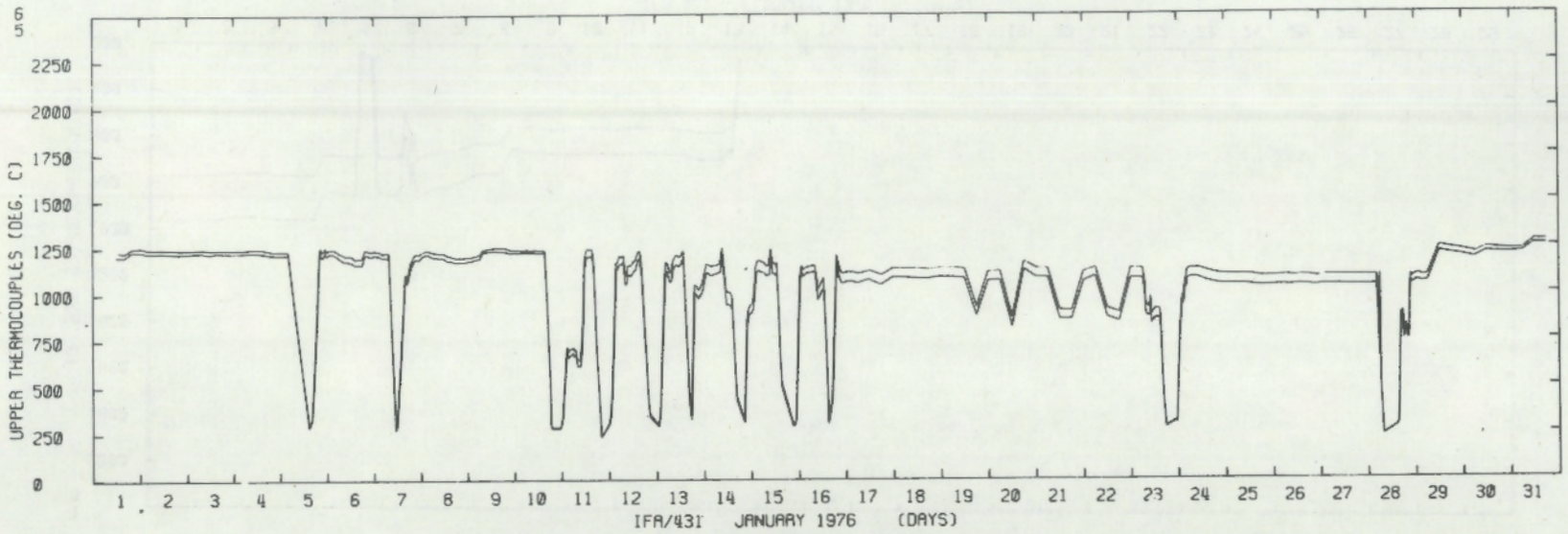

FIGURE B. 35. Upper Thermocouple Readings for Rods 5,6 of IFA 431 - January 1976

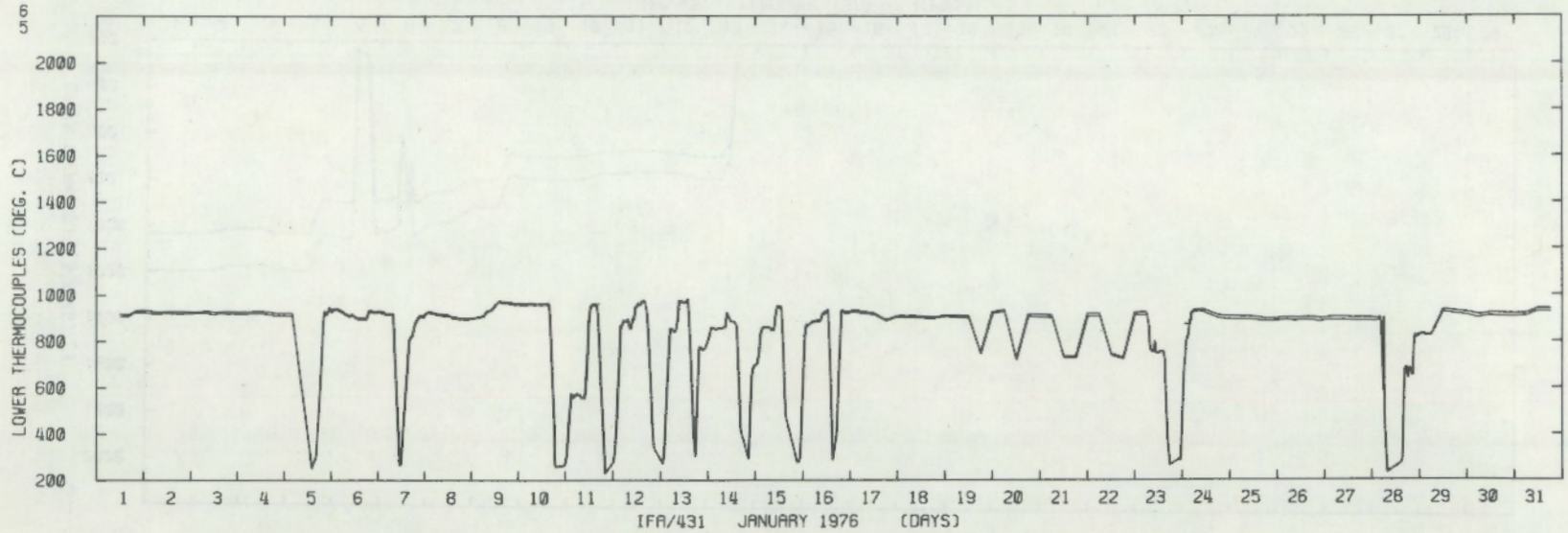

FIGURE B. 36. Lower Thermocouple Readings for Rods 5,6 of IFA 431 - January 1976

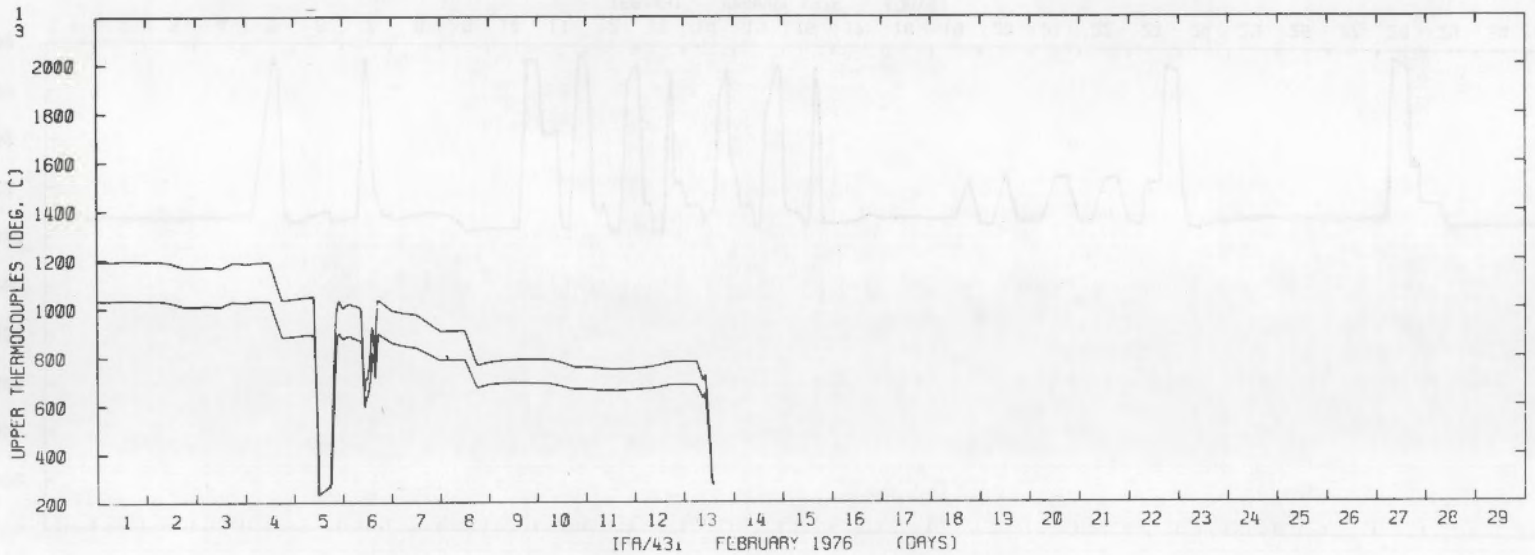

FIGURE B.37. Upper Thermocouple Readings for Rods 1,3 of IFA 431 - February 1976

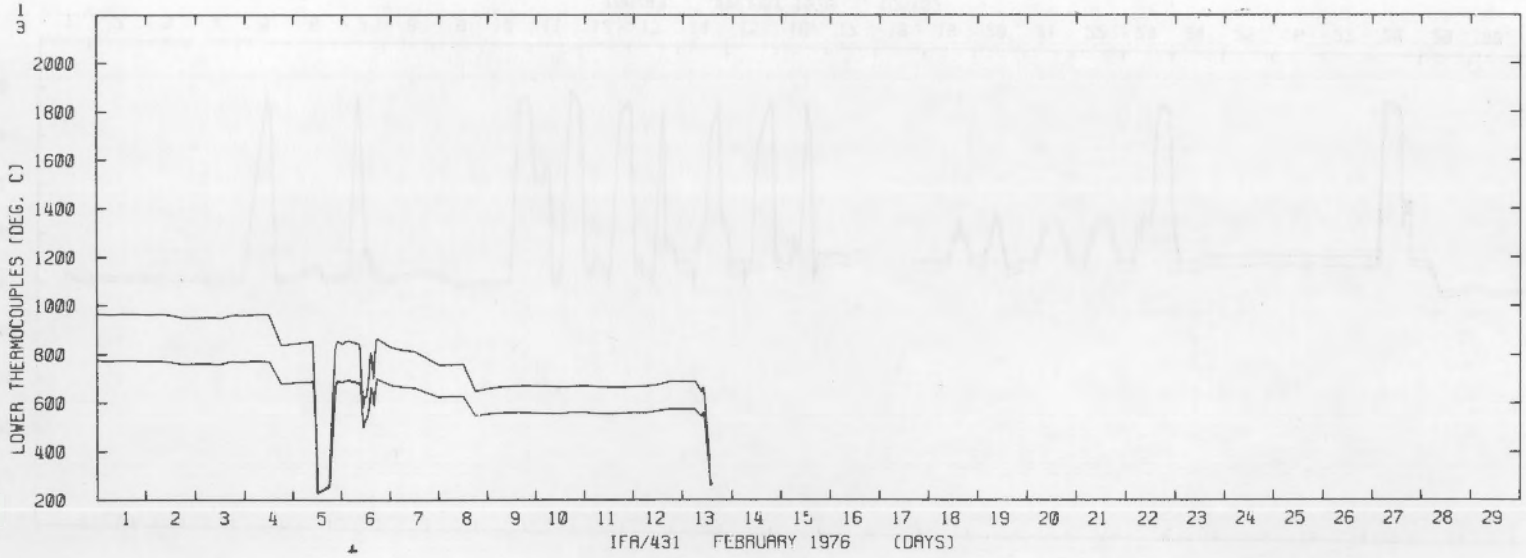

FIGURE B.38. Lower Thermocouple Readings for Rods 1,3 of IFA 431 - February 1976

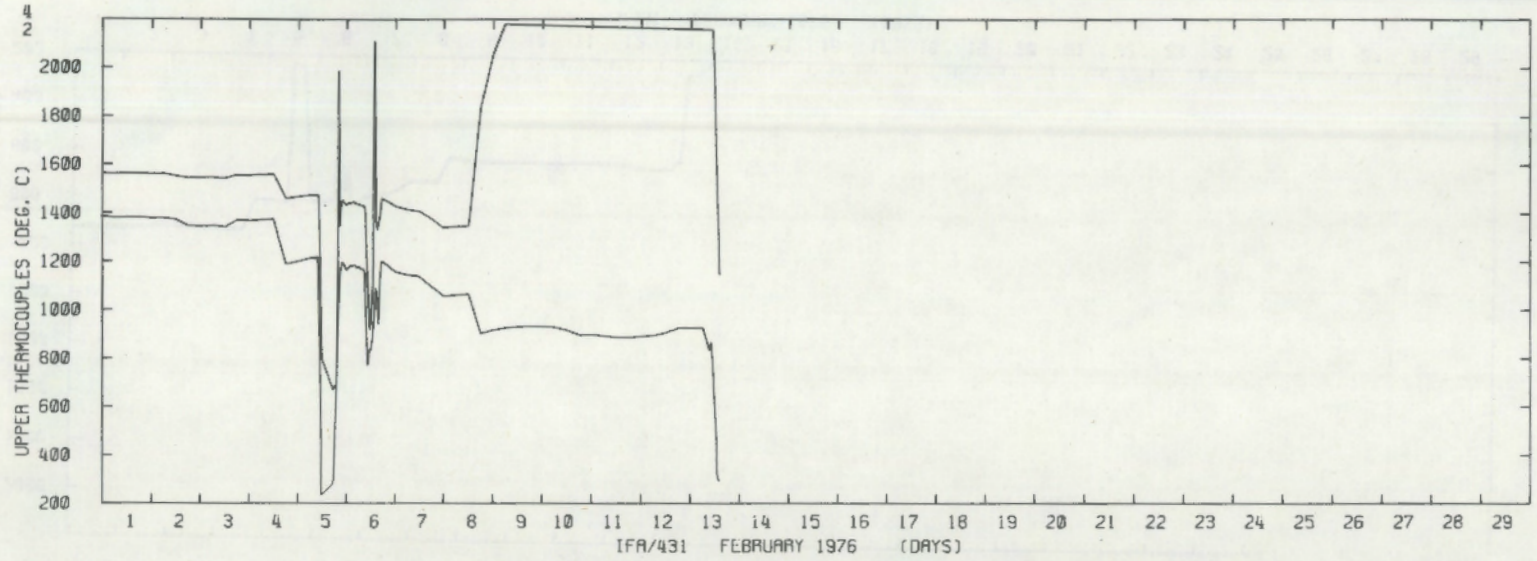

FIGURE B.39. Upper Thermocouple Readings for Rods 2,4 of IFA 431 - February 1976

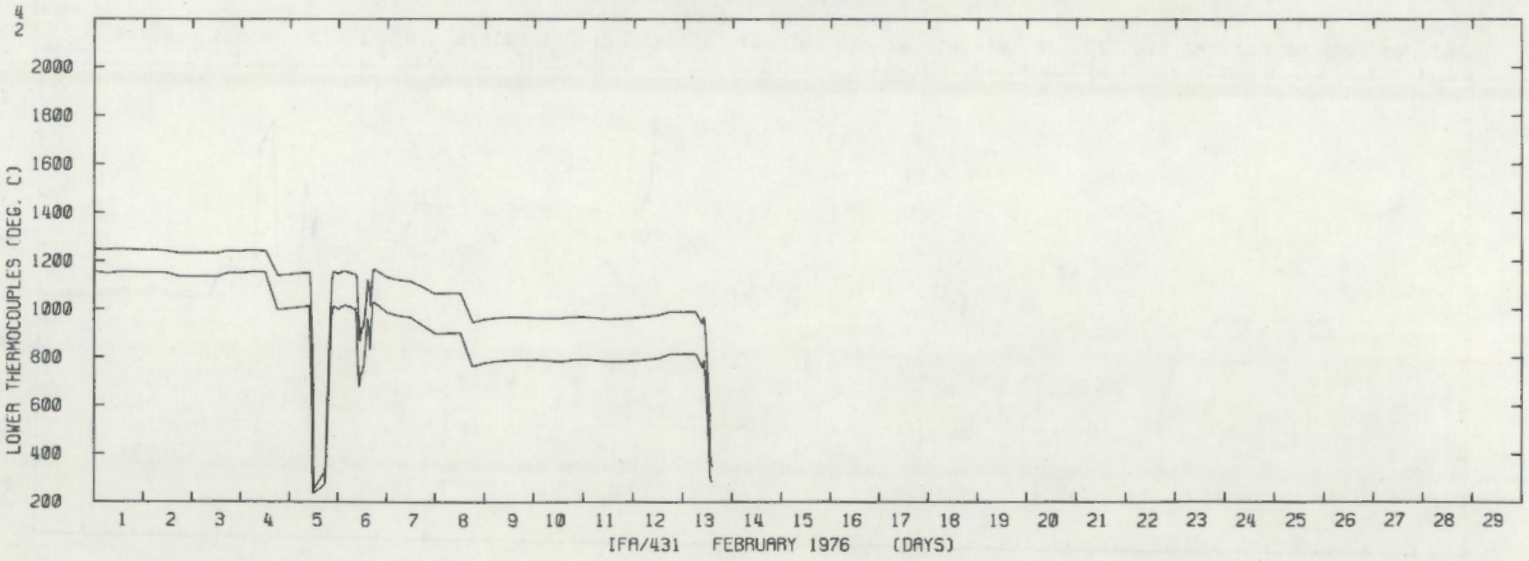

FIGURE B.40. Lower Thermocouple Readings for Rods 2,4 of IFA 431 - February 1976

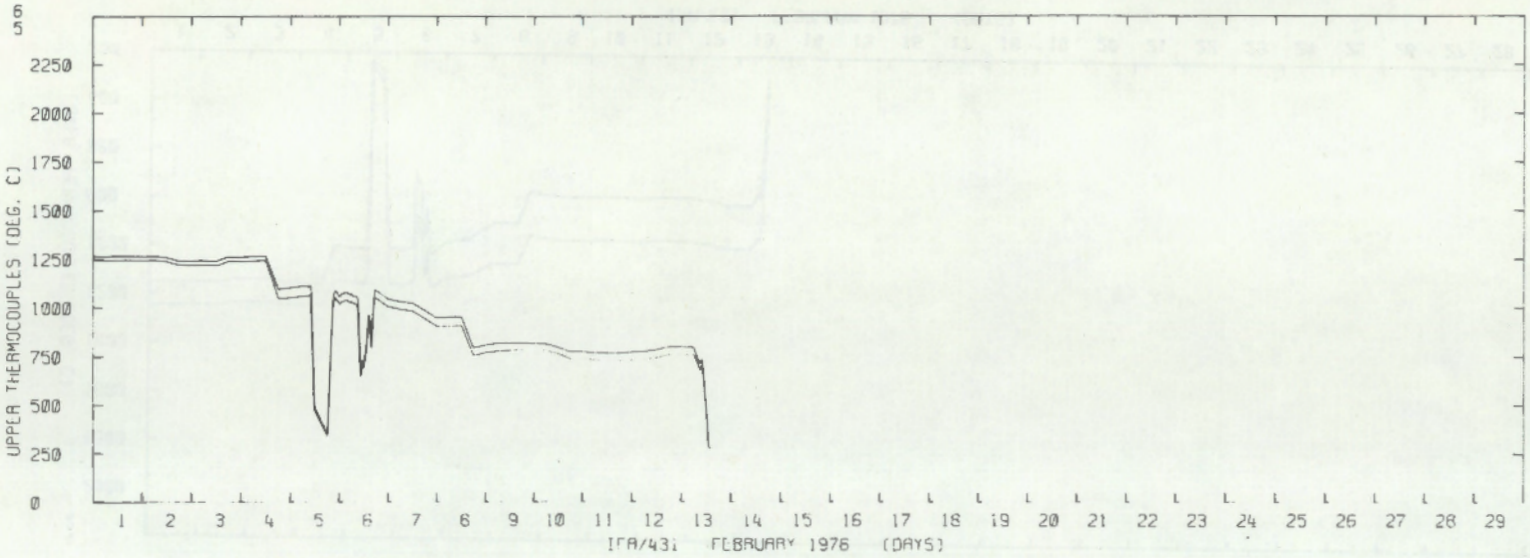

FIGURE B.41. Upper Thermocouple Readings for Rods 5,6 of IFA 431 - February 1976

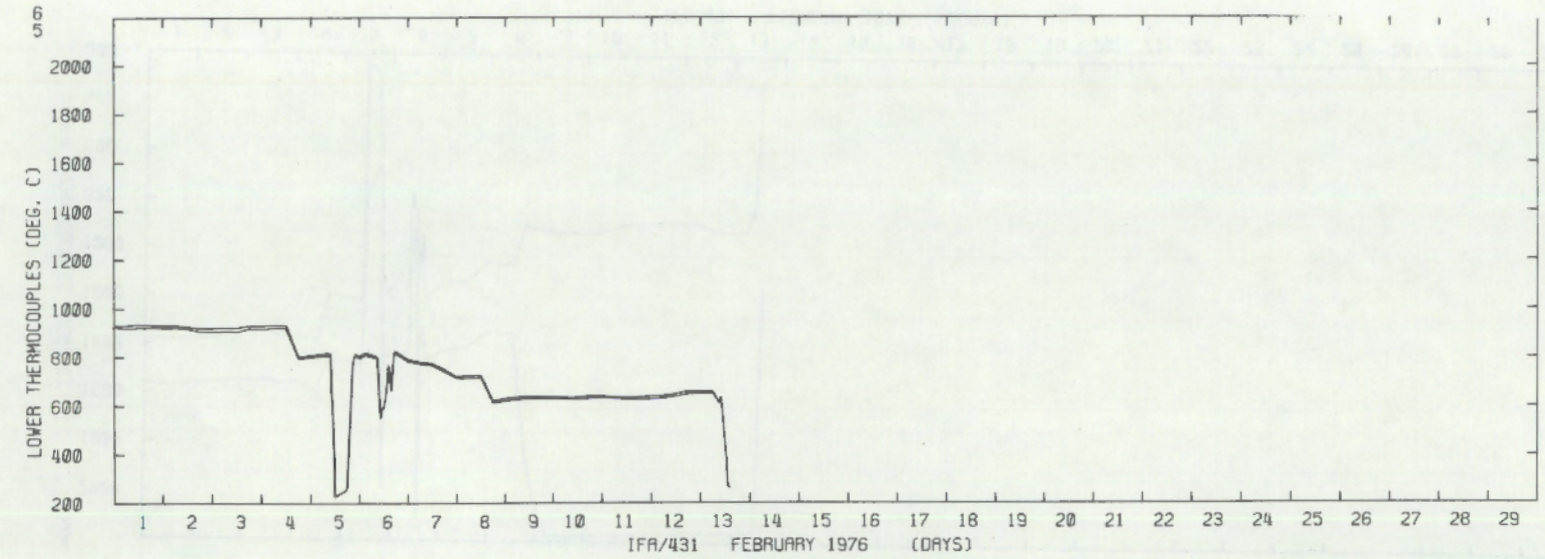

FIGURE B.42. Lower Thermocouple Readings for Rods 5,6 of IFA 431 - February 1976

APPENDIX C

GAMMA SCANS

GAMMA SCANS

This appendix presents the results, for all six IFA-431 rods, of the gamma scans that were performed at Kjeller. Figure C-1 is the gamma spectrum recorded near the lower end of the fuel stack of rod 1. This was done to determine the highest energy peaks in the fuel rods. The average count rates and the axial form factors were computed during gamma scanning, and these results are tabulated in Tables C-1 through C-12. Figures C-2 through C-13 are plots of the gamma scan results. Figure C-14 is a plot of the gamma scanning done at Harwell on rod 6.

Note that two different energy windows were used in the gamma scanning at Kjeller. Channel A was a gross gamma scan with an energy window of 584 to 775 KeV. The double peak of Zr 95/Nb 95 was selected for Channel B. This channel had an energy window of 752 to 770 KeV. The gamma activity at Harwell measured the energy peak that resulted from Cs 137 and Z4 95/Nb 95.

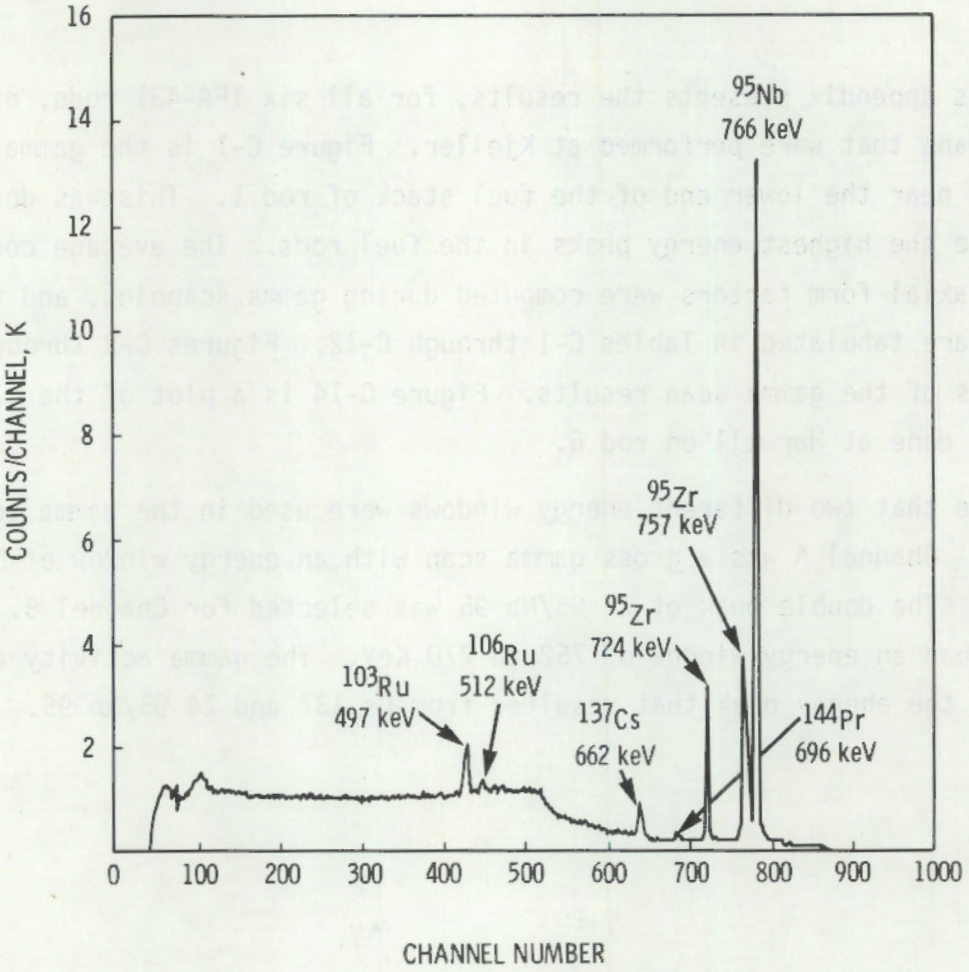

FIGURE C-1. Gamma Ray Spectrum (1024 Channels) Taken Near Lower end of Rod 1 (100 sec counting time)

FIGURE C.2 Axial gamma scan for Rod 1, Channel A

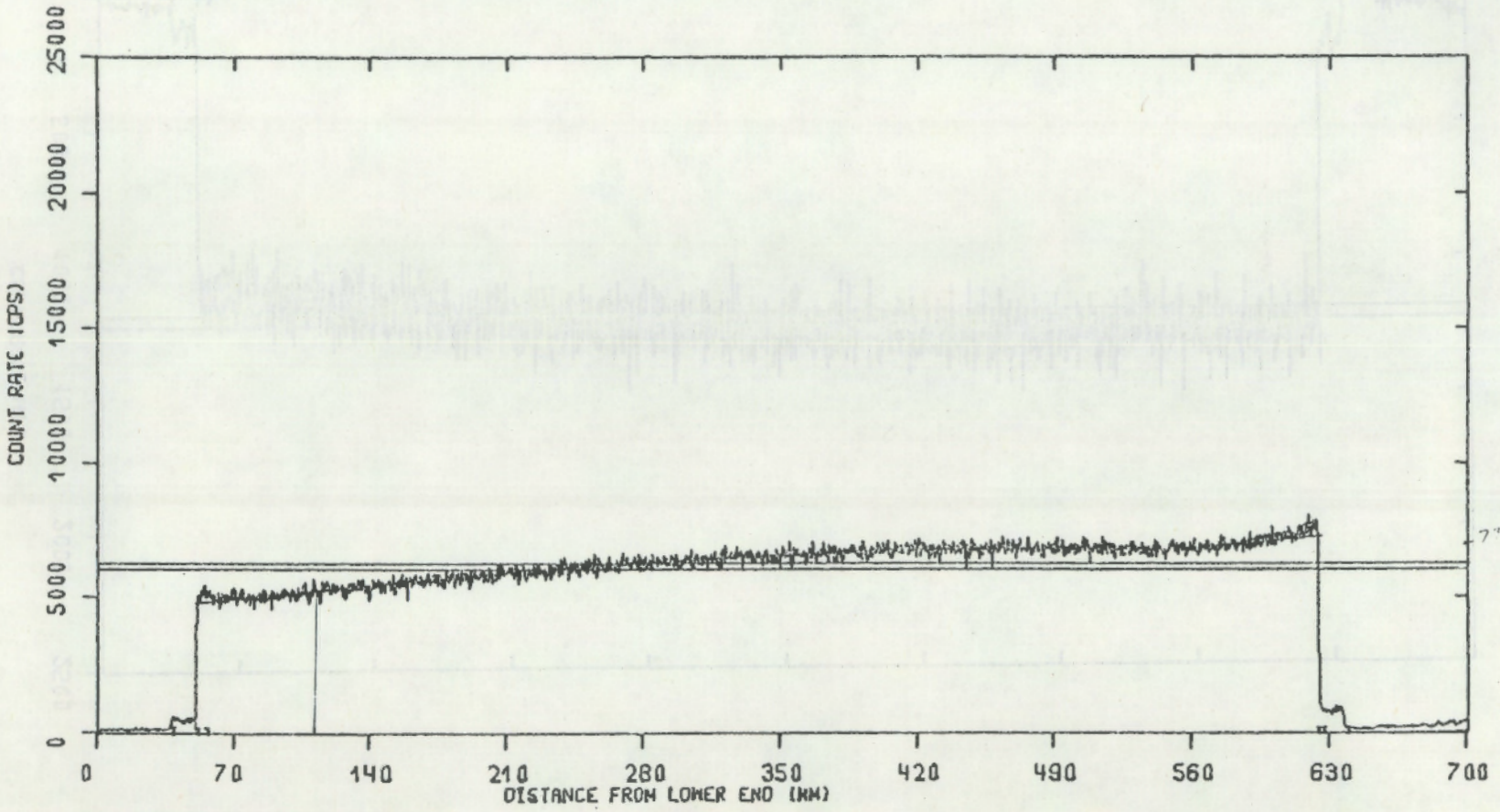

FIGURE C.3 Axial Gamma Scan for Rod 1, Channel B

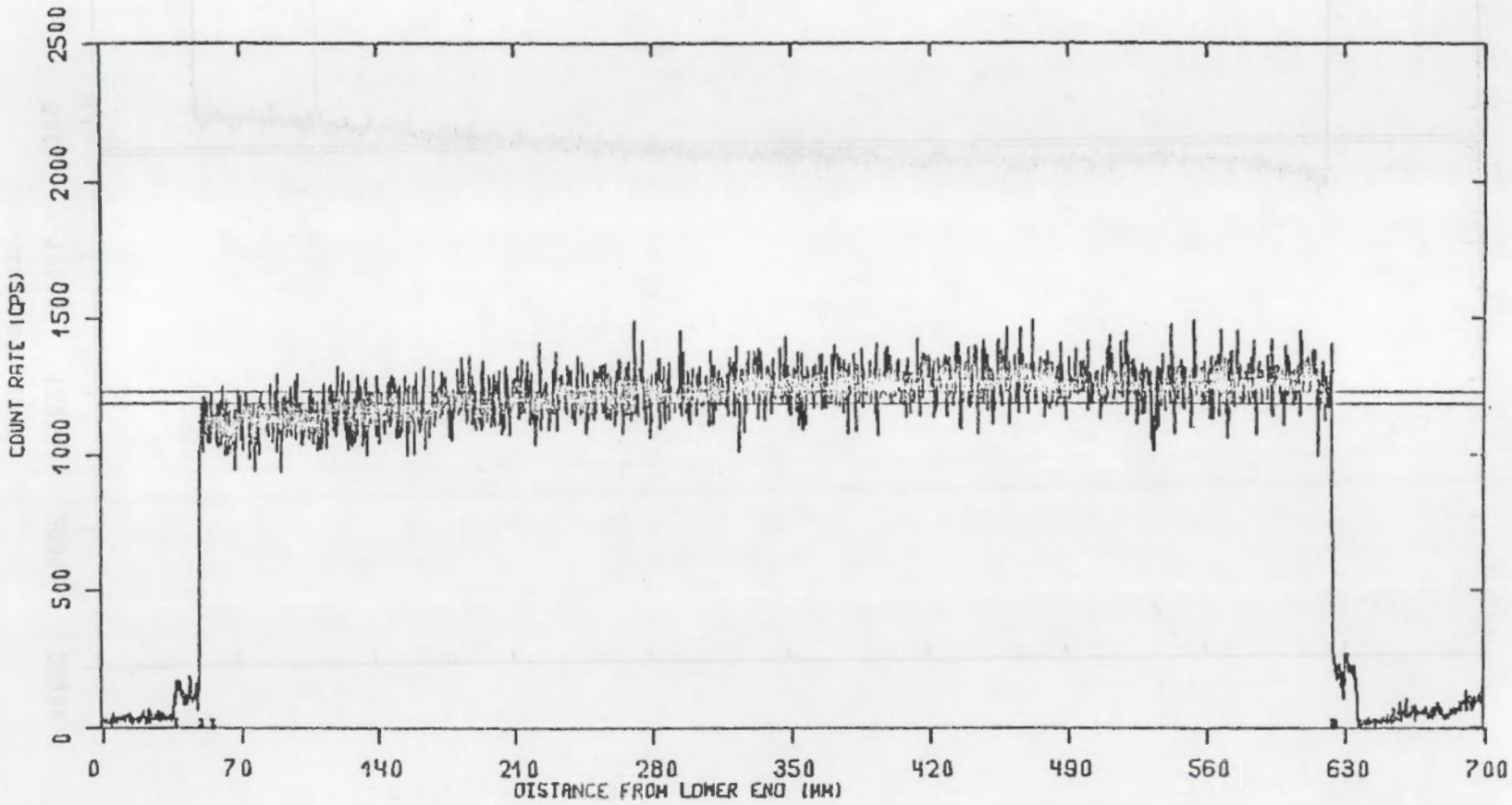

FIGURE C.4 Axial Gamma Scan for Rod 2, Channel A

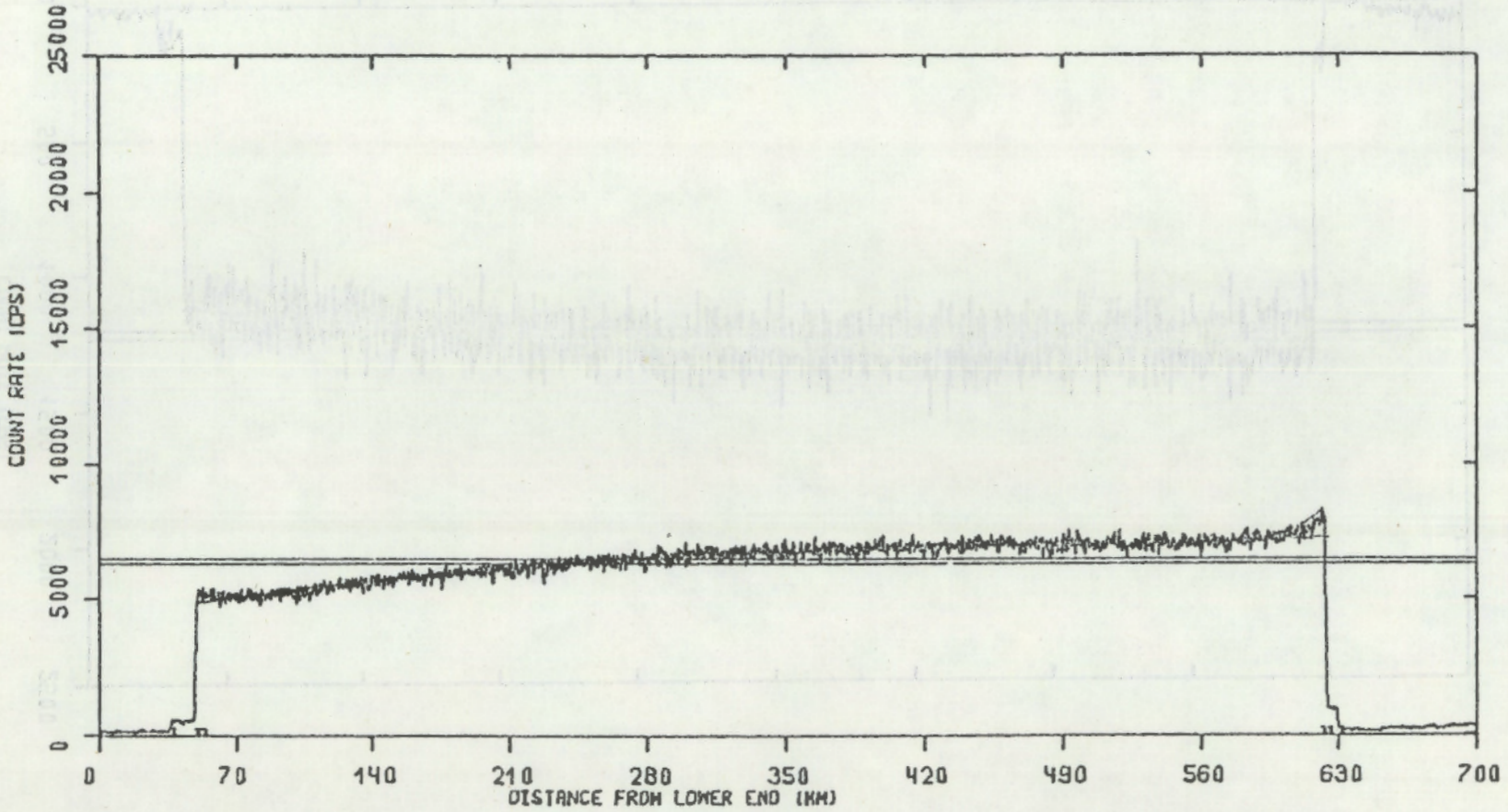

FIGURE C.5 Axial Gamma Scan for Rod 2, Channel B

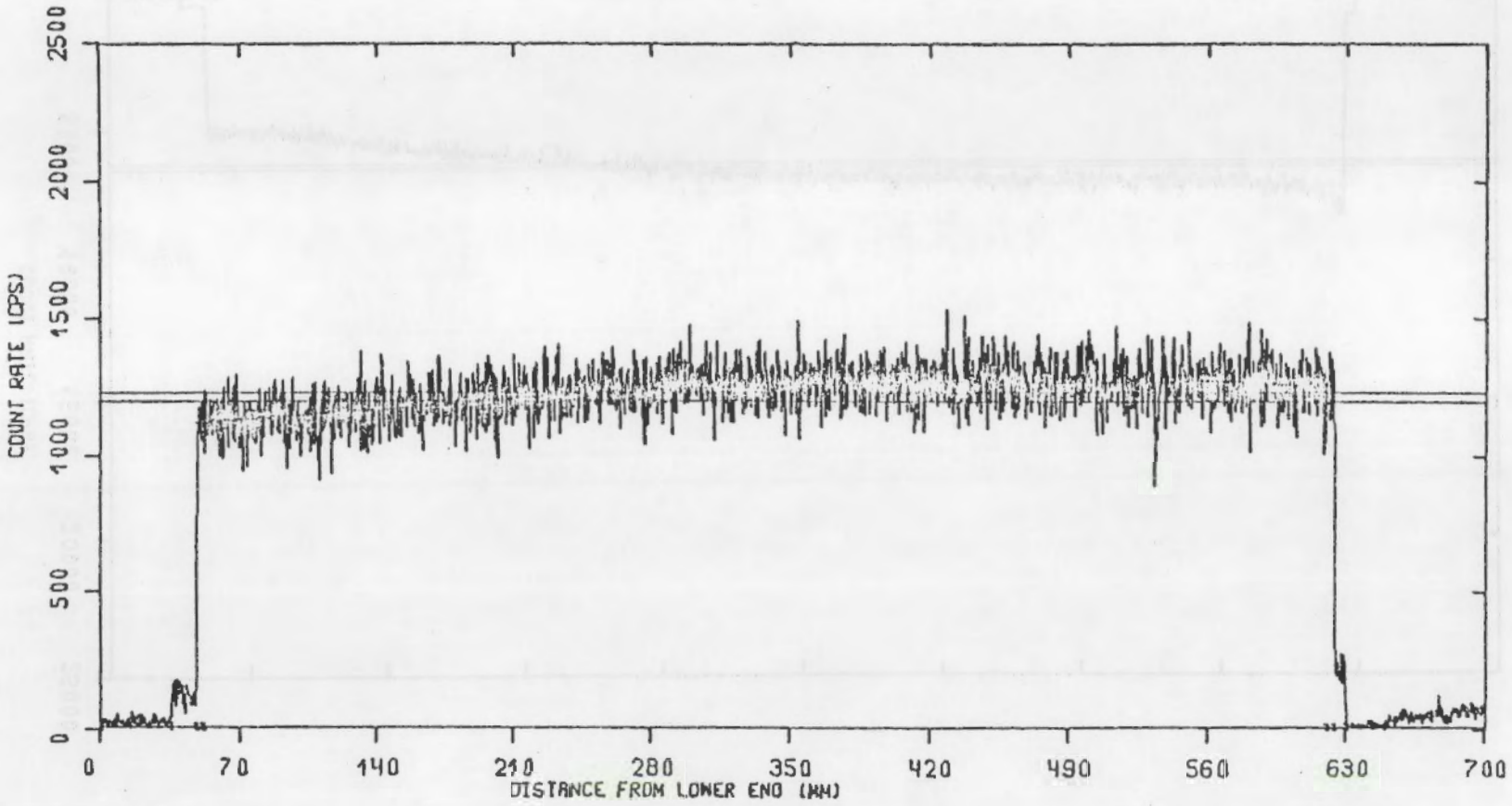

FIGURE C.6 Axial Gamma Scan for Rod 3, Channel A

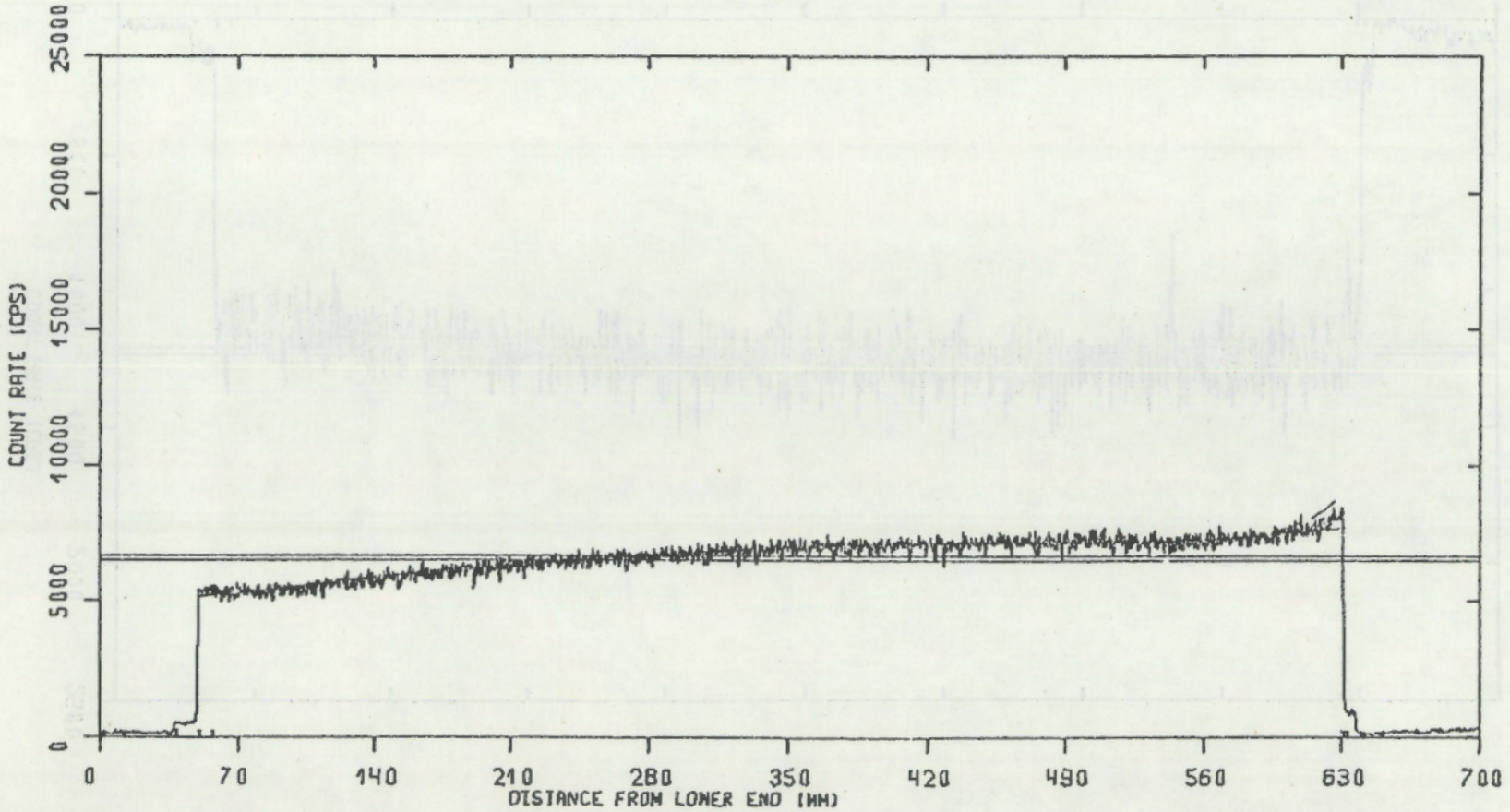

FIGURE C.7 Axial Gamma Scan for Rod 3, Channel B

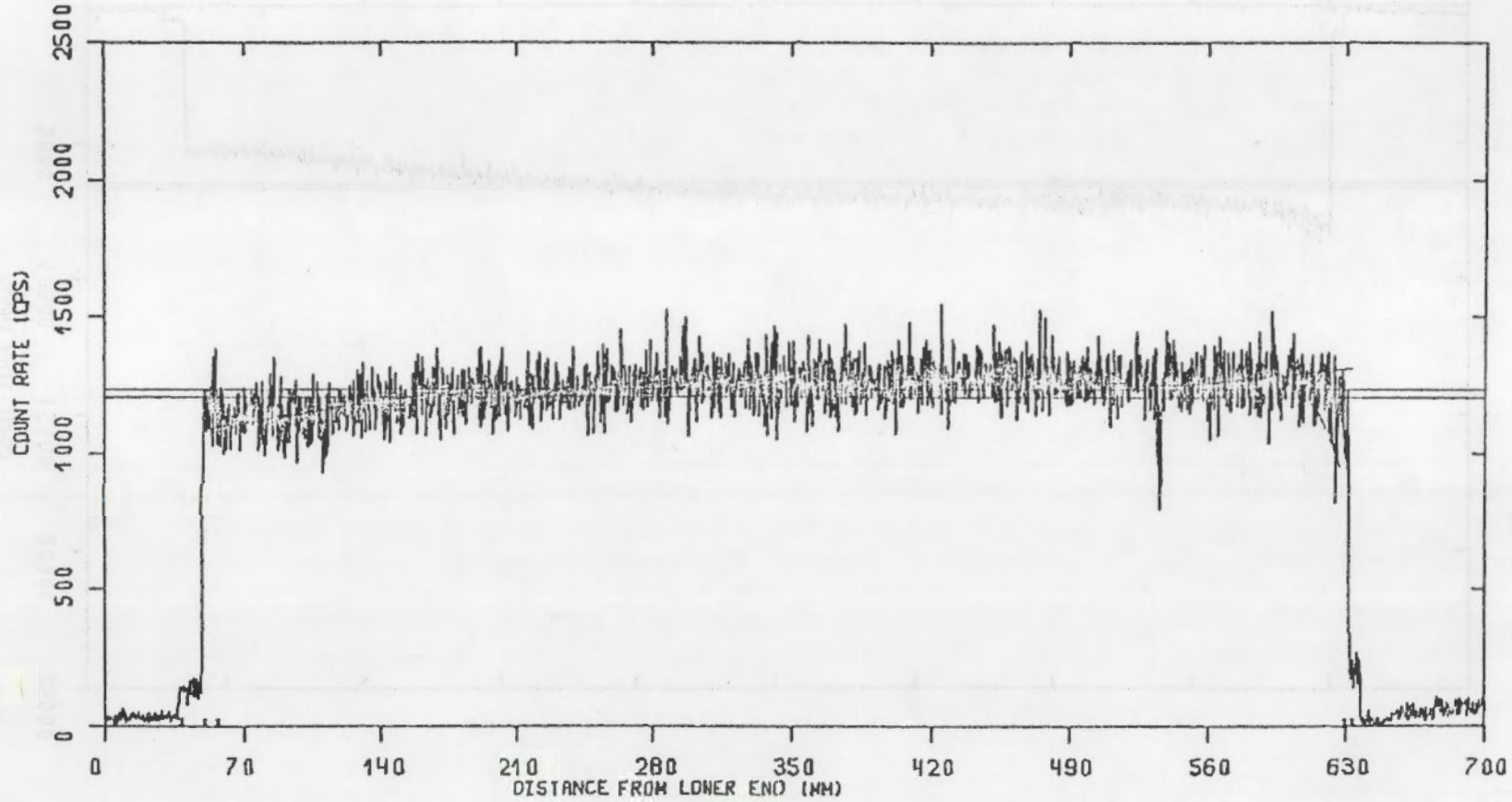

FIGURE C.8 Axial Gamma Scan for Rod 4, Channel A

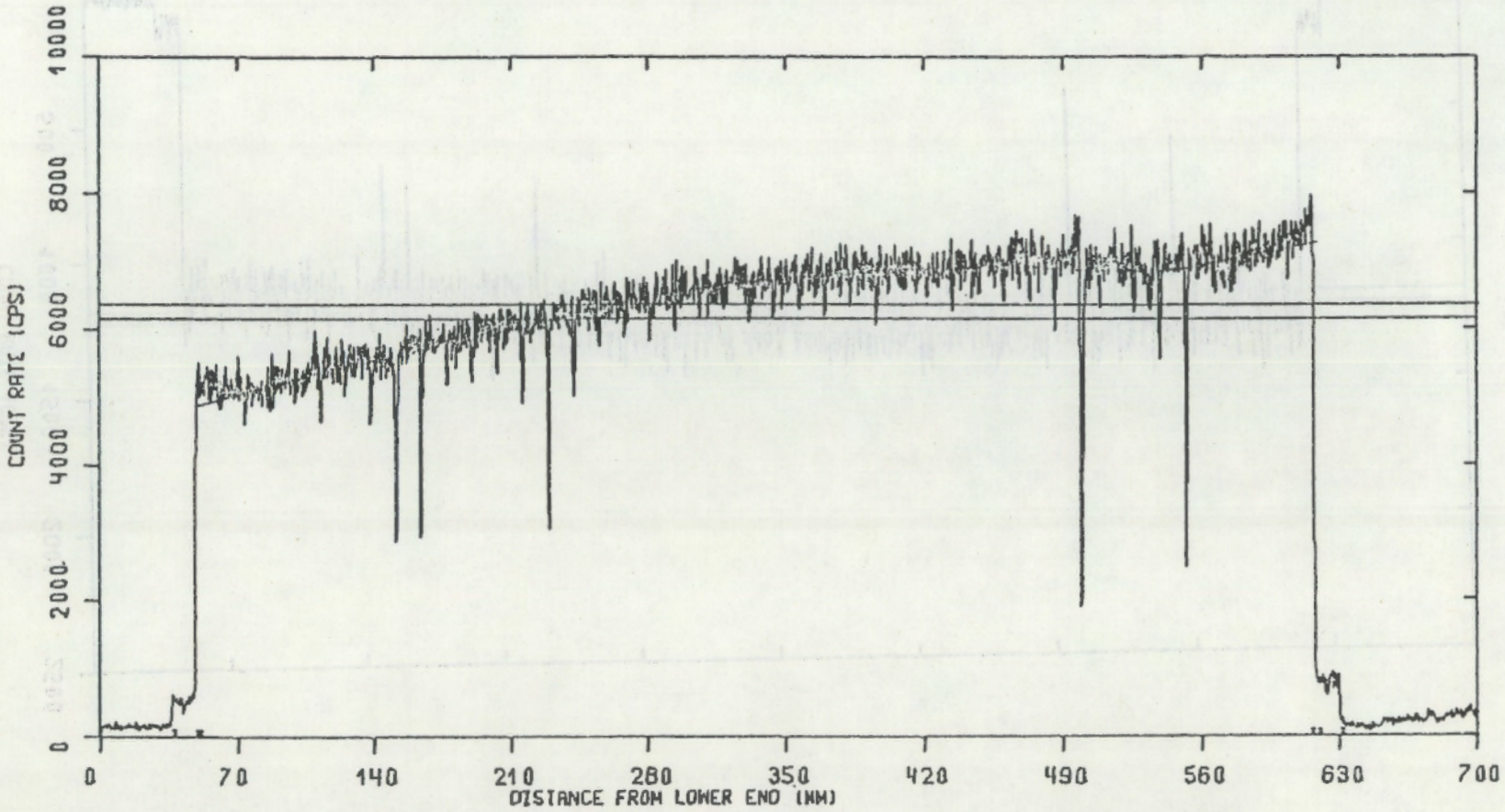

FIGURE C.9 Axial Gamm Scan for Rod 4, Channel B

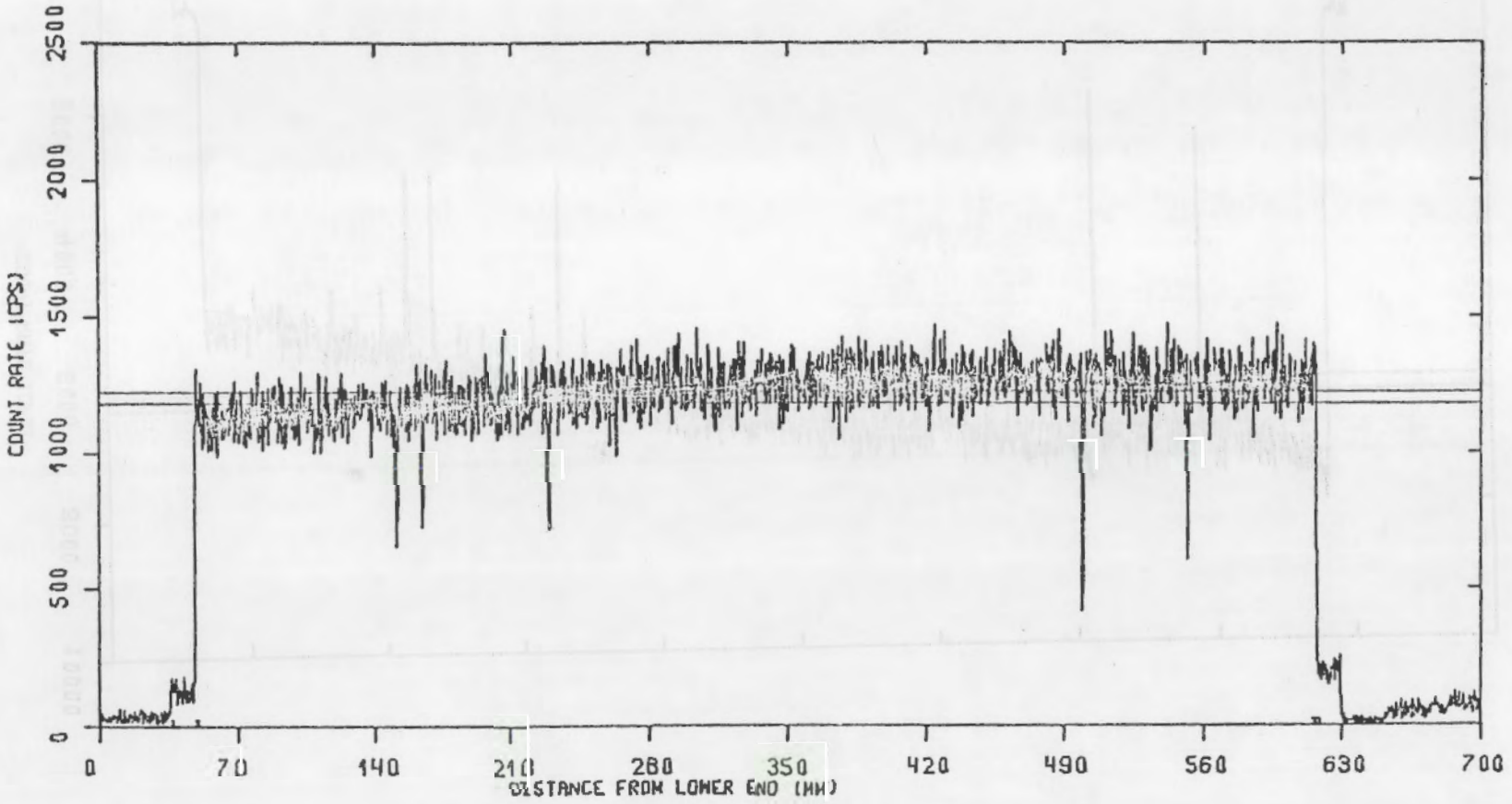

FIGURE C.10 Axial Gamma Scan for Rod 5, Channel A.

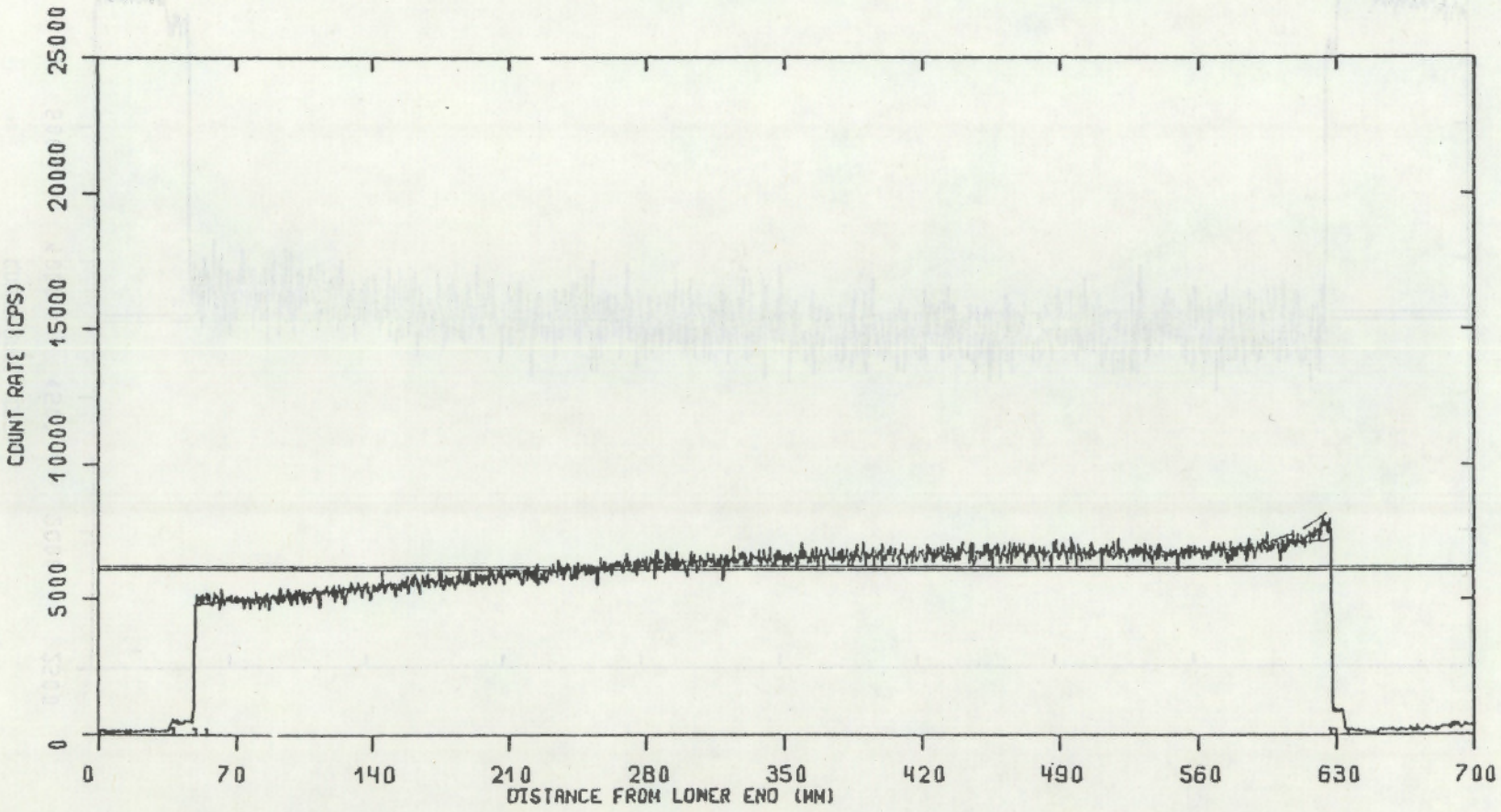

FIGURE C.11 Axial Gamma Scan for Rod 5, Channel B

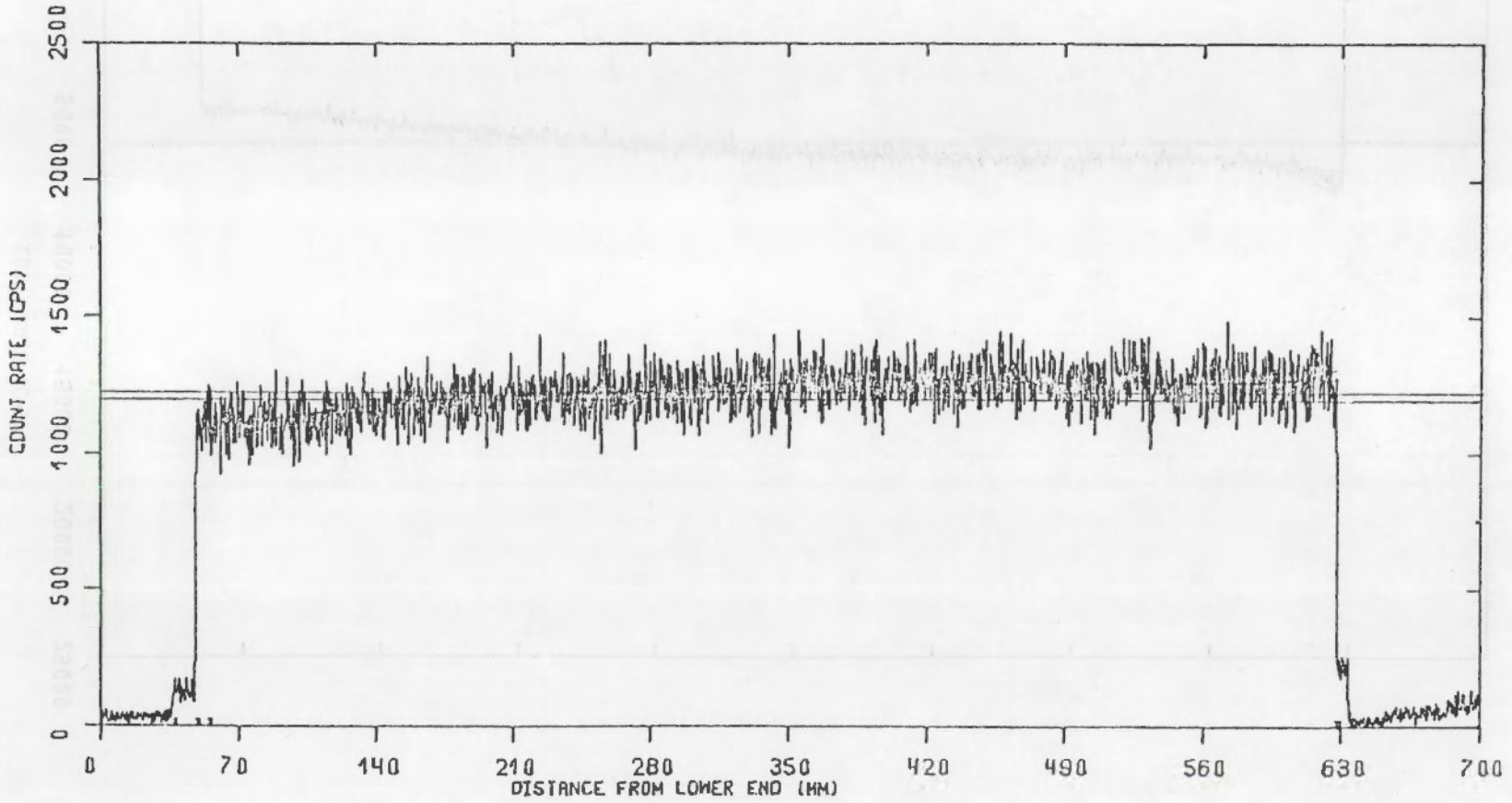

FIGURE C.12 Axial Gamma Scan for Rod 6, Channel A

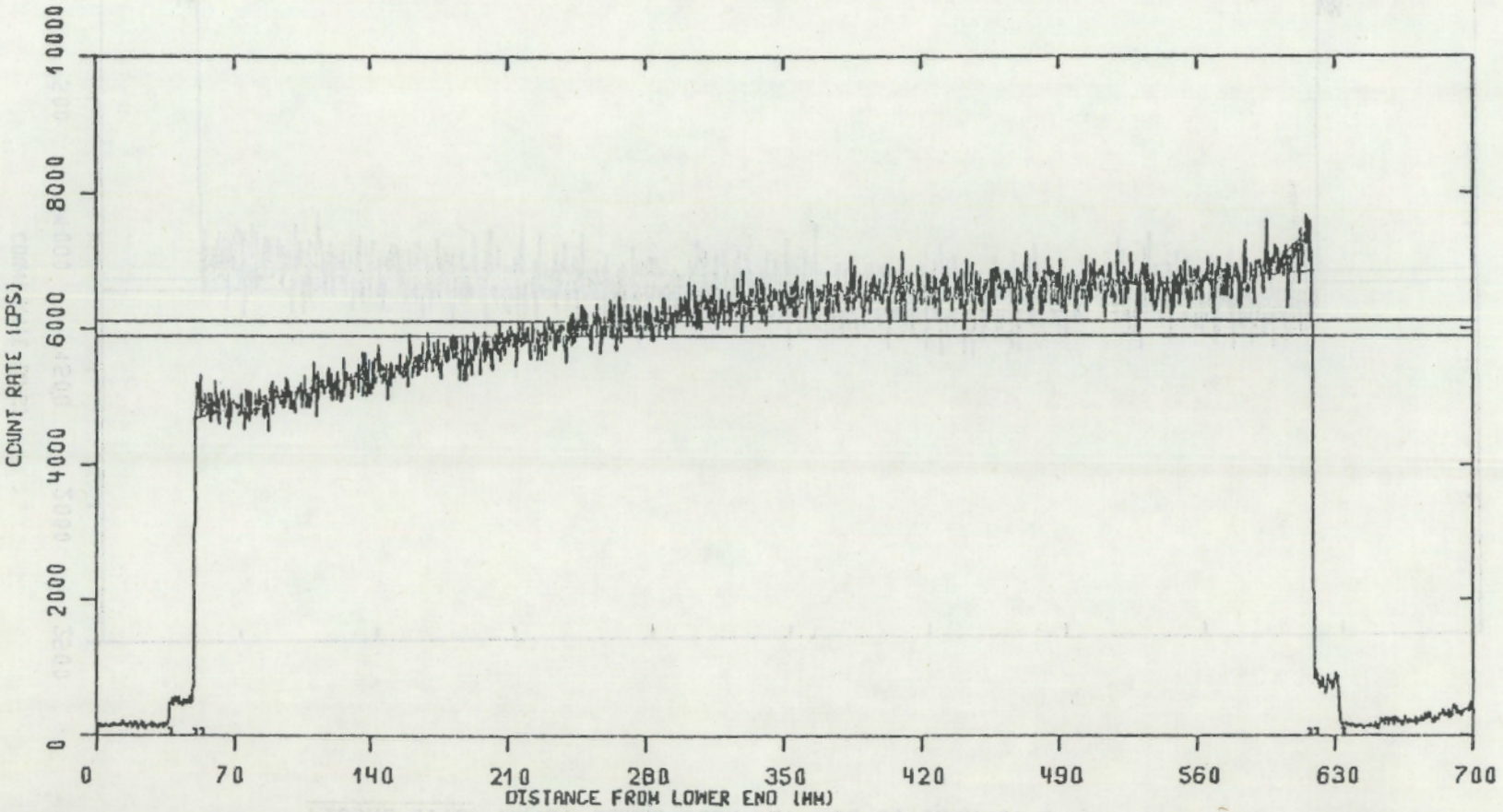

FIGURE C.13 Axial Gamma Scan for Rod 6, Channel B

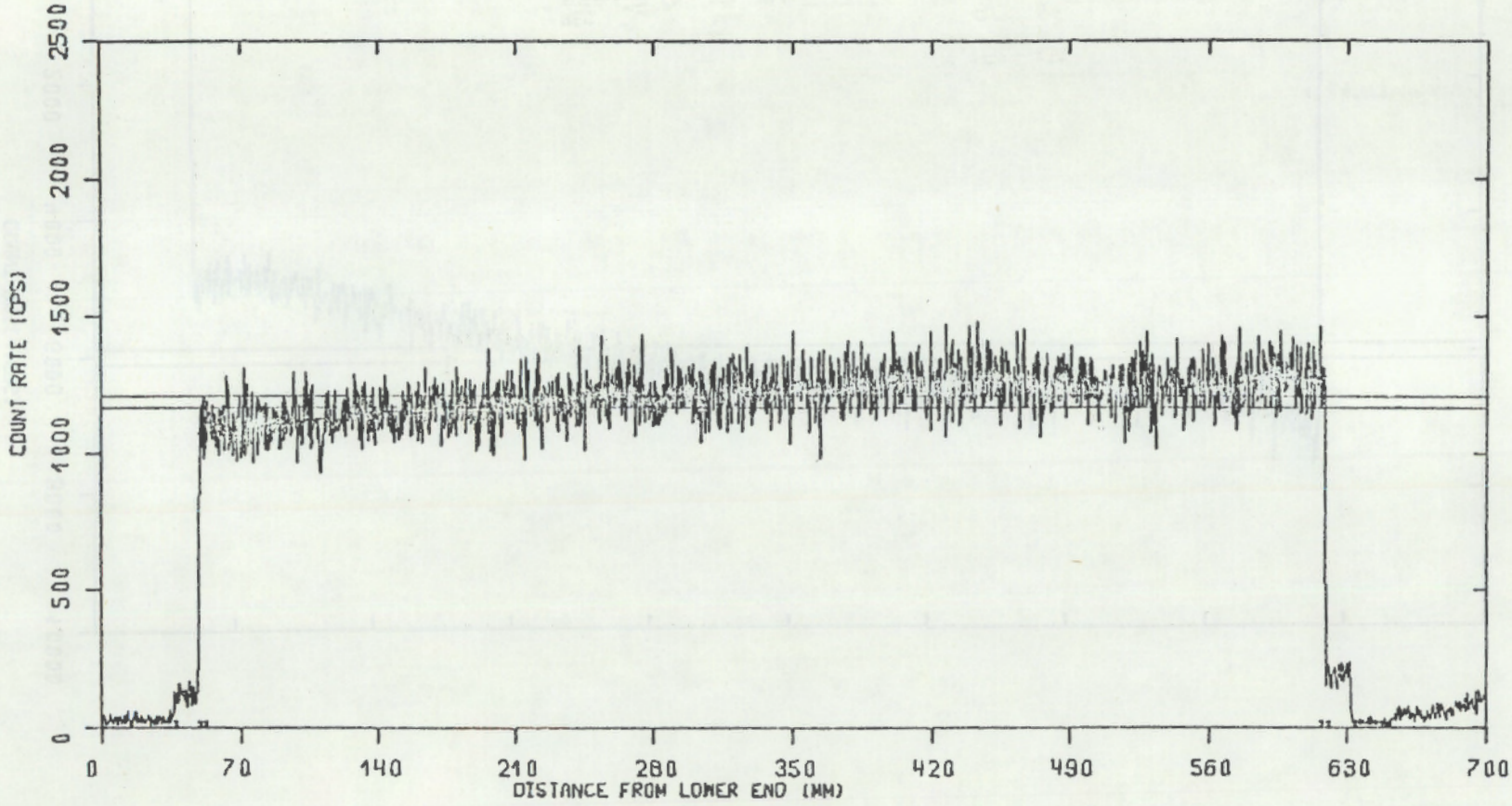

FIGURE C.14. Axial Gamma Scan for Cs 137 and Zr 95/Nb 95 (with Dead Time Correction) of Rod 6, IFA-431

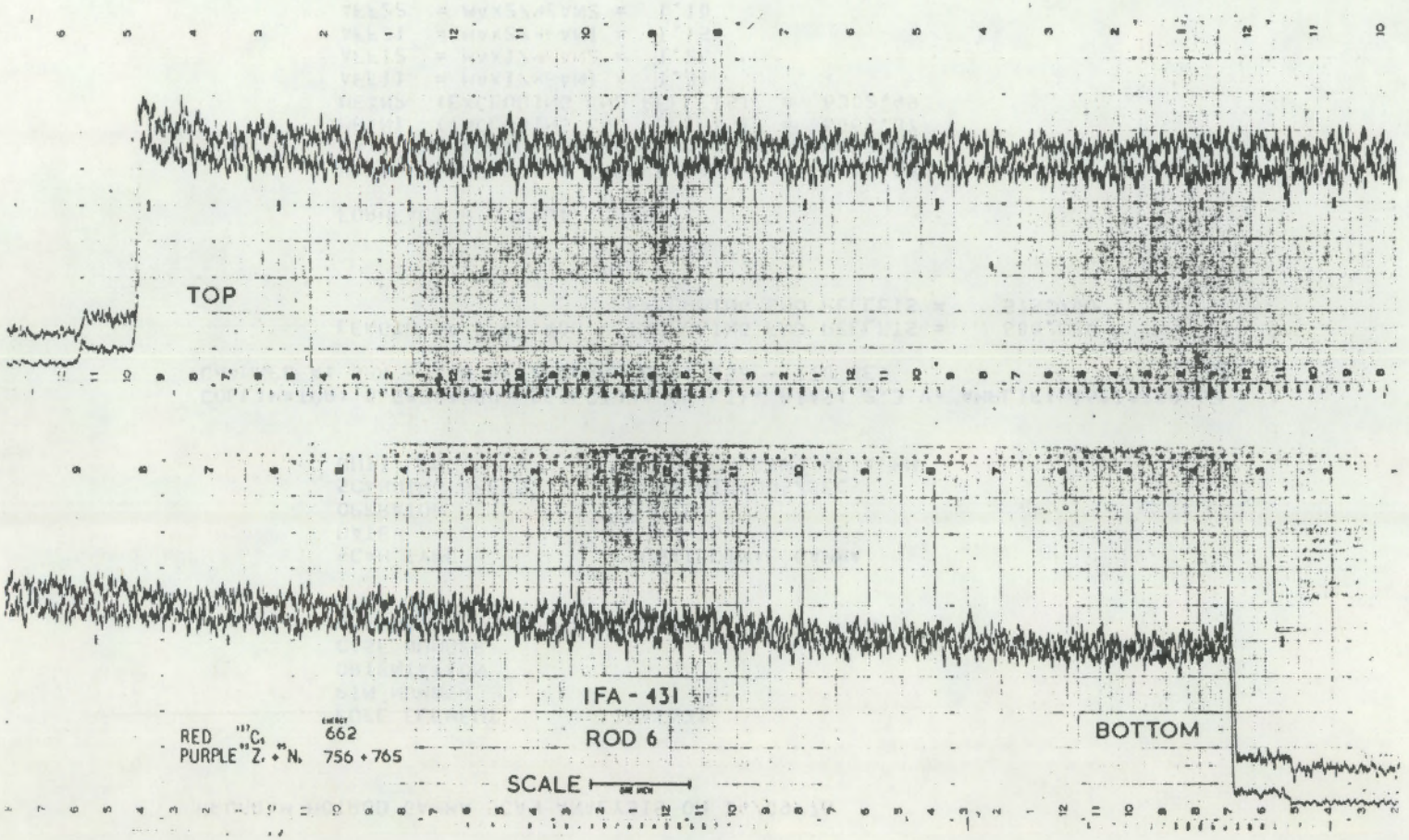

TABLE C.1 Gamma Scanning Results for Rod 1, Channel A

PROGRAM HOTROD GAMMA SCAN ANALYSIS ON 14/09/76

FUEL ELEMENT	IFA 431
PIN NUMBER	1
ORIENTATION	0
CASE NUMBER	1
ENERGY CHANNEL	A
SCAN TYPE	LONGITUDINAL GAMMA
DATE	3/9-76
OPERATOR	O.S.
SCANNING SPEED	500. MICRONS/SEC
UNIT LENGTH	30 HUNDREDTHS OF A MM

COLLIMATOR: 0.5*20*200, DETECTOR: GE(LI), BIAS: 2.3 V. AMPLIF: 16*1*2*0.62
CHANNEL A: 584 - 775 KEV. CHANNEL B: 752 - 770 KEV

LENGTH OF FUEL ROD , INCLUDING END PELLETS = 600.600
EXCLUDING END PELLETS = 575.700

FORMFACTOR OUTPUT

MAX1	(INCLUDING END PEAKS)	= 7919.08
MAX2	(EXCLUDING END PEAKS)	= 6959.19
MEAN1	(INCLUDING END PELLETS)	= 6066.37
MEAN2	(EXCLUDING END PELLETS)	= 6302.49
AFF11	= MAX1/MEAN1 =	1.31
AFF12	= MAX1/MEAN2 =	1.26
AFF21	= MAX2/MEAN1 =	1.15
AFF22	= MAX2/MEAN2 =	1.10

END PEAKING OUTPUT

LOWER END PEAKING =	4.	PERCENT
UPPER END PEAKING =	8.	PERCENT

TABLE C.2 Gamma Scanning Results for Rod 1, Channel B

PROGRAM HOTROD GAMMA SCAN ANALYSIS ON 14/09/76

FUEL ELEMENT	IFA 431
PIN NUMBER	1
ORIENTATION	0
CASE NUMBER	1
ENERGY CHANNEL	B
SCAN TYPE	LONGITUDINAL GAMMA
DATE	3/9-76
OPERATOR	OLS.
SCANNING SPEED	500. MICRONS/SEC
UNIT LENGTH	30 HUNDREDTHS OF A MM

COLLIMATOR: 0.5*20*200, DETECTOR: GE(LI), BIAS: 2.3 V, AMPLIF: 16*1*2*0.62
CHANNEL A: 584 - 775 KEV, CHANNEL B: 752 - 770 KEV

LENGTH OF FUEL ROD , INCLUDING END PELLETS = 600.000
EXCLUDING END PELLETS = 575.100

FORMFACTOR OUTPUT

MAX1	(INCLUDING END PEAKS) =	1277.92
MAX2	(EXCLUDING END PEAKS) =	1274.18
MEAN1	(INCLUDING END PELLETS) =	1179.77
MEAN2	(EXCLUDING END PELLETS) =	1223.84
AFF11	= MAX1/MEAN1 =	1.08
AFF12	= MAX1/MEAN2 =	1.04
AFF21	= MAX2/MEAN1 =	1.08
AFF22	= MAX2/MEAN2 =	1.04

END PEAKING OUTPUT

LOWER END PEAKING =	0.	PERCENT
UPPER END PEAKING =	-9.	PERCENT

TABLE C.3 Gamma Scanning Results for Rod 2, Channel A

PROGRAM HOTROD GAMMA SCAN ANALYSIS ON 14/09/76

FUEL ELEMENT	IFA 431
PIN NUMBER	2
ORIENTATION	0
CASE NUMBER	1
ENERGY CHANNEL	A
SCAN TYPE	LONGITUDINAL GAMMA
DATE	3/9-76
OPERATOR	O.S.
SCANNING SPEED	500. MICRONS/SEC
UNIT LENGTH	30 HUNDREDTHS OF A MM

COLLIMATOR: 0.5*20*200, DETECTOR: GE(LI), BIAS: 2.3 V, AMPLIF: 16*1*2*0.62
CHANNEL A: 584 - 775 KEV, CHANNEL B: 752 - 770 KEV

LENGTH OF FUEL ROD , INCLUDING END PELLETS = 594.000
EXCLUDING END PELLETS = 576.000

FORMFACTOR OUTPUT

MAX1	(INCLUDING END PEAKS)	= 8311.89
MAX2	(EXCLUDING END PEAKS)	= 7126.58
MEAN1	(INCLUDING END PELLETS)	= 6309.02
MEAN2	(EXCLUDING END PELLETS)	= 6487.05

AFF11 = MAX1/MEAN1 = 1.32
AFF12 = MAX1/MEAN2 = 1.28
AFF21 = MAX2/MEAN1 = 1.13
AFF22 = MAX2/MEAN2 = 1.10

END PEAKING OUTPUT

LOWER END PEAKING = 6. PERCENT
UPPER END PEAKING = 14. PERCENT

TABLE C.4 Gamma Scanning Results for Rod 2, Channel B

PROGRAM HOTROD GAMMA SCAN ANALYSIS ON 14/09/76

FUEL ELEMENT	IFA 431
PIN NUMBER	2
ORIENTATION	0
CASE NUMBER	1
ENERGY CHANNEL	B
SCAN TYPE	LONGITUDINAL GAMMA
DATE	3/9-76
OPERATOR	O.S.
SCANNING SPEED	500. MICRONS/SEC
UNIT LENGTH	30 HUNDREDTHS OF A MM

COLLIMATOR: 0.5*20*200, DETECTOR: GE(LI), BIAS: 2.3 V, AMPLIF: 16*1*2*0.62
CHANNEL A: 584 - 775 KEV, CHANNEL B: 752 - 770 KEV

LENGTH OF FUEL ROD , INCLUDING END PELLETS = 594.300
EXCLUDING END PELLETS = 575.700

FORMFACTOR OUTPUT

MAX1	(INCLUDING END PEAKS)	= 1277.27
MAX2	(EXCLUDING END PEAKS)	= 1277.27
MEAN1	(INCLUDING END PELLETS)	= 1199.76
MEAN2	(EXCLUDING END PELLETS)	= 1233.51

AFF11 = MAX1/MEAN1 = 1.06
AFF12 = MAX1/MEAN2 = 1.04
AFF21 = MAX2/MEAN1 = 1.06
AFF22 = MAX2/MEAN2 = 1.04

END PEAKING OUTPUT

LOWER END PEAKING = 1. PERCENT
UPPER END PEAKING = -0. PERCENT

TABLE C.5. Gamma Scanning Results for Rod 3, Channel A

PROGRAM HOTROD GAMMA SCAN ANALYSIS ON 14/09/76

FUEL ELEMENT	IFA 431
PIN NUMBER	3
ORIENTATION	0
CASE NUMBER	1
ENERGY CHANNEL	A
SCAN TYPE	LONGITUDINAL GAMMA
DATE	3/9-76
OPERATOR	O(S.
SCANNING SPEED	500. MICRONS/SEC
UNIT LENGTH	30 HUNDREDTHS OF A MM

COLLIMATOR: 0.5*20*200, DETECTOR: GE(LI), BIAS: 2.3 V, AMPLIF: 16*1*2*0.62
CHANNEL A: 584 - 775 KEV, CHANNEL B: 752 - 770 KEV

LENGTH OF FUEL ROD ,	INCLUDING END PELLETS =	601.800
	EXCLUDING END PELLETS =	582.600

FORMFACTOR OUTPUT

MAX1	(INCLUDING END PEAKS) =	8981.62
MAX2	(EXCLUDING END PEAKS) =	7397.45
MEAN1	(INCLUDING END PELLETS) =	6482.00
MEAN2	(EXCLUDING END PELLETS) =	6675.08
AFF11	= MAX1/MEAN1 =	1.39
AFF12	= MAX1/MEAN2 =	1.35
AFF21	= MAX2/MEAN1 =	1.14
AFF22	= MAX2/MEAN2 =	1.11

END PEAKING OUTPUT

LOWER END PEAKING =	3.	PERCENT
UPPER END PEAKING =	16.	PERCENT

TABLE C.6 Gamma Scanning Results for Rod 3, Channel B

PROGRAM HOTROD GAMMA SCAN ANALYSIS ON 14/09/76

FUEL ELEMENT	IFA 431
PIN NUMBER	3
ORIENTATION	0
CASE NUMBER	1
ENERGY CHANNEL	B
SCAN TYPE	LONGITUDINAL GAMMA
DATE	3/9-76
OPERATOR	O.L.S.
SCANNING SPEED	500. MICRONS/SEC
UNIT LENGTH	30 HUNDREDTHS OF A MM

COLLIMATOR: 0.5*20*200, DETECTOR: GE(LI), BIAS: 2.3 V, AMPLIF: 16*1*2*0.62
CHANNEL A: 584 - 775 KEV, CHANNEL B: 752 - 770 KEV

LENGTH OF FUEL ROD , INCLUDING END PELLETS = 600.900
EXCLUDING END PELLETS = 582.900

FORMFACTOR OUTPUT

MAX1	(INCLUDING END PEAKS)	= 1280.82
MAX2	(EXCLUDING END PEAKS)	= 1280.82
MEAN1	(INCLUDING END PELLETS)	= 1203.84
MEAN2	(EXCLUDING END PELLETS)	= 1235.97
AFF11	= MAX1/MEAN1 =	1.06
AFF12	= MAX1/MEAN2 =	1.04
AFF21	= MAX2/MEAN1 =	1.06
AFF22	= MAX2/MEAN2 =	1.04

END PEAKING OUTPUT

LOWER END PEAKING =	6.	PERCENT
UPPER END PEAKING =	-32.	PERCENT

TABLE C.7 Gamma Scanning Results for Rod 4, Channel A

PROGRAM HOTROD GAMMA SCAN ANALYSIS ON 14/09/76

FUEL ELEMENT	IFA 431
PIN NUMBER	4
ORIENTATION	0
CASE NUMBER	1
ENERGY CHANNEL	A
SCAN TYPE	LONGITUDINAL GAMMA
DATE	3/9-76
OPERATOR	O. S.
SCANNING SPEED	500. MICRONS/SEC
UNIT LENGTH	30 HUNDREDTHS OF A MM

COLLIMATOR: 0.5*20*200, DETECTOR: GE(LI), BIAS: 2.3 V, AMPLIF: 16*1*2*0.62
CHANNEL A: 584 - 775 KEV, CHANNEL B: 752 - 770 KEV

LENGTH OF FUEL ROD , INCLUDING END PELLETS = 593.400
EXCLUDING END PELLETS = 570.000

FORMFACTOR OUTPUT

MAX1	(INCLUDING END PEAKS)	= 7510.30
MAX2	(EXCLUDING END PEAKS)	= 6967.02
MEAN1	(INCLUDING END PELLETS)	= 6155.30
MEAN2	(EXCLUDING END PELLETS)	= 6379.07
AFF11	= MAX1/MEAN1 =	1.22
AFF12	= MAX1/MEAN2 =	1.18
AFF21	= MAX2/MEAN1 =	1.13
AFF22	= MAX2/MEAN2 =	1.09

END PEAKING OUTPUT

LOWER END PEAKING = 8. PERCENT
UPPER END PEAKING = 3. PERCENT

TABLE C.8 Gamma Scanning Results for Rod 4, Channel B

PROGRAM HOTROD GAMMA SCAN ANALYSIS ON 14/09/76

FUEL ELEMENT	IFA 431
PIN NUMBER	4
ORIENTATION	0
CASE NUMBER	1
ENERGY CHANNEL	B
SCAN TYPE	LONGITUDINAL GAMMA
DATE	3/9-76
OPERATOR	OLS.
SCANNING SPEED	500. MICRONS/SEC
UNIT LENGTH	30 HUNDREDTHS OF A MM

COLLIMATOR: 0.5*20*200, DETECTOR: GE(LI), BIAS: 2.3 V, AMPLIF: 16*1*2*0.62
CHANNEL A: 584 - 775 KEV, CHANNEL B: 752 - 770 KEV

LENGTH OF FUEL ROD , INCLUDING END PELLETS = 594.900
EXCLUDING END PELLETS = 568.800

FORMFACTOR OUTPUT

MAX1	(INCLUDING END PEAKS)	= 1284.52
MAX2	(EXCLUDING END PEAKS)	= 1284.52
MEAN1	(INCLUDING END PELLETS)	= 1180.14
MEAN2	(EXCLUDING END PELLETS)	= 1226.49
AFF11	= MAX1/MEAN1 =	1.09
AFF12	= MAX1/MEAN2 =	1.05
AFF21	= MAX2/MEAN1 =	1.09
AFF22	= MAX2/MEAN2 =	1.05

END PEAKING OUTPUT

LOWER END PEAKING = 1. PERCENT
UPPER END PEAKING = -3. PERCENT

TABLE C.9 Gamma Scanning Results for Rod 5, Channel A

PROGRAM HOTROD GAMMA SCAN ANALYSIS ON 14/09/76

FUEL ELEMENT	IFA 431
PIN NUMBER	5
ORIENTATION	0
CASE NUMBER	1
ENERGY CHANNEL	A
SCAN TYPE	LONGITUDINAL GAMMA
DATE	3/9-76
OPERATOR	OLS.
SCANNING SPEED	500. MICRONS/SEC
UNIT LENGTH	30 HUNDREDTHS OF A MM

COLLIMATOR: 0.5*20*200, DETECTOR: GE(LI), BIAS: 2.3 V, AMPLIF: 16*1*2*0.62
CHANNEL A: 584 - 775 KEV, CHANNEL B: 752 - 770 KEV

LENGTH OF FUEL ROD , INCLUDING END PELLETS = 597.900
EXCLUDING END PELLETS = 580.200

FORMFACTOR OUTPUT

MAX1	(INCLUDING END PEAKS)	= 8331.97
MAX2	(EXCLUDING END PEAKS)	= 6909.73
MEAN1	(INCLUDING END PELLETS)	= 6102.93
MEAN2	(EXCLUDING END PELLETS)	= 6271.85
AFF11	= MAX1/MEAN1 =	1.37
AFF12	= MAX1/MEAN2 =	1.33
AFF21	= MAX2/MEAN1 =	1.13
AFF22	= MAX2/MEAN2 =	1.10

END PEAKING OUTPUT

LOWER END PEAKING =	3.	PERCENT
UPPER END PEAKING =	15.	PERCENT

TABLE C.10 Gamma Scanning Results for Rod 5, Channel B

PROGRAM HOTROD GAMMA SCAN ANALYSIS ON 14/09/76

FUEL ELEMENT	IFA 431
PIN NUMBER	5
ORIENTATION	0
CASE NUMBER	1
ENERGY CHANNEL	B
SCAN TYPE	LONGITUDINAL GAMMA
DATE	3/9-76
OPERATOR	OLS.
SCANNING SPEED	500. MICRONS/SEC
UNIT LENGTH	30 HUNDREDTHS OF A MM

COLLIMATOR: 0.5*20*200, DETECTOR: GE(LI), BIAS: 2.3 V, AMPLIF: 16*1*2*0.62
CHANNEL A: 584 - 775 KEV, CHANNEL B: 752 - 770 KEV

LENGTH OF FUEL ROD , INCLUDING END PELLETS = 597.300
EXCLUDING END PELLETS = 579.900

FORMFACTOR OUTPUT

MAX1	(INCLUDING END PEAKS)	= 1314.16
MAX2	(EXCLUDING END PEAKS)	= 1274.97
MEAN1	(INCLUDING END PELLETS)	= 1194.25
MEAN2	(EXCLUDING END PELLETS)	= 1225.13

AFF11 = MAX1/MEAN1 = 1.10
AFF12 = MAX1/MEAN2 = 1.07
AFF21 = MAX2/MEAN1 = 1.07
AFF22 = MAX2/MEAN2 = 1.04

END PEAKING OUTPUT

LOWER END PEAKING = 2. PERCENT
UPPER END PEAKING = 3. PERCENT

TABLE C.11 Gamma Scanning Results for Rod 6, Channel A

PROGRAM HOTROD GAMMA SCAN ANALYSIS ON 14/09/76

FUEL ELEMENT	IFA 431
PIN NUMBER	6
ORIENTATION	0
CASE NUMBER	1
ENERGY CHANNEL	A
SCAN TYPE	LONGITUDINAL GAMMA
DATE	3/9-76
OPERATOR	O.S.
SCANNING SPEED	500. MICRONS/SEC
UNIT LENGTH	30 HUNDREDTHS OF A MM

COLLIMATOR: 0.5*20*200, DETECTOR: GE(LI), BIAS: 2.3 V, AMPLIF: 16*1*2*0.62
CHANNEL A: 584 - 775 KEV. CHANNEL B: 752 - 770 KEV

LENGTH OF FUEL ROD , INCLUDING END PELLETS = 596.100
EXCLUDING END PELLETS = 570.600

FORMFACTOR OUTPUT

MAX1	(INCLUDING END PEAKS)	= 7491.10
MAX2	(EXCLUDING END PEAKS)	= 6714.36
MEAN1	(INCLUDING END PELLETS)	= 5884.25
MEAN2	(EXCLUDING END PELLETS)	= 6120.24

AFF11 = MAX1/MEAN1 = 1.27
AFF12 = MAX1/MEAN2 = 1.22
AFF21 = MAX2/MEAN1 = 1.14
AFF22 = MAX2/MEAN2 = 1.10

END PEAKING OUTPUT

LOWER END PEAKING = 5. PERCENT
UPPER END PEAKING = 9. PERCENT

TABLE C.12 Gamma Scanning Results for Rod 6, Channel B

PROGRAM HOTROD GAMMA SCAN ANALYSIS ON 14/09/76

FUEL ELEMENT	IFA 431
PIN NUMBER	6
ORIENTATION	0
CASE NUMBER	1
ENERGY CHANNEL	B
SCAN TYPE	LONGITUDINAL GAMMA
DATE	3/9-76
OPERATOR	O.L.S.
SCANNING SPEED	500. MICRONS/SEC
UNIT LENGTH	30 HUNDREDTHS OF A MM

COLLIMATOR: 0.5*20*200, DETECTOR: GE(LI), BIAS: 2.3 V, AMPLIF: 16*1*2*0.62
CHANNEL A: 584 - 775 KEV, CHANNEL B: 752 - 770 KEV

LENGTH OF FUEL ROD , INCLUDING END PELLETS = 596.400
EXCLUDING END PELLETS = 570.600

FORMFACTOR OUTPUT

MAX1	(INCLUDING END PEAKS)	= 1282.92
MAX2	(EXCLUDING END PEAKS)	= 1272.73
MEAN1	(INCLUDING END PELLETS)	= 1165.60
MEAN2	(EXCLUDING END PELLETS)	= 1211.42
AFF11	= MAX1/MEAN1 =	1.10
AFF12	= MAX1/MEAN2 =	1.06
AFF21	= MAX2/MEAN1 =	1.09
AFF22	= MAX2/MEAN2 =	1.05

END PEAKING OUTPUT

LOWER END PEAKING =	4.	PERCENT
UPPER END PEAKING =	-1.	PERCENT

APPENDIX D

PROFILOMETRY

PROFILOMETRY

The profilometry results are given in Tables D-1 through D-18 and Figures D-1 through D-24. These profilometry measurements were made at Kjeller.

Three tables are presented for each fuel rod. The first table presents 0^{o} orientation profile information, while the second table shows 90^{o} orientation profile information. Diameter information is tabulated in the third table for each fuel rod.

Four plots of the results are presented for each fuel rod. The first figure for each rod shows the 0^{o} and 90^{o} orientation profiles, while the second figures shows the 180^{o} and 270^{o} orientation profile. These 180^{o} and 270^{o} orientation results were calculated by computer from the 90^{o} orientation profile and the diameter data. The third and fourth figures present diameter plots at 0^{o} orientation and 90^{o} orientation, respectively.

FIGURE 0.1 Profile for Rod 1, 0° and 90° Orientation

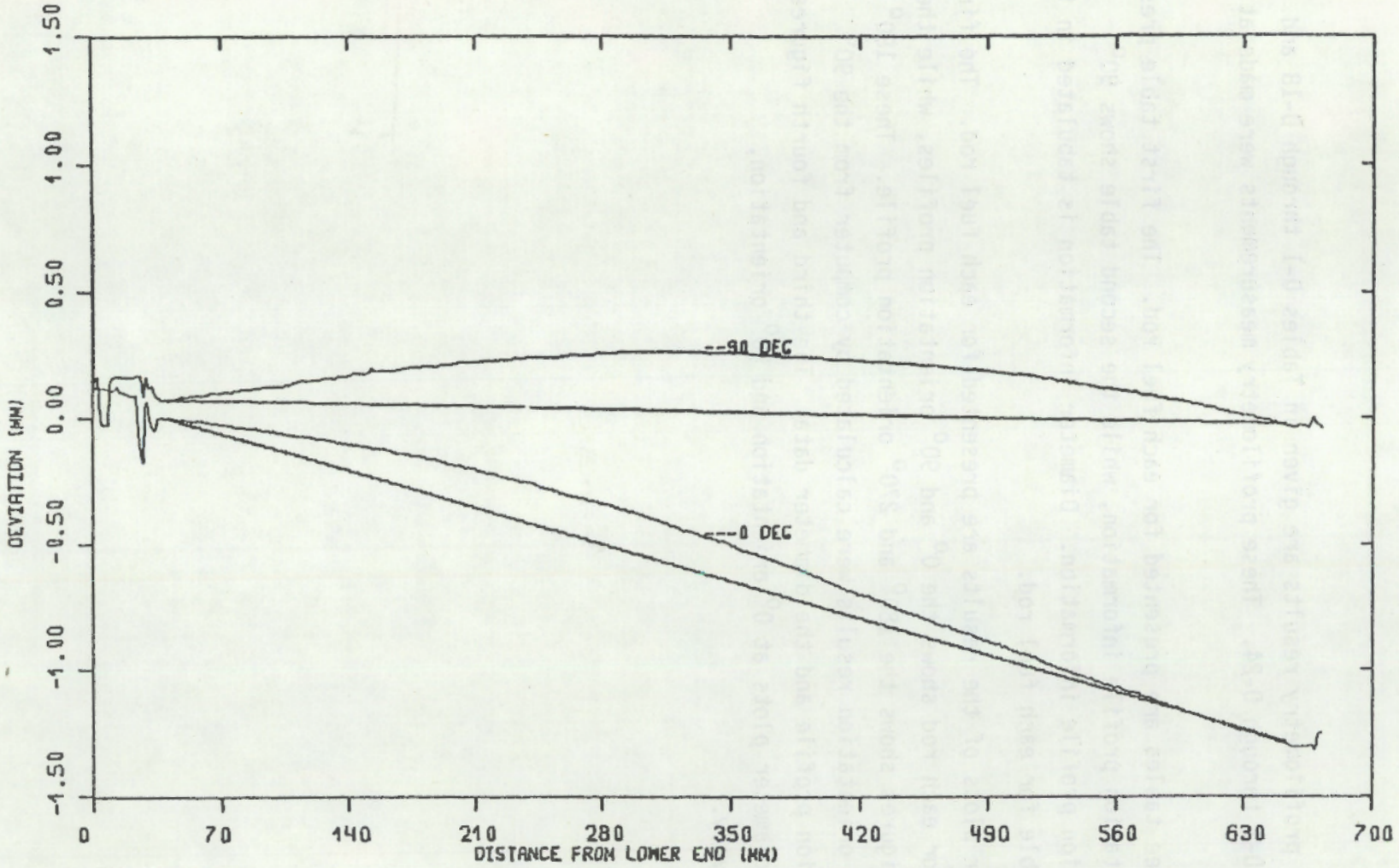

FIGURE D.2 Profile for Rod 1, 180° and 270° Orientation

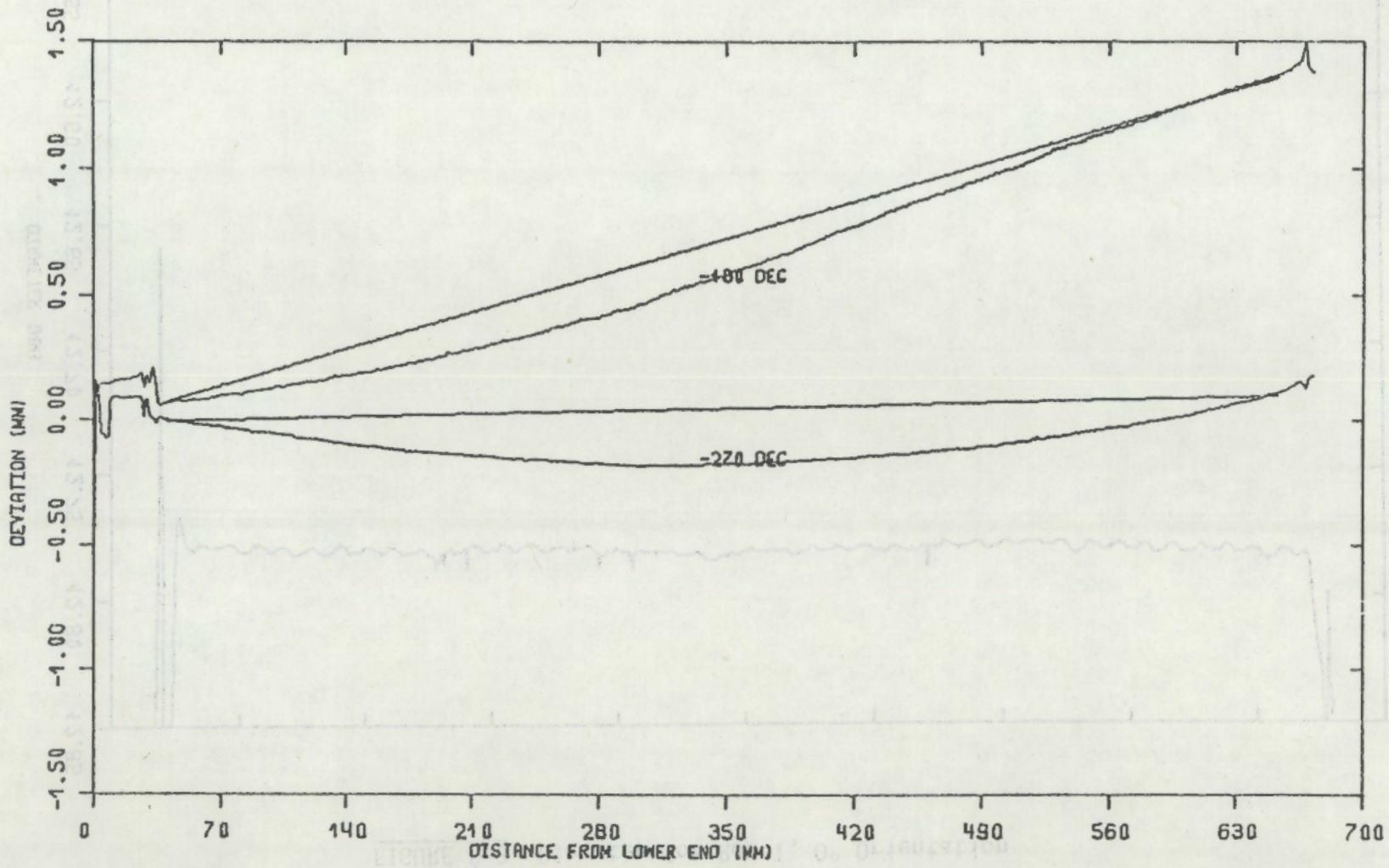

FIGURE D.3 Diameter for Rod 1, 0° Orientation

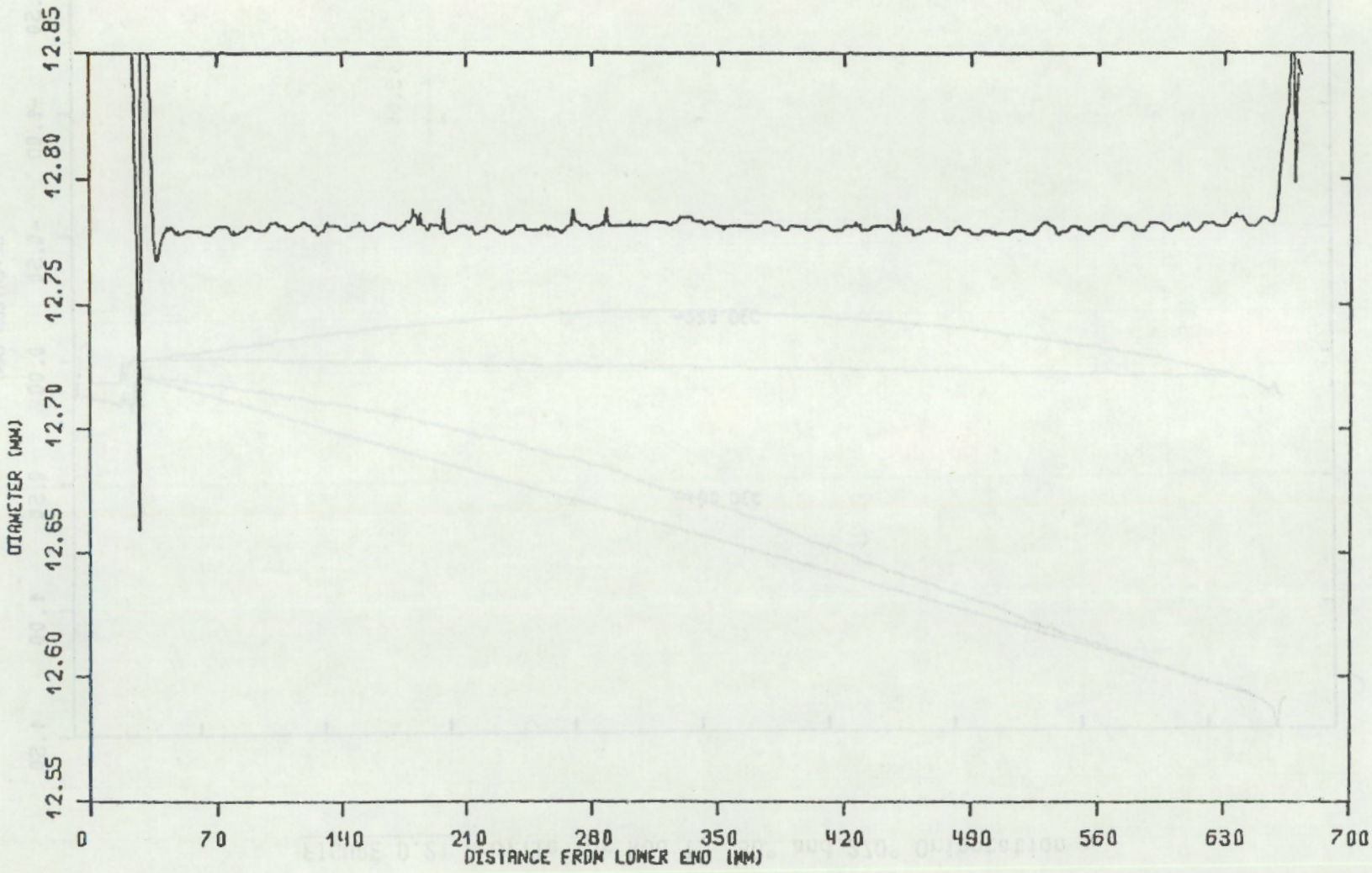

FIGURE D.4 Diameter for Rod 1, 90° Orientation

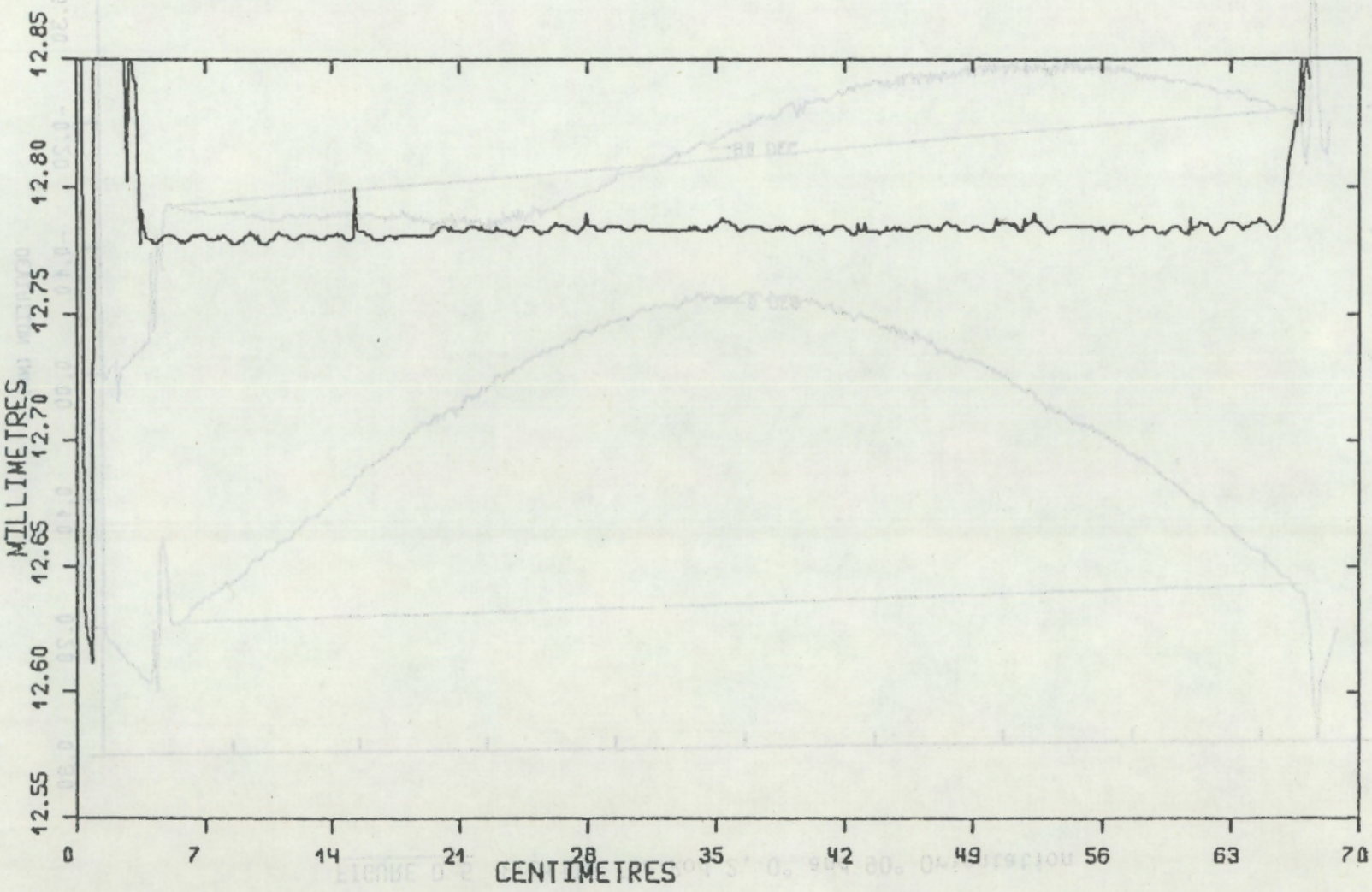

FIGURE D.5 Profile for Rod 2, 0° and 90° Orientation

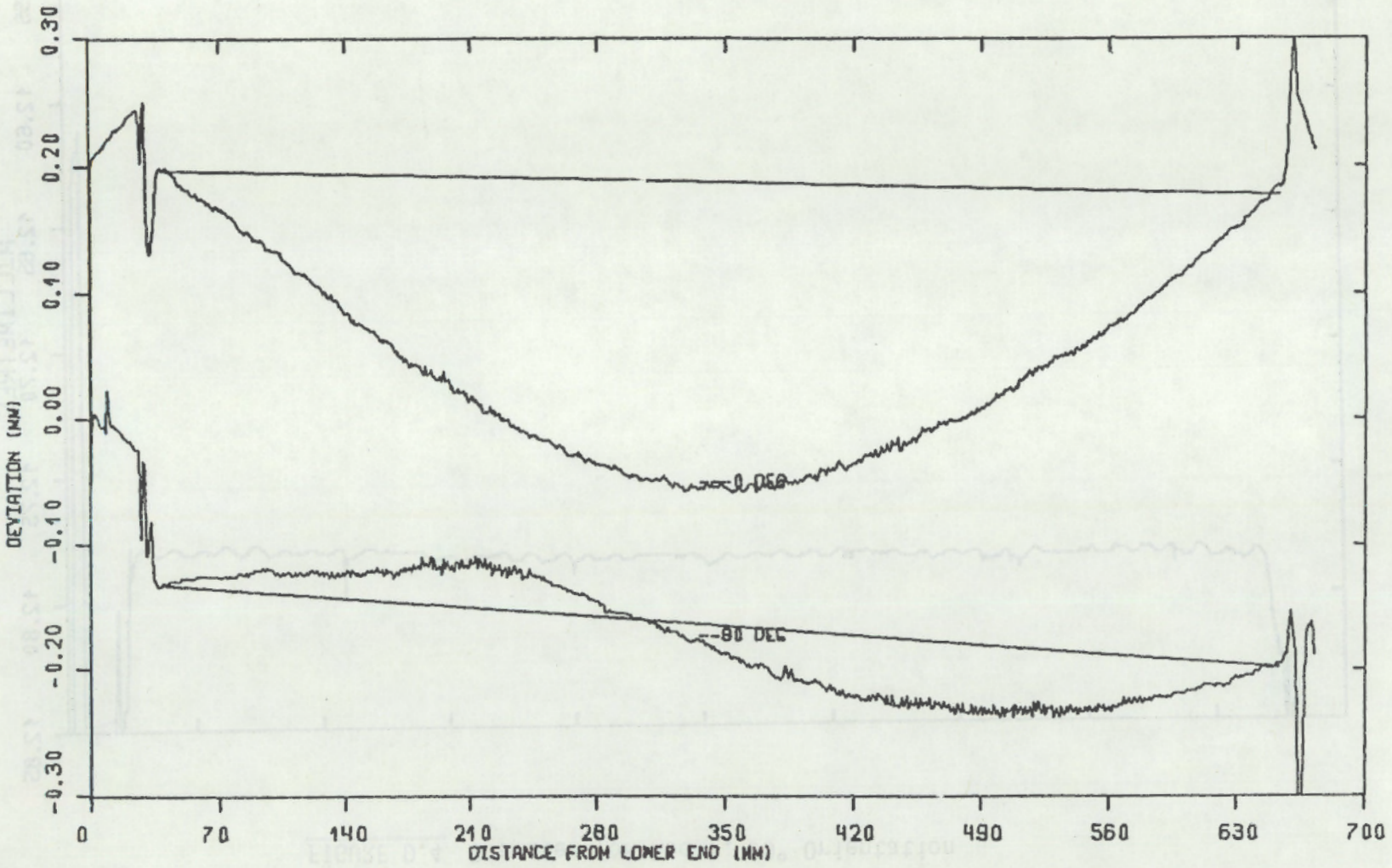

FIGURE D.6 Profile for Rod 2, 180° and 270° Orientation

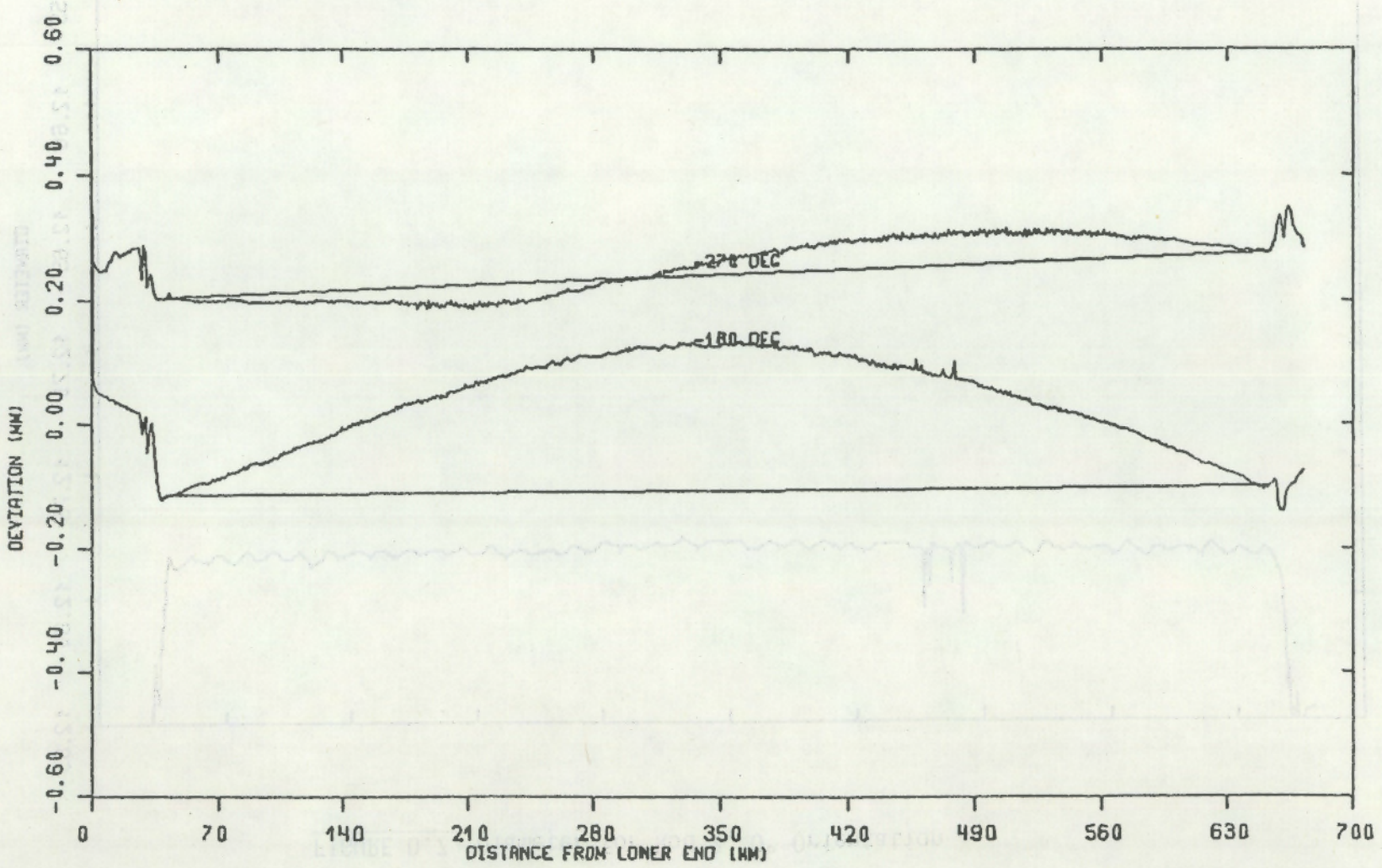

FIGURE D.7 Diameter for Rod 2, 0° Orientation

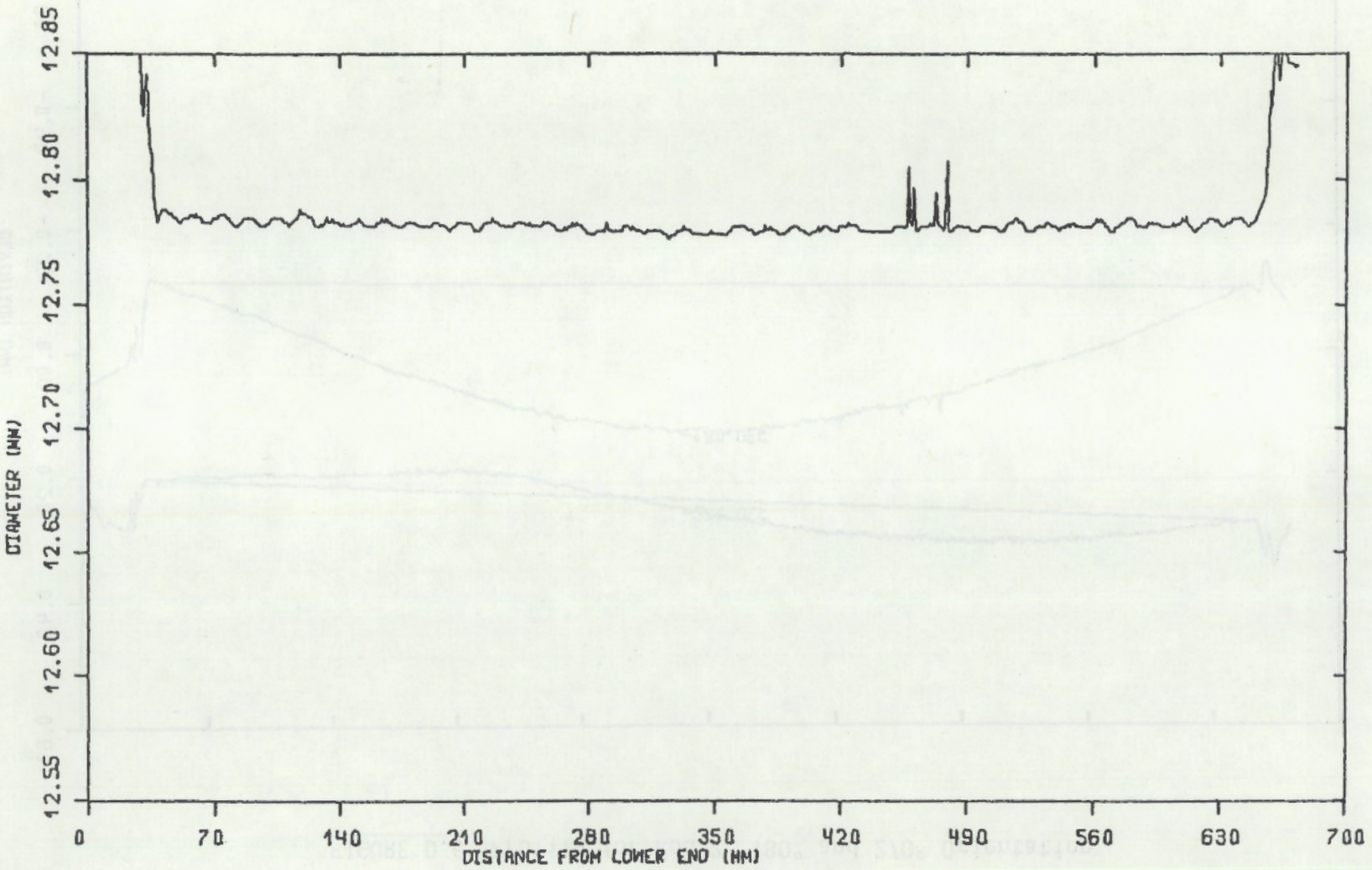

FIGURE D.8 Diameter for Rod 2, 90° Orientation

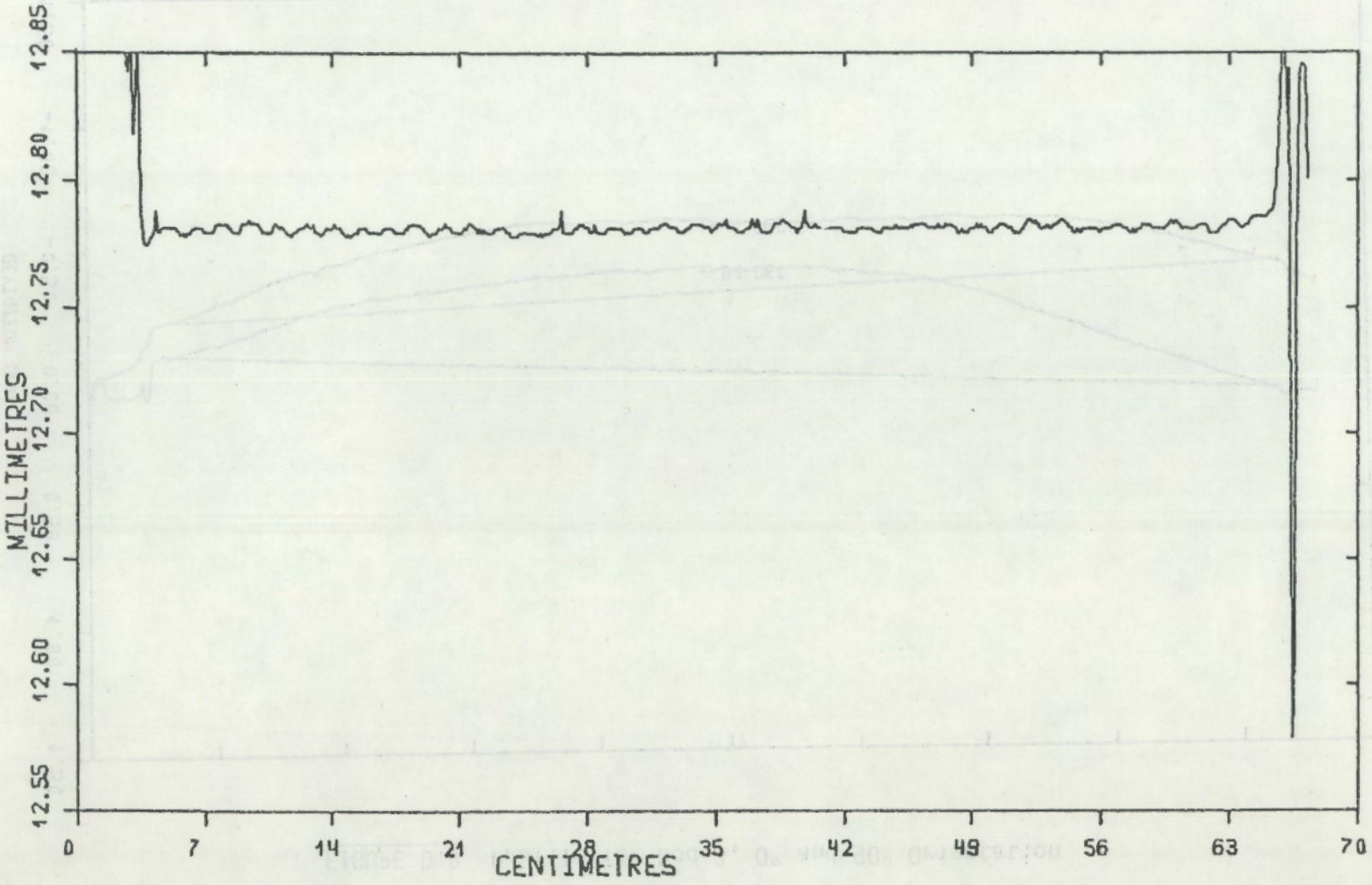

FIGURE D.9 Profile for Rod 3, 0° and 90° Orientation

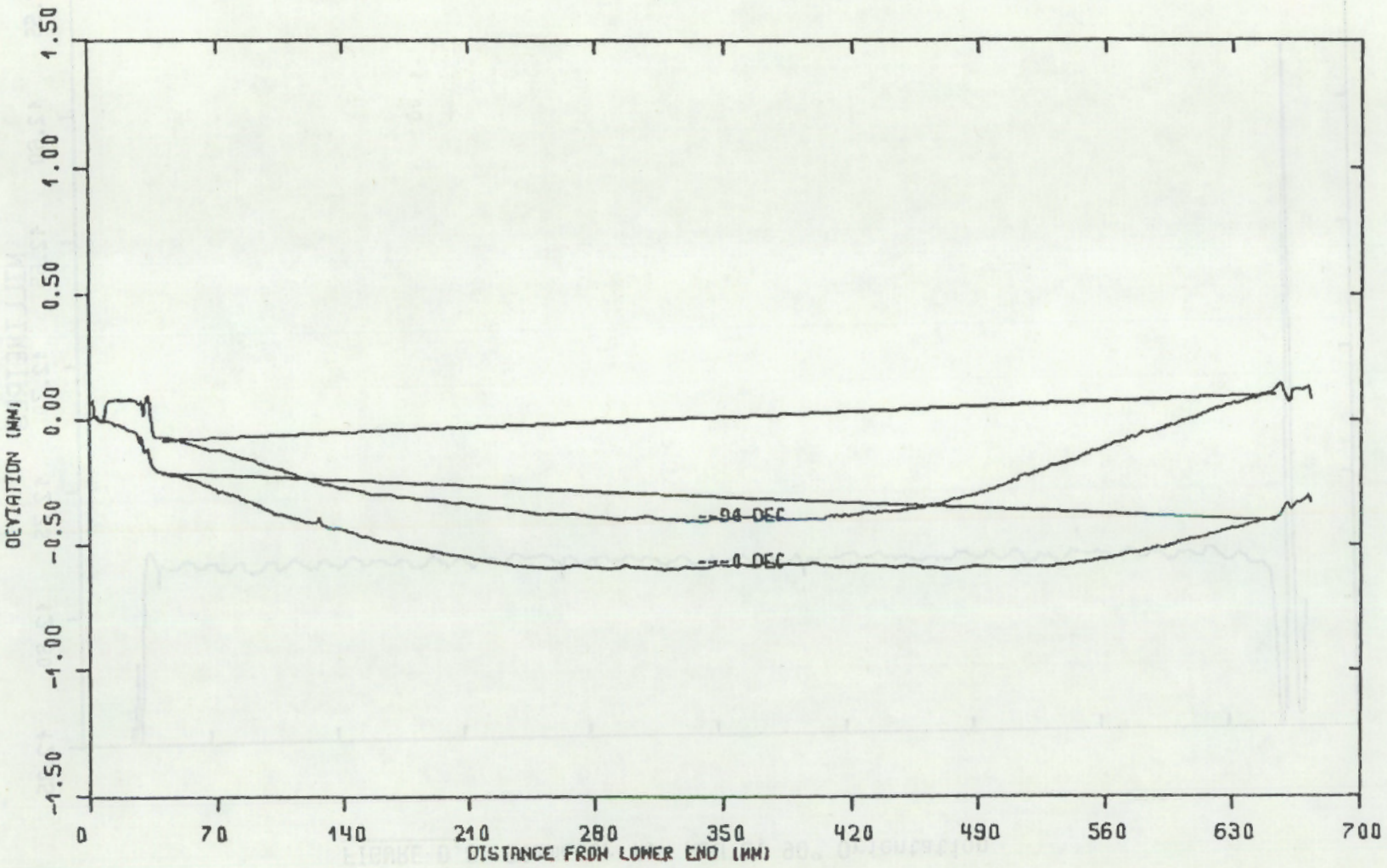

FIGURE D.10 Profile for Rod 3, 180° and 270° Orientation

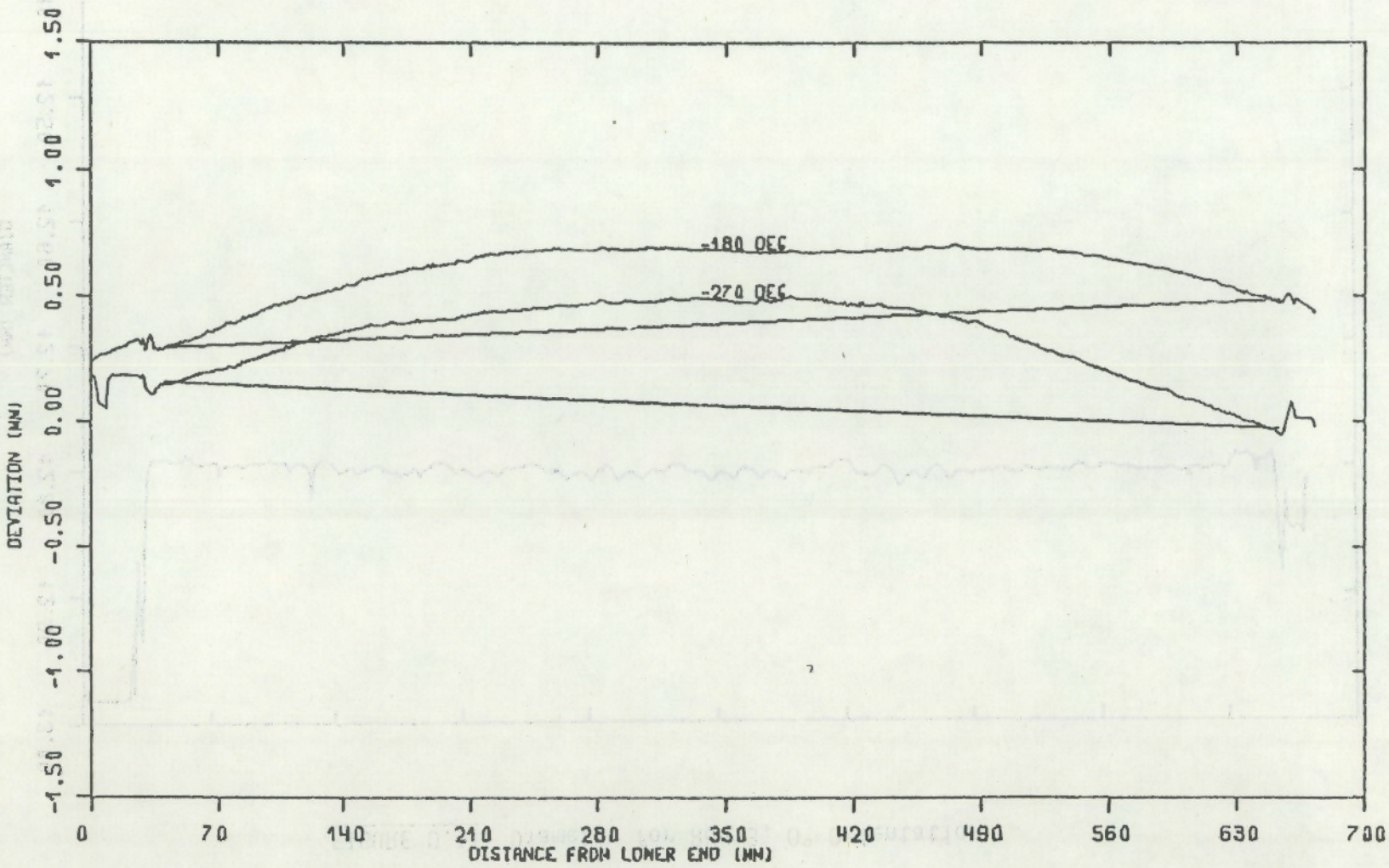

FIGURE D.11 Diameter for Rod 3, 0° Orientation

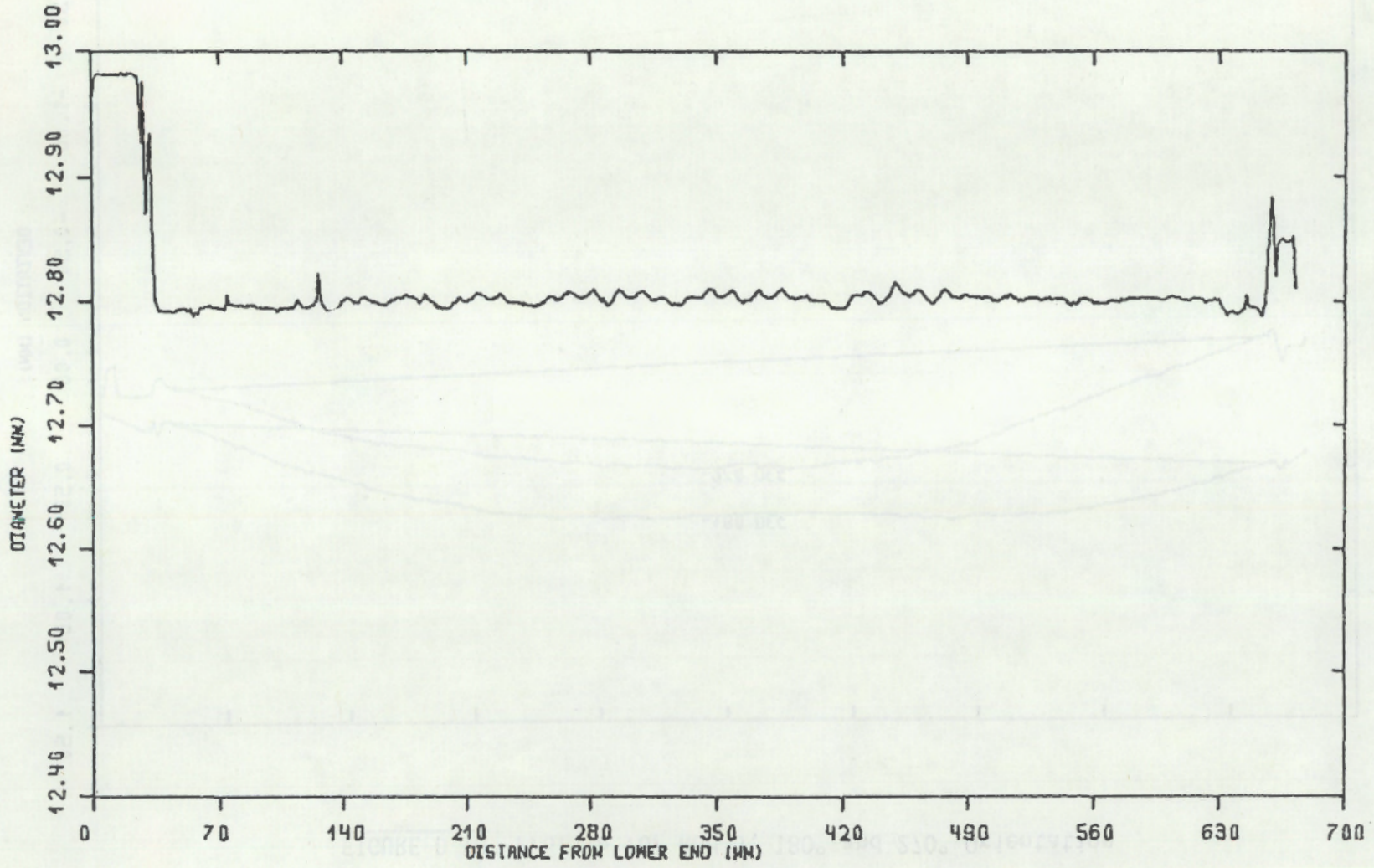

FIGURE D.12 Diameter for Rod 3, 90° Orientation

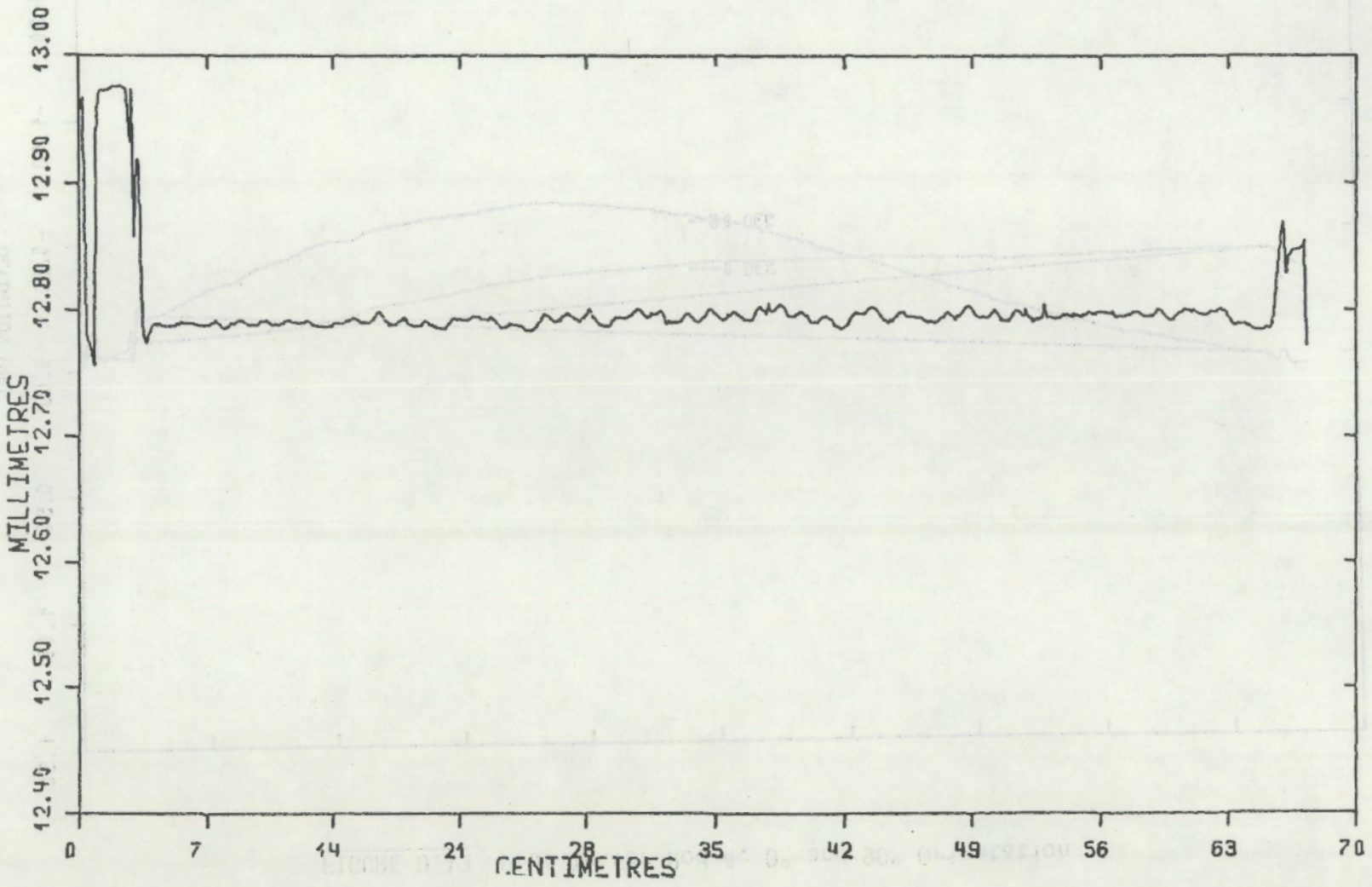

FIGURE D.13 Profile for Rod 4, 0° and 90° Orientation

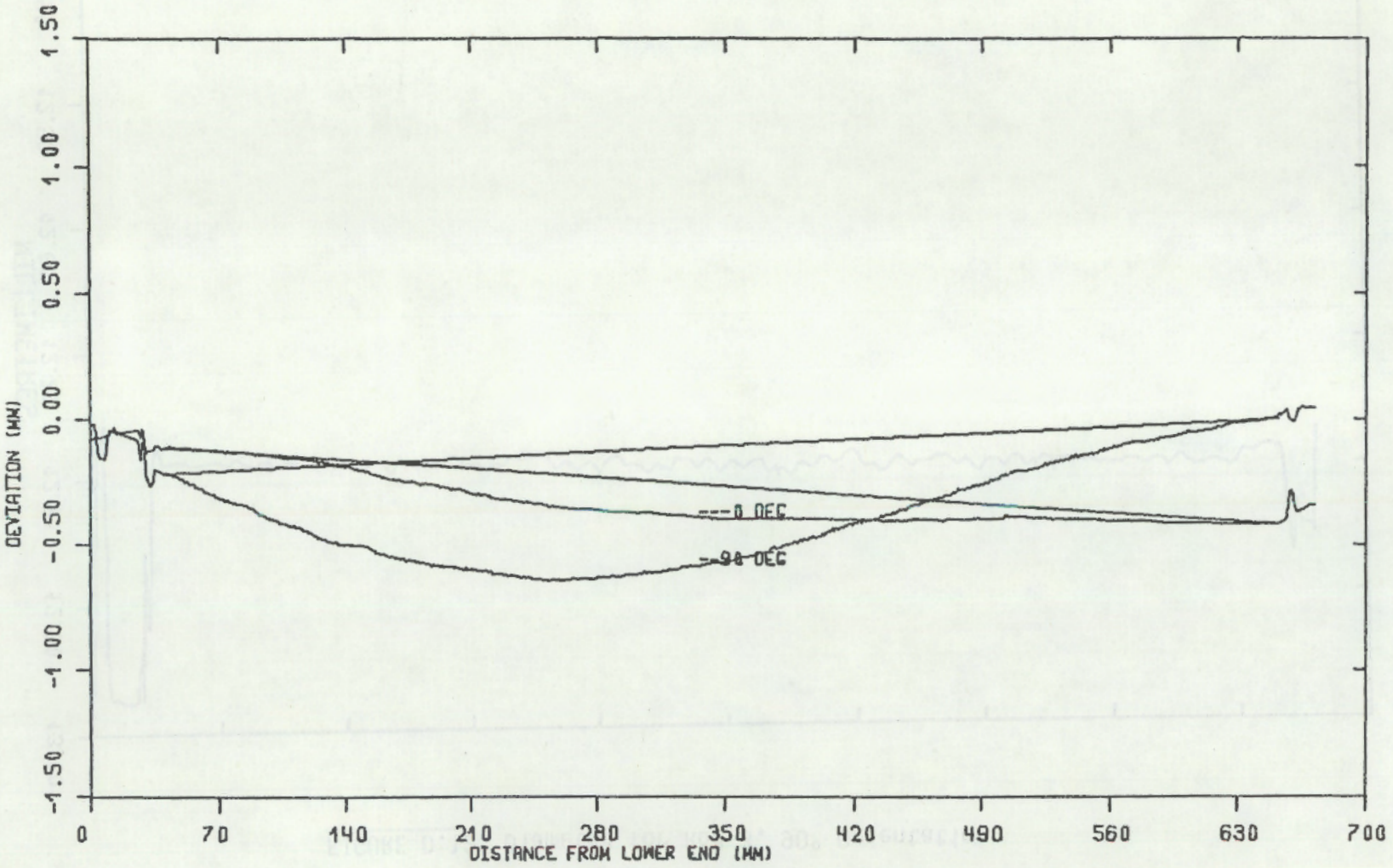

FIGURE D.14 Profile for Rod 4, 180° and 270° Orientation

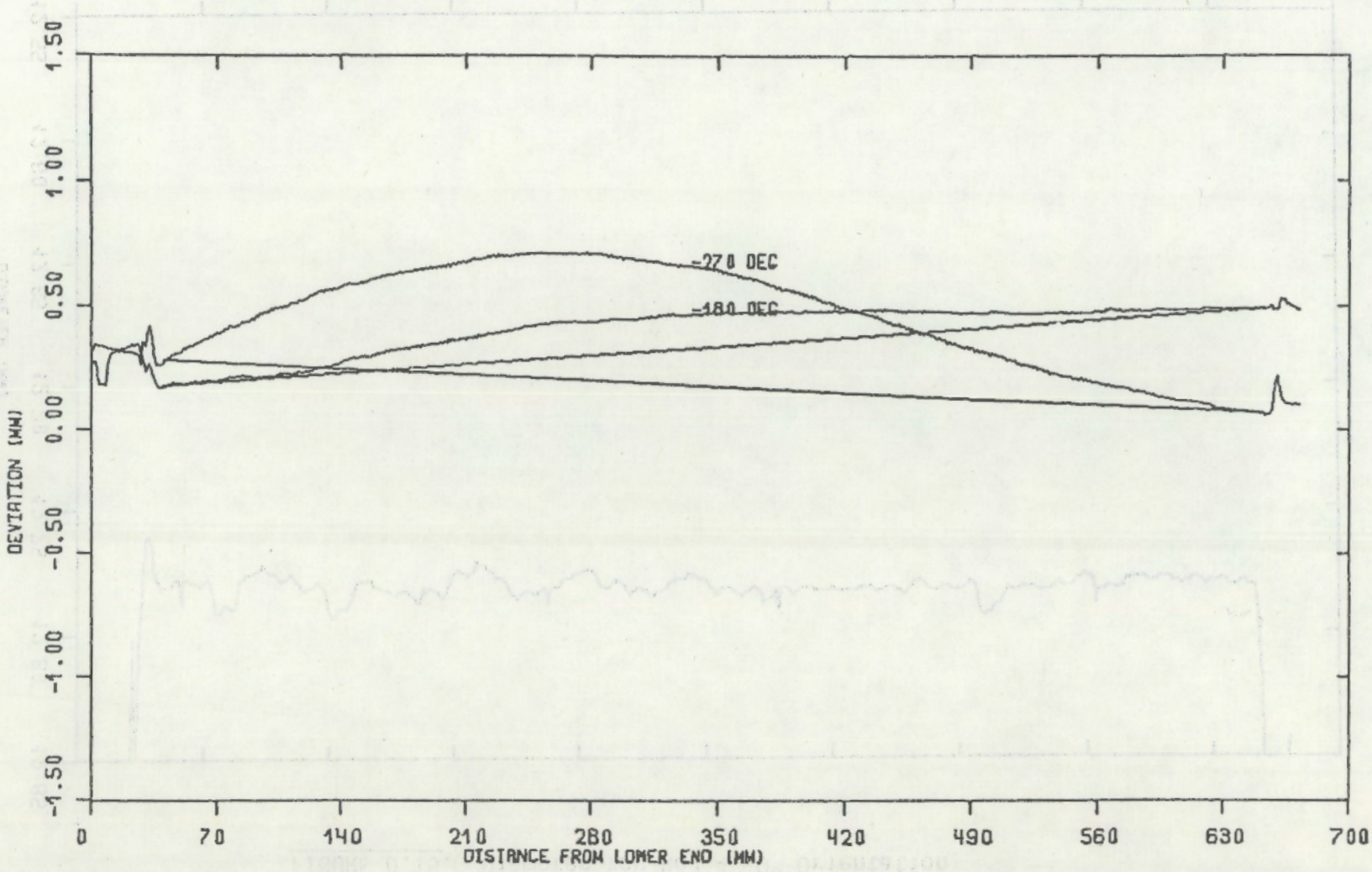

FIGURE D.15. Diameter for Rod 4, 0° Orientation

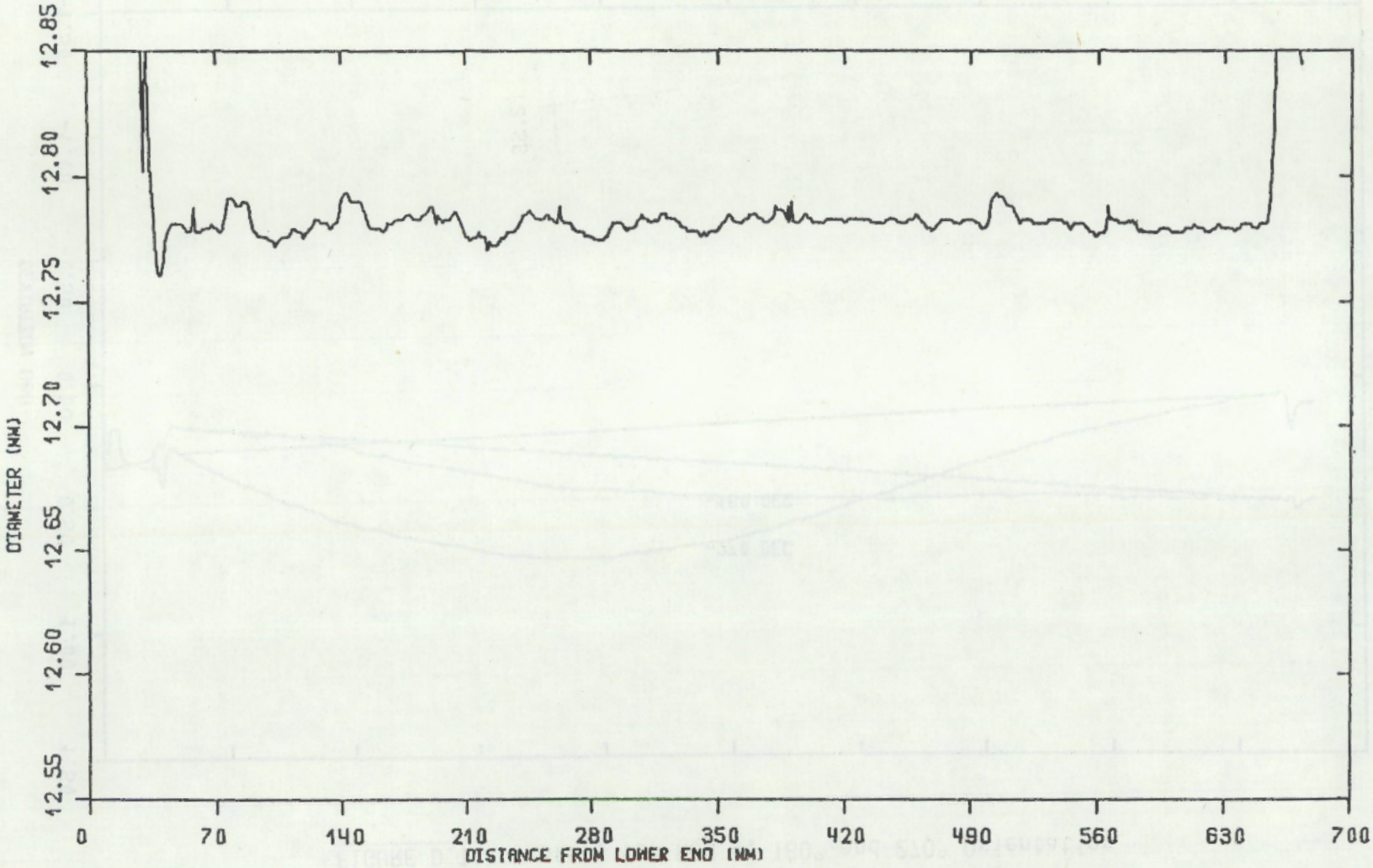

FIGURE D.16 Diameter for Rod 4, 90° Orientation

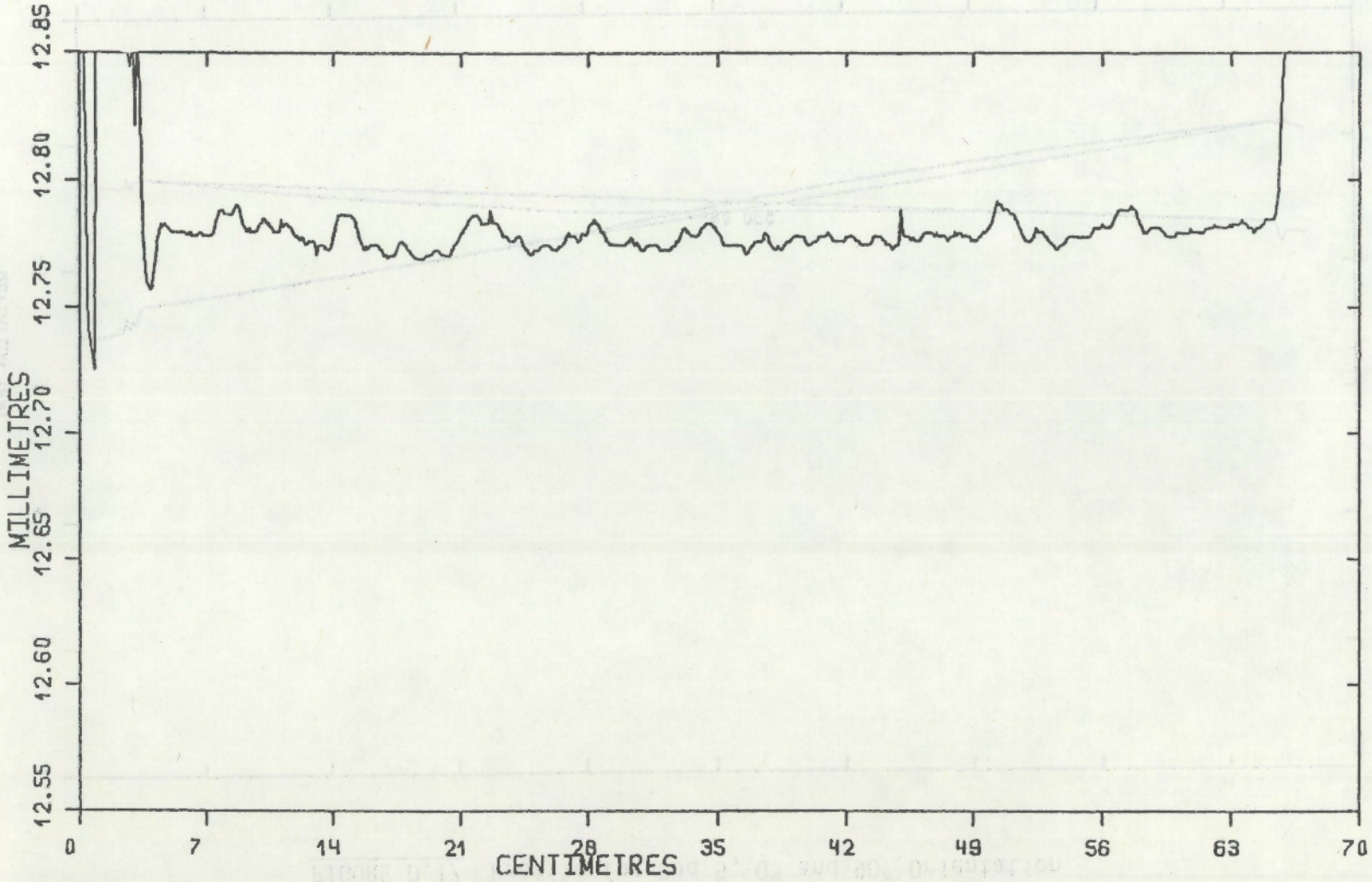

FIGURE D.17 Profile for Rod 5, 0° and 90° Orientation

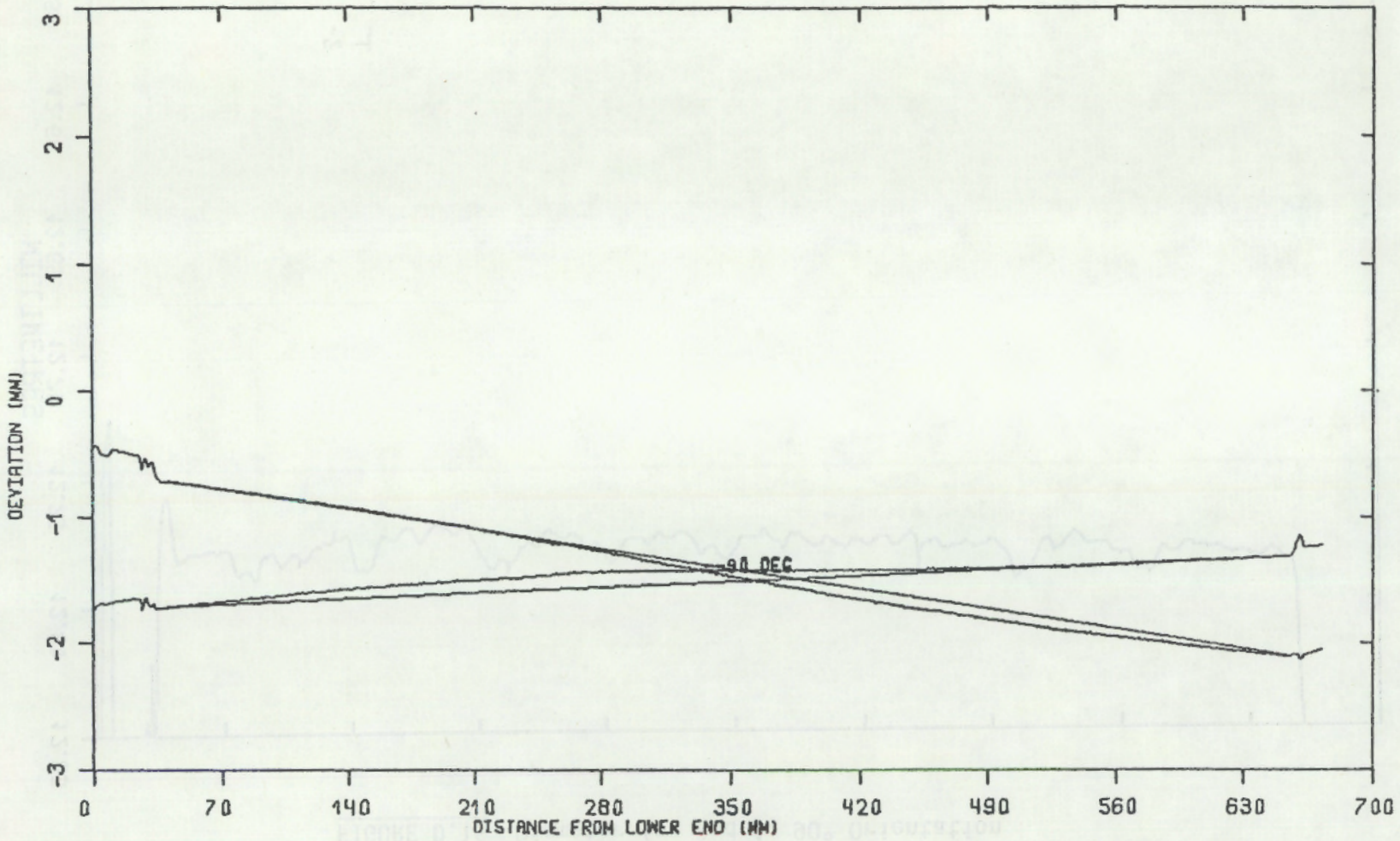

FIGURE D.18 Profile for Rod 5, 180° and 270° Orientation

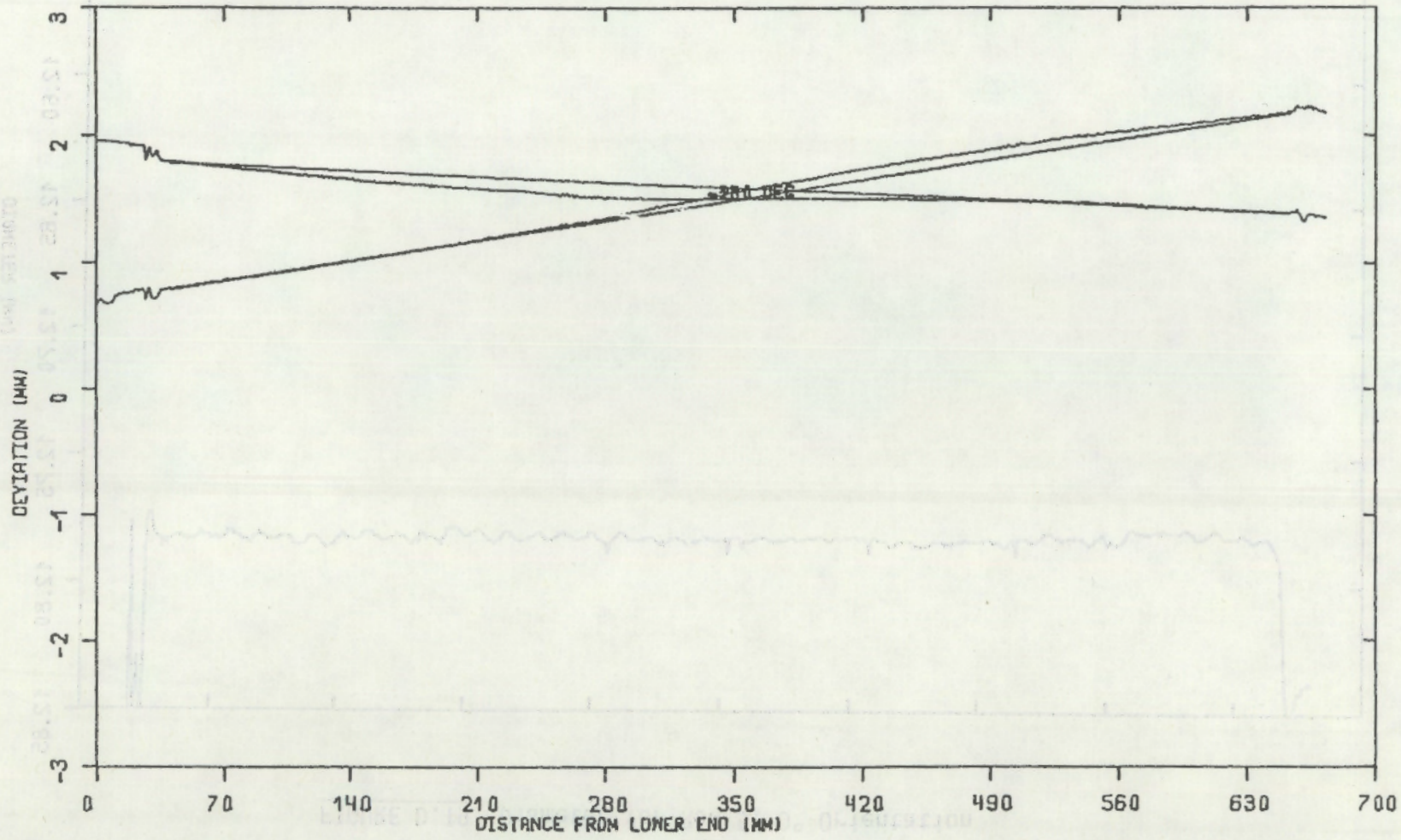

FIGURE D.19 Diameter for Rod 5, 0° Orientation

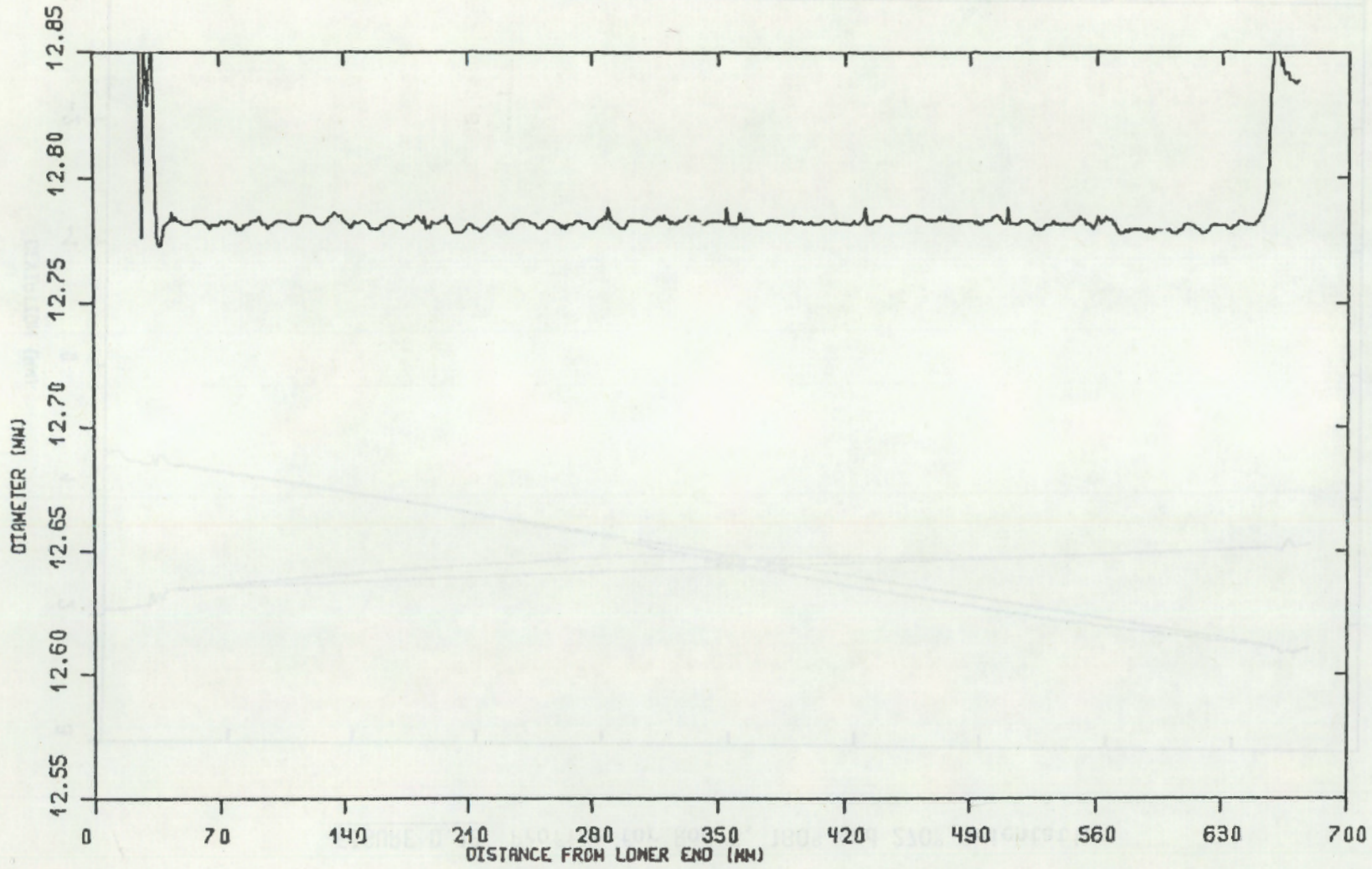

FIGURE D.20 Diameter for Rod 5, 90° Orientation

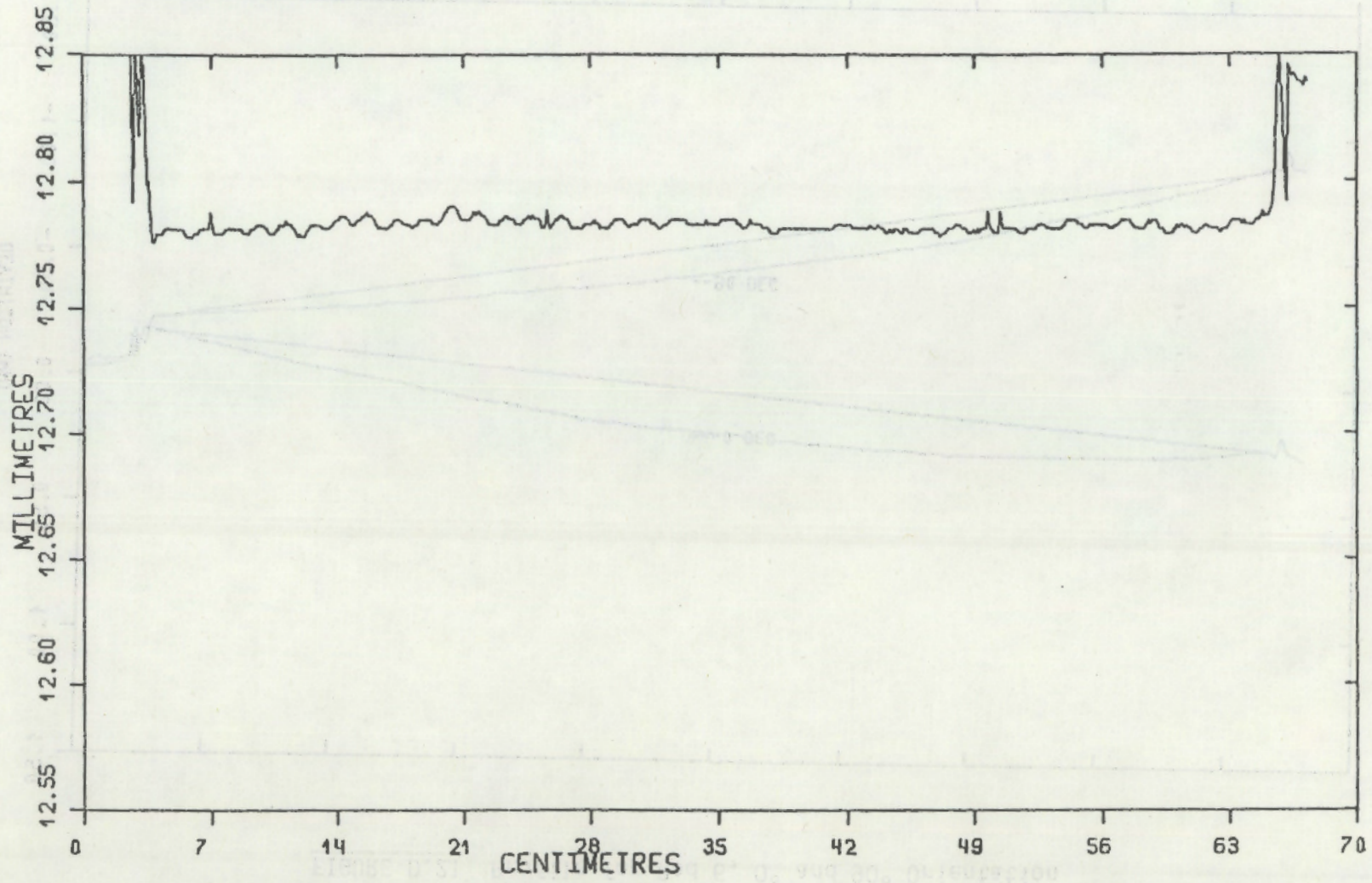

FIGURE D.21 Profile for Rod 6, 0° and 90° Orientation

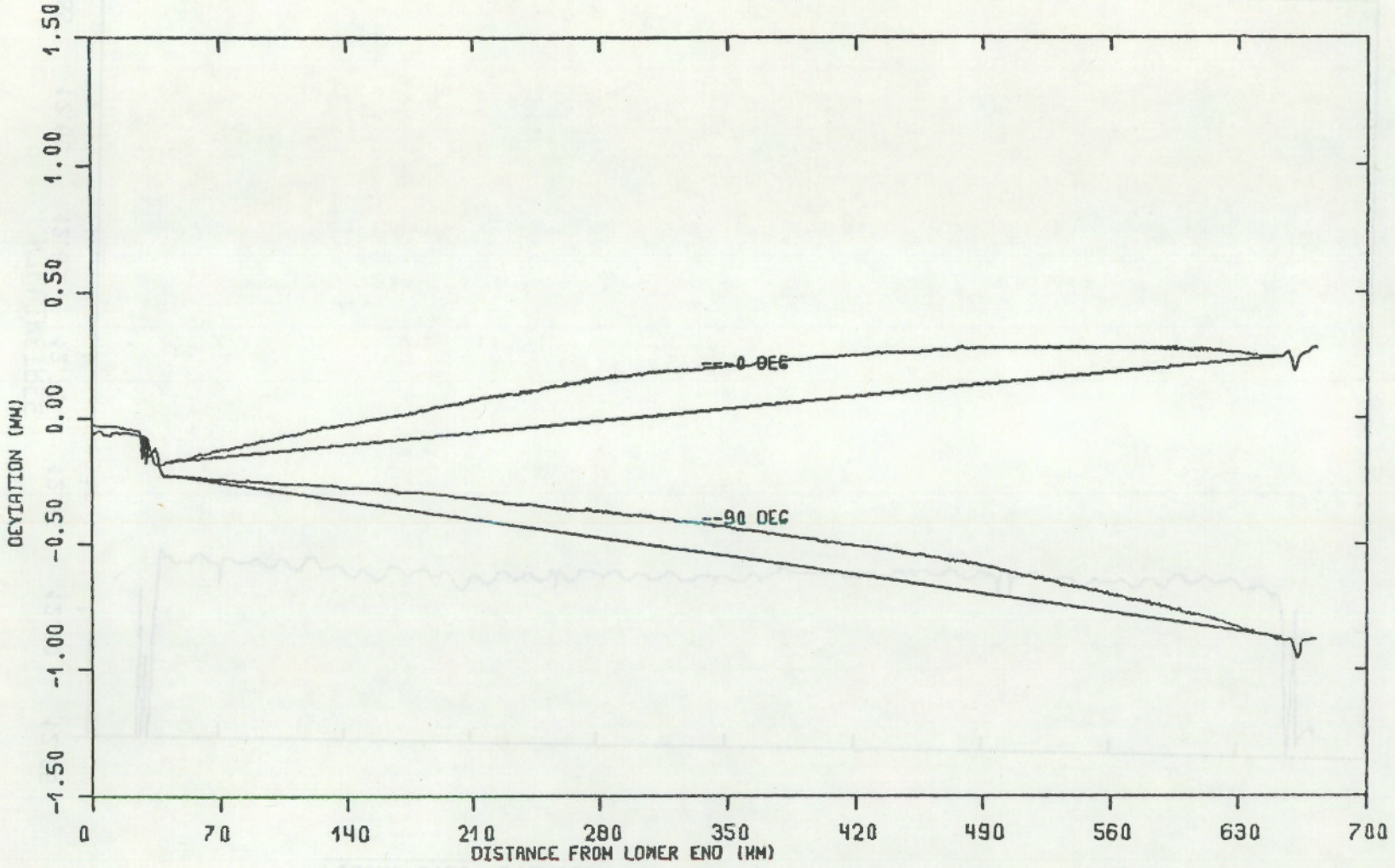

FIGURE D.22 Profile for Rod 6, 180° and 270° Orientation

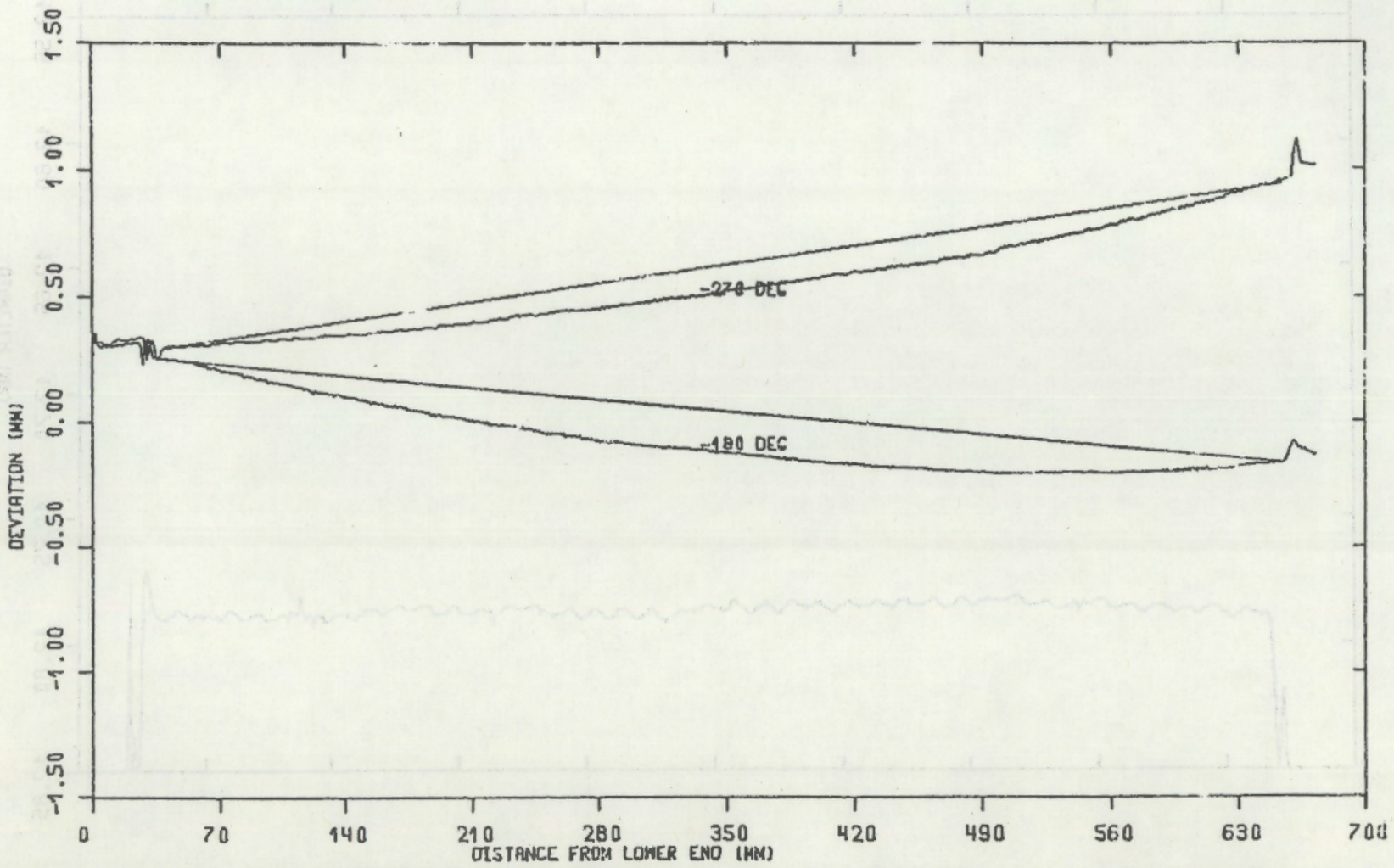

FIGURE D.23 Diameter for Rod 6, 0° Orientation

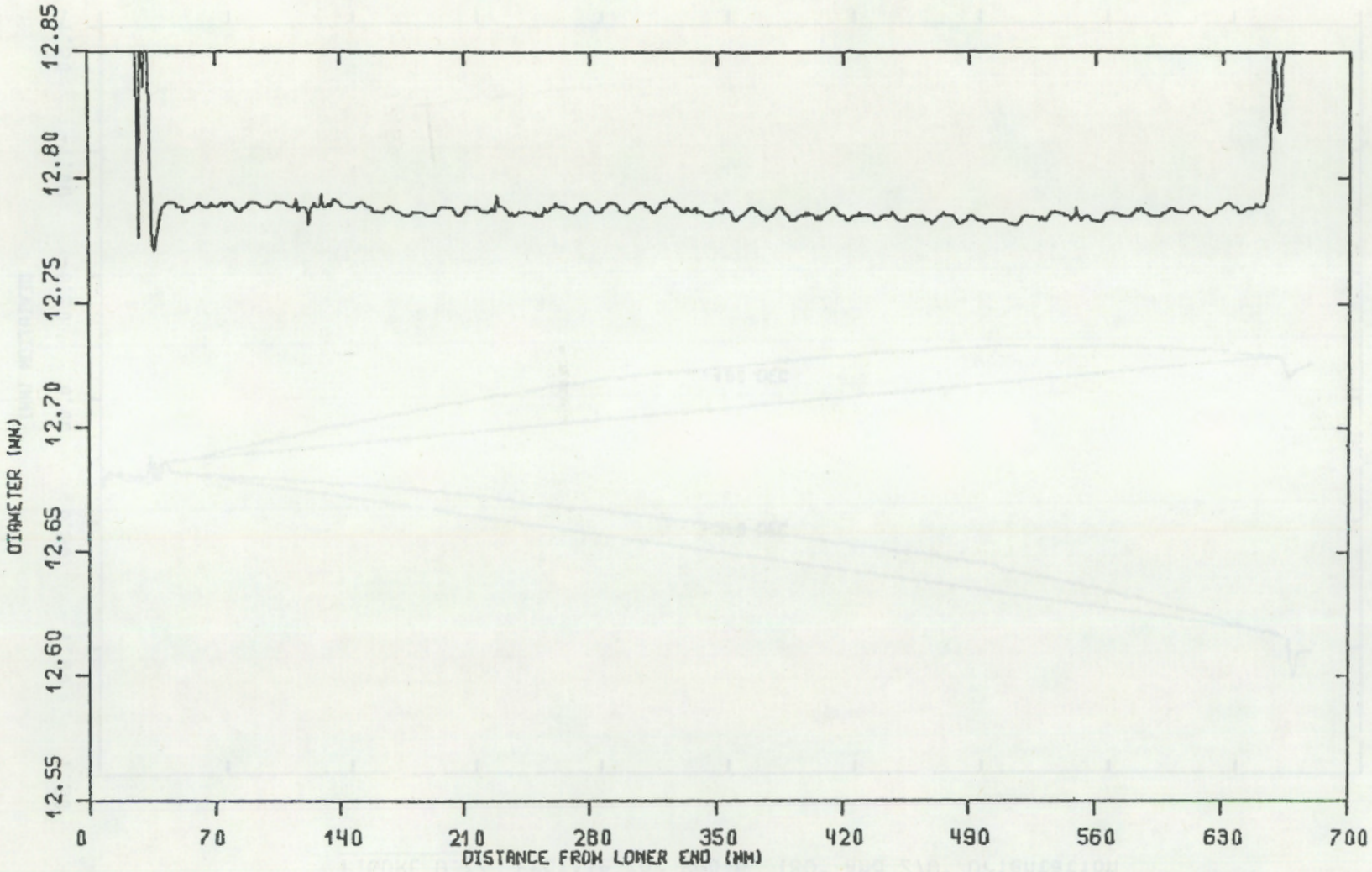

FIGURE D.24 Diameter for Rod 6, 90° Orientation

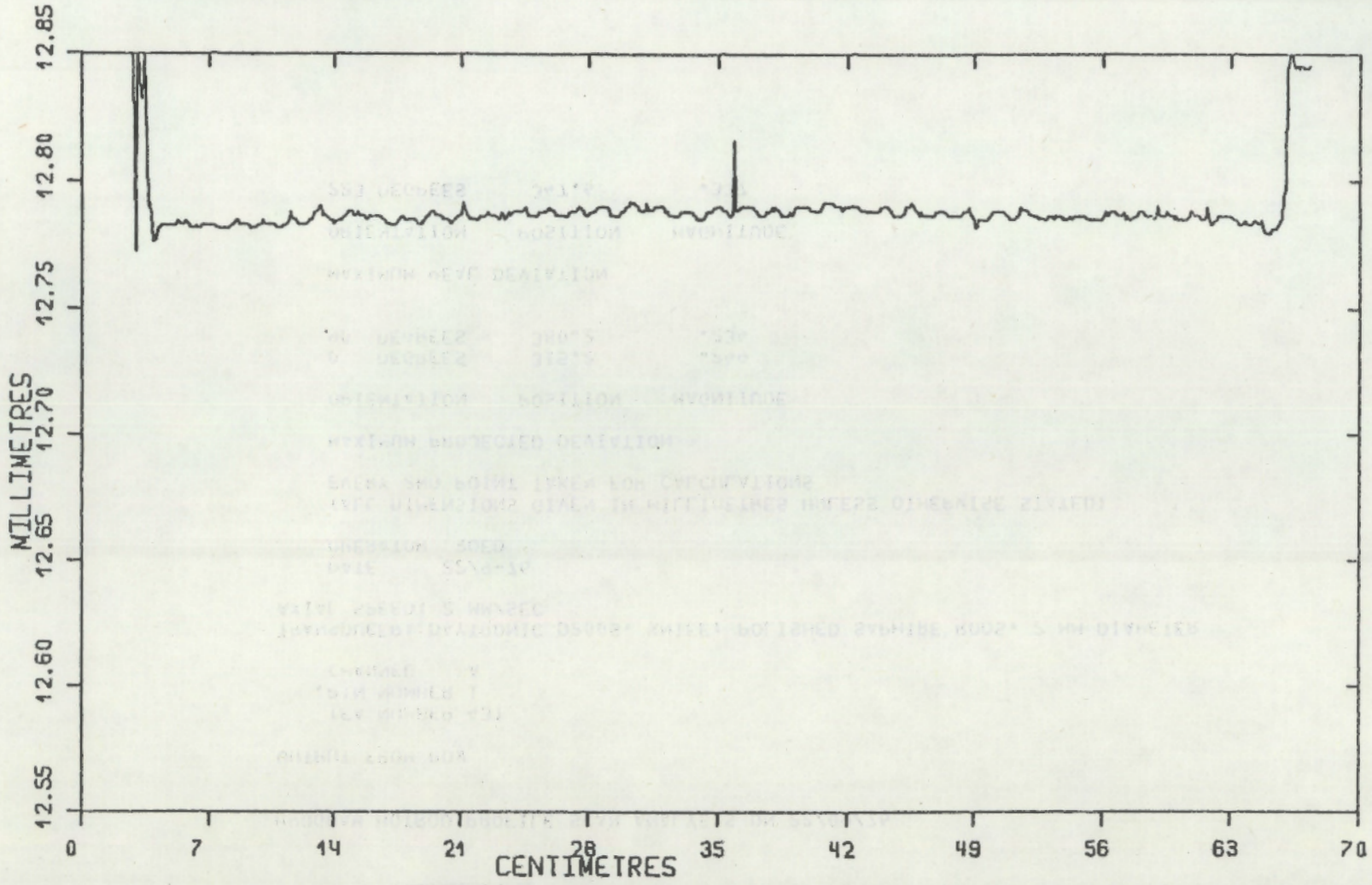

TABLE D.1 Profile for Rod 1, 0° Orientation

PROGRAM HOTROD PROFILE SCAN ANALYSIS ON 22/09/76

OUTPUT FROM ROW

IFA NUMBER 431
PIN NUMBER 1
CHANNEL A

TRANSDUCER: DAYTRONIC D200S, KNIFE: POLISHED SAPHIRE RODS, 2 MM DIAMETER
AXIAL SPEED: 2 MM/SEC

DATE 22/9-76
OPERATOR ROED

(ALL DIMENSIONS GIVEN IN MILLIMETRES UNLESS OTHERWISE STATED)
EVERY 2ND POINT TAKEN FOR CALCULATIONS

MAXIMUM PROJECTED DEVIATION

ORIENTATION	POSITION	MAGNITUDE
0 DEGREES	315.2	.249
90 DEGREES	380.2	.234

MAXIMUM REAL DEVIATION

ORIENTATION	POSITION	MAGNITUDE
223 DEGREES	347.6	.337

TABLE D.2 Profile for Rod 1, 90° Orientation

PROGRAM HOTROD PROFILE SCAN ANALYSIS ON 22/09/76

OUTPUT FROM POW

IFA NUMBER 431
PIN NUMBER 1
CHANNEL B

TRANSDUCER: DAYTRONIC D200S. KNIFE: POLISHED SAPHIRE RODS. 2 MM DIAMETER
AXIAL SPEED: 2 MM/SEC

DATE 22/9-76
OPERATOR ROED

(ALL DIMENSIONS GIVEN IN MILLIMETRES UNLESS OTHERWISE STATED)
EVERY 2ND POINT TAKEN FOR CALCULATIONS

MAXIMUM PROJECTED DEVIATION

ORIENTATION	POSITION	MAGNITUDE
0 DEGREES	318.6	.249
90 DEGREES	377.4	.235

MAXIMUM REAL DEVIATION

ORIENTATION	POSITION	MAGNITUDE
43 DEGREES	348.4	.338

TABLE D.3 Diameter for Rod 1

PROGRAM HOTROD PROFILE SCAN ANALYSIS ON 22/09/76

OUTPUT FROM DIAMETER

IFA NUMBER 431
PIN NUMBER 1

TRANSDUCER: DAYTRONIC D200S, KNIFE: POLISHED SAPHIRE RODS, 2 MM DIAMETER
AXIAL SPEED: 2 MM/SEC

DATE 22/9-76
OPERATOR ROED

EVERY 2ND POINT TAKEN FOR CALCULATIONS
(ALL DIMENSIONS GIVEN IN MILLIMETRES UNLESS OTHERWISE STATED)

POSITION	DIAMETER		MEAN DIAMETER OVER SECTIONS		
	0 DEG.	90 DEG.	SECTION ROUNDS	0 DEG.	90 DEG.
40	12.778	12.779			
90	12.779	12.779	40 - 90	12.780	12.780
140	12.779	12.781	90 - 140	12.781	12.780
190	12.781	12.781	140 - 190	12.782	12.781
240	12.781	12.783	190 - 240	12.780	12.783
290	12.781	12.785	240 - 290	12.781	12.784
340	12.781	12.783	290 - 340	12.782	12.784
390	12.781	12.783	340 - 390	12.781	12.784
440	12.781	12.783	390 - 440	12.781	12.783
490	12.778	12.783	440 - 490	12.779	12.784
540	12.781	12.785	490 - 540	12.779	12.785
590	12.781	12.783	540 - 590	12.781	12.784
640	12.781	12.786	590 - 640	12.782	12.785

MAXIMUM DIAMETER AT 0 DEG. IS 12.792 MM. AT POSITION 176.6 MM.
AT 90 DEG. IS 12.807 MM. AT POSITION 151.4 MM.

MINIMUM DIAMETER AT 0 DEG. IS 12.776 MM. AT POSITION 502.8 MM.
AT 90 DEG. IS 12.778 MM. AT POSITION 104.6 MM.

MEAN DIAMETER AT 0 DEG. IS 12.780 MM.
AT 90 DEG. IS 12.782 MM.

TABLE D.4. Profile for Rod 2, 0° Orientation

PROGRAM HOTROD PROFILE SCAN ANALYSIS ON 22/09/76

OUTPUT FROM ROW

IFA NUMBER 431
PIN NUMBER 2
CHANNEL A

TRANSDUCER: DAYTRONIC D200S. KNIFE: POLISHED SAPHIRE RODS, 2 MM DIAMETER
AXIAL SPEED: 2 MM/SEC

DATE 22/9-76
OPERATOR ROED

(ALL DIMENSIONS GIVEN IN MILLIMETRES UNLESS OTHERWISE STATED)
EVERY 2ND POINT TAKEN FOR CALCULATIONS

MAXIMUM PROJECTED DEVIATION

ORIENTATION	POSITION	MAGNITUDE
0 DEGREES	385.2	.233
90 DEGREES	524.9	.044

MAXIMUM REAL DEVIATION

ORIENTATION	POSITION	MAGNITUDE
4 DEGREES	389.6	.234

TABLE D.5. Profile for Rod 2, 90° Orientation

PROGRAM HOTROD PROFILE SCAN ANALYSIS ON 22/09/76

OUTPUT FROM ROW

IFA NUMBER 431
PIN NUMBER 2
CHANNEL B

TRANSDUCER: DAYTRONIC D200S, KNIFE: POLISHED SAPHIRE RODS, 2 MM DIAMETER
AXIAL SPEED: 2 MM/SEC

DATE 22/9-76
OPERATOR ROED

(ALL DIMENSIONS GIVEN IN MILLIMETRES UNLESS OTHERWISE STATED)
EVERY 2ND POINT TAKEN FOR CALCULATIONS

MAXIMUM PROJECTED DEVIATION

ORIENTATION	POSITION	MAGNITUDE
0 DEGREES	384.8	.241
90 DEGREES	524.6	.047

MAXIMUM REAL DEVIATION

ORIENTATION	POSITION	MAGNITUDE
184 DEGREES	388.9	.242

TABLE D.6 Diameter for Rod 2

PROGRAM HOTROD PROFILE SCAN ANALYSIS ON 22/09/76

OUTPUT FROM DIAMETER

IFA NUMBER 431
PIN NUMBER 2

TRANSDUCER: DAYTRONIC D200S. KNIFE: POLISHED SAPHIRE RODS. 2 MM DIAMETER
AXIAL SPEED: 2 MM/SEC

DATE 22/9-76
OPERATOR ROED

EVERY 2ND POINT TAKEN FOR CALCULATIONS
(ALL DIMENSIONS GIVEN IN MILLIMETRES UNLESS OTHERWISE STATED)

POSITION	DIAMETER		MEAN DIAMETER OVER SECTIONS		
	0 DEG.	90 DEG.	SECTION BOUNDS	0 DEG.	90 DEG.
40	12.786	12.778			
90	12.785	12.783	40 - 90	12.785	12.781
140	12.783	12.783	90 - 140	12.783	12.781
190	12.781	12.779	140 - 190	12.782	12.781
240	12.783	12.779	190 - 240	12.782	12.780
290	12.779	12.781	240 - 290	12.781	12.780
340	12.778	12.781	290 - 340	12.779	12.781
390	12.781	12.779	340 - 390	12.779	12.781
440	12.779	12.781	390 - 440	12.780	12.781
490	12.779	12.783	440 - 490	12.782	12.782
540	12.783	12.779	490 - 540	12.781	12.782
590	12.783	12.783	540 - 590	12.782	12.781
640	12.781	12.786	590 - 640	12.783	12.783

MAXIMUM DIAMETER AT 0 DEG. IS 12.828 MM. AT POSITION 474.0 MM.
AT 90 DEG. IS 12.792 MM. AT POSITION 92.8 MM.

MINIMUM DIAMETER AT 0 DEG. IS 12.776 MM. AT POSITION 321.2 MM.
AT 90 DEG. IS 12.778 MM. AT POSITION 282.8 MM.

MEAN DIAMETER AT 0 DEG. IS 12.781 MM.
AT 90 DEG. IS 12.780 MM.

TABLE D.7. Profile for Rod 3, 0° Orientation

PROGRAM HOTROD PROFILE SCAN ANALYSIS ON 22/09/76

OUTPUT FROM ROW

IFA NUMBER 431
PIN NUMBER 3
CHANNEL A

TRANSDUCER: DAYTRONIC D200S, KNIFE: POLISHED SAPHIRE RODS, 2 MM DIAMETER
AXIAL SPEED: 2 MM/SEC

DATE 22/9-76
OPERATOR ROED

(ALL DIMENSIONS GIVEN IN MILLIMETRES UNLESS OTHERWISE STATED)
EVERY 2ND POINT TAKEN FOR CALCULATIONS

MAXIMUM PROJECTED DEVIATION

ORIENTATION	POSITION	MAGNITUDE
0 DEGREES	303.2	.309
90 DEGREES	436.4	.442

MAXIMUM REAL DEVIATION

ORIENTATION	POSITION	MAGNITUDE
57 DEGREES	393.4	.512

TABLE D.8. Profile for Rod 3, 90° Orientation

PROGRAM HOTROD PROFILE SCAN ANALYSIS ON 22/09/76

OUTPUT FROM ROW

IFA NUMBER 431
PIN NUMBER 3
CHANNEL B

TRANSDUCER: DAYTRONIC D200S, KNIFE: POLISHED SAPHIRE RODS, 2 MM DIAMETER
AXIAL SPEED: 2 MM/SEC

DATE 22/9-76
OPERATOR ROED

(ALL DIMENSIONS GIVEN IN MILLIMETRES UNLESS OTHERWISE STATED)
EVERY 2ND POINT TAKEN FOR CALCULATIONS

MAXIMUM PROJECTED DEVIATION

ORIENTATION	POSITION	MAGNITUDE
0 DEGREES	301.2	.299
90 DEGREES	437.5	.433

MAXIMUM REAL DEVIATION

ORIENTATION	POSITION	MAGNITUDE
237 DEGREES	384.4	.499

TABLE D.9 Diameter for Rod 3

PROGRAM HOTROD PROFILE SCAN ANALYSIS ON 22/09/76

OUTPUT FROM DIAMETER

IFA NUMBER 431
PIN NUMBER 3

TRANSDUCER: DAYTRONIC D200S, KNIFE: POLISHED SAPHIRE RODS, 2 MM DIAMETER
AXIAL SPEED: 2 MM/SEC

DATE 22/9-76
OPERATOR ROED

EVERY 2ND POINT TAKEN FOR CALCULATIONS
(ALL DIMENSIONS GIVEN IN MILLIMETRES UNLESS OTHERWISE STATED)

POSITION	DIAMETER		MEAN DIAMETER OVER SECTIONS		
	0 DEG.	90 DEG.	SECTION BOUNDS	0 DEG.	90 DEG.
40	12.792	12.788			
90	12.795	12.790	40 - 90	12.795	12.789
140	12.802	12.790	90 - 140	12.797	12.789
190	12.797	12.790	140 - 190	12.800	12.791
240	12.797	12.788	190 - 240	12.800	12.790
290	12.804	12.788	240 - 290	12.802	12.791
340	12.806	12.795	290 - 340	12.803	12.794
390	12.800	12.797	340 - 390	12.805	12.797
440	12.802	12.790	390 - 440	12.801	12.794
490	12.804	12.793	440 - 490	12.806	12.796
540	12.799	12.797	490 - 540	12.802	12.795
590	12.802	12.795	540 - 590	12.801	12.797
640	12.795	12.785	590 - 640	12.799	12.795

MAXIMUM DIAMETER AT 0 DEG. IS 12.869 MM. AT POSITION 124.8 MM.
AT 90 DEG. IS 12.818 MM. AT POSITION 513.8 MM.

MINIMUM DIAMETER AT 0 DEG. IS 12.788 MM. AT POSITION 647.0 MM.
AT 90 DEG. IS 12.781 MM. AT POSITION 437.4 MM.

MEAN DIAMETER AT 0 DEG. IS 12.800 MM.
AT 90 DEG. IS 12.792 MM.

TABLE D.10 Profile for Rod 4, 0° Orientation

PROGRAM HOTROD PROFILE SCAN ANALYSIS ON 22/09/76

OUTPUT FROM HOW

IFA NUMBER 431
PIN NUMBER 4
CHANNEL A

TRANSDUCER: DAYTRONIC D200S, KNIFE: POLISHED SAPHIRE RODS, 2 MM DIAMETER
AXIAL SPEED: 2 MM/SEC

DATE 22/9-76
OPERATOR ROED

(ALL DIMENSIONS GIVEN IN MILLIMETRES UNLESS OTHERWISE STATED)
EVERY 2ND POINT TAKEN FOR CALCULATIONS

MAXIMUM PROJECTED DEVIATION

ORIENTATION	POSITION	MAGNITUDE
0 DEGREES	338.0	.115
90 DEGREES	321.0	.519

MAXIMUM REAL DEVIATION

ORIENTATION	POSITION	MAGNITUDE
77 DEGREES	322.0	.531

TABLE D.11 Profile for Rod 4, 90° Orientation

PROGRAM HOTROD PROFILE SCAN ANALYSIS ON 22/09/76

OUTPUT FROM ROW

IFA NUMBER 431
PIN NUMBER 4
CHANNEL 8

TRANSDUCER: DAYTRONIC D200S, KNIFE: POLISHED SAPHIRE RODS, 2 MM DIAMETER
AXIAL SPEED: 2 MM/SEC

DATE 22/9-76
OPERATOR ROED

(ALL DIMENSIONS GIVEN IN MILLIMETRES UNLESS OTHERWISE STATED)
EVERY 2ND POINT TAKEN FOR CALCULATIONS

MAXIMUM PROJECTED DEVIATION

ORIENTATION	POSITION	MAGNITUDE
0 DEGREES	332.6	.112
90 DEGREES	322.2	.521

MAXIMUM REAL DEVIATION

ORIENTATION	POSITION	MAGNITUDE
257 DEGREES	323.0	.533

TABLE D.12. Diameter for Rod 4

PROGRAM HOTROD PROFILE SCAN ANALYSIS ON 22/09/76

OUTPUT FROM DIAMETER

IFA NUMBER 431
PIN NUMBER 4

TRANSDUCER: DAYTRONIC D200S. KNIFE: POLISHED SAPHIRE RODS. 2 MM DIAMETER
AXIAL SPEED: 2 MM/SEC

DATE 22/9-76
OPERATOR ROED

EVERY 2ND POINT TAKEN FOR CALCULATIONS
(ALL DIMENSIONS GIVEN IN MILLIMETRES UNLESS OTHERWISE STATED)

POSITION	DIAMETER		MEAN DIAMETER OVER SECTIONS		
	0 DEG.	90 DEG.	SECTION BOUNDS	0 DEG.	90 DEG.
40	12.762	12.762			
90	12.778	12.781	40 - 90	12.782	12.782
140	12.793	12.783	90 - 140	12.779	12.779
190	12.786	12.771	140 - 190	12.784	12.775
240	12.785	12.778	190 - 240	12.779	12.778
290	12.791	12.774	240 - 290	12.780	12.776
340	12.776	12.783	290 - 340	12.781	12.776
390	12.781	12.778	340 - 390	12.783	12.776
440	12.783	12.774	390 - 440	12.782	12.776
490	12.781	12.779	440 - 490	12.782	12.777
540	12.779	12.778	490 - 540	12.784	12.780
590	12.779	12.778	540 - 590	12.780	12.782
640	12.779	12.783	590 - 640	12.779	12.781

MAXIMUM DIAMETER AT 0 DEG. IS 12.795 MM. AT POSITION 387.0 MM.
AT 90 DEG. IS 12.799 MM. AT POSITION 109.6 MM.

MINIMUM DIAMETER AT 0 DEG. IS 12.762 MM. AT POSITION 40.4 MM.
AT 90 DEG. IS 12.762 MM. AT POSITION 40.2 MM.

MEAN DIAMETER AT 0 DEG. IS 12.780 MM.
AT 90 DEG. IS 12.777 MM.

TABLE 0.13 Profile for Rod 5, 0° Orientation

PROGRAM HOTROD PROFILE SCAN ANALYSIS ON 22/09/76

OUTPUT FROM ROW

IFA NUMBER 431
PIN NUMBER 5
CHANNEL A

TRANSDUCER: DAYTRONIC D200S. KNIFE: POLISHED SAPHIRE RODS. 2 MM DIAMETER
AXIAL SPEED: 2 MM/SEC

DATE 22/9-76
OPERATOR ROED

(ALL DIMENSIONS GIVEN IN MILLIMETRES UNLESS OTHERWISE STATED)
EVERY 2ND POINT TAKEN FOR CALCULATIONS

MAXIMUM PROJECTED DEVIATION

ORIENTATION	POSITION	MAGNITUDE
0 DEGREES	312.2	.089
90 DEGREES	161.8	.105

MAXIMUM REAL DEVIATION

ORIENTATION	POSITION	MAGNITUDE
226 DEGREES	278.5	.121

TABLE D.14 Profile for Rod 5, 90° Orientation

PROGRAM HOTROD PROFILE SCAN ANALYSIS ON 22/09/76

OUTPUT FROM ROW

IFA NUMBER 431
PIN NUMBER 5
CHANNEL B

TRANSDUCER: DAYTRONIC 0200S, KNIFE: POLISHED SAPHIRE RODS, 2 MM DIAMETER
AXIAL SPEED: 2 MM/SEC

DATE 22/9-76
OPERATOR ROED

(ALL DIMENSIONS GIVEN IN MILLIMETRES UNLESS OTHERWISE STATED)
EVERY 2ND POINT TAKEN FOR CALCULATIONS

MAXIMUM PROJECTED DEVIATION

ORIENTATION	POSITION	MAGNITUDE
0 DEGREES	314.2	.087
90 DEGREES	173.2	.106

MAXIMUM REAL DEVIATION

ORIENTATION	POSITION	MAGNITUDE
48 DEGREES	273.8	.121

TABLE D.15 Diameter for Rod 5

PROGRAM HOTROD PROFILE SCAN ANALYSIS ON 22/09/76

OUTPUT FROM DIAMETER

IFA NUMBER 431
PIN NUMBER 5

TRANSDUCER: DAYTRONIC D200S. KNIFE: POLISHED SAPHIRE RODS, 2 MM DIAMETER
AXIAL SPEED: 2 MM/SEC

DATE 22/9-76
OPERATOR ROED

EVERY 2ND POINT TAKEN FOR CALCULATIONS
(ALL DIMENSIONS GIVEN IN MILLIMETRES UNLESS OTHERWISE STATED)

POSITION	DIAMETER		MEAN DIAMETER OVER SECTIONS		
	0 DEG.	90 DEG.	SECTION BOUNDS	0 DEG.	90 DEG.
40	12.791	12.779			
90	12.783	12.779	40 - 90	12.782	12.781
140	12.791	12.786	90 - 140	12.783	12.782
190	12.791	12.785	140 - 190	12.782	12.784
240	12.783	12.783	190 - 240	12.781	12.786
290	12.791	12.785	240 - 290	12.782	12.783
340	12.791	12.785	290 - 340	12.782	12.784
390	12.783	12.781	340 - 390	12.782	12.782
440	12.785	12.781	390 - 440	12.782	12.782
490	12.781	12.781	440 - 490	12.783	12.781
540	12.781	12.785	490 - 540	12.782	12.782
590	12.779	12.779	540 - 590	12.781	12.783
640	12.781	12.785	590 - 640	12.780	12.782

MAXIMUM DIAMETER AT 0 DEG. IS 12.788 MM. AT POSITION 46.4 MM.
AT 90 DEG. IS 12.792 MM. AT POSITION 201.4 MM.

MINIMUM DIAMETER AT 0 DEG. IS 12.778 MM. AT POSITION 616.0 MM.
AT 90 DEG. IS 12.778 MM. AT POSITION 467.4 MM.

MEAN DIAMETER AT 0 DEG. IS 12.781 MM.
AT 90 DEG. IS 12.782 MM.

TABLE D.16 Profile for Rod 6, 0° Orientation

PROGRAM HOTROD PROFILE SCAN ANALYSIS ON 22/09/76

OUTPUT FROM ROW

IFA NUMBER 431
PIN NUMBER 6
CHANNEL A

TRANSDUCER: DAYTRONIC D200S, KNIFE: POLISHED SAPHIRE RODS, 2 MM DIAMETER
AXIAL SPEED: 2 MM/SEC

DATE 22/9-76
OPERATOR ROED

(ALL DIMENSIONS GIVEN IN MILLIMETRES UNLESS OTHERWISE STATED)
EVERY 2ND POINT TAKEN FOR CALCULATIONS

MAXIMUM PROJECTED DEVIATION

ORIENTATION	POSITION	MAGNITUDE
0 DEGREES	391.8	.139
90 DEGREES	452.0	.156

MAXIMUM REAL DEVIATION

ORIENTATION	POSITION	MAGNITUDE
228 DEGREES	430.4	.208

TABLE D.17 Profile for Rod 6, 90° Orientation

PROGRAM HOTROD PROFILE SCAN ANALYSIS ON 22/09/76

OUTPUT FROM POW

IFA NUMBER 431
PIN NUMBER 6
CHANNEL B

TRANSDUCER: DAYTRONIC D200S, KNIFE: POLISHED SAPHIRE RODS, 2 MM DIAMETER
AXIAL SPEED: 2 MM/SEC

DATE 22/9-76
OPERATOR ROED

(ALL DIMENSIONS GIVEN IN MILLIMETRES UNLESS OTHERWISE STATED)
EVERY 2ND POINT TAKEN FOR CALCULATIONS

MAXIMUM PROJECTED DEVIATION

ORIENTATION	POSITION	MAGNITUDE
0 DEGREES	374.8	.137
90 DEGREES	448.0	.162

MAXIMUM REAL DEVIATION

ORIENTATION	POSITION	MAGNITUDE
50 DEGREES	422.2	.211

TABLE D.18 Diameter for Rod 6

PROGRAM HOTROD PROFILE SCAN ANALYSIS ON 22/09/76

OUTPUT FROM DIAMETER

TFA NUMBER 431
PIN NUMBER 6

TRANSDUCER: DAYTRONIC D200S, KNIFE: POLISHED SAPHIRE RODS, 2 MM DIAMETER
AXIAL SPEED: 2 MM/SEC

DATE 22/9-76
OPERATOR ROED

EVERY 2ND POINT TAKEN FOR CALCULATIONS
(ALL DIMENSIONS GIVEN IN MILLIMETRES UNLESS OTHERWISE STATED)

POSITION	DIAMETER		MEAN DIAMETER OVER SECTIONS		
	0 DEG.	90 DEG.	SECTION BOUNDS	0 DEG.	90 DEG.
40	12.788	12.778			
90	12.790	12.783	40 - 90	12.789	12.783
140	12.788	12.785	90 - 140	12.789	12.784
190	12.785	12.786	140 - 190	12.787	12.785
240	12.786	12.788	190 - 240	12.787	12.786
290	12.790	12.786	240 - 290	12.787	12.788
340	12.785	12.788	290 - 340	12.788	12.788
390	12.793	12.790	340 - 390	12.786	12.789
440	12.785	12.788	390 - 440	12.785	12.789
490	12.783	12.785	440 - 490	12.784	12.787
540	12.785	12.786	490 - 540	12.784	12.786
590	12.785	12.786	540 - 590	12.785	12.787
640	12.788	12.785	590 - 640	12.787	12.785

MAXIMUM DIAMETER AT 0 DEG. IS 12.802 MM. AT POSITION 222.6 MM.
AT 90 DEG. IS 12.816 MM. AT POSITION 355.2 MM.

MINIMUM DIAMETER AT 0 DEG. IS 12.781 MM. AT POSITION 512.4 MM.
AT 90 DEG. IS 12.778 MM. AT POSITION 40.2 MM.

MEAN DIAMETER AT 0 DEG. IS 12.786 MM.
AT 90 DEG. IS 12.786 MM.

APPENDIX E

PELLET POSITIONS

PELLET POSITIONS

Pellet position numbers have been used in the discussion of the destructive examination done at Harwell. The pellet identity numbers for each position are given below.

Pellet Position	Pellet Identity	Type	Pellet Position	Pellet Identity	Type
1A)	-	Hollow poison	35	742	Solid
1B)		(2-half length)	36	687	"
2	647	Hollow	37	713	"
3	646	"	38	746	"
4	652	"	39	704	"
5	653	"	40	740	"
6	661	"	41	688	"
7	641	"	42	640	Hollow
8	649	"	43	645	"
9	656	"	44	669	"
10	734	Solid	45	642	"
11	706	"	46	654	"
12	718	"	47A)	-	Hollow-poison
13	745	"	47B)		(2-half length)
14	712	"			
15	748	"			
16	743	"			
17	755	"			
18	727	"			
19	701	"			
20	693	"			
21	756	"			
22	747	"			
23	732	"			
24	711	"			
25	722	"			
26	731	"			
27	681	"			
28	699	"			
29	721	"			
30	690	"			
31	719	"			
32	733	"			
33	741	"			
34	735	"			

DISTRIBUTION

No. of Copies

OFFSITE

A. A. Churm
DOE Patent Division
9300 S. Cass Avenue
Argonne, IL 60439

350 Nuclear Regulatory Commission
Division of Technical Information and Document Control
7920 Norfolk Avenue
Bethesda, MD 20014

2 DOE Technical Information Center

4 W. V. Johnston
Chief, Fuel Behavior Research Branch
Division of Reactor Safety Research
U.S. Nuclear Regulatory Commission
Washington, DC 20555

ONSITE

48 Pacific Northwest Laboratory

W. J. Bailey
J. O. Barner
E. R. Bradley
E. L. Courtright
M. E. Cunningham (10)
M. D. Freshley
R. L. Goodman
R. J. Guenther
C. M. Hagen
C. R. Hann (3)
P. L. Hendrick
K. A. Hsieh
O. D. Lanning (5)
R. K. Marshall

ONSITE

Pacific Northwest Laboratory (contd)

C. L. Mohr (3)
C. Nealley (3)
F. E. Panisko
P. J. Pankaskie
W. N. Rausch
R. E. Schreiber
G. D. White
R. E. Williford
Technical Information (5)
Publishing Coordination (2)